CORROSION OF TITANIUM FOR BIOMEDICAL APPLICATIONS

by

Fei Yu

A thesis submitted to the University of Birmingham for the degree of DOCTOR OF PHILOSOPHY

School of Metallurgy and Materials

University of Birmingham

March 2015

ABSTRACT

Ti and its alloys have been widely used in the manufacture of biomedical implanted devices since the 1950s because of their biocompatibility, corrosion resistance and suitable mechanical properties. However, corrosion-related failures of Ti implants are observed. It has also been found that the corrosion products, including metal ions and/or debris/particles, can induce unfavourable biological responses which in turn may lead to the failure of Ti implants.

In the current study, the corrosion of three grades of Ti (CP-Ti Grade 2, CP-Ti Grade 4 and Ti6Al4V) in a series of simulated peri-implant environments has been characterised by measuring ion release and characterising surface morphology. Electrochemical tests have been used to identify the mechanisms leading to the observed corrosion behaviour. Corrosion in the presence of chemical species found in the peri-implant environment (lipopolysaccharide (LPS), a component of Gram-negative bacterial cell walls and a potent mediator of peri-implant inflammation, albumin, an abundant protein, and H_2O_2, an important inflammation product) was studied. Corrosion mediated by the presence of bacteria (early colonisers of Ti surfaces in the oral environment) and abundant immune cells (neutrophils) found in peri-implant sites was investigated. Finally a novel apparatus was designed and fabricated to simulate mechanically-assisted crevice corrosion (MACC) of Ti implants in representative physiological solutions.

LPS was observed to enhance Ti corrosion in slightly acidic and neutral conditions (pH 4-7) whilst it inhibited Ti dissolution in highly acidic environments (pH 2). Both albumin and H_2O_2 influenced the corrosion of Ti and the co-existence of both species considerably enhanced the corrosion of Ti6Al4V more than either species in isolation. The β phase of Ti6Al4V was found to be preferentially attacked in the presence of H_2O_2. The presence of an early bacterial

coloniser of dental implants *Streptococcus sanguinis* and the presence of human neutrophils promoted Ti release from all three grades of Ti. In addition, MACC simulation was demonstrated and the development of aggressive crevice chemistry observed. The presence of albumin decreased the abrasion charge of Ti6Al4V during MACC while LPS and H_2O_2 did not show a measurable change.

Predicting the behaviour of metallic biomaterials in physiological conditions is essential to inform medical device manufacture and prevent adverse outcomes for patients. Despite this unfavourable biological responses to materials that are in widespread use are reported, *in vitro* simulation of materials behaviour is often highly simplistic and fails to account for the complexity of the peri-implant environment. In this study it was demonstrated that chemical species (pH, LPS, H_2O_2 and albumin), biological cells (early colonising bacteria and innate immune cells) and MACC may significantly modify the corrosion properties of biomedical Ti alloys.

ACKNOWLEDGEMENT

TABLE OF CONTENTS

LIST OF SYMBOLS AND DEFINITIONS

Symbol	Definition
CP-Ti	Commercially pure Ti
CP-Ti-G2	Commercial purity ASTM Grade 2 Ti
CP-Ti-G4	Commercial purity ASTM Grade 4 Ti
Ti6Al4V	ASTM Grade 5 Ti
Ti6Al4V-ELI	ASTM Ti Grade 23, ELI: Extra low interstitial
BAHA	Bone-anchored hearing aids
MACC	Mechanically-assisted crevice corrosion
ICP-MS	Inductively coupled plasma mass spectrometry
SLA	Sandblasted-acid-etched
G2P	Mirror-polished CP-Ti-G2
G4P	Mirror-polished CP-Ti-G4
G5P	Mirror-polished Ti6Al4V
G2S	Sandblasted-acid-etched CP-Ti-G2
G4S	Sandblasted-acid-etched CP-Ti-G4
G5S	Sandblasted-acid-etched Ti6Al4V
E	Potential
E_{pp}	Primary passivation potential
i_{crit}	Critical anodic current density
i_{pass}	Passive current density
E_{corr}	Corrosion potential
i_{corr}	Corrosion current
OCP	Open circuit potential
CE	Counter electrode
RE	Reference electrode
WE	Working electrode
ACM	Potentiostat (ACM Instruments, UK)
SCE	Saturated calomel electrode
NHE	Normal hydrogen electrode
EIS	Electrochemical impedance spectroscopy

R_p	Polarisation resistance
E_a	Activation energy
T	Absolute temperature
R	Gas constant
LPS	Lipopolysaccharide
PS	Physiological saline
PBS	Phosphate buffered saline
S. sanguinis	*Streptococcus sanguinis*
S. mutans	*Streptococcus mutans*
S. mitis	*Streptococcus mitis*
Neutrophils	Polymorphous nuclear leukocytes (neutrophils)
Tris-buffer	Tris-buffered saline
Ops *Sa*	Opsonised *Staphylococcus aureus*
TSB	Tryptone soya broth
ROS	Reactive oxygen species
H_2O_2	Hydrogen peroxide
O_2^-	Superoxide
HOCl	Hypochlorous acid
SEM	Scanning electron microscopy
SE	Secondary electron SEM image
BSE	Backscatter electron SEM image
EDX	Energy dispersive X-ray spectroscopy
AFM	Atomic force microscopy

1   INTRODUCTION

Ti and Ti alloys are routinely used for biomedical applications such as dental implants, bone anchorage of extra-oral prostheses, bone fixation systems and orthopaedic devices. Ti and its alloys are employed because of their perceived biocompatibility, suitable mechanical properties and corrosion resistance [1]. The favourable cellular responses to Ti that are reported are conferred by the presence on the Ti surface of a thin passive oxide film which provides chemical stability [1-3]. It has been established in *in vitro* experiments that Ti and its biomedical alloys are highly resistant to pitting corrosion and crevice corrosion at temperatures below 65 °C [4-6]. Therefore corrosion of Ti leading to the release of particles and ions into surrounding tissues is rarely considered by surgeons and patients as a likely event.

However, corrosion-related failures of implanted Ti devices and prostheses have been regularly reported within the medical literature e.g. [7-9]. Using mass spectrometry, investigators have shown that Ti levels can be significantly elevated in compartments remote from the implant site such as in the serum of patients with indwelling Ti fixation devices [10-13]. The presence of Ti particles/debris in a form of Ti metallic, TiO_2 as rutile and TiO_2 as anatase have been found in peri-implant soft tissues retrieved from patients [14-16]. Macroscopic wear/tribocorrosion processes may be the underlying cause, however, there is increasing evidence to suggest that Ti implants are deteriorating in physiological environments in the absence of any significant tribiological process [7, 8, 14].

The physiological environment into which a Ti implant is placed varies with site and with the device application, but is always a complex system containing various inorganic and organic components such as ions, amino acids and proteins and living cells. The specific composition

1

of this environment can also change in either health or disease due to physiological processes such as peri-implant inflammation [14] or as a direct consequence of the deterioration of the implant itself [7].

It has been previously reported that products of normal cellular metabolism such as hydrogen peroxide (H_2O_2) [17] or bacterial products such as lipopolysaccharide (LPS) [18], both of which are important species associated with the inflammation in peri-implant sites can influence the corrosion resistance of Ti implants. The current body of evidence however contains results which are inconsistent or incomplete and typically consider factors which may affect corrosion individually. For example proteins readily adsorb on *in vivo* surfaces of Ti implants, which may modify the corrosion behaviour of the substrate and the interaction of a further chemical species with the Ti surface. Albumin is an abundant protein found in blood and the extracellular environment and its influence on the corrosion behaviour of metallic implants (including Ti) has been reported [19-24]. However there remains disagreement amongst investigators as to whether the presence of albumin enhances or inhibits corrosion of Ti alloys [20, 25-28]. Although clarification of the influence of adsorbed proteins on Ti corrosion is important, it is also necessary to study the combination effect of such species with other biomolecules which are abundant in the peri-implant environment and may subsequently promote or prevent Ti corrosion.

It has been suggested that the human cells and bacteria that can form a surface biofilm may have an influence on corrosion properties of biomedical implants [29-32]. However, the mechanisms underlying the cellular effects on the corrosion resistance of Ti alloys in the body are poorly characterised and require further investigation.

In addition to biologically-mediated release of Ti from implants, mechanically-assisted crevice corrosion (MACC) has been proposed to contribute to the accumulation of Ti products in peri-implant tissues in situations where the implant is not subjected to macroscopic wear [7, 14, 33]. To date most laboratory efforts have focussed on studying tribocorrosion or "fretting corrosion" with small scale motion [34-36], which fails to generate the typical features proposed to be associated with MACC of implanted devices. MACC of metallic implants has not been studied extensively, and to date there is no report of apparatus which could be considered to fully simulate the specific conditions that occur during MACC, with the exception of measurements made on assembled implants using real orthopaedic components [37, 38]. However, none of the work to date has considered the effect of biologically-relevant species such as albumin, LPS and H_2O_2 on the crevice chemistry.

This thesis considers the current evidence and experimentally addresses how specific components of the peri-implant physiological environment including chemical species (pH, LPS, H_2O_2 and albumin), biological cells (early colonising bacteria and innate immune cells) and MACC influence the corrosion properties of biomedical Ti alloys.

2   LITERATURE REVIEW

2.1 Ti and its alloys

2.1.1   Biomedical applications

Ti and its alloys are among the most important metals in the biomedical field. Ti alloys have good mechanical properties, including low elastic modulus, low density and high tensile strength, yielding an excellent strength-to-weight ratio [1, 2]. Ti alloys also show outstanding chemical properties such as good corrosion resistance and thermal stability [1]. In addition, Ti can osseointegrate with living bone after implantation [39]. Therefore, Ti and its alloys have been routinely used in the manufacture of biomedical implants since the 1950s [3]. It is reported that over 1000 tonnes of Ti are used as biomedical devices every year and in modern dentistry the use of Ti implants has revolutionised patient care resulting in a global market value for these interventions at over $4.5 billion [14].

ASTM International recognises 31 grades of Ti and Ti alloys, of which 23 are classified as biomedical materials [3]. There are several kinds of components fabricated from Ti that are used in biomedical devices for various applications in the human body as shown in Figure 2-1 [1, 31]. Ti is used biomedically as parts of joint replacements in the hip and knee; as fixation devices such as bone screws and plates and as anchorage devices to retain artificial teeth or facial prostheses. Ti alloys can also serve as artificial heart valves or artificial vascular stents [1, 31]. Of the available biomedical Ti substrates, commercially pure Ti (CP-Ti) and Ti6Al4V are the most commonly used [40].
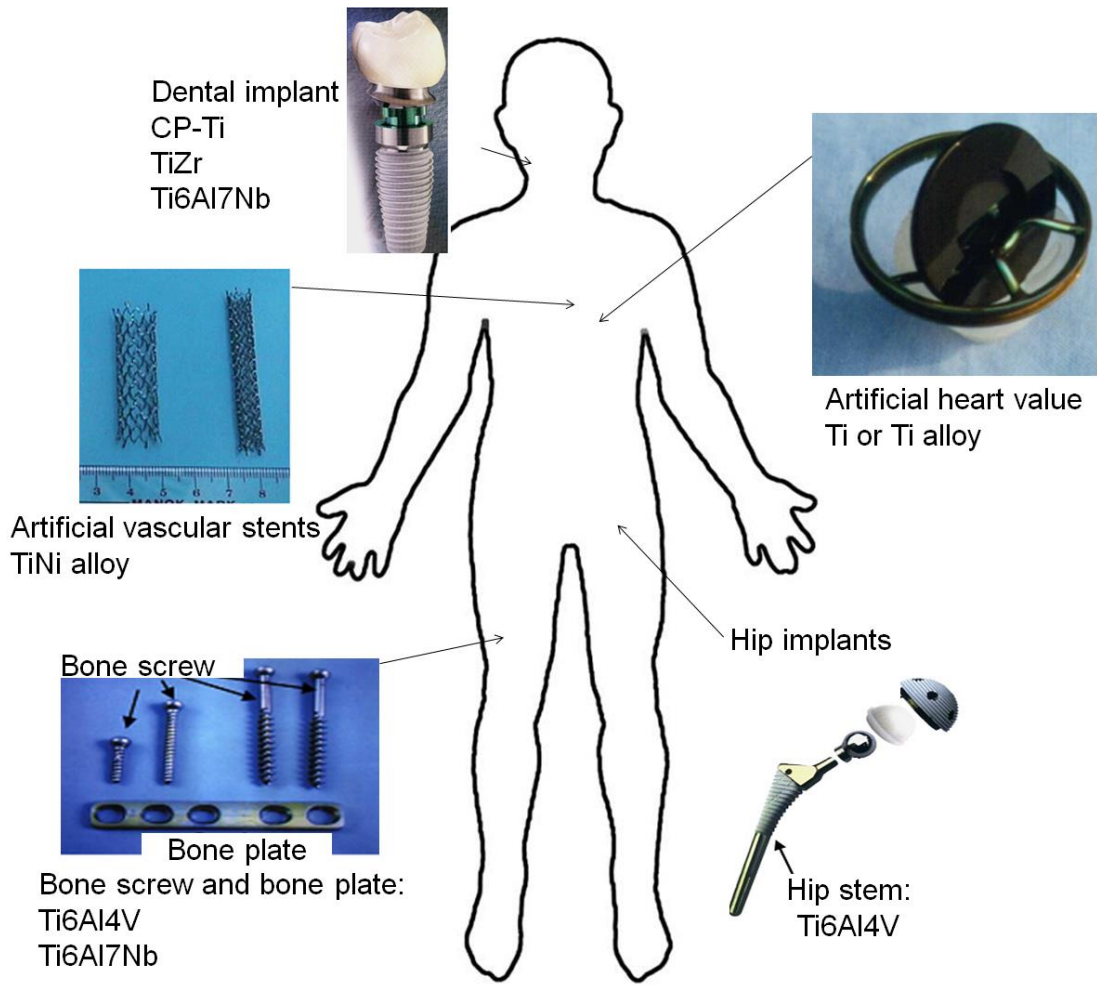
Figure 2-1 Examples of Ti use as biomedical devices-adapted from previous work [1, 31].

2.1.2   CP-Ti and Ti6Al4V

2.1.2.1 Mechanical properties

CP-Ti is classified by ASTM as Grade 1-4, and is mostly used for cranial anchorage devices and dental implants for which relatively low tensile strength is required. Ti6Al4V alloy is classified by ASTM as Grade 5 and is used in orthopaedic components which are subjected to large external loads, because of its high tensile strength of 860 MPa (Table 2-1) [40].

Table 2-1 Mechanical properties of CP-Ti and Ti6Al4V [2, 40].

	Yield Strength (MPa)	Ultimate Tensile Strength (MPa)	Elongation (%)	Elastic Modulus (GPa)
CP-Ti Grade 1	170	240	24	103-107
CP-Ti Grade 2	275	345	20	103-107
CP-Ti Grade 3	380	450	18	103-107
CP-Ti Grade 4	483	550	15	103-107
Ti6Al4V (Grade 5)	795	860	10	117-120
Bone	-	150-400	-	10-40

2.1.2.2 Microstructure

Ti has a high melting point (1668 °C) and has a hexagonal close-packed crystal structure (hcp, α) below the transformation temperature (883 °C). When the temperature is higher than the transformation temperature, the crystal structure of Ti transforms into body centred cubic structure (bcc, β). Both types of the crystal structures are shown in Figure 2-2 [41]. According to the microstructure at room temperature, Ti alloys may be classified into five categories: α, near α, α + β, metastable β and stable β [2]. Accordingly, alloying elements can be classified into (i) α-stabilisers, such as Al, N, (ii) β-stabilisers, such as V or Fe or (iii) neutral, such as Zr.

For example, CP-Ti, which is classified by ASTM as Grades 1-4, is unalloyed Ti with an α-phase structure, while Ti6Al4V, which contains ~4wt% V (a β-stabiliser), is an α+β alloy. Figure 2-3 shows the microstructure of CP-Ti Grade 2 (CP-Ti-G2) with various contents of Fe as impurity [42]. Ti6Al4V has three characteristic microstructures: fully equiaxed, bimodal, and fully lamellar as shown in Figure 2-4. The different microstructures can be obtained through different thermomechanical treatments [43].
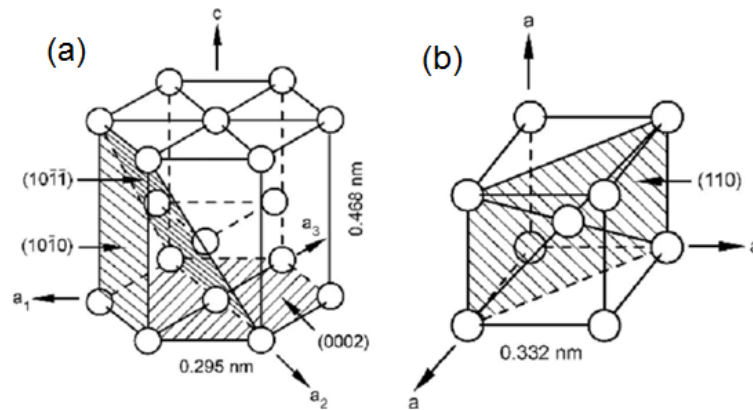
Figure 2-2 Crystal structure of Ti, (a) α phase and (b) β phase [41].
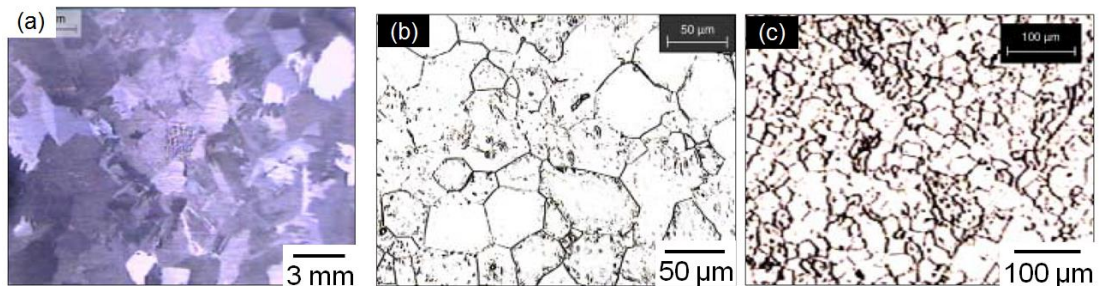
Figure 2-3 Micrographs of CP-Ti Grade 2 (CP-Ti-G2) materials with different contents of Fe: (a) 0.042 wt%; (b) 0.078 wt%; (c) 0.12 wt% [42].
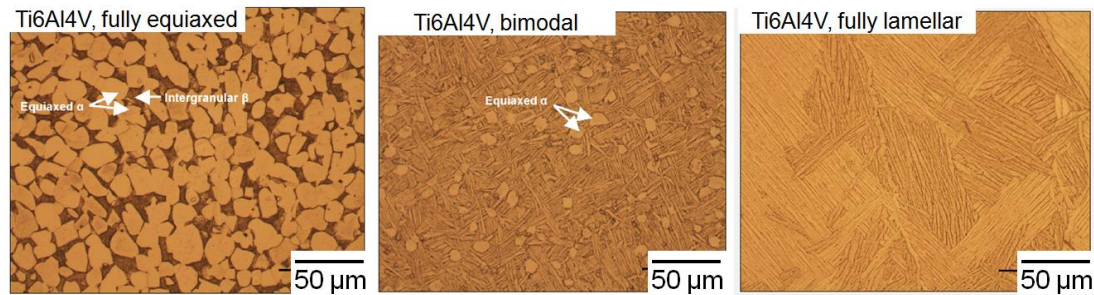
Figure 2-4 Microstructures of Ti6Al4V: fully equiaxed, bimodal, and fully lamellar [43].

2.2 Corrosion of Ti alloys

2.2.1 Ti surface

All Ti alloys, when exposed to air or water, form a tightly adherent passive oxide layer on the surface due to the high reactivity between Ti and oxygen. The oxide layer normally grows to several nanometres thick forming rapidly in a few seconds. The surface oxide film is very stable rendering Ti corrosion resistant and chemically and thermally stable [44]. The oxide film mainly consists of TiO_2, which may be amorphous or crystalline according to the growth conditions [45, 46]. At higher temperatures crystallisation of anodic oxide films occurs (e.g. at 60 °C the oxide film commonly contain anatase) [46]. In terms of the stability of the oxide film, it has been reported that the electrochemical potential may have an influence: the stability of the oxide film decreased and more reactive sites appeared when the applied potential becomes very negative [47].

2.2.2 Electrochemistry of Ti corrosion

Ti is a passive metal that shows active behaviour at low potentials. A schematic polarisation curve is shown in Figure 2-5 [48, 49]. With an increase in the potential, the

8

corrosion/dissolution rate of Ti increases (active region) until a potential of E_{pp} (primary passivation potential) is reached. The current density at this potential is defined as i_{crit} (critical anodic current density), which represents the highest dissolution rate of metal in the figure. When the potential is higher than E_{pp}, a decrease in current density occurs and there is no significant change in current density when the potential is further increased. This current density is nominated as i_{pass} (passive current density). Under some conditions, the value of i_{crit} can be over several orders of magnitude greater than that of i_{pass}.
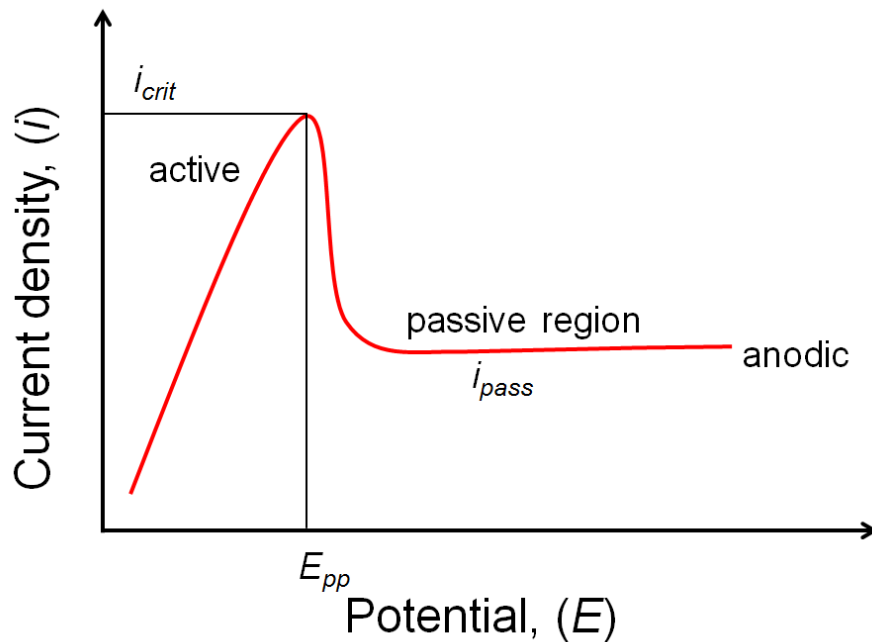
Figure 2-5 Schematic diagram of the anodic polarisation curve of Ti; E_{pp}: primary passivation potential; i_{crit}: critical anodic current density; i_{pass}: passive current density [48, 49].

To determine the corrosion/dissolution rate of Ti, the nature of the environment and the kinetics of cathodic reactions are very important. When the rate of the cathodic reaction is low, the corrosion potential (E_{corr}) is in the active region, and Ti will undergo uniform dissolution (Figure 2-6, cathodic-1) and the corrosion rate increases with the cathodic reaction rate

(Figure 2-6, cathodic-2). When the cathodic reaction rate is very high, E_{corr} is noble to E_{pp}, Ti is passive at the open circuit, and the corrosion rate can be represented by i_{pass} (Figure 2-6, cathodic-3) [48, 50]. This last case is the basis of adding noble metals such as Pd to Ti to protect it from corrosion, and is known as "cathodic modification" [51, 52].
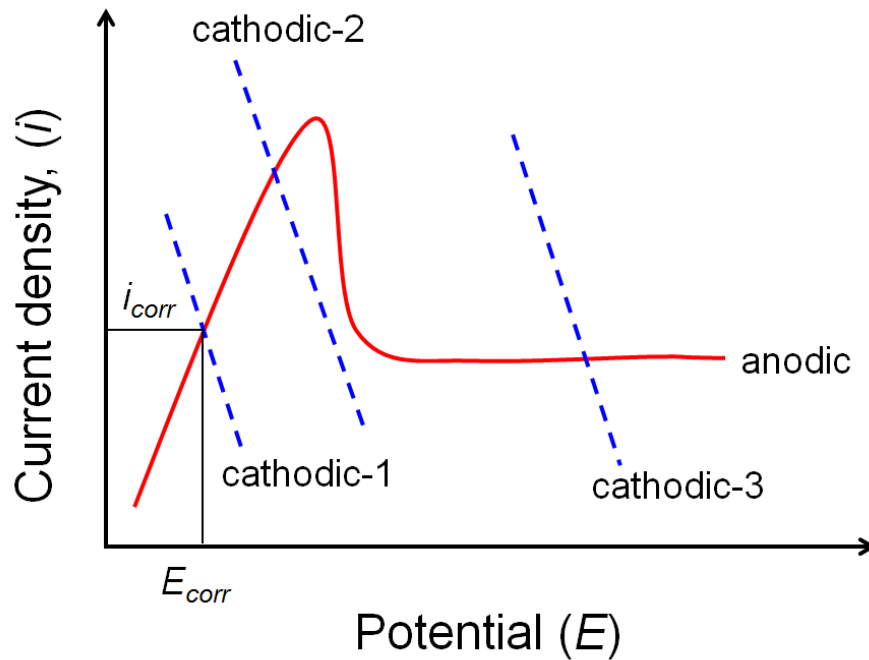
Figure 2-6 Schematic Evans diagram: anodic reaction (red) and three types of cathodic reactions (blue) for low (1), moderate (2), and high (3) cathodic reaction rates [48].

2.2.3   General corrosion of Ti

Ti and its alloys are protected by a spontaneously-formed stable passive surface film which reduces the dissolution of underlying metallic Ti. In addition, in the presence of some oxidising solutions such as chromic acid, Ti can be easily oxidised to form stable TiO_2 [53]. General corrosion of Ti can take place in the presence or absence of passive film, e.g. when Ti is immersed in concentrated reducing acids like HCl [53, 54].

When Ti is in the active region as shown in Figure 2-5 (e.g. immersed in concentrated HCl), homogeneous dissolution of the passive film and the underlying Ti metal can take place. The dissolution of the Ti oxide film has been proposed to occur via direct chemical dissolution or electrochemical dissolution [55, 56]. By direct chemical dissolution, TiO_2 is dissolved to cations (Ti^{4+}) in the form of TiO^{2+} or $Ti(OH)_3^+$ (Equation 2-1) [56]. In terms of the electrochemical pathway, it was proposed by Dyer and Leach [55] that the reduction reaction of Ti^{4+} in TiO_2 and oxidation reaction of Ti substrate can form Ti^{3+} in the form of TiOOH or $TiOOH \cdot H_2O$ at the open circuit (Equation 2-2), followed by chemical dissolution of TiOOH or $TiOOH \cdot H_2O$ to Ti^{3+} (Equation 2-3) [53, 55].

Equation 2-1 $\qquad TiO_2 + H_2O + H^+ \rightarrow Ti(OH)_3^+$

Equation 2-2 $\qquad Ti + 3TiO_2 + 6H_2O \rightarrow 4TiOOH \cdot H_2O$

Equation 2-3 $\qquad TiOOH \cdot H_2O + 3H^+ \rightarrow Ti^{3+} + 3H_2O$
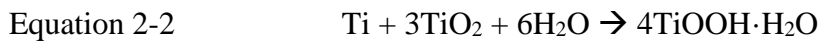
When Ti is in the passive region shown in Figure 2-5 (i.e. E_{corr} is above E_{pp}), the passive film on Ti surface is thermodynamically stable across a wide range of potentials and pH [57]. The solubility of the passive film is dependent upon the solutions and the corrosion rate can be represented by the passive current (i_{pass}) [48, 50].

2.2.4 Pitting corrosion of Ti

When Ti alloys are protected by a passive oxide film they can still become vulnerable to localised corrosion at specific sites on the surface. A common form of localised corrosion is pitting corrosion, in which small cavities are created on the surface, however there are relatively few papers on pitting corrosion of Ti alloys. In early studies the effect of different factors such

as halide type, concentration, and temperature on the pitting corrosion were investigated [58]. It is reported that Ti is highly resistant to pitting corrosion in Cl^- containing solutions [6]. The pitting potential of Ti is very high ~8 V [59, 60] and for a freely corroding Ti electrode this potential is hard to reach, especially in the body where the relevant potential is <1 V [61]. Recently, Burstein et al. [62, 63] reported observations of pit nucleation events but not propagation in Ringer's solution (0.65% NaCl and low concentrations of other salts such as KCl, $NaHCO_3$ and $CaCl_2$) which was proposed to be physiologically representative.

2.2.5 Crevice corrosion of Ti

Crevice corrosion is an important type of localised corrosion for Ti. It occurs where a crevice-former presses against the metal surface as illustrated in Figure 2-7 [64]. The crevice-former serves as a ready-made initiation site. Inside a restricted crevice, dissolved O_2 would be used up quickly. If the environment is neutral or alkaline, O_2 is reduced as described in Equation 2-4 and if under acidic conditions the reaction occurs as described in Equation 2-5. The metal inside the crevice becomes the anode whilst the part outside the crevice is the cathode. Ti ions accumulate in the crevice and undergo a hydrolysis reaction (Equation 2-6, Equation 2-7, and Equation 2-8 [4]). Accordingly more H^+ ions are produced and the crevice becomes more acidic. Because of electro-neutrality, Cl^- ions are drawn into the crevice which makes the solution more aggressive and favours dissolution of Ti metal over repassivation. This aggressive chemistry with a high level of acidity and high chloride concentration is critical for the propagation of localised corrosion.

Equation 2-4 $\qquad\qquad O_2 + 2H_2O + 4e^- \rightarrow 4OH^-$

Equation 2-5 $\qquad\qquad O_2 + 4H^+ + 4e^- \rightarrow 2H_2O$

Equation 2-6 $\qquad$ $Ti \rightarrow Ti^{4+} + 4e^-$

Equation 2-7 $\qquad$ $Ti^{4+} + 2H_2O \rightarrow [Ti(OH)_2]^{2+} + 2H^+$

Equation 2-8 $\qquad$ $Ti^{4+} + 4H_2O \rightarrow Ti(OH)_4 + 4H^+$
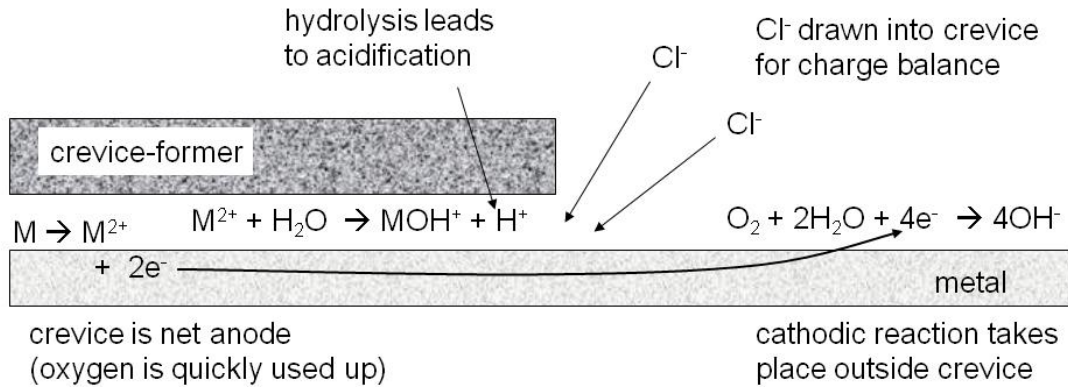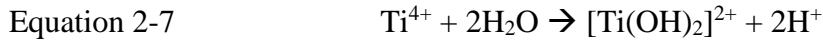
Figure 2-7 Schematic illustration of crevice corrosion in the presence of Cl^- [64].

Many researchers have studied the influence of alloy composition, temperature and surface modification on crevice corrosion of Ti [4, 5, 42]. However it is reported that crevice corrosion on Ti is not likely to occur in static neutral chloride-containing solutions when the temperature is below 65 °C [4], which suggests that crevice corrosion should not occur in the human body (37 °C). Further studies have confirmed that CP-Ti and Ti6Al4V are very resistant to crevice corrosion in physiological saline (0.9% NaCl) or Hank's solution (0.8% NaCl and low concentrations of other salts such as KCl, $NaHCO_3$ and $MgCl_2$) at 37 °C [65, 66].

2.2.6   Mechanically-assisted crevice corrosion (MACC)

Although crevice corrosion of Ti alloys is not predicted to occur in physiological environments, severe corrosion of Ti implants has been observed on devices implanted in the human body

13

(37 °C). The observation of corrosion has been ascribed to mechanically-assisted crevice corrosion (MACC) which was firstly proposed by Gilbert et al. in 1993 [33]. This type of corrosion is sometimes referred to as fretting crevice corrosion or fretting corrosion [34] however this terminology is not always applied appropriately and can cause some confusion within the literature. MACC is dependent on small scale of movement (e.g. micro-motion) between the two relatively large surfaces that geometrically form a (occluded) crevice. During MACC the passive oxide film becomes susceptible to rupture due to this motion leading to a burst of dissolution. Since the motion is on a relatively small scale, the geometry of the crevice and the development of aggressive solution chemistry inside crevice are maintained so that crevice corrosion can propagate -as described in Section 2.2.5. The stability of the passive film is further decreased in this more aggressive environment resulting in active attack of Ti and an increase of corrosion rate.

MACC should be distinguished from another type of corrosion - tribocorrosion (corrosive wear, sometimes also called fretting corrosion) for which the motion is on a large scale (e.g. macro-motion) between the two relatively small surfaces. A gap between the surfaces might be changed depending on different movement modes (e.g. the gap is changed for linear sliding movement, but not for rotating movement, which is against the same metal surface). This motion between the two relatively small surfaces can also destroy the passive film leading to a burst of dissolution. However, the amplitude of motion in tribocorrosion is large enough so that fresh solution can refresh the surface environment quickly (for linear sling movement) or be "pumped" into the gap (for rotating movement) therefore the crevice chemistry cannot be maintained and the metal is able to repassivate quickly.

It should be noted that the reports of simulation of "fretting corrosion" which employ small amplitude movements between two surfaces with relatively small contact areas are not necessarily simulating MACC, because the contact area is of an insufficient size to be able to develop effective crevice chemistry. The crevice between small contact surfaces is readily refreshed by the bulk solution and the aggressive crevice chemistry cannot be maintained.

2.3 Characterisation of Ti corrosion in the body

2.3.1 Introduction

Ti and its alloys are generally corrosion resistant due to the presence of a stable passive oxide film on the surface. However, significantly elevated Ti levels have been detected in humans or animals that have Ti implants [10-12, 67-69]. In addition to the detection of metal ions, Ti particles/debris including Ti metal, TiO_2 as anatase and rutile have been found in analysis of peri-implant tissues and more distant tissues retrieved from patients [14, 15, 70-73]. Corrosion features and/or abrasion scars have also been clearly observed on areas of some Ti implants and their generation has been attributed to MACC [7, 8, 33, 74-78]. The consequences of released Ti corrosion products interacting with the host tissues include adverse biological outcomes such as allergic and inflammatory reactions which can manifest as pain and ultimately failure of the integration of the Ti implant itself [7, 8, 14].

2.3.2 Metal ion release

Many *in vivo* studies have demonstrated Ti ion release or high Ti levels in the serum of patients with Ti implants [67-69]. Elevated Ti levels have also been found in the organs far from the implant sites (e.g. spleen, liver, kidney) in patients implanted with Ti6Al4V hip or knee

prostheses [10] or in animals whose limbs have been implanted with CP-Ti wire [12]. Macroscopic tribological processes leading to the generation of wear debris may account for high concentrations of Ti local to the implant. However, systemically distributed Ti and increased Ti levels in tissues next to implants where there are no obvious wear processes have been observed, which indicate that corrosion of Ti implants does occur *in vivo* [11]. It has also been demonstrated that greater Ti release has been found in patients with peri-implantitis (where inflammation is present) than that in patients without peri-implant disease [71]. This observation is significant as many species and biomolecules generated locally in inflammation potentially have the capacity to influence Ti corrosion.

2.3.3   Detection of Ti particles/debris in human tissues

Ti particles/debris have been detected in peri-implant tissues around different types of implants, e.g. dental implants [15, 71], bone-anchored hearing aids (BAHA) (Figure 2-8) [14] and interfaces of modular hip implants [70, 76]. Both metallic Ti and Ti oxide particles in the form of anatase and rutile have been observed in the retrieved tissues [14, 15]. Various characterisation methods have been used to analyse the peri-implant tissues, including light microscopy [71], X-ray scanning microscopy [15], X-ray fluorescence and X-ray absorption spectroscopy [14]. In many situations Ti has been detected around implants that have not been subjected to obvious macroscopic wear processes and MACC has been proposed to be contributory to the release of Ti debris/particles [14, 33].
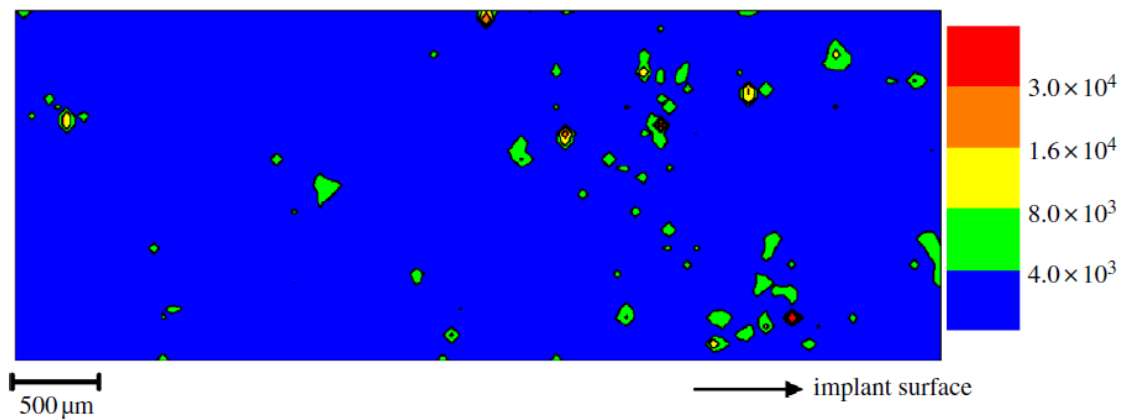
Figure 2-8 An X-ray fluorescence map (5300 μm×2000 μm) of Ti distributed in peri-implant soft tissue taken from around a CP-Ti BAHA fixture which is not subjected to obvious wear [14]. Scale refers to fluorescence intensity in arbitrary units.

2.3.4 Mechanically-assisted crevice corrosion (MACC) of Ti implants

2.3.4.1 Corrosion features of Ti femoral stem of orthopaedic implants

Evidence of corrosion of the intramedullary Ti stem component of total hip replacements has been reported by a number of clinical investigators [7, 8, 79]. In one report it was observed that the normal polished surface of a Ti6Al4V cemented stem became modified after 78 months implantation with the surface covered by thick white layers (Figure 2-9a) [8]. The part of the femoral stem most affected was the distal end which would be at the "base" of the potential crevice formed between bone/cement and the Ti implant. Another case with obvious corrosion features and visible debris on the surface of a cemented Ti hip stem was also reported after 3 years of service (Figure 2-9b). It was identified that although the Ti stem was still well-fixed in bone the patient suffered severe pain. On removal of the Ti implant it was found that the mean pH of the body fluid around the distal tip was as low as 2.5, indicating a highly acidic peri-implant environment had formed (Figure 2-9c) [7].

17
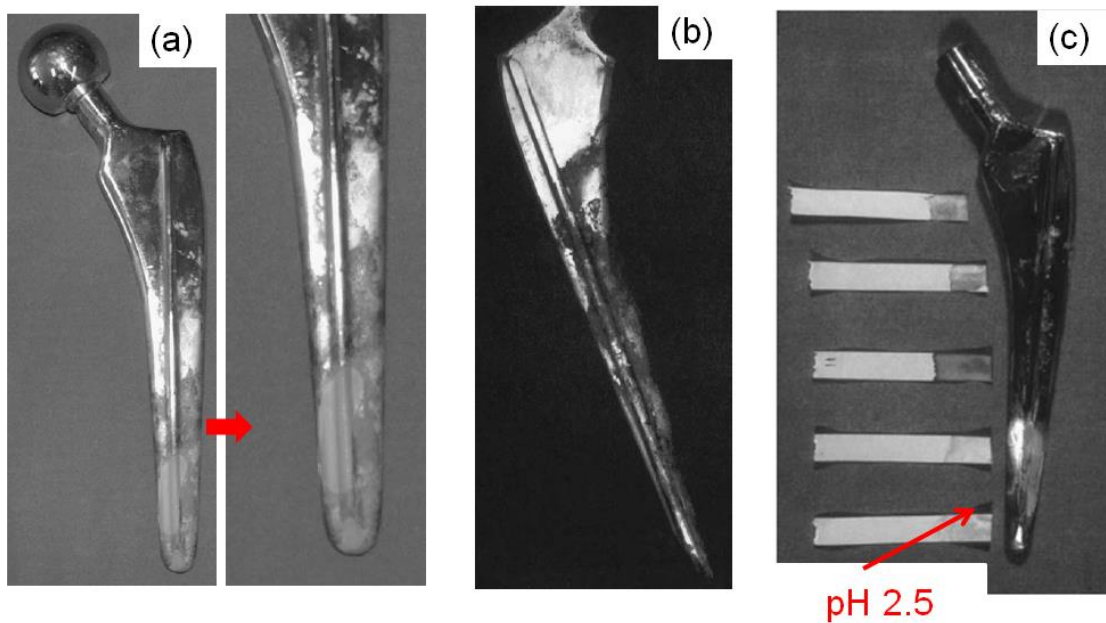
Figure 2-9 Images showing distal corrosion features of retrieved Ti6Al4V femoral stem (a) after mean 78 months implantation [8]; (b) after over 3 years of service [7]; (c) pH 2.5 of body fluid around at the distal end (the red arrow was added to point towards the highly acidic observation) [7].

Ti femoral stems and similar fixation devices such as intramedullary nails are routinely fixed into bone with or without a cement (usually PMMA). During human gait and cyclic stressing, the displacement between bone/bone cement and the femoral stem is on a small scale (<300 μm [80]). MACC is more likely to take place at the distal end of the femoral stem (Figure 2-10) and acidification of the peri-implant fluid environment would result in implant surface degradation. In addition a series of biological responses to both the corrosion products and the local acidification would be initiated, which would ultimately lead to a decreased lifetime of the device itself.
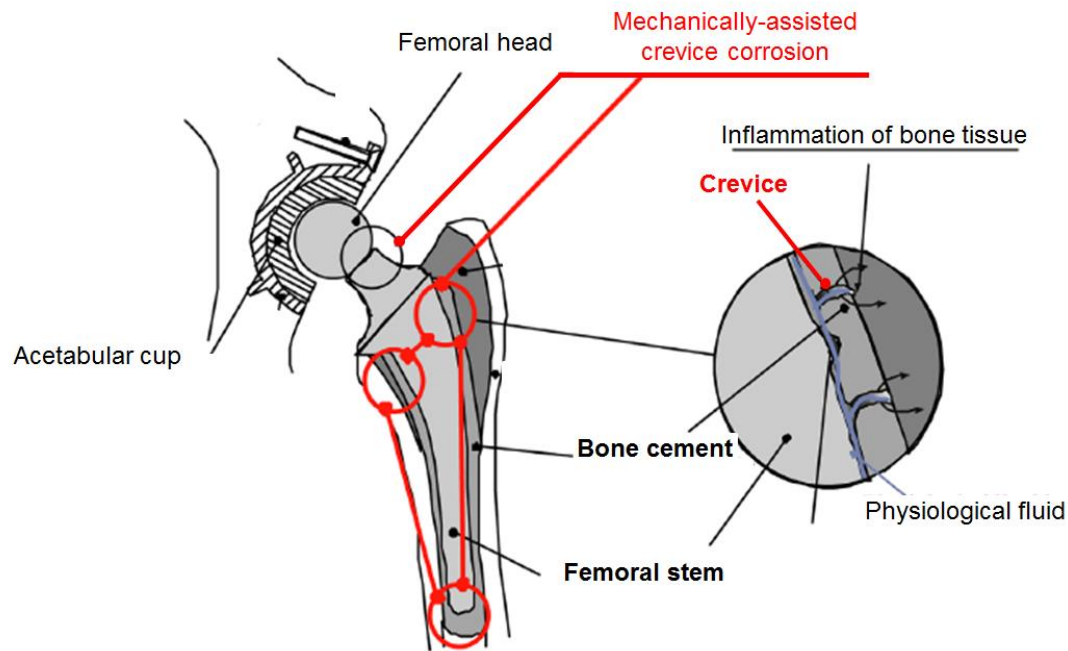
Figure 2-10 Schematic image of the presence of MACC (highlighted in red) at a total hip implant with cement (the image was adapted from [81])

2.3.4.2 Corrosion features of modular tapers

Modular orthopaedic implant systems are widely used as modularisation allows the surgeon intra-operative flexibility to optimise implant fixation and the restoration of function [82, 83]. However, modularisation does introduce interfaces and in total hip arthroplasty systems in particular, "Morse" taper interfaces are commonly used to link the femoral head and stem components together. Severe degradation of these contacting interfaces (e.g. the neck-stem interface) has been widely observed in modular joint prostheses (Figure 2-11) [33, 74-76]. Although the modular tapers have been designed in different ways by different manufacturers (Figure 2-11a-d) [74-76], significant discoloration and severe corrosion attack (e.g. etching, delamination, surface cracking) have often been seen following implantantion and their generation has been attributed to MACC.

19

In addition, fractures of modular tapers have been documented [78, 83]. In the analysis of retrieved fractured components, investigators have proposed that the severely corroded regions of the taper indicate a high concentration of hydrogen which has favoured the formation of titanium hydride, leading to hydrogen embrittlement further leading to fracture [74]. In addtion, it was recently reported that the β phase of Ti6Al4V taper was preferentially attacked, at least initially, followed by the attack on α phase as shown in Figure 2-11f [75].
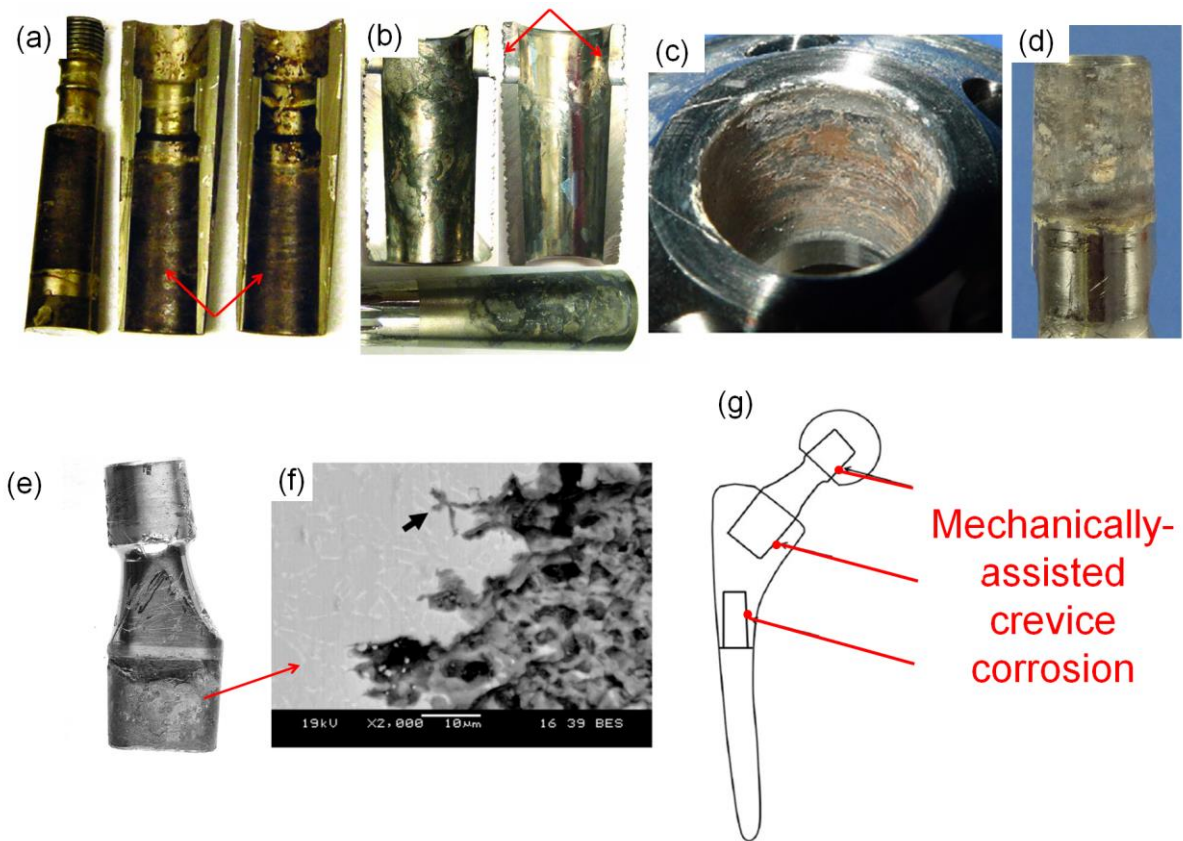
Figure 2-11 Images of severe corrosion features of retrieved taper samples (a) lateral male taper and medial half-sleeve female tapers (Ti6Al4V) after 22 months implantation [74]; (b) proximal female tapers and male taper (Ti6Al4V) after 27 months implantation [74]; (c) female taper adapter (Ti6Al4V) and (d) male Ti6Al4V stem taper after 43 months implantation [76]; (e) Ti6Al4V neck-stem taper after 6 years implantation [75]; (f) backscattered electron image showing the β phase (black arrow) of Ti6Al4V preferentially attacked than the α phase at the interface shown in (e) [75]; (g) schematic image of the presence of MACC at a modular hip implants (the image was adapted from [75], red parts point towards the possible sites of MACC due to the small scale movement of modular taper (<250 μm [78, 83])).

MACC may take place in all Ti devices implanted in human body because of the presence of peri-prosthetic crevices formed between the device and the adjacent tissues (usually bone) when the metal ions cannot escape through tissue. In addition in modular prostheses, including joint replacements, bone fixation systems and dental implants, crevices can form between components in association with micro-motion make these systems particularly susceptible to MACC [14, 33]. For example MACC of dental implants could potentially take place at the interface between the implant and bone, between the implant and a connected abutment (fabricated from a variety of substrates including metal alloys and ceramics) and between the abutment and the superstructure (e.g. crowns) - in all cases driven by low amplitude micro-motion associated with functional loading (chewing).

2.3.5 Effects on human tissues

The biological consequences of released Ti corrosion products are now receiving considerable attention. Clinical observations include bony reactions manifested as hypertrophy (swelling) (Figure 2-12) associated with clearly discoloured neighbouring tissues around the implanted device [7, 8]. Reactive soft tissue lesions correlated with Ti have also been observed in the peri-implant tissue of dental implant [72]. In 2006, the Medicines and Healthcare products Regulatory Agency (MHRA) in conjunction with the Committee on the Safety of Devices (CSD) in reviewing the available literature on the consequences of Ti release reported genotoxicity in patients who were implanted with Ti6Al4V hip replacements amongst a wide range of potential biological outcomes [84].

The deterioration of implanted Ti has been associated with both acute and chronic inflammatory reactions [71, 85] and with modification of adjacent tissue architecture [73, 86]. Importantly in

sites where there is associated peri-implant inflammation there is an inflammatory cell infiltrate (including macrophages and neutrophils) in the zone adjacent to the implants [71, 87]. This is significant as the relationship between tissues and Ti corrosion is interactive. The degradation of Ti implants has a significant impact on human tissue and cells, however the cellular response may also play a role in corrosion of the metallic implant itself (discussed in details in Section 2.4.6).
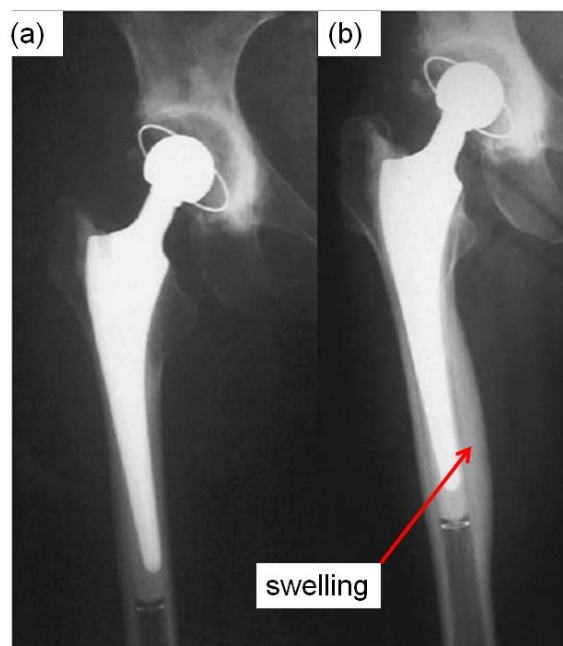
Figure 2-12 Radiographs of Ti total hip replacement (a) after two days' implantation and (b) after two year's implantation, showing a bony hypertrophy (swelling) of femur around distal hip stem [7]

2.4 Corrosion of Ti alloys *in vitro* studies

2.4.1   Introduction

Biomedical implants are exposed to complex physiological environments after implantation, which contain various substances including inorganic species, organic species (e.g. proteins,

organic acids) as well as living eukaryotic cells and/or bacteria. The corrosion behaviour of implanted Ti is well known to be influenced by alloy types [88, 89] and the alloy microstructures [43, 90], but much less is known about the impact of the peri-implant environment.

The presence or absence of different physiological species in simulated physiological environments has been reported to influence corrosion behaviour of Ti alloys, such as pH [89, 91, 92], certain inorganic species (e.g. H_2O_2 or fluoride ions [17, 93, 94]), organic species (e.g. lipopolysaccharide (LPS) [18], serum [95, 96] and proteins such as albumin [25-28, 97]. However, limited work has been carried out relating to the biological effects of prokaryotic cells (bacteria) [29, 98, 99] and human cells [30, 32, 100] on the corrosion of Ti alloys.

2.4.2   Effect of environment acidity on corrosion of Ti alloys

2.4.2.1 Introduction

Physiological fluids are buffered solutions and the pH usually remains around 7. However, in the presence of inflammation around the implants and/or in conditions associated with MACC, the environment can be changed resulting in local acidification. It has also been demonstrated clinically that the pH of the fluid around corroded Ti stem can be as low as 2.5 (Figure 2-9) [7].

In a dental context, acidogenic bacteria are principal components of the biofilm which forms on Ti dental implants. The bacteria can produce acid (e.g. lactic acid), resulting in a local pH change to below 4.5 [29, 91, 93, 101]. The pH of the oral environment may also change from 2 to 11 because of consumed foods or beverages. It is clear that acidic environments can be generated in the body which is a hazard for metallic implants. It is therefore necessary to evaluate the effect of local acidification on Ti implant degradation.

2.4.2.2 Effect of pH on corrosion of Ti alloys

To investigate the effect of pH on Ti corrosion, solution analysis or electrochemical methods have been used. By measuring the concentration of released Ti in the solution, a Ti release rate in the range of 0-0.3 $\mu gcm^{-2}d^{-1}$ has been reported under acidic conditions (lactic acid, acetate acid in combination with chloride) at 37 °C [89, 94]. The concentration of released Ti decreased with increasing pH and was significantly reduced at pH 4 and above [89, 91].

For studies using electrochemical methods, it was found that CP-Ti, Ti6Al4V and Ti13Nb13Zr were spontaneously passivated in acidic artificial saliva (pH 3) [102] or acidic Ringer's solution (pH 5.5) [103]. Increased ion exchange and corrosion rates were reported in acidic environments and no significant difference was found for CP-Ti and Ti6Al4V [102, 103].

2.4.2.3 Effect of HCl on corrosion of Ti alloys

It has been found that both the concentration of acid and the temperature have influence on the stability of the protective oxide film [53, 54, 56, 104]. An abrupt negative shift of the OCP of CP-Ti-G2 (indicating an activation behaviour) was observed in deaerated ≥ 1 M HCl while it did not show any activation behaviour in deaerated 0.1 M HCl at 37 °C (Figure 2-13a) [53]. In addition, the time before activation has been found to vary with temperatures in concentrated HCl (Figure 2-13b) [53]. According to Kelly's observation [104], the condition for a stable active state is pH <2.3 in 1 M Cl⁻ at 30 °C. Blackwood et al. [56] believes that uniform dissolution of oxide film rather than localised attack leads to breakdown of the passive film on the Ti surface. After activation, the dissolution of Ti is in an active steady state (active dissolution) [104].
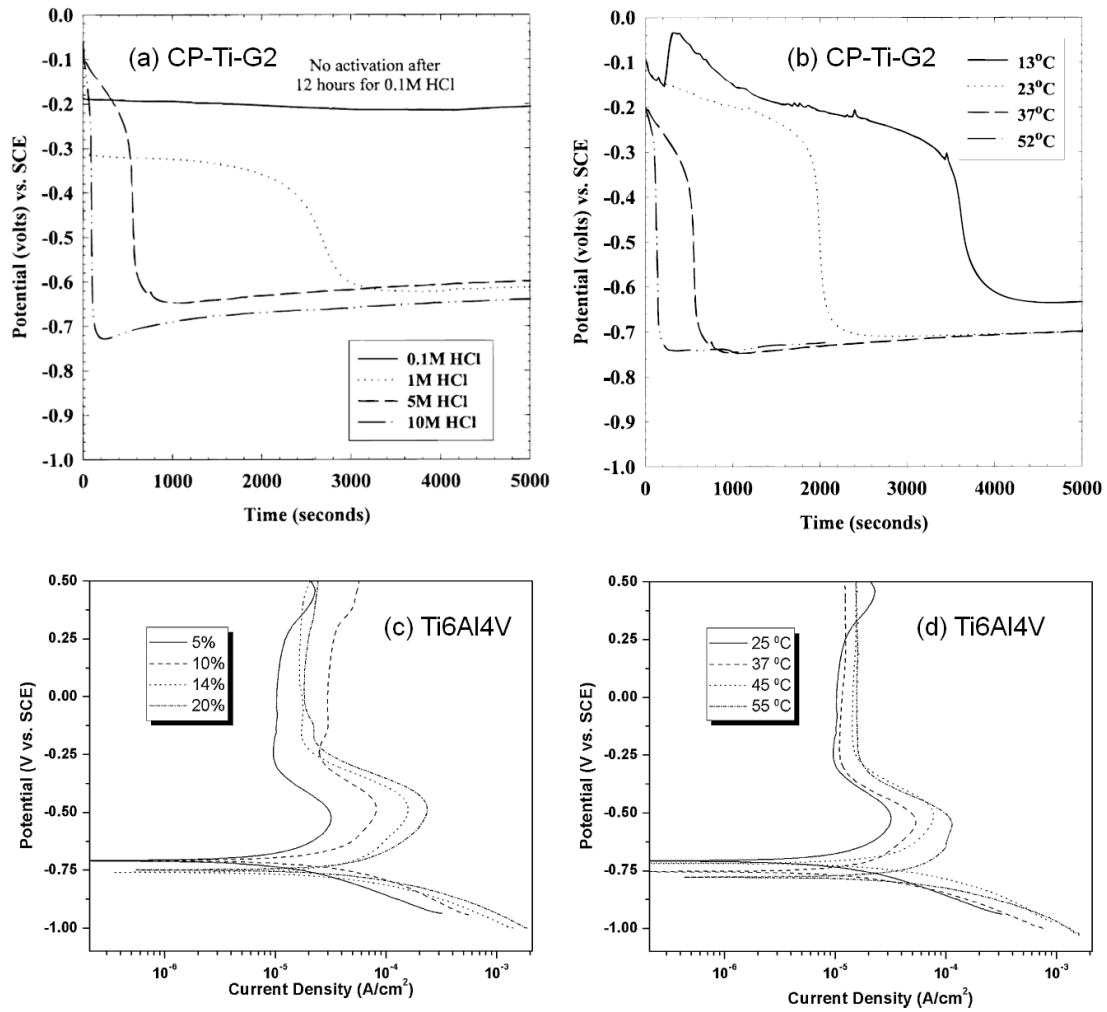
Figure 2-13 (a) OCP of CP-Ti-G2 with an air-formed oxide in various concentrations of deaerated HCl (0.1, 1, 5, 10 M) at 37 °C [53]; (b) OCP of CP-Ti-G2 with an air-formed oxide in deaerated 5 M HCl at various temperatures (15, 23, 37, 52 °C) [53]; (c) anodic polarisation of Ti6Al4V in different concentrations (5, 10, 14, 20%) of HCl at 25 °C [90]; (d) anodic polarisation of Ti6Al4V in 5% HCl at various temperatures (25, 37, 45, 55 °C) [90].

It has also been reported that the concentration of acid and temperature have significant effects on the active-passive transition behaviour of Ti alloys in acidic chloride solutions (Figure 2-13c and Figure 2-13d) [90, 104]. It has been found that Ti6Al4V with different microstructures (i.e. fully equiaxed, bimodal, and fully lamellar) exhibited similar corrosion rates [43]. Specifically, the β phase in Ti6Al4V-ELI (ASTM Ti Grade 23, is similar to Ti6Al4V but contains lower

content of C, N, O and Fe) was preferentially attacked when immersed in 5 M HCl at 37 °C for 50 h (Figure 2-14) [105].
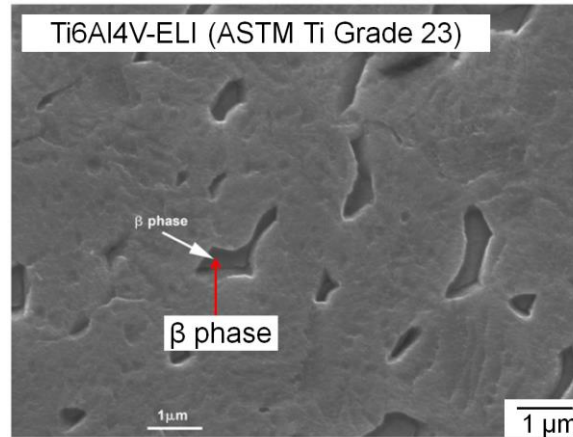
Figure 2-14 Surface morphology of Ti6Al4V-ELI (ASTM Ti Grade 23) after immersing in 5 M HCl at 37 °C for 50 h [105].

2.4.3 Effect of inorganic species on corrosion of Ti alloys

In vitro corrosion investigations of Ti alloys have focused on the effects of fluoride ions (F^-) and hydrogen peroxide (H_2O_2) because fluoride is often present in commercially fluoridated toothpastes and H_2O_2 is regarded as an important product of inflammation [88, 93, 106]. It has been shown that the presence of fluoride ions and H_2O_2 drastically increase Ti release and surface roughness [88, 93, 94]. However, the mechanisms differ: fluoride ions can form complexes with Ti ions and generate soluble species such as TiF_4, leading to further corrosion [93, 107], whilst the interaction between H_2O_2 and Ti is more complicated and the corrosion products formed are still not explicit [17, 106, 108-110].

It is well known that H_2O_2 is a strong oxidiser and Ti/TiO_2 is reported to be able to catalyse the decomposition of H_2O_2 by electron-producing and electron-consuming reactions taking place

simultaneously (Equation 2-9, Equation 2-10 and Equation 2-11) [17, 106]. Tengvall et al. [106] believes that the decomposition of H_2O_2, the oxidation/corrosion of Ti and the formation of Ti-H_2O_2 complex can take place concurrently when Ti is incubated in H_2O_2 solutions. In addition, it has been reported that H_2O_2 acts as both oxidising and reducing agents under certain potentials (Equation 2-9 and Equation 2-10). When a potential is within the green region (below line ① and above line ②) in Figure 2-15, H_2O_2 is doubly unstable and chemically decomposed into H_2O and O_2, which is regarded as an electrochemical catalysis effect [57].

Equation 2-9 $\quad\quad\quad H_2O_2 + 2H^+ + 2e^- = 2H_2O$;

E (V vs. SCE) = 1.54 - 0.059pH + 0.029log[H_2O_2]

Equation 2-10 $\quad\quad\quad H_2O_2 = O_2 + 2H^+ + 2e^-$;

E (V vs. SCE) = 0.44 - 0.059pH + 0.029logp(O_2)/[H_2O_2]

Equation 2-11 $\quad\quad\quad H_2O_2 \rightarrow H_2O + O_2$;
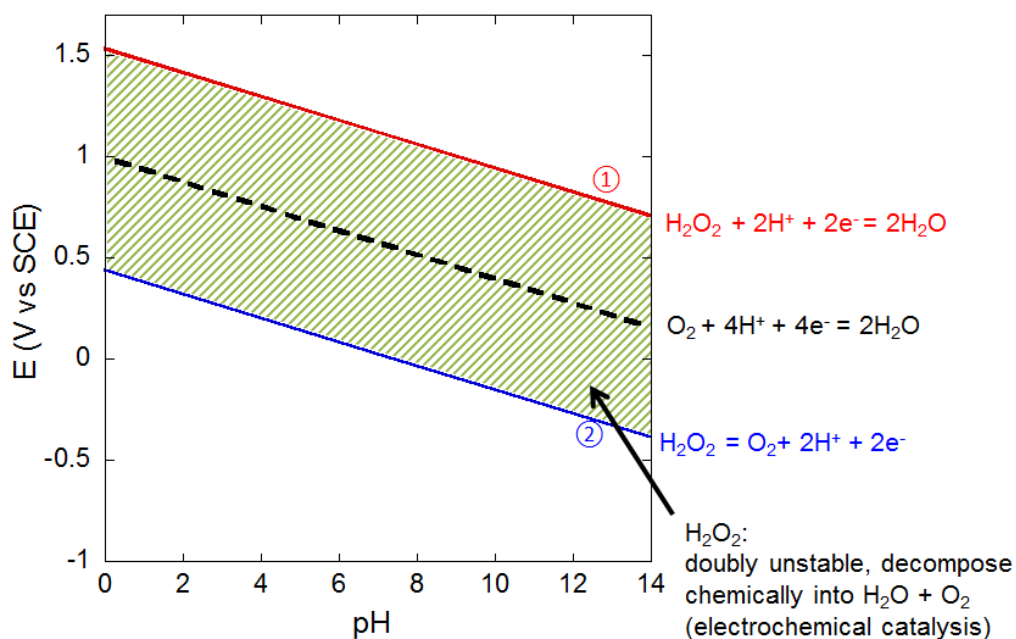
Figure 2-15 E-pH (Pourbaix) diagram for H_2O/H_2O_2 system at room temperature adapted from [57].
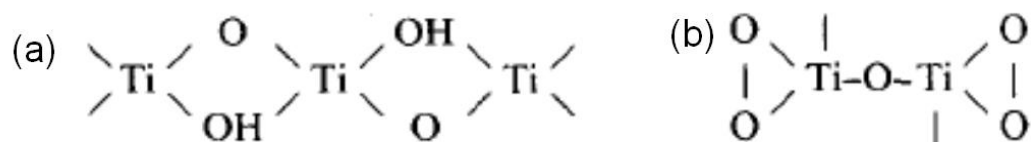
Figure 2-16 (a) and (b) proposed structures of Ti(IV)-H_2O_2 complex [108].

Both the Ti-H_2O_2 complex and different oxides have been reported to form on the Ti surface following immersion in H_2O_2 solutions. The proposed structures of the strongly hydrated Ti(IV)-H_2O_2 complex, (i.e. TiOOH(H_2O)$_n$) are shown in Figure 2-16 [108]. Mohanchandra et al. [109] confirmed the presence of TiO on a Ni-Ti surface when treated with 30% H_2O_2. In contrast, Pan et al. [17] found that the composition of the oxide film on CP-Ti surface after being immersed in H_2O_2 solutions was mainly TiO_2 without any trace TiO or Ti_2O_3.

Whilst Assis and Costa [110] reported that Ti_2O_3 and TiO_2 were detected on the surface of Ti13Nb13Zr after 125 days immersion in Hank's solution in the presence of H_2O_2.

Studies of the surface morphologies of Ti alloys after being immersed in H_2O_2 solution have shown both surface roughening [111, 112] and unchanged surface morphology [88]. In terms of Ti6Al4V, Noguchi et al. [88] reported discoloration of Ti6Al4V but no change of surface morphology was observed when immersed in H_2O_2. However, Gilbert et al. [113, 114] reported selective dissolution of the β phase of Ti6Al4V after electrochemical treatment in H_2O_2 solutions (Figure 2-17). Besides, a clear porous structure of corrosion product on CP-Ti surface was observed by SEM after immersion in H_2O_2 [111, 112]. It has also been found that the surface roughness of CP-Ti became increased by AFM after immersion in the presence of H_2O_2 [93].
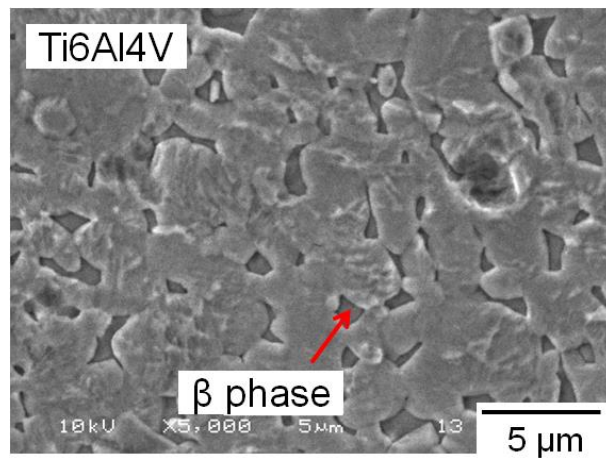
Figure 2-17 Selective dissolution of the β phase of Ti6Al4V after electrochemical treatment with H_2O_2 [113, 114]. (The red arrow was added to point towards the β phase).

2.4.4   Effect of organic species on corrosion of Ti alloys

2.4.4.1 Introduction

It has not yet been fully defined whether the organic species (e.g. serum, albumin, collagen and fibrinogen) relevant to the peri-implant environment accelerate or inhibit the corrosion rate of metallic materials. It is however well known that many organic molecules strongly adsorb on implant surfaces (including Ti) and therefore their potential role in modifying corrosion resistance is clinically relevant but both a decrease [19, 27, 95, 115] and increase [25, 116-119] in corrosion resistance have been reported.

Following implantation, Ti implants are exposed to blood and to tissue fluids where the most abundant protein is albumin (~0.6 mM) and studies of the impact of albumin on Ti corrosion have been reported [20, 24, 26, 27]. However, very little attention has been paid on the corrosion behaviour of Ti alloys in more realistic combined conditions such as albumin and the inflammatory product H_2O_2.

Recently, another important biomolecule, lipopolysaccharide (LPS), has received much attention because of its abundance and its crucial role as a mediator of peri-implant inflammation [18, 120, 121]. Therefore the effects of LPS on the corrosion behaviour of Ti implant are of interest to the recent studies.

2.4.4.2 Effect of albumin on corrosion of Ti alloys

It is understood that a layer of proteins (e.g. albumin) can quickly form on the surface of an implant following implantation (e.g. Ti [24] and stainless steel [19]). However, the effect of albumin on the corrosion rate of Ti and other biomedical alloys is still controversial [19, 26, 28,

122, 123]. The presence of albumin can lead to the decreased corrosion rate of CP-Ti [116], Ti6Al4V [25, 117], stainless steel and CoCrMo [26, 28], the increased corrosion rate of Ti6Al4V [27], stainless steel [19, 115] and CoCrMo [124, 125] and no change on corrosion resistance of CP-Ti [20, 126], Ti6Al4V [122, 123]. It is however agreed that the addition of albumin decreases the cathodic current of Ti alloys indicating that albumin serves as a cathodic inhibitor [20, 116, 122].

In addition, the concentration of albumin has been shown to influence the corrosion behaviour of metallic implants (e.g. Ti6Al4V [28], CoCrMo [127] and Nb [22]). Karimi et al. [26, 28] reported that the presence of albumin decreased the stability of the passive film on the surface of Ti6Al4V in the concentration range of 0.02-0.2% in phosphate buffered saline (PBS, 0.8% NaCl and low concentration of other salts such as KCl, KH_2PO_4 and Na_2HPO_4), whilst it enhanced the stability at the concentration of 0.4%. However, Huang and Lee [123] reported that the presence of albumin in the range of 0.01-0.5% had no influence on the corrosion resistance of Ti6Al4V in artificial saliva. These conflicting results demonstrate that the influence of albumin on Ti alloys is still in debate.

2.4.4.3 Combination effect of albumin and H_2O_2

There have been extensive investigations into the influence of organic species (e.g. albumin in Section 2.4.4.2) or inorganic species (F^-, H_2O_2 in Section 2.4.3) on the corrosion behaviour of Ti alloys, but much fewer studies have reported the influence of the combination of multiple species.

It has been reported that the addition of albumin in F^--containing solutions significantly increased corrosion resistance and decreased i_{corr} and i_{pass}, which protected Ti6Al4V from

31

attack of F[-] [118, 123]. A similar protecting effect of albumin on CP-Ti and TiZr alloys was also reported [128].

In terms of albumin and H_2O_2, it has been observed that increased adsorption of albumin occurred on a H_2O_2 treated Ti surface [129, 130]. However, to our knowledge, the combination effect of H_2O_2 and albumin on the corrosion of Ti alloys has not yet been reported. Padilla and Bronson [25] mentioned the possible effect of H_2O_2 and albumin since H_2O_2 was regarded as an intermediate species in oxygen reduction, however, there was no direct investigation on the synergistic effect of the two species.

2.4.4.4 Effect of LPS on corrosion of Ti alloys

Significant levels of adherent LPS have been found to be present on Ti implant surfaces [131] and as LPS is a constituent of the cell wall of Gram-negative bacteria, any implant with a biofilm is likely to be associated with elevated LPS in the immediate environment. However, the influence of LPS on Ti corrosion behaviour has received little attention and the findings that have been reported to date are inconclusive [18]. By using electrochemical impedance spectroscopy (EIS) and cyclic polarisation methods, it has been reported that the corrosion of CP-Ti-G2 was increased in LPS-containing solution [18]. However, in the reported EIS results, the polarisation resistance (R_p) of Ti in the presence of LPS was increased when compared with that in the absence of LPS, indicating a lower corrosion rate [132]. Therefore the results appear to be inconsistent. The influence of LPS on the corrosion behaviour of Ti alloys needs to be clarified.

2.4.5   Effect of prokaryotic cells (bacteria) on corrosion of Ti alloys

Biomedical implanted devices that penetrate skin or the oral mucosa will be associated with surface biofilms [133, 134]. The bacteria in the oral environment readily accumulate on teeth and adhere onto Ti dental implants, resulting in the formation of highly complex biofilms often described as "plaque" [135]. The presence of a surface biofilm may in certain cases induce peri-implant infection and/or lead to a peri-implant inflammatory response. This can take place early and/or late following the implantation process [136].

For dental implants, there are two common types of surface finishes. One is a highly polished surface and the other is rough surface usually obtained by a sandblasted (large grit)-acid-etched (SLA) surface treatment. The highly polished surface is used as the top part of the dental implant to inhibit the adhesion of bacteria. However, the surface of the bottom part is generally roughened SLA surface in order to promote osseointegration after bony implantation [137-139]. Most studies on cellular interactions with Ti implant surfaces have focused on either the effect on osseointegration and/or bacteria adhesion [135, 137-139] with much less attention paid to the biological effects of bacteria on corrosion properties of Ti dental implant [93, 140].

It has been recently reported that Ti is susceptible to corrosion in the presence of *Actinomyces naeslundii* [98] or *Streptococcus mutans* (*S. mutans*) [29, 141] by comparing the corrosion resistance before and after exposure to the bacterial culture. In addition to comparing corrosion resistance, *Streptococcus sanguinis* (*S. sanguinis*) and *Lactobacillus salivarius* were reported to induce deterioration of the mechanical properties of the Ti implant [99] and the presence of *Streptococcus mitis* (*S. mitis*) was found to lead to increased surface roughness of CP-Ti [93].

Human oral flora is polymicrobial. *Actinomyces naeslundii* is able to co-aggregate with oral streptococci (including *S. mitis*, *S. sanguinis*, and *S. mutans*), which were encountered in dental plaque, caries or related to periodontal diseases [98, 142]. The influence of *S. sanguinis* may be a particular interest. *S. sanguinis* is a Gram-positive bacterium and usually serves as an early coloniser which facilitates adhesion of later species onto the surface of the biomaterial during formation of dental plaque [142]. It has been shown that *S. sanguinis* is both acidogenic and when cultured in aerobic environment it produces millimolar levels of H_2O_2 [143-145], which may lead to degradation of the Ti implant.

2.4.6   Effect of human cells (leukocytes) on corrosion of Ti alloys

Studies on a variety of cell types found in the peri-implant environment (fibroblasts, osteoclasts and macrophages) have demonstrated that cellular interactions with surfaces can cause changes in corrosion properties of certain metallic implants including CP-Ti [30, 146-148], Ti6Al4V [100, 149], stainless steel [147, 150] and CoCrMo [151].

It has been demonstrated that the pH values around the surfaces of CP-Ti decreased in the presence of fibroblasts, which play an important role in wound healing process [146, 147]. It has also been reported that the human osteoclast (bone resorption cells) could take up Ti ions when cultured on Ti foil [148]. As shown in Figure 2-18, the presence of cells on an implant surface is believed to retard diffusion of dissolved oxygen and ions and suppress the cathodic reaction. Meanwhile, metal ions can be accumulated and hydrolysed at the interface, resulting in a very localised pH reduction and destabilisation of the surface passive film [31].
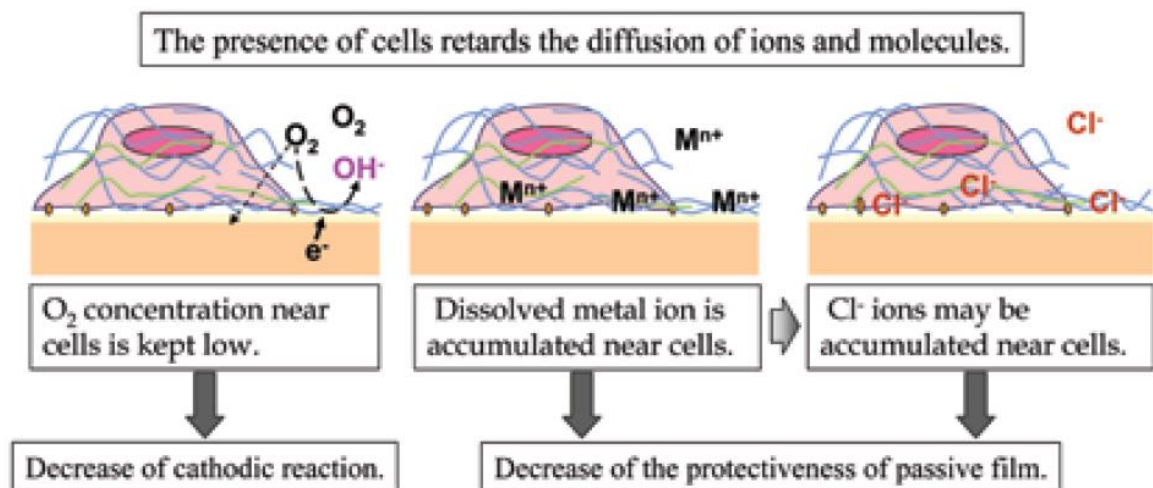
Figure 2-18 Influence of the presence of adhered cells on the corrosion of metallic biomaterials [31].

Studies into the cellular effects on Ti corrosion often produce conflicting findings. It has been reported that Ti release from CP-Ti surfaces was accelerated in the presence of rat macrophages (an innate immune cell) [30], however other investigators have reported that the stability of the oxide layer on Ti6Al4V surface was enhanced and the corrosion rate was reduced in the presence of the mouse macrophage cell line [100, 149].

In vivo, following implantation or during inflammation both polymorphous nuclear leukocytes (neutrophils) and macrophages migrate into the peri-implant environment. Although there has been considerable focus on macrophages, it is neutrophils that are the first to arrive and in larger numbers (54-65%) than macrophages [152]. Neutrophils are short lived (2-4 days) and are formed from stem cells in the bone marrow and migrate from the circulation to the site of injury or infection led by the release of signalling molecules at the damaged site. Neutrophils play a critical role in dental peri-implant inflammation and have a number of microbiocidal killing mechanisms [153, 154]. Importantly neutrophils can generate reactive oxygen species (ROS),

including superoxide (O_2^-), hypochlorous acid (HOCl), H_2O_2 and chloramines [153, 155, 156], which may be implicated in the degradation of the Ti implant. To date, most studies have focused on the effect of corrosion products like TiO_2 on the function and morphology of neutrophils [152, 157, 158], but there has been little attention paid on the role of these cells playing in the initial generation of these products.

2.4.7 *In vitro* studies on mechanically-assisted crevice corrosion (MACC)

2.4.7.1 Introduction

Mechanical disruption of passive films on Ti alloys can influence corrosion process and lead to degradation of implants *in vivo*. Due to the inferior wear resistance, Ti alloys are normally not used for the articulating surfaces of the femoral head/acetabular cup [159]. In a very few cases Ti6Al4V has been used in the acetabular cup to support a polymer liner [160]. Ti alloys are more widely used for hip stems and the modular tapers, which are susceptible to MACC. However, most laboratory investigations have focused on tribocorrosion [36, 121, 161, 162] or "fretting corrosion" with small scale movement [34, 35, 82] whilst very few studies have focused on MACC [37, 38].

2.4.7.2 Experimental methods: apparatus

Devices with ball-on-disc, disc-on-block (or ball-on-pin), and pin-on-disc geometries are commonly used to study tribocorrosion or "fretting corrosion" of the bearing interfaces between Ti alloys and the counterbodies. The most commonly used counterbodies are Al_2O_3 spheres with different diameters, however, some investigators have employed 30CrNiMo8 steel [163],

Ti6Al4V [34], or CoCrMo [34] counterbodies against Ti alloys. Table 2-2 contains a summary

about previously reported testing apparatus.

Table 2-2 Summary of apparatus used for tribocorrosion, "fretting corrosion" and MACC. The contact area diameter was calculated by Hertzian contact stress calculator [164] except that *shows the contact area and **shows the diameter of pin part.

Type	Reference	Geometry	Contact area diameter	Movement mode	Amplitude of vibration
Tribo-corrosion Type 1 (Figure 2-19a)	Komotori [165]	ball-on-disc	fresh contact ~0.02 mm	reciprocating linear	10 mm
	Dimah [166]	ball-on-disc	fresh contact ~0.1 mm	circumferential sliding	19 mm
	Runa [36]	ball-on-disc	fresh contact ~0.07 mm	N/A	2 mm
	Licausi [162]	ball-on-disc	fresh contact ~0.1 mm	circumferential sliding	-
Tribo-corrosion Type 2 (Figure 2-19b)	Mathew [121, 161]	ball-on-pin	same contact ~0.27 mm	rotation (28 mm diameter)	-
	Cvijovic-Alagic [163]	disc-on-block	same contact ~0.37 mm	rotation (35 mm diameter)	-
	Lomholt [160]	disc-on-block	N/A	rotation	N/A
Abrasion (Figure 2-20)	Contu [167]	tube-on-disc	same contact ~0.2*	rotation	0
"Fretting corrosion" (Figure 2-21)	Barril [35, 168, 169]	ball-on-disc	~150 μm	reciprocating linear	180 μm
	Hiromoto [122]	ball-on-disc	~230 μm	reciprocating linear	100 μm
	Baxmann [82]	ball-on-disc	~650 μm	reciprocating linear	10-50 μm
	Vieira [170]	ball-on-disc	~90 μm	reciprocating linear	200 μm
	Swaminathan and Gilbert [34, 171]	pin-on-disc	350-800 μm**	reciprocating linear	50 μm
MACC (Figure 2-22)	Goldberg and Gilbert [37, 38]	assembling manufactured modular taper	~400 mm^2*	cyclic loading (Figure 2-22)	<250 μm [78, 83]

Figure 2-19 shows two types of tribocorrosion tests. The device can be a commercialised tribometer or similar apparatus with adjustment. The geometry in tribocorrosion type 1 (Figure 2-19a) is normally ball-on-disc and the contact area is relatively small (Table 2-2). Importantly, the contact area is always fresh due to linear sliding or circumferential sliding movement. Crevice geometry and crevice chemistry that would be observed during MACC cannot be developed.

The geometries with ball-on-pin or disc-on-block are more commonly used in tribocorrosion type 2 setups (Figure 2-19b). A ball or disc with a relatively large diameter is rotated against the metal (pin or block) surface. The abrasion area on the metal surface is always located in the same region (Table 2-2). However, the solution in the environment of the abrasion area is readily refreshed by the bulk solution during this motion and the metal substrate tends to repassivate quickly.
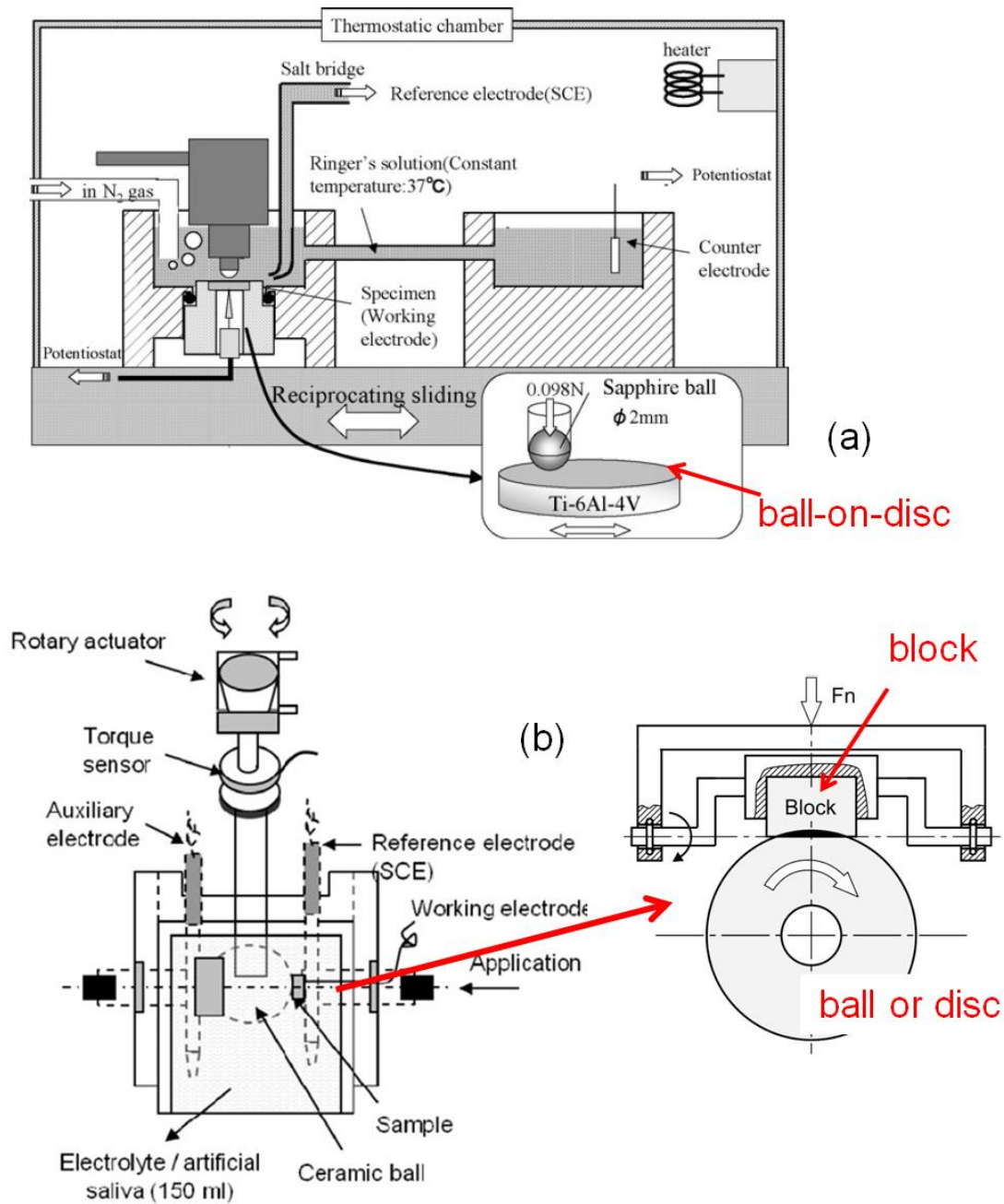
Figure 2-19 (a) An example of tribocorrosion using similar commercialized tribometer with ball-on-disc geometry and with 10 mm linear sliding replacement [165]; (b) an apparatus with ball-on-pin [121] (or disc-on-block [163]) geometry with rotating ball (or disc) on metallic pin (or block). The geometry was highlighted in red.

Figure 2-20 shows an apparatus with a small diameter rotating Al_2O_3 tube (inner diameter 0.24 mm and outer diameter 0.52 mm) on a metallic disc [167]. During rotation, there was no abrasion area (~0.2 mm^2) contacting with the bulk solution. However, as long as the mechanical stress stopped, the metal substrate was repassivated and the crevice cannot be maintained.
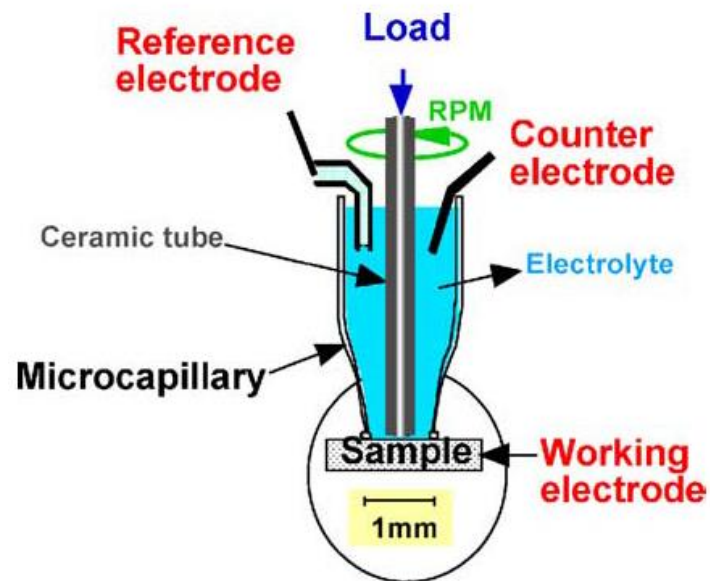
Figure 2-20 Abrasion setup with alumina tube on Ti surface with rotating periodical movement [167].

The "fretting corrosion" apparatus normally has a ball/pin-on-disc geometry and a horizontal periodical micro-motion (<200 µm) [34, 35, 82, 170]. Figure 2-21 shows two examples of devices with linear displacement generated by moving an Al_2O_3 ball or Ti6Al4V pad (with a spherical head at the tip) against the Ti6Al4V surface [35, 82]. During the "fretting corrosion" process the majority of the small contact area (Table 2-2) is readily flushed by bulk solution (Table 2-2). The geometry of crevice and the development of an aggressive solution chemistry inside crevice cannot be maintained. Although Swaminathan and Gilbert [34] reported the possibility of crevice corrosion in their designed "fretting corrosion" apparatus, there was no direct evidence except for a slight increase in recovery time after long time fretting under high loads.
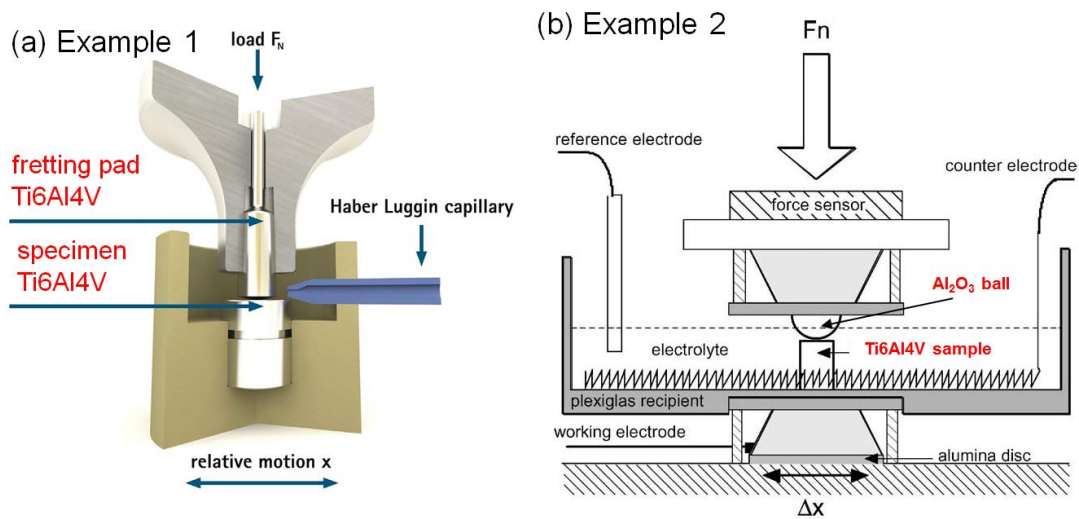
Figure 2-21 "Fretting corrosion" devices with ball-on-disc geometry and small amplitude of motion (<200 µm) between the two bearing surfaces [35]. Fretting pad in (a) consisted of a spherical head at the tip (radius of 16 mm) [82].

Figure 2-22 shows an apparatus using typical manufactured implants to investigate MACC of head-neck taper by Goldberg and Gilbert [37, 38]. It has been found that the OCP became decreased and current became increased during long-term cyclic loading. In addition, the pH in the gap between head and neck was also decreased by 0-3 units [37]. It was also observed that the magnitudes of OCP change and current change were smaller after long-term cyclic loading when compared with the change prior to the long-term cyclic loading [38]. It can be concluded that currently there is no specific laboratory apparatus focusing on simulating MACC.
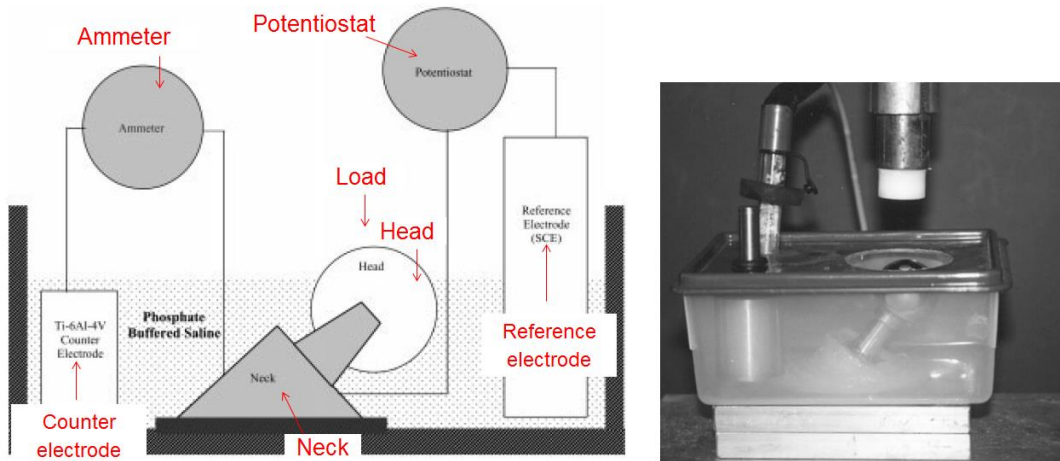
Figure 2-22 Schematic diagram of fretting crevice corrosion of head-neck taper by Goldberg and Gilbert [38].

2.4.7.3 Effect of mechanical parameters

It has been reported that mechanical factors including load, amplitude of movement and frequency/speed influence tribocorrosion or "fretting corrosion" of Ti alloys. It has been observed that stick, slip or partial slip fretting regimes can be achieved by applying different loads and different amplitudes of movement in the "fretting corrosion" apparatus [34, 168]. Decreased OCP or increased anodic current (potentiostatic measurement) during the abrasion

process in tribocorrosion or "fretting corrosion" have been observed, due to the mechanical rupture of passive film and exposure of the bare metal to the surrounding solution [162, 170].

In addition, the OCP under the abrasion condition was reported to decrease with increasing loads [38, 167] or abrasion speed [165], while the abrasion current increased with increasing load [122] or abrasion frequency [165, 169, 171], probably because of more effective rupture of the passive film. However, Swaminathan and Gilbert [34] found that the abrasion current was increased first and then decreased with increasing load during their "fretting corrosion" experiments. They explained that sticking condition might appear under much higher loads, which resulted in less effective displacement between two contacting surfaces. Therefore, different phenomenon may be observed by using different apparatus.

2.4.7.4 Effect of chemical species

An increase, a decrease and no change of albumin on abrasion current of Ti alloys have been reported, possibly due to the different experimental conditions (e.g. type of apparatus or applied potential) [36, 122, 166]. For example, during "fretting corrosion", it has been reported that the abrasion current of Ti6Al4V did not significantly change in the solution with or without albumin [122]. However, it was also observed that during tribocorrosion the presence of albumin slightly decreased the abrasion current of Ti6Al4V at a low potential but it increased the abrasion current at a high potential [36]. In addition, it has been reported that the presence of albumin decreased the wear accelerated corrosion of Ti6Al4V-ELI during tribocorrosion [166].

Very little attention has been paid to the effect of LPS and H_2O_2 on the tribocorrosion or "fretting corrosion" of Ti alloys. One paper reported that the presence of LPS induced higher

43

weight loss of CP-Ti and Ti6Al4V after tribocorrosion test [121]. The presence of H_2O_2 was reported to increase weight loss and Ti release from a manual assembly containing a Ti6Al4V plate and Ti6Al4V screw [172].

In summary, the effects of albumin, LPS and H_2O_2 on tribocorrosion or "fretting corrosion" behaviour of Ti alloys still not fully understood, and further investigations are necessary. To our knowledge, there is no report about their effect on MACC of Ti alloys.

2.5 Summary and aims

The aim of this project is to investigate how the simulated physiological environment including chemical species (pH, LPS, H_2O_2 and albumin), biological cells (bacteria and neutrophils) and MACC can influence the corrosion properties of Ti alloys.

The presence of bacteria has been observed in the peri-implant environment and can induce peri-implant infection and inflammation. An important Gram-negative bacterial product, LPS, has also been found to adhere to Ti surfaces and also serves as an important mediator of peri-implant inflammation. However, the effects of bacteria and bacterial products on the corrosion resistance of Ti are poorly understood. In addition, the role of the neutrophils the most abundant immune cells during the peri-implant inflammation on corrosion behaviour of Ti alloys has not been considered previously. The aim of this part of the study is to determine the effects of bacteria bacterial products and neutrophils on Ti corrosion.

The effect of albumin on the corrosion of biomedical implant alloys is still debated and the effect of H_2O_2 on Ti corrosion has also been the subject of considerable attention. However, the combination of albumin and H_2O_2 has not been considered although this is a better approximation of the peri-implant environment under inflammatory conditions. The aim of this

part of the study is to determine the combined effect of albumin and H_2O_2 on corrosion behaviour of Ti alloys.

MACC has been previously been reported as a key degradation mechanism of Ti implants, but relatively little investigation has focused on electrochemical aspects of MACC of Ti alloys under realistic conditions where an aggressive solution develops in the crevice between the two components. The aim was to develop and fabricate a MACC simulation apparatus to investigate the effect of the chemical species (albumin, LPS, and H_2O_2) on MACC of Ti alloys.

3   MATERIALS AND METHODS

3.1 Ti sample preparation

3.1.1   Mirror-polished surface

Commercial purity ASTM Grade 2 Ti (lower Fe content, CP-Ti-G2), commercial purity ASTM Grade 4 Ti (higher Fe content, CP-Ti-G4) and ASTM Grade 5 Ti (Ti6Al4V) were commercially sourced (Titanium Products Ltd, Solihull, UK) and the compositional analysis was acquired (Table 3-1). Nominally identical disc-shaped specimens of CP-Ti-G2 and CP-Ti-G4 (14 mm diameter and 1 mm thickness) were machined by the supplier (Titanium Products Ltd, Solihull, UK). The surfaces were subsequently ground to a consistent finish using sequential grades of SiC abrasive paper from P400, through P800, P1200, P2400 to P4000 grit with deionised water as a lubricant. Ti6Al4V disc-shaped specimens (14 mm diameter and 1.2 mm thickness) were prepared using abrasive cloths MD-Piano (Struers, Rotherham, UK) with deionised water as a lubricant, followed by MD-Largo with a 9 μm diamond suspension as a lubricant. Finally all three grades of Ti were polished with a MD-Chem polishing cloth (Struers, Rotherham, UK) using 0.04 μm OP-S Colloidal Silica suspension (Struers, Rotherham, UK) to produce a mirror finish on both sides. All samples were thoroughly cleaned in acetone, ethanol, and deionised water sequentially using ultrasonic agitation for 10 min at each stage. Specimens were finally dried in an air stream before further experiments.

Table 3-1 The composition of CP-Ti-G2, CP-Ti-G4 (Manufactures compositional certificate, wt%) and Ti6Al4V (ASTM standard F1108-97A, wt%).

Substrate	N	C	H	Fe	O	Residual	Al	V	Ti
CP-Ti-G2	<0.01	0.01	0.002	0.03	0.11	<0.1			Bal.
CP-Ti-G4	0.006	0.007	0.002	0.22	0.30	<0.1			Bal.
Ti6Al4V	max. 0.05	max. 0.08	max. 0.015	max. 0.3	max. 0.2		5.5-6.8	3.5-4.5	Bal.

3.1.2 Sandblasted-acid-etched (SLA) surface

A SLA surface was obtained by sandblasting both sides of all three grades of Ti discs (CP-Ti-G2, CP-Ti-G4 and Ti6Al4V, all of which had been previously ground to a P400 finish with SiC abrasive paper) with 250 µm corundum particles (Korox®, BEGO) (SANDIMAT, Local exhaust ventilation, Allianz Engineering Inspection Service Ltd, Italy), and then cleaning in deionised water using ultrasonic agitation for 15 min. The samples were then etched in the combination solutions of 37% HCl and 98% H_2SO_4 (1:1) at 80 °C for ~4 min and then washed in deionised water. All samples were thoroughly cleaned in acetone, ethanol, and deionised water sequentially using ultrasonic agitation for 10 min at each stage. Specimens were finally dried in an air stream before further experiments. It can be seen that the home-produced SLA surfaces of three grades of Ti are consistent with the commercial dental implant SLA surface finish (Figure 3-1).
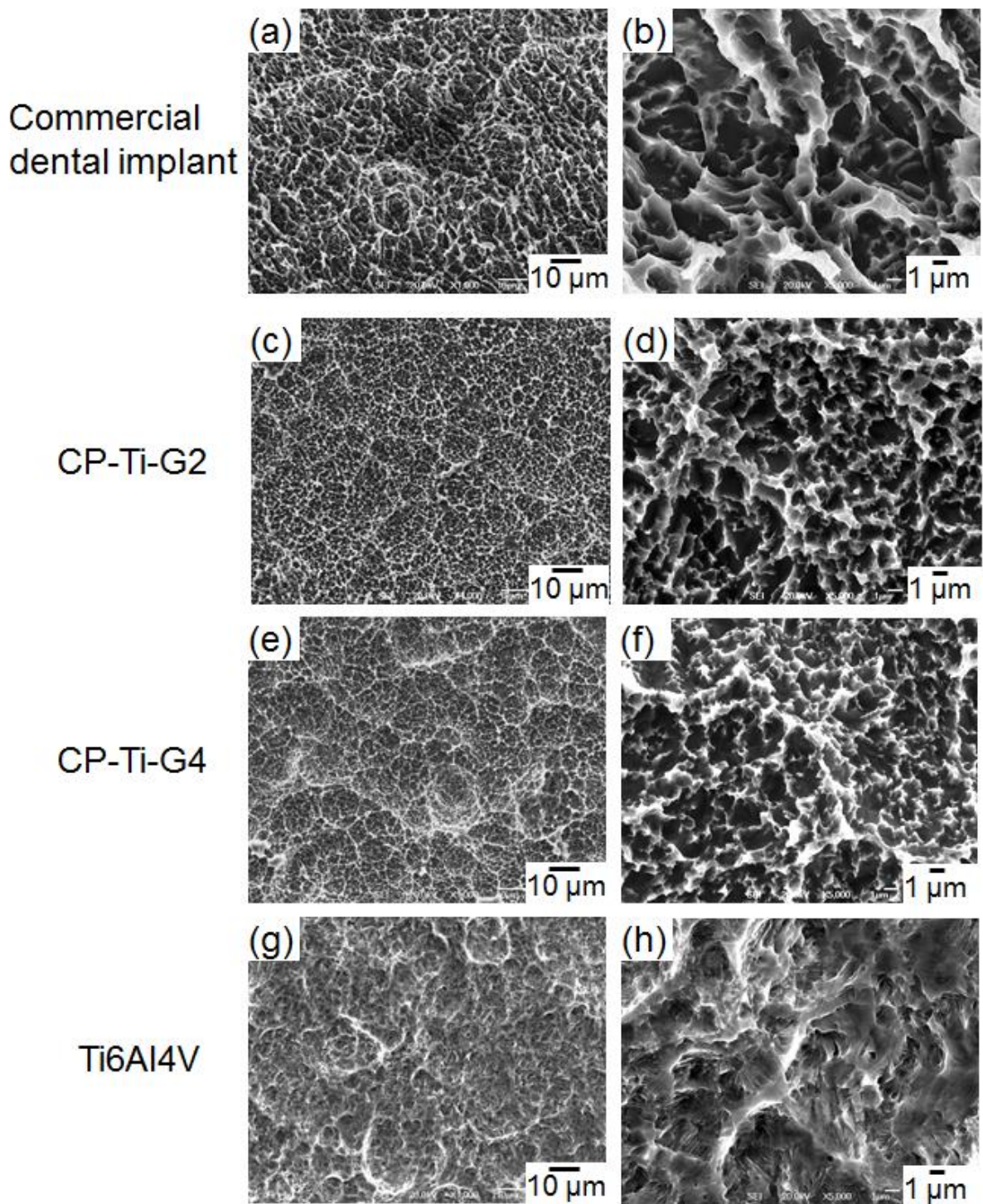
Figure 3-1 SEM images of SLA surface finish of (a-b) a commercial CP-Ti dental implant (Straumann® SP Ø4.1 RN SLA, Institute Straumann AG) and home-produced (c-d) CP-Ti-G2; (e-f) CP-Ti-G4; and (g-h) Ti6Al4V.

3.2 Immersion tests

3.2.1 Effect of pH and lipopolysaccharide (LPS) on Ti corrosion

Physiological saline (0.9% NaCl, w/v (i.e. 0.9 g NaCl in 100 mL solution)) (ASTM F1801-97(2009)e1) was used as an immersion solution for metal release measurements. The use of more complex physiological solutions containing phosphates was avoided to reduce the risk of polyatomic interferences occurring in inductively coupled plasma mass spectrometry (ICP-MS) measurements of solutions containing Ti [173]. Each solution was modified according to two experimental factors, pH (at 4 levels) and LPS (with or without the addition of LPS). The pH value was measured with a calibrated Ø40 pH meter (Beckman Instruments, California, USA) and subsequently modified to pH 7, 5.5, 4 or 2 by adding lactic acid (Sigma-Aldrich, Dorset, UK) or NaOH (Sigma-Aldrich, UK). To investigate the effect of LPS, a further series of test solutions at each pH were prepared containing 150 µg/mL of LPS (*Escherichia coli* LPS 055:B5, Sigma-Aldrich) with the pH re-measured immediately after LPS addition. To minimise contamination with elements of interest for subsequent mass spectrometry measurements, ultrapure water (Gibco®, life technologies™, Paisley, UK) and mass spectrometry grade reagents were used.

All prepared mirror-polished Ti samples were immersed in 2 mL of test solution in a 30 mL universal tube (transparent polystyrene with conical bottom) which was sealed to prevent evaporation. For each experimental condition, three samples of each Ti grade (CP-Ti-G2, CP-Ti-G4, and Ti6Al4V) were immersed in separate containers and incubated at 37 °C. The samples were consistently positioned so that the periphery of each disc made multiple point contacts with the radius of the container but allowed the majority of the surface area to be

exposed to the immersion solutions. Samples were gently agitated on an A500 orbital mixer (Denley, UK) for 1 hour per day. For each sample, the test solution was retrieved and replaced with fresh solution after 7 days. The pH of the prepared test solutions were measured immediately before use on each occasion. Following 4 weeks of immersion, the retrieved solutions for each sample were pooled together to form a total of 8 mL which was then used for ICP-MS measurements. The exposed surface area of Ti6Al4V samples was ~2% greater (due to the thicker discs) than CP-Ti-G2 and CP-Ti-G4 samples, but this was not taken into account in the interpretation of the ICP-MS data as the difference was significantly smaller than the typical variation in the results.

3.2.2 Effect of H_2O_2 on Ti corrosion

H_2O_2 (30% w/v (i.e. 30 g H_2O_2 in 100 mL solution), BDH, England, UK) was added into physiological saline (0.9% NaCl, pH 6.7-7, 0.15 M) to create the immersion solutions with four concentrations of H_2O_2: 0.1% (0.03 M), 0.5% (0.15 M), 1% (0.3 M) and 10% (3 M). Due to the decomposition of H_2O_2, all the prepared H_2O_2-containing solutions and the original H_2O_2 were stored at 4 °C in dark environment and used within 1 month. The experimental procedures for immersion testing and ICP-MS measurements are described in Section 3.2.1.

3.2.3 Effect of H_2O_2 in combination with albumin on Ti corrosion

To investigate the effect of the combination of H_2O_2 and albumin on Ti6Al4V corrosion, four concentrations of bovine serum albumin (≥ 98% (agarose gel electrophoresis) lyophilised powder, Sigma-Aldrich, Dorset, UK), i.e., 0.2% (0.03 mM), 0.4% (0.06 mM), 1% (0.15 mM), 4% (0.6 mM), were added into the previously prepared 0.1% H_2O_2 in physiological saline. The storage method for the prepared solutions was the same as described in Section 3.2.2.

The experimental procedures for immersion testing were otherwise the same as described in Section 3.2.1 except for the immersion period. The test solution for each sample was retrieved and replaced with fresh solution after 7 days. Following 2 weeks of immersion, the retrieved solutions were pooled together to form a total of 4 mL for ICP-MS measurements.

3.3 Culture of *Streptococcus sanguinis* (*S. sanguinis*) on Ti surfaces

The prepared mirror-polished and SLA samples (including CP-Ti-G2, CP-Ti-G4 and Ti6Al4V) were autoclaved for 30 min at 120 °C 24 hours prior to use. *S. sanguinis* were pre-incubated on horse blood agar (SR0050B, Oxoid) overnight in an anaerobic chamber with environmental conditions of 10% CO_2, 10% hydrogen and 80% nitrogen as the balance (Don Whitley Scientific, Molecular Atmosphere Controlled System, CAL-3200, Shipley UK). Following pre-incubation, *S. sanguinis* was transferred into 10 mL of autoclaved artificial saliva (composition identified in Table 3-2) [174] and then cultured in an aerobic incubator overnight at 37 °C (NB-205, N-BIOTEK, Inc., Korea) with agitation at 100 rpm. 100 μL of the bacterial suspension (average $\sim4\times10^5$ CFU/mL) was then added into 5 mL of artificial saliva into which a Ti disc-shaped sample had been pre-immersed. Three Ti samples were used for each condition. The Ti discs submerged in the inoculated artificial saliva were subsequently incubated aerobically at 37 °C.

In order to maintain bacterial viability over the prolonged immersion time (30 days), the immersion culture-media was retrieved and replaced with 5 mL of fresh artificial saliva every 3 days. At each renewal of the culture-media a further 100 μL of bacterial inoculum (average $\sim4\times10^5$ CFU/mL) was introduced. Over 30 days the culture was replaced on nine occasions. The retrieved culture-medium was centrifuged at 4000 rpm for 10 min at 4 °C to obtain

bacterial pellets (~0.1 mL) and a separated supernatant. The supernatant collected on day 3, day 12, day 21, and day 30 were stored at 4 °C for elemental concentration measurements. After 30 days, the 10 retrieved bacterial pellets were lysed in 100 μL 69% nitric acid (BDH, UK) and then pooled. Subsequently the pooled solutions were diluted to a 2% concentration of nitric acid using ultrapure water and then stored at 4 °C before ICP-MS measurements.

Mirror-polished and SLA treated Ti control samples were also immersed in artificial saliva without bacteria. The test-samples were immersed in 5 mL of artificial saliva and incubated for 4 weeks. For each sample, the test culture-medium was retrieved and replaced with new solutions after 7 days. Following 4 weeks of immersion, the retrieved solutions for each sample were pooled together for ICP-MS measurements.

To visualise the formation of a *S. sanguinis* biofilm on the Ti surfaces after 30 days of incubation, the retrieved Ti samples were fixed with 2.5% glutaraldehyde (EM grade, Agar Scientific, UK) in 0.1 M sodium cacodylate for 1 hour. Dehydration and cell conservation prior to electron microscopy imaging were performed by immersing the Ti discs serially into from 30%, 40%, 50%, 60%, 70%, 80%, 90%, 95% (twice), 100% (twice) ethanol for at least 10 min at each stage of the gradient. Final drying was achieved using a critical pointer dryer.

Table 3-2 The composition of artificial saliva [174].

Substance	Concentration	Supplier
NaCl	0.35 g/L	Sigma-Aldrich, UK
KCl	0.2 g/L	BDH, UK
CaCl$_2$	0.2 g/L	BDH, UK
Lab lemco powder	1 g/L	Oxoid Limited, UK
Yeast extract	2 g/L	Oxoid Limited, UK
Mucin	2.5 g/L	Sigma-Aldrich, UK
Peptone	5 g/L	Fluka, US
Sterile filtered urea	40% (1.25 ml per 1L)	Sigma-Aldrich, UK
Ultrapure water	N/A	Gibco®, life technologies™, UK

3.4 Incubation of Ti with isolated human neutrophils

3.4.1 Incubation of isolated human neutrophils on Ti surfaces

Peripheral blood neutrophils were isolated from the whole blood of healthy volunteers and the detailed procedures followed those originally described in reference [16]. Briefly, ~6 mL of whole blood was collected into a lithium heparin coated tube using standard venepuncture techniques. The whole blood was then transferred onto a Percoll® gradient (by layering 8 mL of 1.079 Percoll® density over 8 mL 1.098 of Percoll® density, GE Heathcare, Buckinghamshire, UK) (Table 3-3) and centrifuged (8 min at 150 rcf and then 10 min at 1200 rcf) to separate the cellular contents into different layers. The top plasma layer and lymphocyte layer were carefully discarded by using a plastic pipette. The target neutrophil layer located below these two and at the top of the red blood cell layer was then transferred to a 50 mL centrifuge tube which contained 15 mL of prepared lysis buffer (Table 3-4) and was then incubated at room temperature for 5 min to lyse any contaminant red blood cells

(erythrocytes). A concentrated neutrophil pellet was subsequently obtained by further centrifuging (6 min at 500 rcf) and discarding the supernatant. The pellet was further cleaned in lysis buffer once, in phosphate buffered saline (PBS, 7.75 g/L NaCl (Sigma-Aldrich, UK), 0.2 g/L KH_2PO_4 (Sigma-Aldrich, UK) and 1.5 g/L K_2HPO_4 (Sigma-Aldrich, UK)) twice, and then finally in 0.25 mM of Tris-buffered saline (Tris-buffer, 1 mM $MgCl_2$ (BDH, UK), 1.5 mM $CaCl_2$ (BDH, UK) and 1 mM glucose (Sigma-Aldrich, UK)) three times with centrifugation for 6 min at 500 rcf at each stage.

The number of isolated neutrophils was counted by using a light microscope (LeitzLaborlux S, Germany) and a haemocytometer (Neubauer, Reichart, Germany). The viability of neutrophils (10 µL) was determined using Trypan Blue exclusion (Sigma-Aldrich, UK) and was typically >98%. The neutrophils were used by re-suspending into Tris-buffer to obtain a concentration of 2.5×10^6 cells/mL for the *in vitro* neutrophil incubation assays.

Table 3-3 The composition of Percoll® densities [16]

Density (g/mL)	1.079	1.098
Percoll®	19.708 mL	24.823 mL
Deionised water	11.792 mL	6.677 mL
1.5 M NaCl	3.5 mL	3.5 mL

Table 3-4 The composition of lysis butter [16]

Substance	Concentration	Supplier
NH_4Cl	8.3 g/L	Sigma-Aldrich, UK
$KHCO_3$	1 g/L	Sigma-Aldrich, UK
$C_{10}H_{14}N_2Na_2O_8 \cdot 2H_2O$	0.04 g/L	Sigma-Aldrich, UK
Bovine serum albumin	2.5 g/L	Sigma-Aldrich, UK
Sterile deionised water	N/A	Versol, Somerset, UK

0.5 mL of the neutrophil suspension was added into 24 well cell culture plates, in which mirror-polished Ti discs of three grades (CP-Ti-G2, CP-Ti-G4 and Ti6Al4V) had been placed. The experimental groups were designated as Cell-Control (with no Ti discs), CP-Ti-G2-Cell, CP-Ti-G4-Cell and Ti6Al4V-Cell. All samples were incubated in 5% CO_2 at 37 °C for 8 h. Half of the samples from each group were stimulated by the addition of 12.5 μL of opsonised *Staphylococcus aureus* (Ops *Sa*, the preparation of Ops *Sa* shown in Section 3.4.2) and designated as Ops *Sa*-Control, CP-Ti-G2-Ops *Sa*, CP-Ti-G4-Ops *Sa* and Ti6Al4V-Ops *Sa*. Tris-buffer solution without neutrophils was also added into the cell culture plates with mirror-polished Ti discs as the blank control groups. After 8 h incubation, the Tris-buffer solutions or neutrophil suspensions were pooled together for each control group and each experimental group. It should be noted that the sample measured by ICP-MS for each test of each group was created by pooling together 24 identical experimental repeat samples generated under the same conditions to achieve the required volume for the ICP-MS measurements (Figure 3-2). For each ICP-MS test, neutrophils were isolated from 4 or 5 individuals (due to different numbers of neutrophils in different people) to obtain enough cells to be distributed among the experiment groups (n=24 per group, 8 groups in total) (see Figure 3-2). Three ICP-MS tests were carried out for each group. It is worth noting that neutrophils were sourced from 12 different volunteers for all experiments (see Figure 3-2). All the collected solutions in each test were lysed by adding 300 μL 69% nitric acid for 3 days, and were refrigerated at 4 °C prior to elemental concentration measurement.

To characterise the neutrophils on Ti discs, samples previously incubated with neutrophils for 8 h were fixed with 2.5% glutaraldehyde in PBS for 1 h. Cell dehydration and subsequent procedures were the same as described in Section 3.3.

	Cell-Control group	CP-Ti-G2-Cell group	CP-Ti-G4-Cell group	Ti6Al4V-Cell group	Ops Sa-Control group	CP-Ti-G2-Ops Sa group	CP-Ti-G4-Ops Sa group	Ti6Al4V-Ops Sa group	blank control groups
ICP-MS test 1	●●●●●● ●●●●●● ●●●●●● ●●●●●●	●●●●●● ●●●●●● ●●●●●● ●●●●●●	●●●●●● ●●●●●● ●●●●●● ●●●●●●	●●●●●● ●●●●●● ●●●●●● ●●●●●●	●●●●●● ●●●●●● ●●●●●● ●●●●●●	●●●●●● ●●●●●● ●●●●●● ●●●●●●	●●●●●● ●●●●●● ●●●●●● ●●●●●●	●●●●●● ●●●●●● ●●●●●● ●●●●●●	○○○○○○ ○○○○○○ ○○○○○○ ○○○○○○
ICP-MS test 2	●●●●●● ●●●●●● ●●●●●● ●●●●●●	●●●●●● ●●●●●● ●●●●●● ●●●●●●	●●●●●● ●●●●●● ●●●●●● ●●●●●●	●●●●●● ●●●●●● ●●●●●● ●●●●●●	●●●●●● ●●●●●● ●●●●●● ●●●●●●	●●●●●● ●●●●●● ●●●●●● ●●●●●●	●●●●●● ●●●●●● ●●●●●● ●●●●●●	●●●●●● ●●●●●● ●●●●●● ●●●●●●	○○○○○○ ○○○○○○ ○○○○○○ ○○○○○○
ICP-MS test 3	●●●●●● ●●●●●● ●●●●●● ●●●●●●	●●●●●● ●●●●●● ●●●●●● ●●●●●●	●●●●●● ●●●●●● ●●●●●● ●●●●●●	●●●●●● ●●●●●● ●●●●●● ●●●●●●	●●●●●● ●●●●●● ●●●●●● ●●●●●●	●●●●●● ●●●●●● ●●●●●● ●●●●●●	●●●●●● ●●●●●● ●●●●●● ●●●●●●	●●●●●● ●●●●●● ●●●●●● ●●●●●●	○○○○○○ ○○○○○○ ○○○○○○ ○○○○○○

- ● neutrophils from volunteer 1
- ● neutrophils from volunteer 2
- ● neutrophils from volunteer 3
- ● neutrophils from volunteers 4 and 5
- ● neutrophils from volunteer 6
- ○ without neutrophils
- ● neutrophils from volunteer 7
- ● neutrophils from volunteer 8
- ● neutrophils from volunteers 6 and 9
- ● neutrophils from volunteer 10
- ● neutrophils from volunteers 11
- ● neutrophils from volunteer 12

Figure 3-2 The experimental procedures for ICP-MS tests for all the experimental and control groups in the absence or presence of un-stimulated (Cell group) or stimulated neutrophils by Ops Sa (Ops Sa group). For each test, neutrophils were isolated from 4 or 5 individuals (due to different numbers of neutrophils in different people) to obtain enough cells to be distributed among the experiment groups (solid circles with different colours representing different neutrophils sources). The sample was created by pooling together 24 experimental repeat samples (each circle stands for one sample, also meaning different ICP-MS test has different neutrophils). In the absence of neutrophils, samples in blank control groups (including CP-Ti-G2, CP-Ti-G4 and Ti6Al4V) were also obtained by pooling 24 identical samples.

3.4.2 Preparation of opsonised *Staphylococcus aureus* (Ops *Sa*)

To prepare Ops *Sa*, sterile tryptone soya broth (TSB) was inoculated by transferring *Staphylococcus aureus* (*Sa*) grown on a Mannitol salt agar (ThermoFisher Scientific, Oxford, UK) plate using a flame sterilised loop to TSB. The bacteria were then cultured overnight in an anaerobic chamber comprised of 10% CO_2, 10% hydrogen and 80% nitrogen at 37 °C. The bacterial suspension was centrifuged (5 min at 3800 rcf) to obtain a pellet, which was re-suspended in PBS. The procedure was repeated three times before the bacterial pellet was

finally re-suspended in 3% formaldehyde (P6148, Sigma-Aldrich, UK) in PBS and incubated for 1 h at room temperature. The bacteria were again centrifuged and re-suspended in PBS three times. The concentration of bacteria was then estimated according to spectrophotometry measurement to obtain a concentration of 1×10^9 bacteria per mL. The bacteria suspension was heat-killed at 80 °C for 20 min. After this, 33 μL Vigam liquid (5 mg/mL IgG, Bio Products Laboratory, Hertfordshire, UK) per mL of bacteria suspension was added into the bacteria suspension, which was incubated overnight at room temperature to allow opsonisation. The final bacteria suspension was obtained by being centrifuged and re-suspended in PBS twice and stored at -80 °C. Bacterial numbers were estimated according to spectrophotometry measurement to achieve a concentration of 6×10^8 bacteria/mL.

3.5 Determination of released metal concentration

The retrieved and pooled solutions for ICP-MS test in Section 3.2.1, Section 3.2.2 and Section 3.2.3 were syringe-filtered (Acrodisc® 32 mm syringe filter with 0.45 μm Supor® membrane, Pall Newquay, UK) and refrigerated at 4 °C prior to measurement of elemental concentration. Elemental Ti, Al and V concentrations in the immersion solutions were quantified using ICP-MS (University of Birmingham, Agilent 7500ce ICP-MS, Agilent Technologies, UK) where the detectable limits for Ti, Al and V were 0.2 ppb.

The supernatant, the bacterial pellet samples and the control samples in Section 3.3 or the pooled culture-media from the neutrophil incubation group in Section 3.4 were also syringe-filtered and refrigerated at 4 °C prior to ICP-MS measurement (Agilent 7500ce ICP-MS or Agilent 7700x ICP-MS (measurements commercially sourced with Butterworth Laboratories, Company registration No. 1185121, Teddington, UK)) where the detectable limit for Ti was

0.2 ppb for Agilent 7500ce ICP-MS and 1 ppb for Agilent 7700x ICP-MS (the values reported below 1 ppb are just for information to indicate below detectable limit).

For the effect of pH and LPS on Ti release, initially two-way Analyses of Variance (ANOVA) were used to identify significant differences between ICP-MS measurements (α =0.05) where the factors were Ti grade (at 3 levels) and pH (at 4 levels) with tests run independently for samples with and without LPS. Subsequently, further two-way ANOVAs were conducted for each Ti grade where the factors were LPS (at 2 levels) and pH (at 4 levels). Post-hoc Tukey tests (α =0.05) were used to identify significant differences between individual groups.

3.6 Electrochemical tests

3.6.1 General procedures

A standard three-electrode cell with reference electrode, counter electrode and working electrode is shown in Figure 3-3. The counter electrode (CE) was a Pt mesh (working area ~4 cm^2) and the reference electrode (RE) was a commercial saturated calomel electrode (SCE). The potential was controlled with a potentiostat (ACM Instruments, UK). Ti discs were mounted in VARI-SET cold mounting acrylic (MetPrep Ltd, UK) and used as working electrode (WE, working area 1.5 cm^2). The electrode was polished to a mirror surface using identical sample preparation methods as detailed previously in Section 3.1.1. To obtain a good reproducibility, the time between polishing and electrochemical measurements was controlled using the following procedures throughout. After final polishing with an MD-Chem polish cloth, the samples were immediately cleaned with deionised water (Millipore, 18 MΩ), then dried in an air stream and left in open air for 5 min before immersing in test solutions (which were defined as freshly polished samples). Due to the preparatory procedures of setting up the

electrochemical cell, there was a 5 min gap between the initial immersion of the sample and acquisition of the first measurement.

The electrochemical cell was immersed in a water bath (Bennett Scientific Limited, Nickel Electro LTD, England, UK) with high temperature stability (±1 °C). The temperature was monitored with a thermocouple (YC-727UD date logger thermometer, Taiwan) connected to the computer (Figure 3-3).
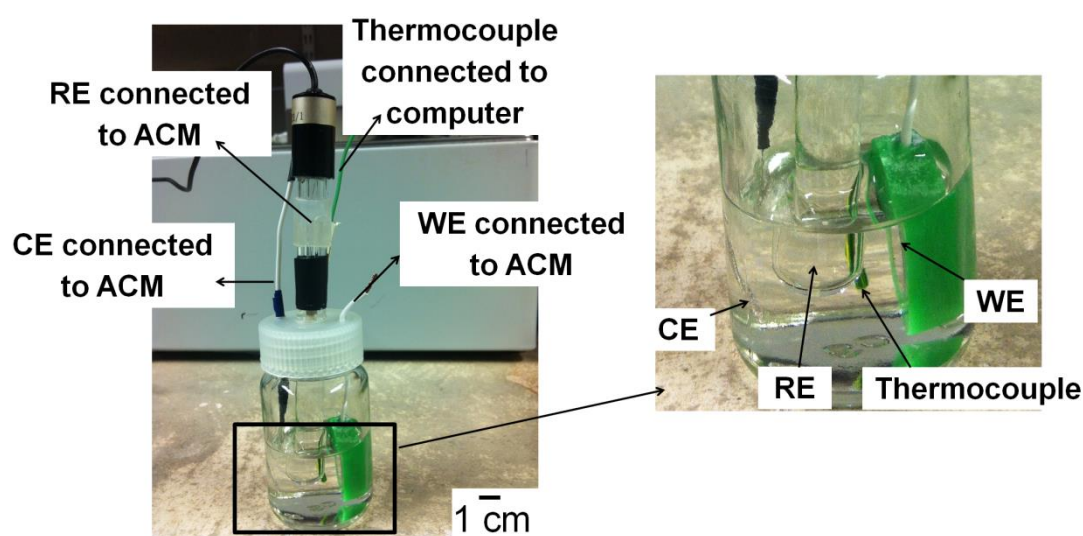
Figure 3-3 The experiment setup of the electrochemical cell; RE: reference electrode, CE: counter electrode, WE: working electrode. ACM: Potentiostat (ACM Instruments, UK).

3.6.2 Potentiodynamic polarisation curves

3.6.2.1 Measurements in HCl

Freshly polished CP-Ti-G2, CP-Ti-G4 and Ti6Al4V electrodes were immersed in 2 M HCl at 37 °C. The open circuit potential (OCP) was measured for 1 h and then anodic polarisation curves were measured by sweeping the potential from -50 mV below the OCP to 0 mV vs. SCE

at a rate of 1 mV/s. The anodic polarisation curves were measured three times for each condition, using a freshly polished sample and fresh solution in each case.

3.6.2.2 Effect of pH and LPS on Ti corrosion

Anodic and cathodic polarisation curves were measured separately. Freshly polished CP-Ti-G4 and Ti6Al4V electrodes were immersed in physiological saline solutions (0.9% NaCl, which was adjusted to either pH 2 or pH 4 with lactic acid, with or without the addition of LPS) at 37 °C. OCP was measured for 1 h. Anodic polarisation curves were measured by sweeping the potential from -50 mV below the OCP to 600 mV vs. SCE while cathodic polarisation curves were obtained by sweeping the potential from 50 mV above OCP to -900 mV vs. SCE at a rate of 1 mV/s. The polarisation curves were measured three times for each condition, using a freshly polished sample and fresh solution in each case.

3.6.2.3 Effect of H_2O_2 on Ti corrosion

To investigate the effect of H_2O_2, anodic polarisation curves of freshly polished CP-Ti-G4 and Ti6Al4V were measured in physiological saline (0.9% NaCl, pH 6.7-7, 0.15 M) with and without different levels of H_2O_2 (0.1%, 1% and 10%). The experimental procedures were the same as described in Section 3.6.2.2 except that anodic polarisation curves were measured by sweeping the potential from -50 mV below the OCP to 1200 mV (instead of 600 mV) vs. SCE while cathodic polarisation curves were obtained by sweeping the potential from 50 mV above OCP to -1400 mV (instead of -900 mV) vs. SCE.

3.6.2.4 Effect of the combination of H_2O_2 and albumin on Ti corrosion

To investigate the effect of the combination of H_2O_2 and albumin on the corrosion behaviour of Ti6Al4V, the anodic and cathodic polarisation curves of freshly polished Ti6Al4V were measured in four concentrations of albumin (0.2%, 0.4%, 1%, and 4%) with and without 0.1% H_2O_2 in physiological saline. The experimental procedures were the same as described in Section 3.6.2.3 except that the polarisation curves for Ti6Al4V in the mixed solutions of albumin and H_2O_2 were measured twice for each condition, using a freshly polished sample and fresh solution in each case.

3.6.3 Potentiostatic measurements

3.6.3.1 Measurements in HCl

The corrosion behaviour of Ti6Al4V in the presence of 2 M HCl was studied by potentiostatic measurements at various temperatures (28 °C, 31 °C, 34 °C, 37 °C, 40 °C, and 43 °C). The temperature was controlled by water bath and the temperature was recorded by a thermocouple, which was immersed in the solution (Figure 3-3). Freshly polished Ti6Al4V was immersed in 2 M HCl. OCP was measured for 30 min and then -510 mV vs. SCE was applied for 3 h.

In addition, the surface morphology of Ti6Al4V was compared using SEM before and after potentiostatic measurements on the same sample at 37 °C. Briefly, to easily locate a same region for comparison, one region of the mirror-polished sample was identified by a hardness mark (Vickers hardness test, load: 300 g, MVK-H1 hardness testing machine, Akashi Corporation Sagami Plant, Mitutoyo, Zama Kanagawa, Japan), which was characterised by SEM. The carbon layer on the surface from SEM was removed by quickly (~10 s) polishing the sample

on an MD-Chem polish cloth with OP-S Colloidal Silica suspension, so that it would not affect the electrochemical experiments.

3.6.3.2 Effect of pH and LPS on Ti corrosion

Potentiostatic studies were performed to investigate the effect of the addition of LPS on the passive current density of CP-Ti-G4 and Ti6Al4V at pH 2 and pH 4. Freshly polished CP-Ti-G4 or Ti6Al4V discs were immersed in physiological saline which had been adjusted to pH 2 or pH 4, and a potential of 600 mV vs. SCE was applied. After 1000 s, LPS was added to obtain a concentration of 150 µg/mL in the immersion solution. Following the LPS addition, the solution was stirred continuously for 100 s. To investigate the effects of agitation of the immersion solution on the passive current, the immersion solution was stirred again for 100 s following 1000 s intervals on two separate occasions. The experiment was repeated twice for each Ti grade and each pH condition, using a fresh polished sample and solution in each case. Control experiments were conducted using an identical method with the exception of LPS addition.

3.6.3.3 Effect of H_2O_2 on surface morphology of Ti6Al4V

The surface morphology of Ti6Al4V was compared using both SEM and AFM before and after the potentiostatic measurement in the presence of H_2O_2. Mirror-polished Ti6Al4V was immersed in 10% H_2O_2 in physiological saline at 37 °C. OCP was measured for 1 h and then a potential of 600 mV vs. SCE was applied for 30 min. The methods for identifying the same region of the sample and removing the carbon layer from SEM are the same as the procedures described in Section 3.6.3.1.

3.6.3.4 Effect of the combination of H_2O_2 and albumin on Ti corrosion

Potentiostatic measurements were performed to investigate the effect of addition of albumin and H_2O_2 on the anodic and cathodic steady state currents for Ti6Al4V in physiological saline. Table 3-5 shows the detailed experimental procedures. The experiment was repeated twice for each condition using a freshly polished sample and fresh solution in each case.

Table 3-5 Experimental procedures for potentiostatic measurements of Ti6Al4V at different applied potentials (-800 mV, 400 mV, 800 mV vs. SCE) in physiological saline (PS) with different sequences for H_2O_2 and/or albumin addition at 37 °C. The solution was stirred for ~100 s at ~1000 s intervals to ensure complete mixing; for some experiments, a specific amount of H_2O_2 or albumin (in PS) was added at ~1000 s intervals immediately before stirring to give a final concentration of 0.1% or 1%.

1st ~1000 s	100 s stir	2nd ~1000 s	100 s stir	3rd ~1000 s	100 s stir	1000 s
PS	+1% albumin		+0.1% H_2O_2			
PS			+0.1% H_2O_2		+1% albumin	
PS			+0.1% H_2O_2			

3.6.4 Long-time (24 h) open circuit potential (OCP) measurement

3.6.4.1 Effect of combination of H_2O_2 and albumin on Ti corrosion

The OCP of mirror-polished Ti6Al4V in physiological saline with and without addition of H_2O_2 and/or albumin were all monitored for 24 h at 37 °C. Table 3-6 shows the detailed experimental procedures. The experiment was repeated twice for each condition using a freshly polished sample and fresh solution in each case.

Table 3-6 Experimental procedure for 24 h OCP measurement of mirror-polished Ti6Al4V in physiological saline (PS) with different sequences for H_2O_2 and/or albumin addition at 37 °C. The solution was stirred for ~200 s at ~1 h and ~4 h to ensure complete mixing; for some experiments, a specific amount of H_2O_2 or albumin (in PS) was added at ~1 h or ~4 h immediately before stirring to give a final concentration of 0.1% or 4%.

Time ~1 h	200 s stir	Time ~3 h	200 s stir	Time ~20 h
PS	+0.1% H_2O_2			
PS				
PS	+0.1% H_2O_2		+4% albumin	
PS	+4% albumin		+0.1% H_2O_2	
PS	+4% albumin			

3.7 Mechanically-assisted crevice corrosion (MACC)

3.7.1 Development of an MACC electrochemical cell

An MACC apparatus was designed (Figure 3-4), manufactured and developed in the current study. It comprised a standard three-electrode cell with RE, CE and WE (Figure 3-5) and was controlled with a potentiostat. The CE was a Pt mesh and the RE was an Ag/AgCl electrode. All potentials in the context of MACC are quoted against this reference scale.
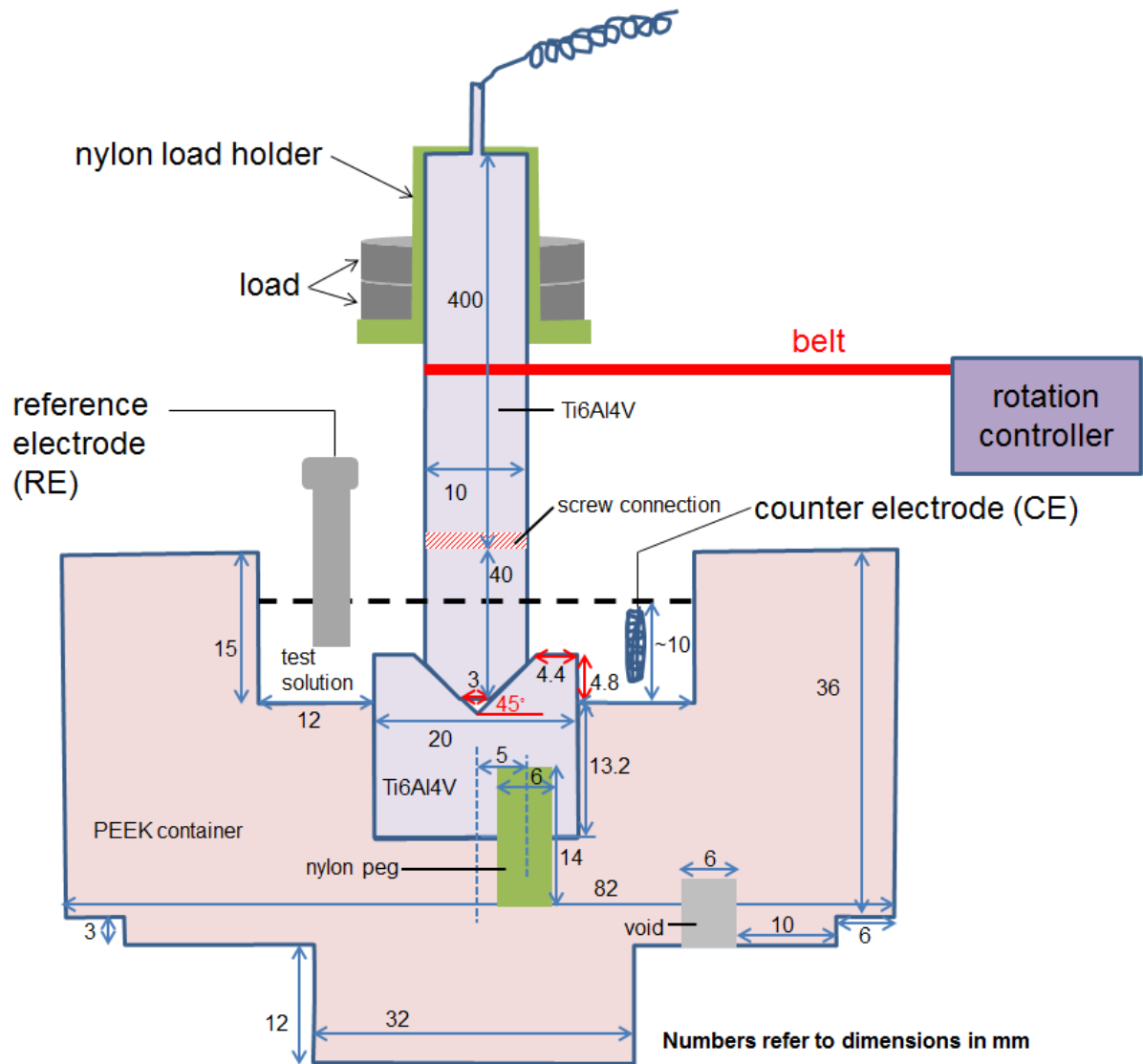
Figure 3-4 Schematic diagram of the designed MACC apparatus. The dimensions of the vertical section have been shown. The vertical loads (250 g to 3200 g) can be adjusted by adding different weights of the metal substrates. The vertical section was controlled by a rotation controller, which made the section rotate clockwise or anti-clockwise in a rotating speed of 0.1-10 rpm in a step of 0.1 rpm.

Figure 3-4 shows the vertical section of MACC apparatus with dimensions. The rotation of the device was controlled by a step-motor with a good control of the speed (Powermax II®, Model: M22NRXB-LNN-NS-OO, Pacific scientific, USA). The rotation speed can be varied from 0.1 to 10 rpm in a step of 0.1 rpm. The direction of the rotation can be clockwise and anti-clockwise.

65

However, all abrasion experiments were carried out in the clockwise direction in this study. In addition, various vertical loads (250 g to 3200 g) can be applied by adding different weights of the metal substrates (Figure 3-5).
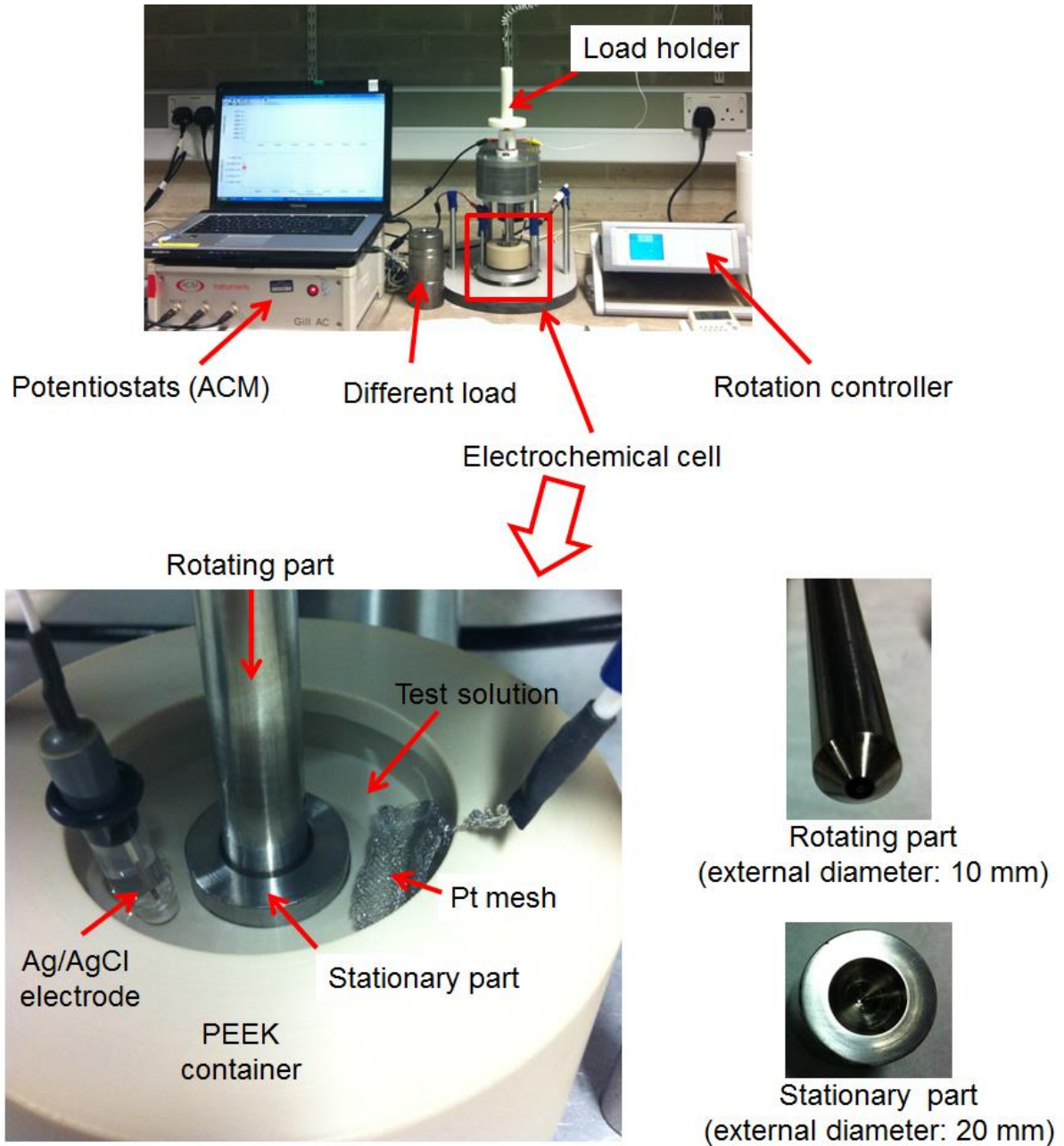
Figure 3-5 Picture of the experiment setup of the MACC electrochemical cell.

The Ti6Al4V couple comprised a "male" rotating component (external diameter 10 mm) which was lowered into a "female" stationary component (external diameter 20 mm) with a cavity facing upwards (Figure 3-5). The female component was prevented from rotating by a nylon peg (Figure 3-5).

The working electrode (WE) connection was made to the male component, but when the two component were in mechanical contact, current could flow between them. The total working area of the WE (the area immersed in the solution) was 910 mm^2 when the volume of test solution was 15 mL. The macroscopic contact area between the rotating part and stationary part was ~110 mm^2 (Figure 3-6), and the abraded area was difficult to define, so the current rather than current density is reported.
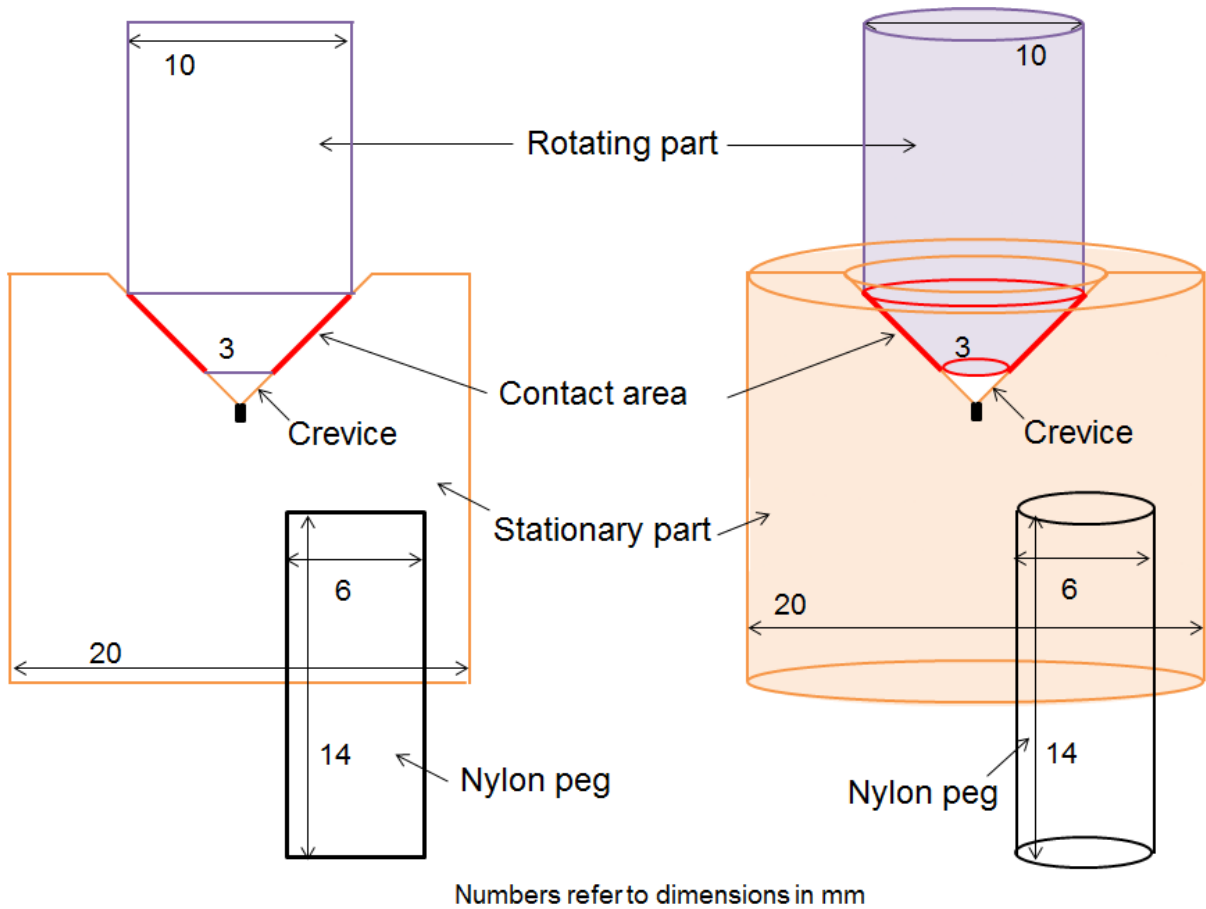
Figure 3-6 Schematic diagram of the vertical section of the MACC couple and the crevice geometry. Nylon peg is used to prevent the stationary part from rotating.

3.7.2 General procedures

The two components of the Ti6Al4V couple, including the Ti6Al4V rotating part and Ti6Al4V stationary part, had an as-machined surface finish. The two components were re-used for all of the tests. The contact surfaces were just cleaned with deionised water (no other treatment) before each test. Generally, the Ti6Al4V couple was separately immersed in the physiological saline (0.9% NaCl, pH 6.7-7, 0.15 M) for 300 s. Then the two parts were connected by applying vertical loads and OCP was measured concurrently. Afterwards, potentiostatic or potentiodynamic measurements were conducted in different tests.

There were both solutions and black debris found in the cavity in the stationary part of the couple. Due to the small volume of the solution (~0.02 mL) in the cavity, the pH was corrected by measuring the pH of the diluted solution (by adding 2-3 mL physiological saline (pH 6.7-7)), and adjusting the value to take account of the dilution.

3.7.3 Effect of the crevice geometry

The crevice geometry of the MACC apparatus was manifested in physiological saline with pH indicator (MACC test-1, Figure 3-7). After static OCP (no rotation) measurement, a potential was applied and according current was monitored. Photos have been taken to show the pH change of the solution during the static and abrasion processes. Before uncoupling the two parts, the solution was collected in a container by a syringe. After uncoupling, the collected solution was added to the cavity in the stationary part and PEEK container for comparison (Figure 3-7).

The crevice geometry was also manifested in physiological saline with pH indicator at free corrosion condition. OCP variation was monitored under static and abrasion conditions. Photos have also been taken to show pH change of the solution.
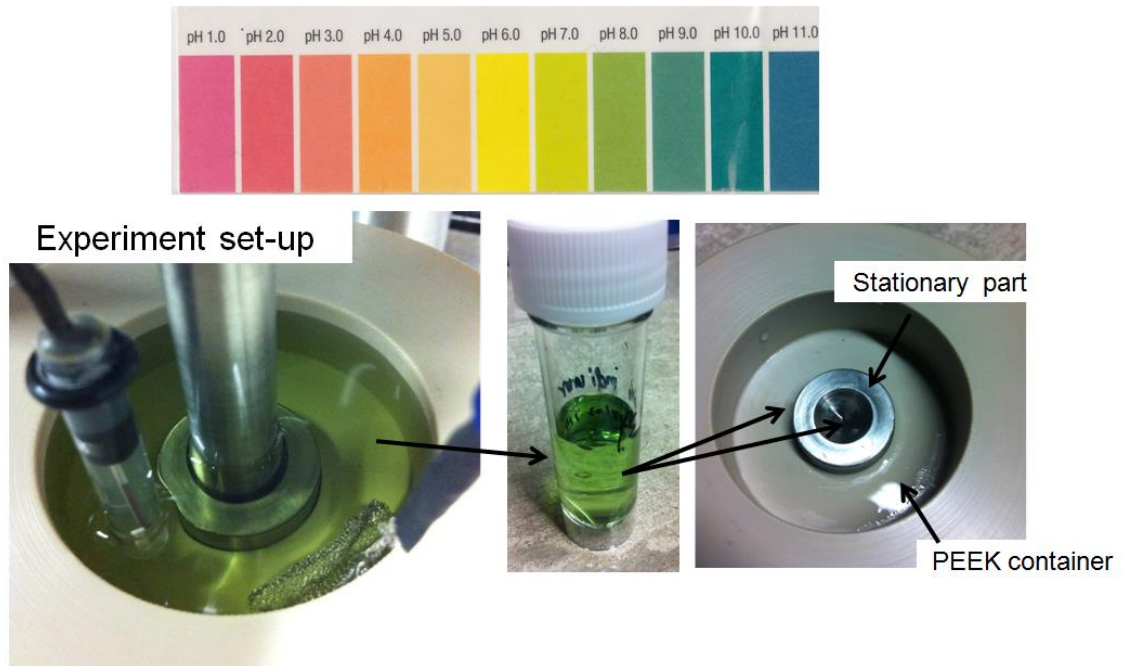
Figure 3-7 Pictures of the Ti6Al4V couples (MACC test-1) immersed in the physiological saline (pH 6.7-7) with pH indicator. The solution was collected in a container as shown in the figure before uncoupling, and then added again into the cavity of the stationary part and PEEK container after uncoupling for pH comparison.

3.7.4 Surface morphology of abrasion scars and abrasion debris

The morphology of the stationary part has been characterised by optical microscope and SEM after MACC-test 1. To investigate the surface morphology of the black debris, another MACC test (MACC test-2) was conducted in physiological saline without pH indicator. After the MACC test-2, black debris in the cavity of the stationary part were collected carefully with a syringe and cleaned with deionised water. One droplet of the debris solution was put onto a carbon or copper tape and left to dry overnight, and then it was characterised with SEM.

3.7.5 Effect of rotation speed on abrasion OCP

To investigate the effect of rotation speed on abrasion OCP of the Ti6Al4V couple in physiological saline, different rotation speeds were applied sequentially with 600 s interval between each two speeds. The Ti6Al4V couple was cleaned with deionised water (no other treatment) before the application of each sequence of rotation speeds. The tests were measured twice for each condition, using a fresh solution in each case.

3.7.6 Effect of rotation speed on abrasion current

The static OCP of the Ti6Al4V couple was measured for 600 s before a potential of 0 mV vs. Ag/AgCl was applied. Different rotation speeds were applied sequentially with 200 s intervals between every period of revolution. The tests were measured twice for each condition, using a fresh solution in each occasion.

3.8 Surface characterisation

3.8.1 SEM

Ti surfaces before and after immersion or electrochemical tests were characterised by scanning electron microscopy (SEM), which was undertaken on Philip XL-30 (Electron source: LaB_6, Fei, Nederlands) or JEOL 7000 (Japan Electron Optics Laboratory Co., Ltd. accelerating voltage is 20 kV, beam current is ~70 µA). Both secondary electron mode (SE) and backscatter electron mode (BSE) were used.

3.8.2 EDX

The elemental composition of Ti surfaces before and after immersion or electrochemical tests was analysed by energy dispersive X-ray spectroscopy (EDX detector model: 7558 for JEOL 7000 and 6650 for Philip XL-30; collecting window: ATW 2; acquisition time: 60 s; quantification method: standardless; Oxford Instrument, UK).

3.8.3 AFM

The surface change of Ti6Al4V was characterised by atomic force microscopy (AFM, Mode: contact mode; Material of tip: silicon; Digital Instruments, Veeco Metrology Group; Model No.: MMAFMLN; Serial No.: 1871EX; California, USA) before and after potentiostatic measurement in 10% H_2O_2 at 37 °C.

4   EFFECT OF PH AND LIPOPOLYSACCHARIDE (LPS) ON TI CORROSION[1]

4.1 Introduction

The aim of the work described in this chapter was to investigate the effect of pH and lipopolysaccharide (LPS), a constituent of the cell walls of Gram-negative bacteria and important mediator of peri-implant inflammation, on the corrosion behaviour of Ti alloys. The corrosion of Ti alloys in 2 M HCl, a very aggressive environment that simulates the crevice chemistry of mechanically-assisted crevice corrosion (MACC), was also investigated. Firstly, the three grades of Ti (CP-Ti-G2, CP-Ti-G4 and Ti6Al4V) used in this study were characterised using SEM and EDX. Then the preliminary investigations of Ti in 2 M HCl were conducted by using electrochemical tests, including potentiodynamic polarisation and potentiostatic measurements. In addition, the corrosion of three grades of Ti in physiological saline with different pH in the absence and presence of LPS was investigated by measuring Ti released in immersion tests and using SEM to characterise surface morphology at the end of tests.

4.2 Characterisation of the Ti samples

Figure 4-1 shows the surface morphology and EDX analysis of three grades of Ti with mirror-polished surfaces. CP-Ti-G2 shows no significant second phase particles, whereas CP-Ti-G4 (higher Fe level) contains $TiFe_x$ intermetallic particles, which agrees with the reported compositions (Table 3-1). Ti6Al4V shows the characteristic two-phase (α and β) microstructure. There was more V and Fe in the β phase and more Al in the α phase (Figure 4-2 and Table 4-1).

When as-polished samples were etched in Kroll's etchant (HF (2%) and HNO_3 (10%) mixed solution) for ~5 s, CP-Ti-G2 and CP-Ti-G4 showed equiaxed α grains with grain size from several to hundreds of micrometres while a uniform distribution of $TiFe_x$ intermetallic particles was only present on CP-Ti-G4 (Figure 4-3). The β phase was clearly observed on Ti6Al4V after being etched in Kroll's etchant (Figure 4-3).
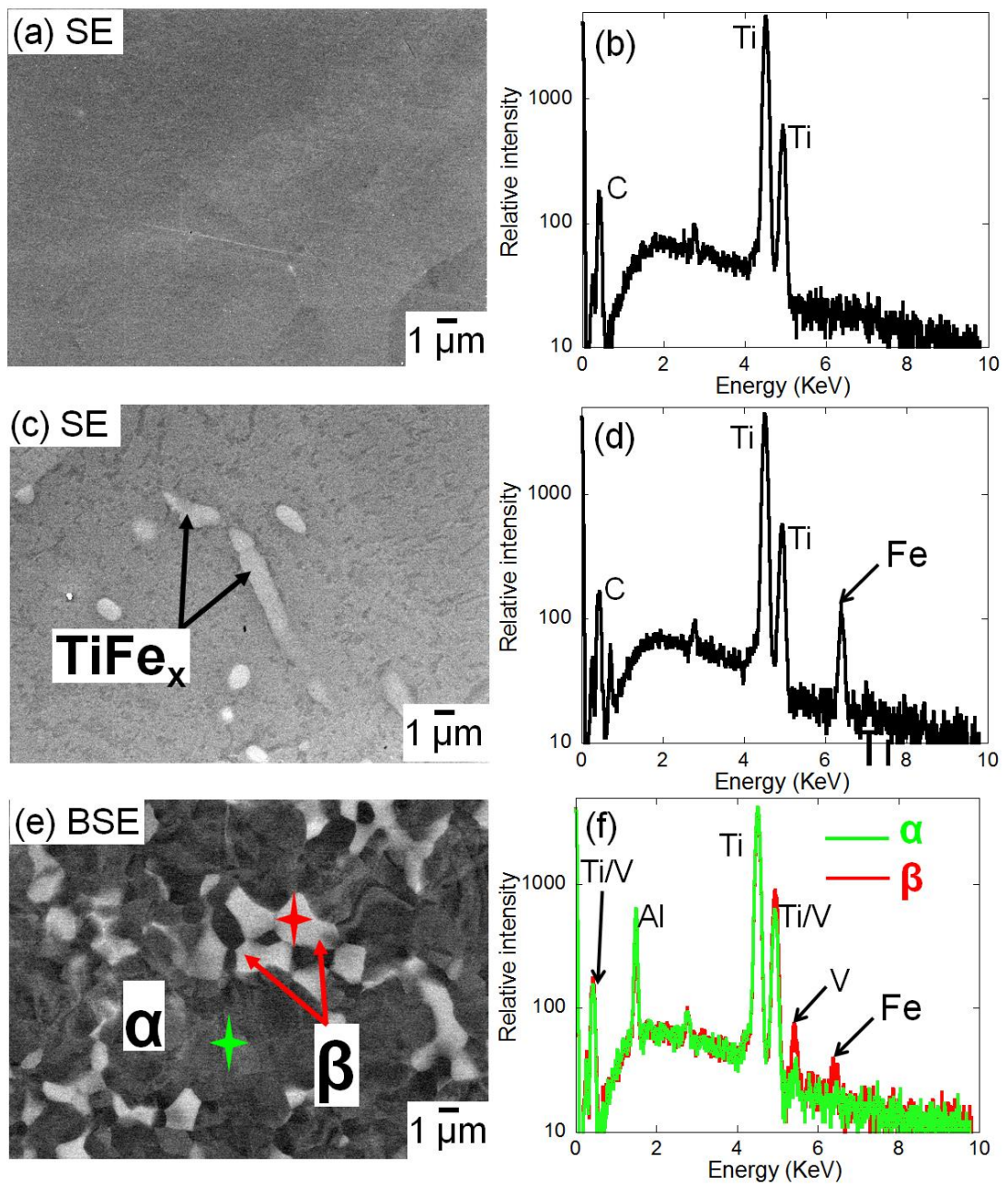
Figure 4-1 SEM image and EDX analysis of the mirror-polished samples of (a) (b) CP-Ti-G2, (c) (d) CP-Ti-G4, (e) (f) Ti6Al4V. SE: secondary electron mode SEM image; BSE: backscatter electron mode SEM image.
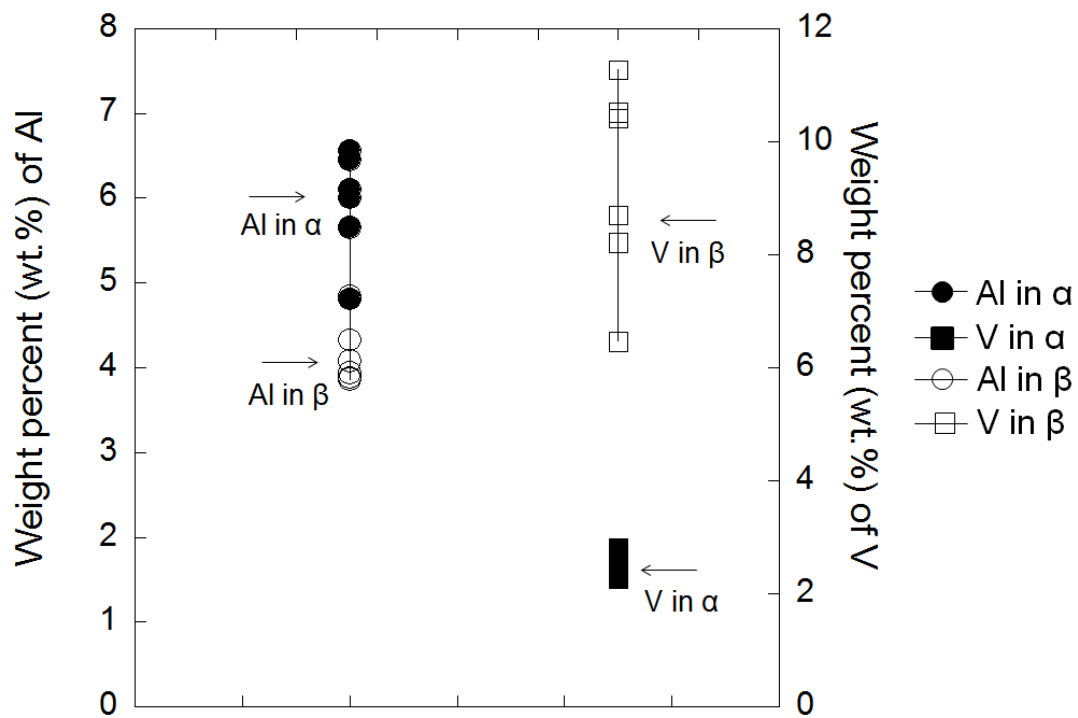
Figure 4-2 The weight percent (wt.%) of Al and V in α phase and β phase of mirror-polished Ti6Al4V based on the EDX analysis of randomly chosen points on the sample.

Table 4-1 The weight percent (wt.%) of Al, V and Fe in α phase and β phase of mirror-polished Ti6Al4V based on the EDX analysis of randomly chosen points on the sample.

	Al in α	Al in β	V in α	V in β	Fe in β
weight percent (wt.%) (randomly chosen points on the sample)	6	4.1	2.3	8.7	0.5
	4.8	3.9	2.8	11.3	0.9
	6.5	3.9	2.4	10.4	0.8
	6.6	4.3	2.7	8.2	0.5
	5.7	3.9	2.4	10.5	0.7
	6.1	4.9	2.6	6.5	0.4
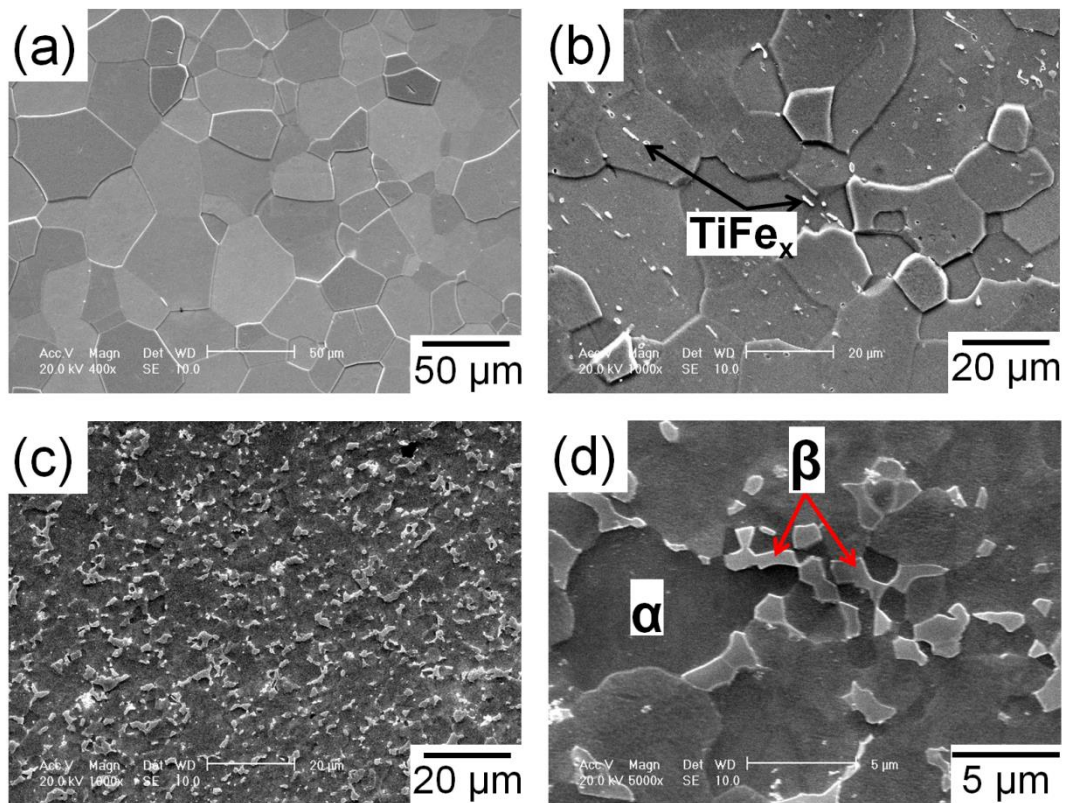
Figure 4-3 Microstructure of etched (a) CP-Ti-G2; (b) CP-Ti-G4; (c) low magnification (d) high magnification of Ti6Al4V in Kroll's etchant (HF (2%) and HNO$_3$ (10%) mixed solution) for ~5 s.

4.3 Effect of HCl on Ti corrosion

4.3.1 OCP measurement

Figure 4-4 shows the OCP as a function of time for mirror-polished CP-Ti-G2, CP-Ti-G4 and Ti6Al4V in naturally-aerated 2 M HCl. The OCP started from ~-350 mV vs. SCE and then abruptly decreased to ~-640 mV vs. SCE for CP-Ti-G2 and CP-Ti-G4 and ~-670 mV vs. SCE for Ti6Al4V, indicating dissolution of the air-formed passive film and surface activation in 2 M HCl.
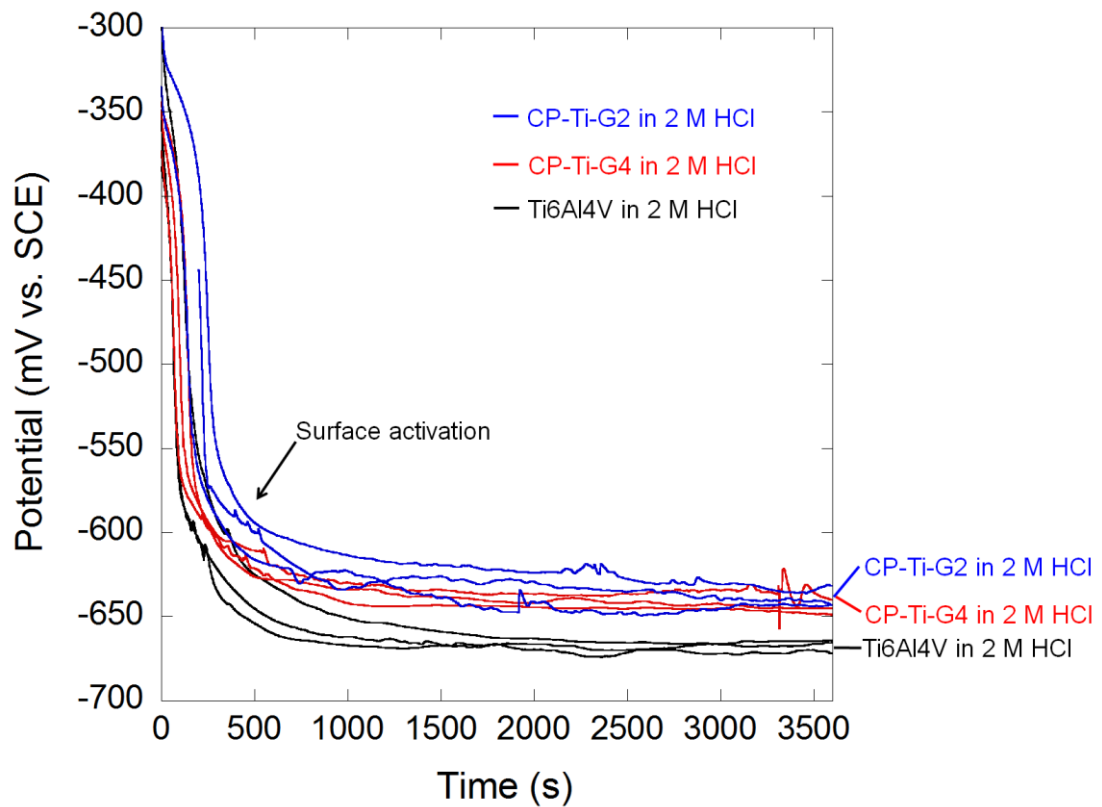
Figure 4-4 OCP as a function of time for mirror-polished CP-Ti-G2, CP-Ti-G4 and Ti6Al4V in 2 M HCl at 37 °C.

4.3.2 Anodic polarisation

Figure 4-5 shows that three grades of Ti (CP-Ti-G2, CP-Ti-G4 and Ti6Al4V) exhibited obvious active peaks during anodic polarisation. The critical anodic current densities (i_{crit}) were similar among the three grades of Ti, while passive current density (i_{pass}) of Ti6Al4V exhibited a slightly higher value when compared with CP-Ti-G2 and CP-Ti-G4 (Figure 4-5). The primary passivation potential (E_{pp}) of the three grades of Ti is ~-510 mV vs. SCE.
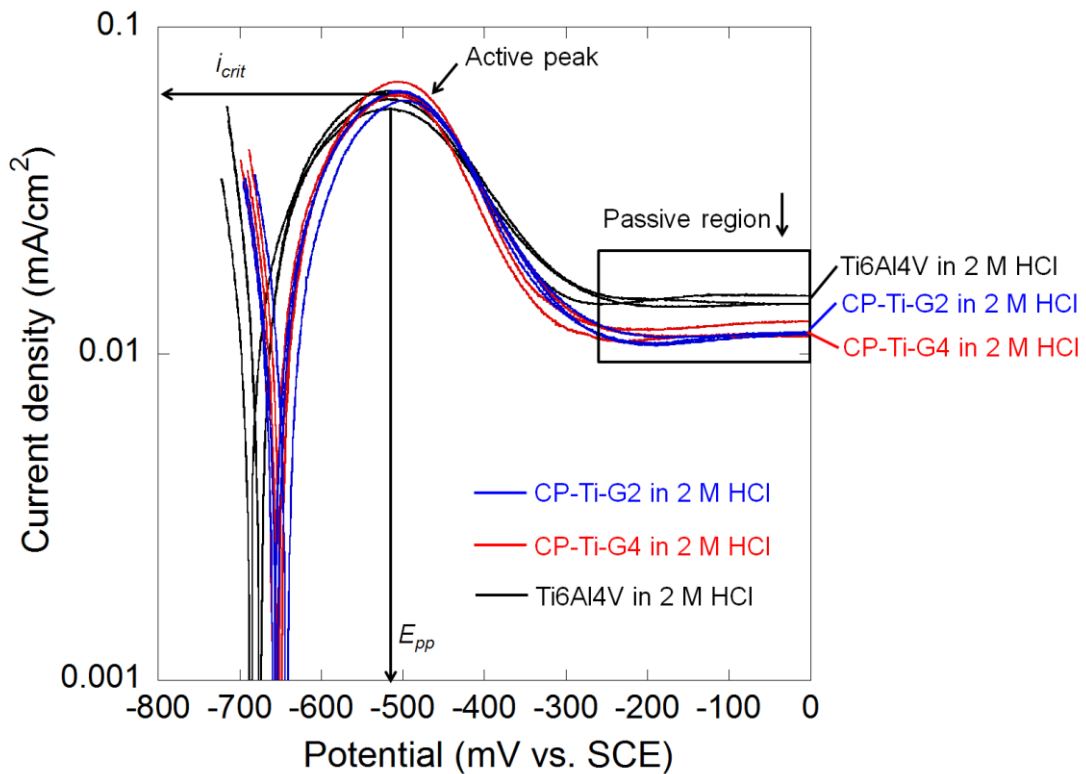
Figure 4-5 Anodic polarisation curves of mirror-polished CP-Ti-G2, CP-Ti-G4 and Ti6Al4V in 2 M HCl at 37 °C (i_{crit}: critical anodic current density; i_{pass}: passive current density; E_{pp}: primary passivation potential).

4.3.3 Temperature dependence of corrosion behaviour of Ti6Al4V

Figure 4-6 shows potentiostatic measurements of mirror-polished Ti6Al4V in 2 M HCl at different temperatures. Figure 4-7 shows that the steady state current density of Ti6Al4V was sensitive to temperature. It can be seen from Figure 4-7a that the corrosion process at 28 °C is slightly different from the others at above 28 °C since the current density of Ti6Al4V was gradually decreased within the measured time until ~4000 s (before reaching a relative steady state). Figure 4-7b shows that the steady state current density of Ti6Al4V was increased with increasing temperature at above 28 °C (i.e. 31 °C, 34 °C, 37 °C, 40 °C and 43 °C).
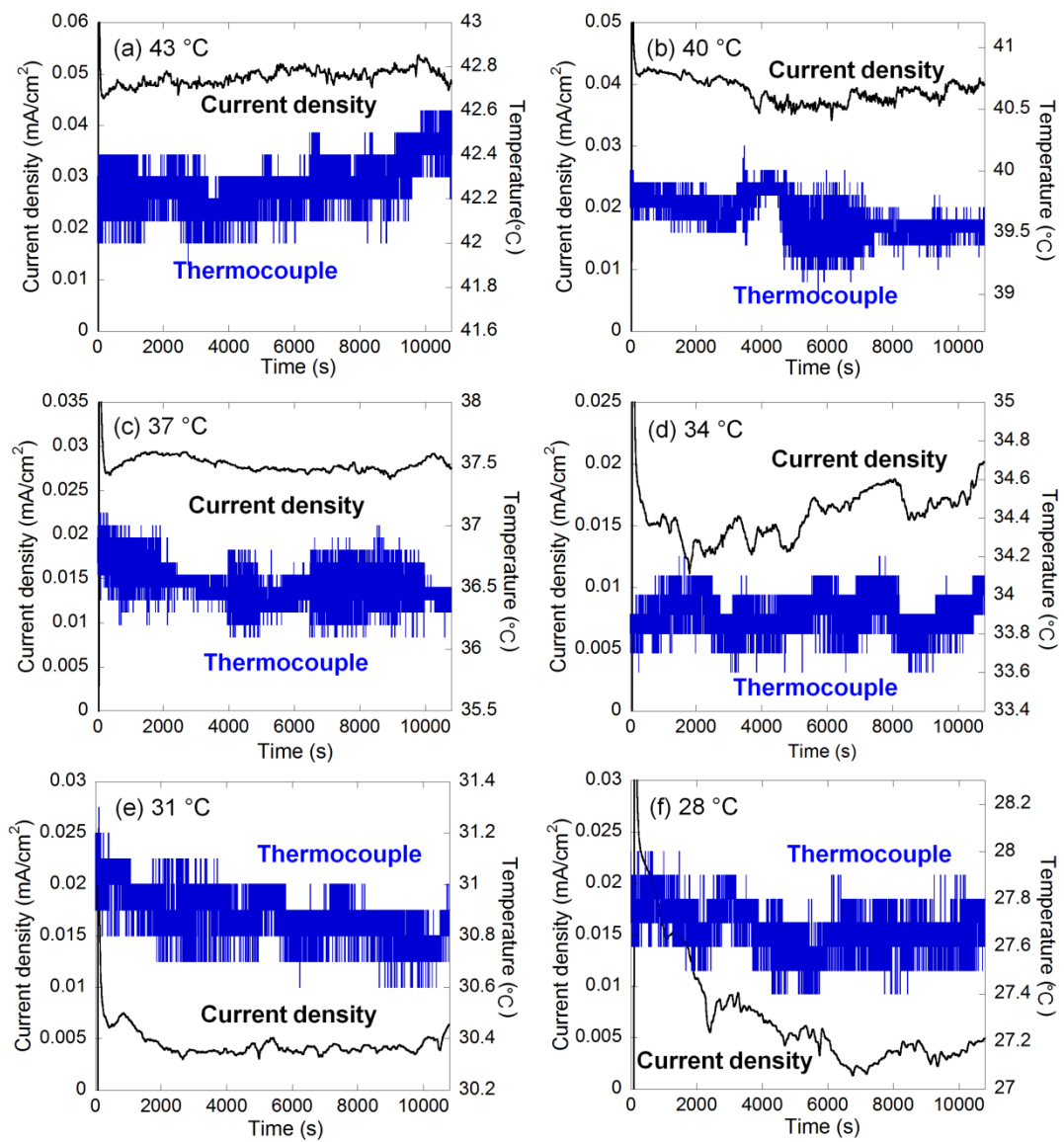
Figure 4-6 Potentiostatic measurements of mirror-polished Ti6Al4V in 2 M HCl at -510 mV vs. SCE for 3 h at different temperatures.
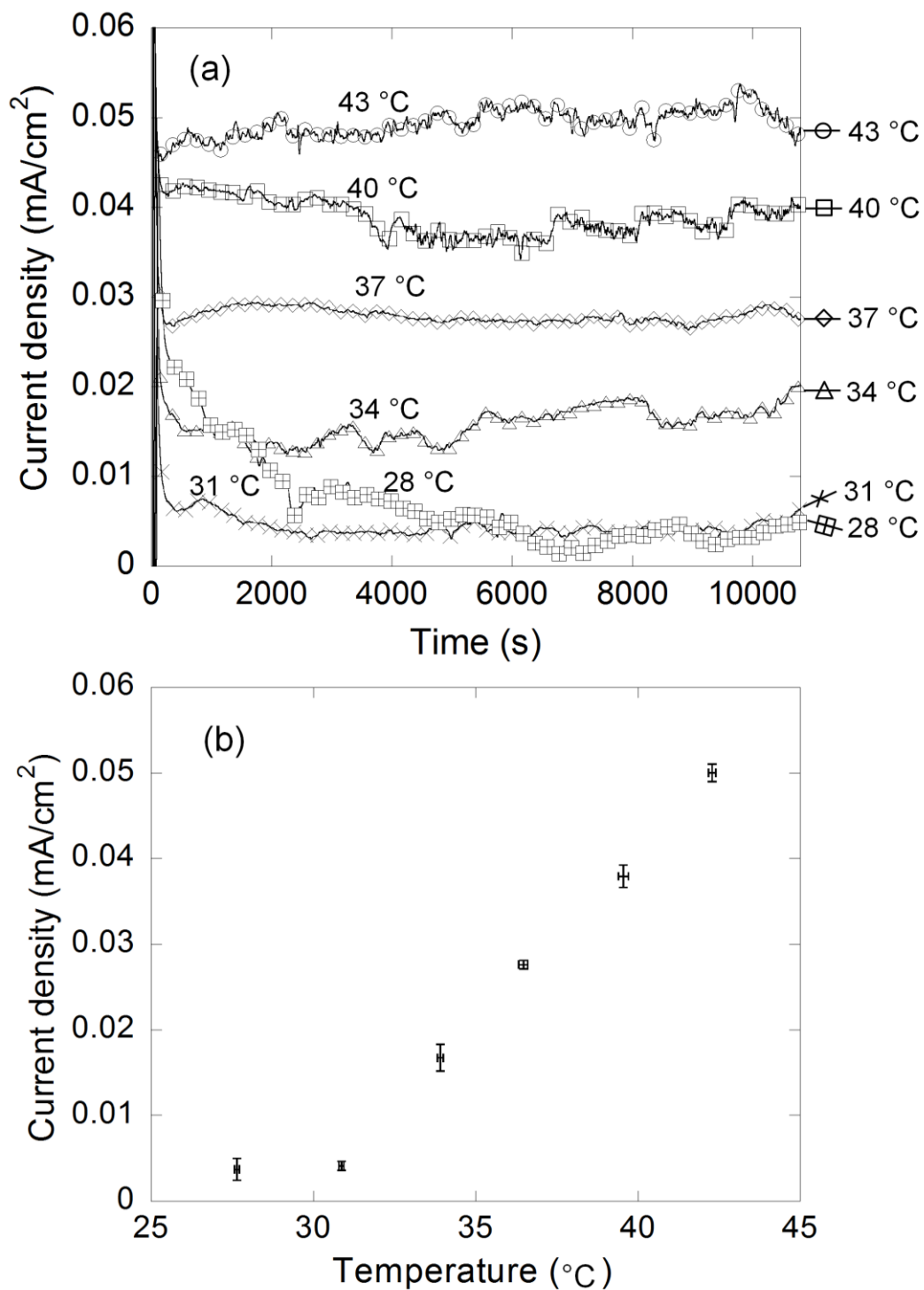
Figure 4-7 (a) Potentiostatic measurements of mirror-polished Ti6Al4V at -510 mV vs. SCE in 2 M HCl at different temperatures and (b) the relationship between the anodic steady state current density and temperature (the values were chosen from 4000 s to 10800 s). Error bars refer to 1 standard deviation.

4.3.4 Surface morphology of Ti6Al4V after potentiostatic tests

Figure 4-8 compares the surface morphologies of mirror-polished Ti6Al4V before and after potentiostatic test at -510 mV vs. SCE (E_{pp} at 37 °C) in 2 M HCl. It can be seen that Ti6Al4V shows a characteristic α/β two phase microstructure based on the BSE image and there is no sign of corrosion on the SE image before the test. However, the α phase of Ti6Al4V was found to be attacked more than the β phase after the test.
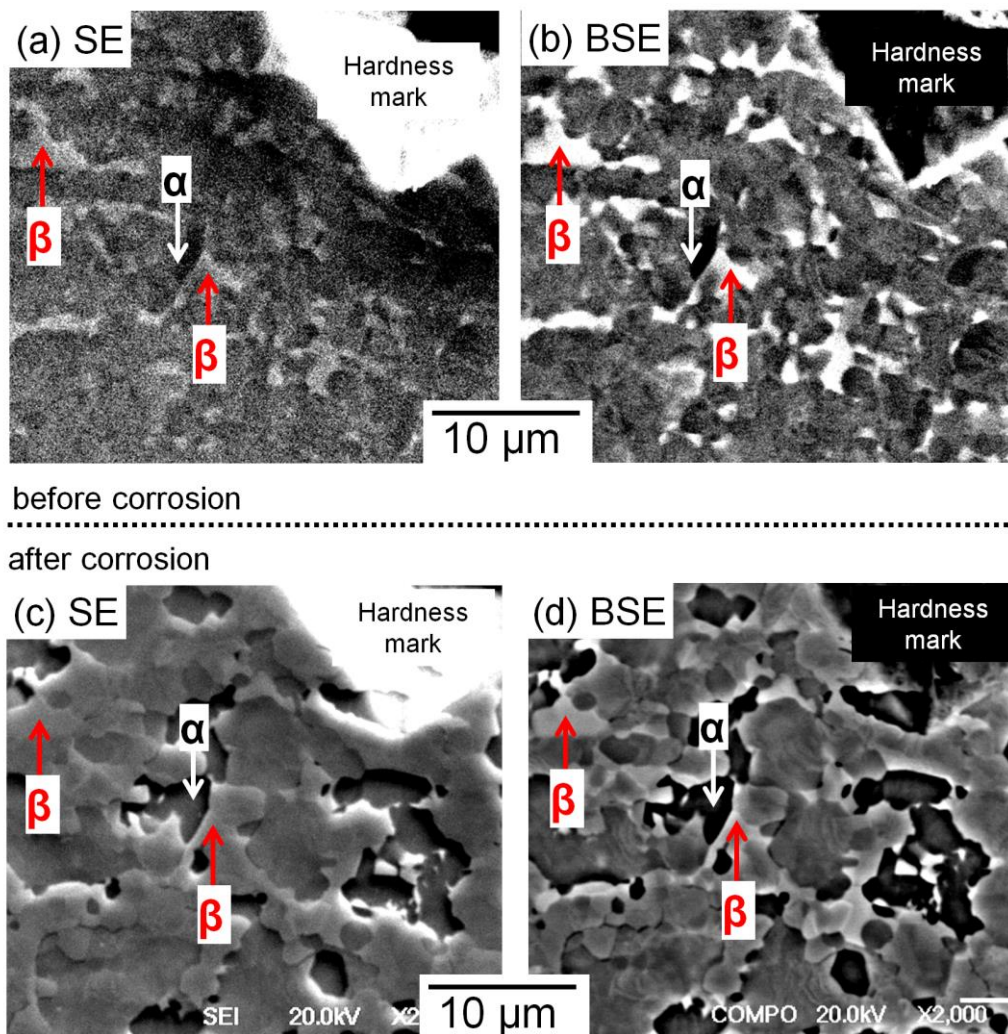
Figure 4-8 SEM image of mirror-polished Ti6Al4V (a) (b) before and (c) (d) after potentiostatic test in 2 M HCl at -510 mV vs. SCE for 30 min at 37 °C. SE: secondary electron mode SEM image; BSE: back scattered electron mode SEM image.

4.4 Effect of pH and LPS on Ti corrosion

4.4.1 Quantification of Ti release

Figure 4-9 and Table 4-2 show that there is no significant difference between the three Ti grades on the magnitude of Ti release into physiological saline following immersion in both LPS-free and LPS containing solutions (Two way ANOVAs demonstrated $p > 0.05$), whereas pH significantly influenced the detected Ti elemental concentration ($p < 0.01$). It also can be seen that Ti release was significantly increased at pH 2 for all Ti grades in comparison with pH ≥ 4.

Further Two-way ANOVAs run independently for each Ti Grade demonstrated that LPS significantly modified the mean Ti concentration of the immersion solution ($p < 0.01$). At pH 2, the addition of LPS caused a significant decrease in the mean Ti concentration in the solution ($p < 0.01$), whereas for the pH of 4-7, LPS addition significantly increased the detected Ti levels ($p < 0.01$) (Figure 4-9). Ti levels in the control immersion solutions with and without LPS were negligible.

The action of LPS as a potential buffer was tested with pH measurements during solution preparation before and after LPS addition. It has been found that the addition of LPS had no detectable effect on the pH of the solution. pH was recorded again following the collection of the test solutions after the immersion period, prior to elemental quantification (Figure 4-9). A significant reduction in the pH of the solutions prepared at pH 7 was observed following the immersion period (to pH 5.8). All remaining immersion solutions were not significantly affected (Figure 4-9).
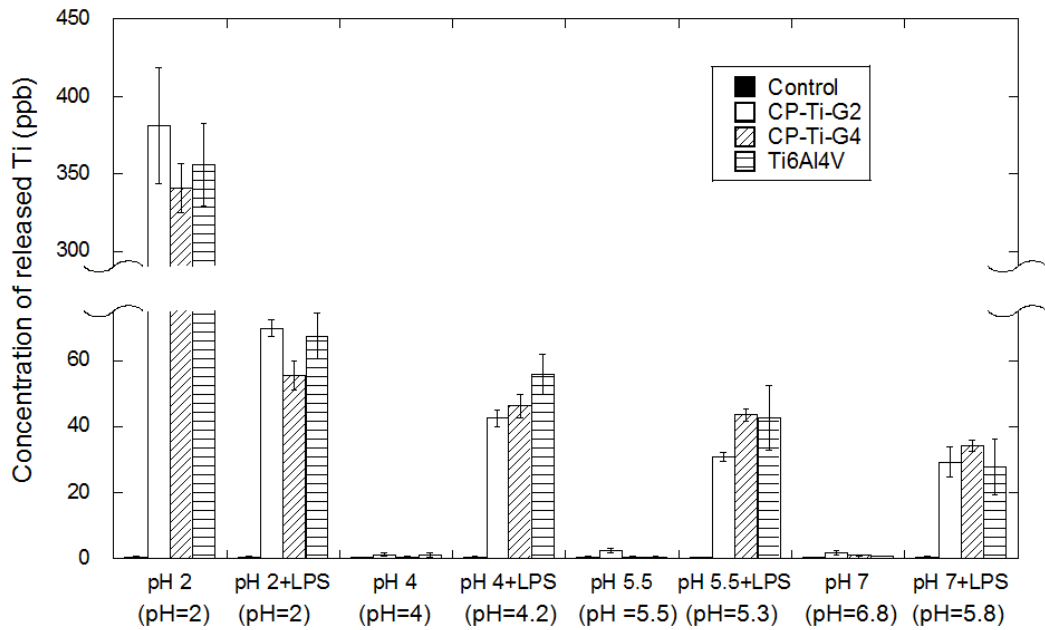
Figure 4-9 Mean concentrations (ppb) of Ti released measured with ICP-MS from mirror-polished CP-Ti-G2, CP-Ti-G4, and Ti6Al4V following immersion in physiological saline with and without LPS for 4 weeks at 37 °C. The final immersion solution pH values measured after the immersion period are provided below the initial values. Error bars refer to 1 standard deviation (n=3); control group: solutions without any Ti disc.

Table 4-2 Mean concentrations and standard deviations (ppb) of Ti released measured with ICP-MS from mirror-polished CP-Ti-G2, CP-Ti-G4, and Ti6Al4V following immersion in physiological saline with and without LPS for 4 weeks at 37°C (n=3); control group: solutions without any Ti disc.

	Control Group	CP-Ti-G2 Group	CP-Ti-G4 Group	Ti6Al4V Group
pH 2	0.5±0.3	380±40	340±20	360±30
pH 2+LPS	0.4±0.3	70±3	56±4	67±7
pH 4	0.2±0.01	1±1	0.5±0.01	1±1
pH 4+LPS	0.4±0.4	43±2	46±4	56±6
pH 5.5	0.4±0.3	3±1	0.5±0.4	0.4±0.2
pH 5.5+LPS	<0.2	31±1	43±2	43±10
pH 7	<0.2	1.7±0.6	1±0.2	0.7±0.1
pH 7+LPS	0.4±0.3	29±5	34±2	28±9

4.4.2 Anodic polarisation

Figure 4-10 shows the anodic polarisation curves of mirror-polished Ti6Al4V and CP-Ti-G4 measured in physiological saline at pH 2 and 4 in the absence and presence of LPS after 1 h immersion at OCP. The OCP of both Ti6Al4V and CP-Ti-G4 showed a relatively small increasing trend in physiological saline with and without LPS (data not shown) and the final OCP value is listed in Table 4-3.

Table 4-3 Mean final OCP and standard deviations of mirror-polished CP-Ti-G4 and Ti6Al4V after 1 h of immersion in physiological saline with and without LPS at 37 °C (n=6).

	CP-Ti-G4 Group (mV vs. SCE)	Ti6Al4V Group (mV vs. SCE)
pH 2	-370±20	-340±20
pH 2+LPS	-390±30	-360±20
pH 4	-330±30	-320±20
pH 4+LPS	-390±50	-380±30

It can be seen from Figure 4-10 that both Ti6Al4V and CP-Ti-G4 showed passive behaviour in physiological saline with and without LPS. A higher anodic current density was measured for both Ti6Al4V and CP-Ti-G4 at pH 2 compared with measurements at pH 4 (Figure 4-10). For the solution adjusted to pH 2 containing LPS, the anodic current density decreased for both Ti6Al4V and CP-Ti-G4 when compared with the LPS-free solution. In contrast at pH 4, an increased anodic current density was observed for both Ti6Al4V and CP-Ti-G4 in the LPS-containing physiological saline when compared with the LPS-free solution (Figure 4-10). It should be noted that the addition of LPS had no detectable effect on the pH of the solution.
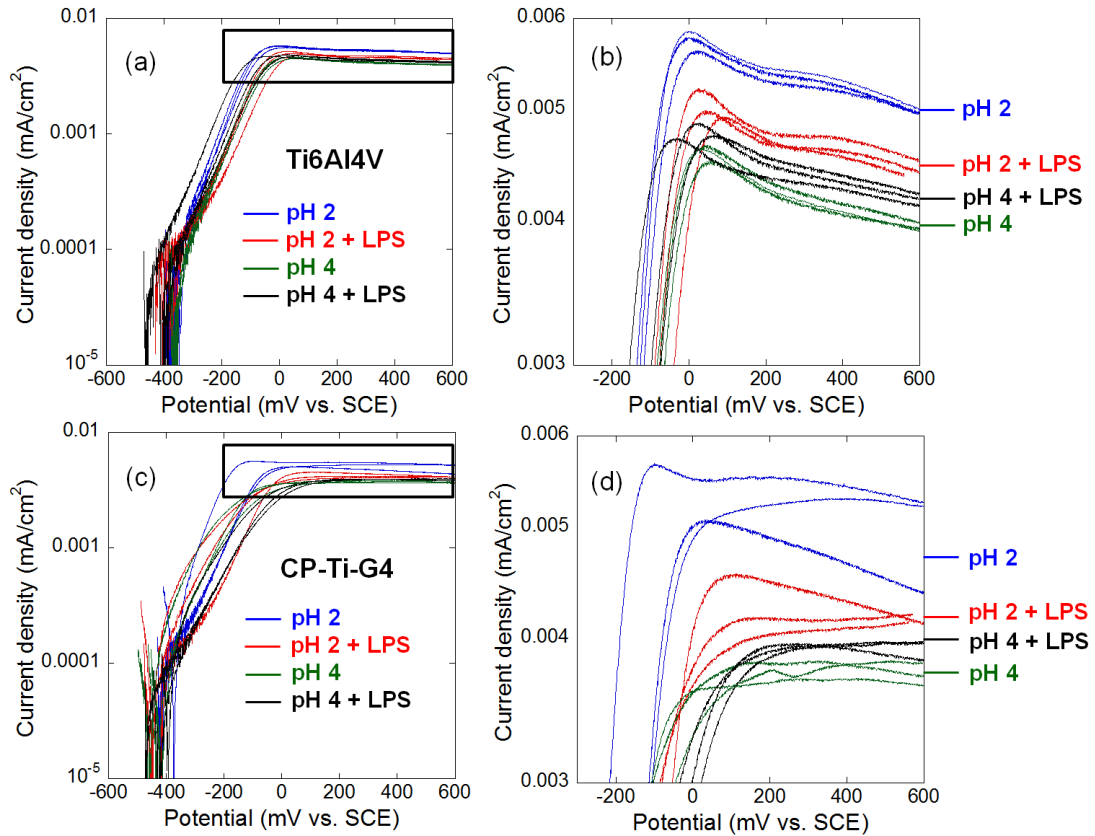
Figure 4-10 Anodic polarisation curves of (a) Ti6Al4V, (b) enlarged image of the region outlined in (a) and (c) CP-Ti-G4, (d) enlarged image of the region outlined in (c) in physiological saline solution adjusted to pH 2 and pH 4 in the absence and presence of LPS at 37 °C. Anodic polarisation curves were measured by sweeping the potential from -50 mV below the OCP to 600 mV vs. SCE at a rate of 1 mV/s.

4.4.3 Cathodic polarisation

Cathodic polarisation curves of Ti6Al4V and CP-Ti-G4 were measured separately from the anodic measurements (Figure 4-11). A higher cathodic current density was observed for Ti6Al4V and CP-Ti-G4 at pH 2 when compared with that at pH 4 (Figure 4-11). In the presence of LPS, the cathodic current decreased slightly for both Ti6Al4V and CP-Ti-G4 at pH 2, but showed a very slight increase at pH 4 when compared with the solution without LPS.
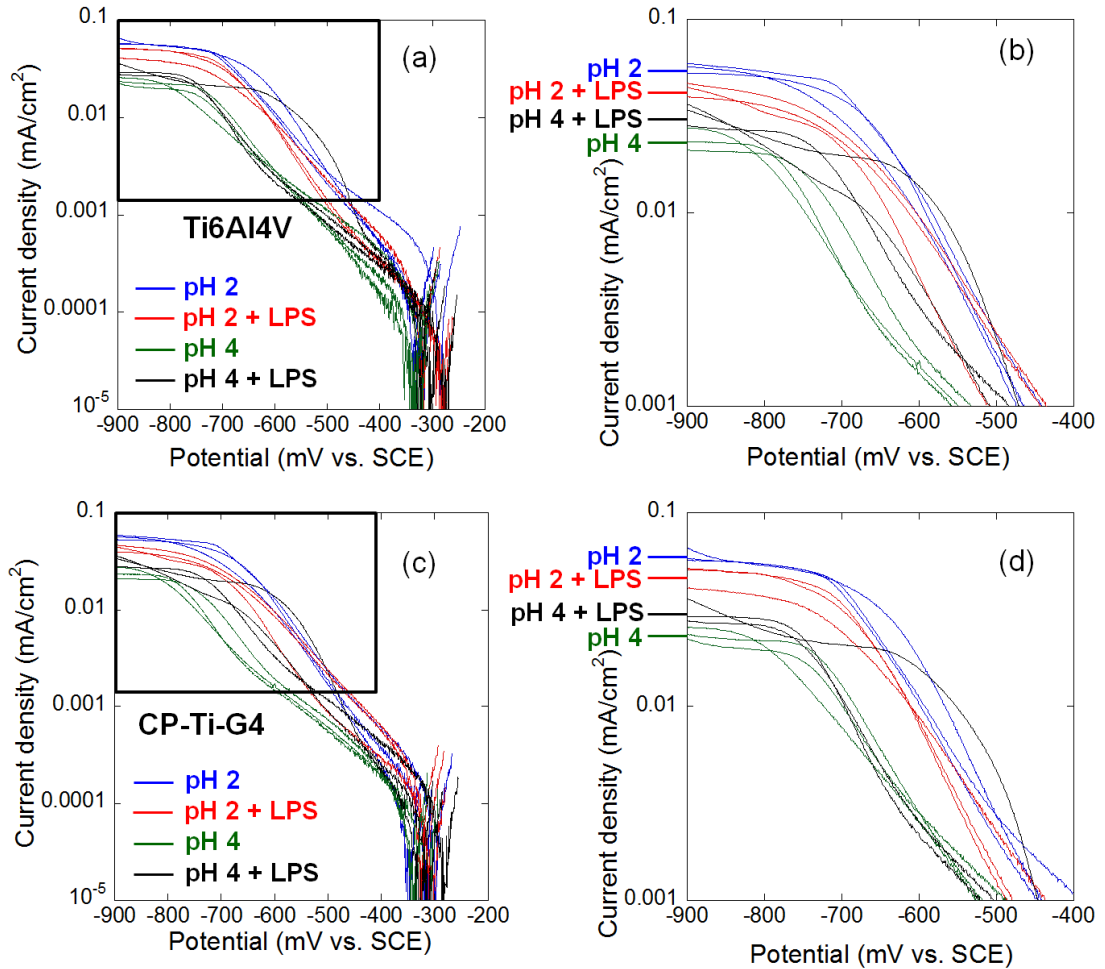
Figure 4-11 Cathodic polarisation curves of (a) Ti6Al4V, (b) enlarged image of the region outlined in (a) and (c) CP-Ti-G4, (d) enlarged image of the region outlined in (c) in physiological saline solution adjusted to pH 2 and pH 4 in the absence and presence of LPS at 37 °C. Cathodic polarisation curves were obtained by sweeping the potential from 50 mV above OCP to -900 mV vs. SCE at a rate of 1 mV/s.

4.4.4 Potentiostatic study

Figure 4-12 shows potentiostatic measurements of mirror-polished Ti6Al4V and CP-Ti-G4 in physiological saline at a pH 2 and 4 with and without the addition of LPS. The potential was maintained at 600 mV vs. SCE, which is in the passive region. The solution was stirred at intervals to ensure complete mixing. LPS was added just prior to stirring at ~1000 s for some of the measurements. It is clear that the passive current density of both grades of Ti was greater

at pH 2 than at pH 4 (Figure 4-12). After the addition of LPS, the current density measured for samples immersed at pH 2 decreased rapidly (within 1000 s) to the value found for samples immersed at pH 4. However, LPS was found to have no effect on the passive current density at pH 4. It should be noted that the addition of LPS had no detectable effect on the pH of the solution.
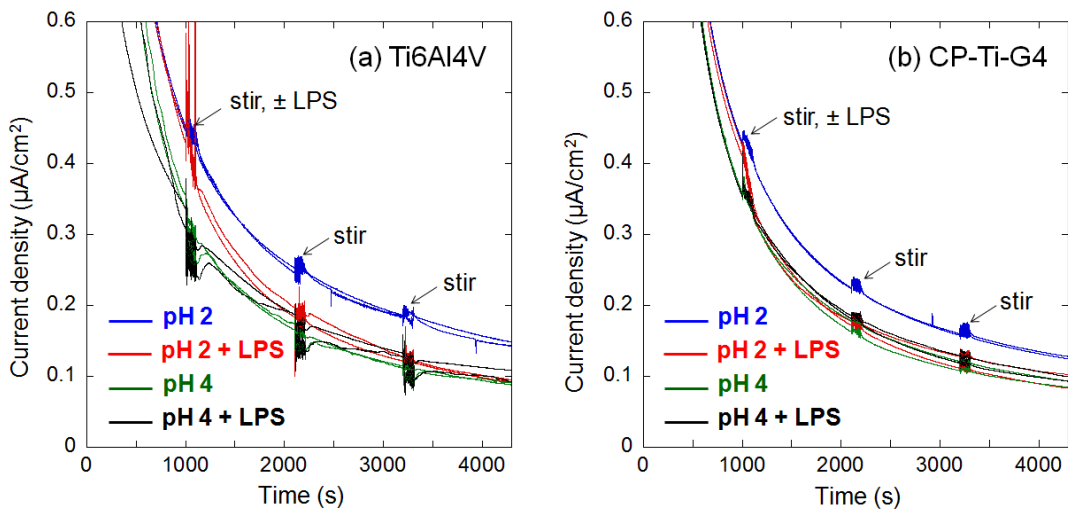
Figure 4-12 Potentiostatic study (600 mV vs. SCE) of (a) Ti6Al4V and (b) CP-Ti-G4 in physiological saline adjusted to pH 2 or pH 4 at 37 °C; the solution was stirred for ~100 s at ~1000 s intervals to ensure mixing; for some experiments, LPS (in physiological saline) was added at ~1000 s immediately before stirring to give a final concentration of 150 μg/mL.

4.4.5 Surface morphology after immersion tests in physiological saline

Figure 4-13 shows the surface morphologies of all three grades of Ti in the as-polished condition and following immersion for 4 weeks in physiological saline at pH 7 and pH 2. No significant difference on the surface morphology before and after immersion was observed even for physiological saline at pH 2, which showed the highest metal release for all of the conditions studied with and without LPS (Figure 4-9).
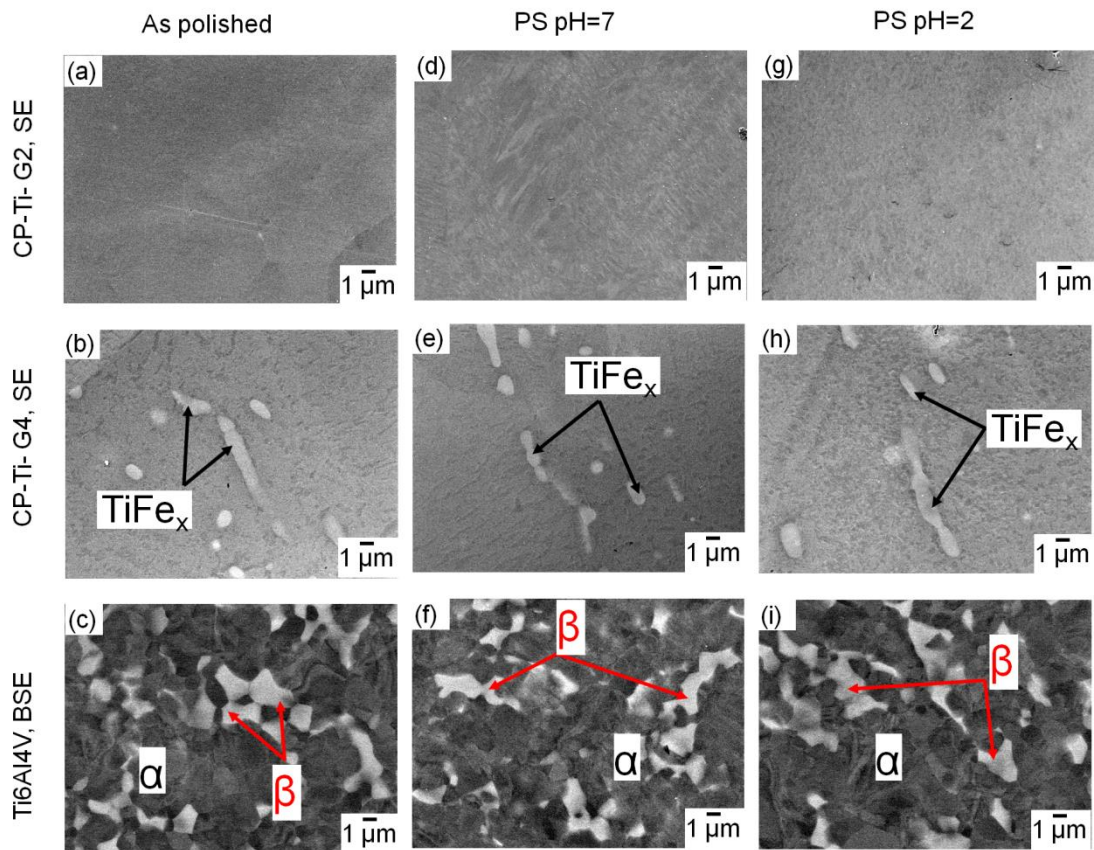
Figure 4-13 SEM images of mirror-polished surfaces of Ti and its alloy: CP-Ti-G2, CP-Ti-G4 and Ti6Al4V before and after immersion for 4 weeks at 37 °C in physiological saline (PS) adjusted to pH 7 or pH 2. SE: secondary electron mode SEM image, BSE: backscatter electron mode SEM image.

4.5 Discussion

4.5.1 Effect of HCl on Ti corrosion

The current study demonstrated that three grades of Ti were activated in naturally-aerated 2 M HCl, which agrees with other studies, i.e. Ti6Al4V in naturally-aerated 1.5 M HCl [43] and CP-Ti in deaerated 1-10 M HCl [53]. It has also been reported that there was no activation of CP-Ti at pH 1 (0.1 M HCl) after 12 h immersion at open circuit [53].

The E-pH diagram (Pourbaix diagram) at 37 °C (Figure 4-14) provides preliminary information about the thermodynamically stable state of Ti^{3+} within a wide range of potentials at pH <1.5 [175]. In the presence of 2 M HCl (pH -0.3), OCP of three grades of Ti were between -640 mV and -670 mV vs. SCE (Figure 4-4) (the SCE scale was converted to NHE by adding 240 mV [48]), in which Ti^{3+} is the thermodynamically stable state, and therefore chemical dissolution of Ti oxide passive film occurred at the first stage before surface activated, resulting in abrupt drop in OCP. The dropped OCP values of three grades of Ti also agree with other studies [43, 53, 176].

In addition, a clear characteristic active-passive transition was exhibited during anodic polarisation in 2 M HCl. Similar E_{pp} and i_{crit} have also been reported, i.e. Ti6Al4V in aerated 1.5 M HCl [43] and in deaerated 5% (1.3 M) HCl [90] at 37 °C. Higher i_{crit} of CP-Ti was reported in Yu and Scully's studies [54, 175] since a high concentration of HCl was used (5 M HCl).
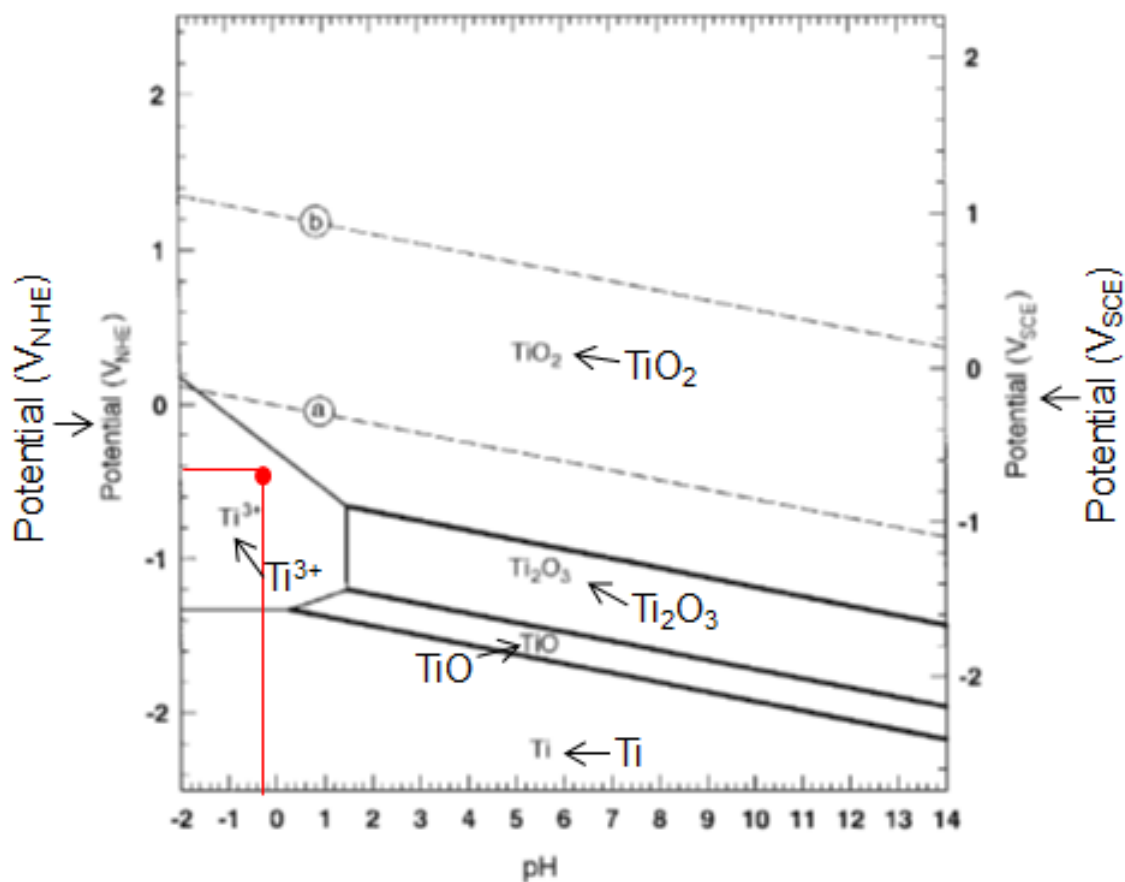
Figure 4-14 E-pH diagram (Pourbaix diagram) for Ti-H₂O system at 37 °C. Ti species are at an activity of 10^{-6}. Line (a) and (b) refers to the regions of water stability [175]. NHE: normal hydrogen electrode. The red spot shows the OCP of CP-Ti and Ti6Al4V in this study.

4.5.2 Temperature dependence of Ti6Al4V in 2 M HCl

The steady state current density of Ti6Al4V at -510 mV vs. SCE (E_{pp} at 37 °C) has been observed to be increased with increasing temperature at above 28 °C (i.e. 31 °C, 34 °C, 37 °C, 40 °C and 43 °C) (Figure 4-7). Assuming the corrosion process of Ti6Al4V in this study can be analysed by a simple Arrhenius expression (Equation 4-1) based on that the corrosion rate can be represented by current density:

Equation 4-1 $\ln i = a - \dfrac{E_a}{RT}$

where E_a is the activation energy of the corrosion process during potentiostatic polarisation, T is the absolute temperature (K) and R is the gas constant (8.3 J/mol·K).
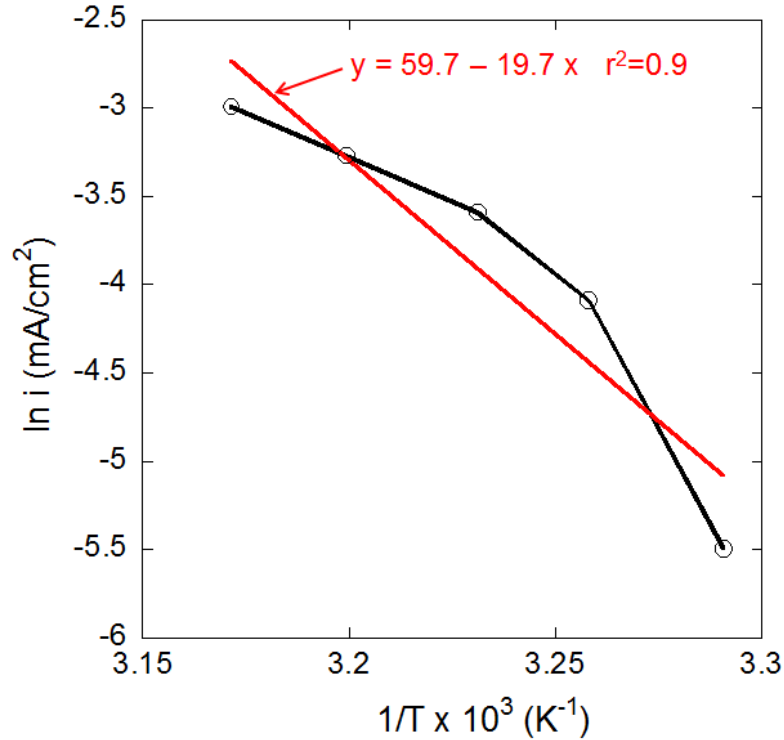
Figure 4-15 A plot of steady state current at -510 mV vs. SCE vs. temperature for mirror-polished Ti6Al4V in 2 M HCl. The red line shows the fitted linear Arrhenius plot.

It can be seen from Figure 4-15 that the relationship between natural logarithm of current density and reciprocal temperature is non-linear (black line in Figure 4-15) and does not obey linear Arrhenius expression. The corrosion process of Ti6Al4V cannot be analysed by a simple Arrhenius expression. However, to compare with other works [53, 56, 90], a fitted Arrhenius plot was conducted (red line in Figure 4-15) and the calculated activation energy was 164 kJ/mol.

Different activation energies were also reported (e.g. 27 kJ/mol by Atapour et al. [90], 57 kJ/mol by Yu et al. [53] and 63 kJ/mol by Blackwood et al. [56]), which may be attributed

to the different methods used. The activation energies reported by Yu et al. [53] and Blackwood et al. [56] are related to the dissolution/corrosion of Ti oxide on CP-Ti in deaerated 5 M HCl or 3 M H_2SO_4 based on the surface activation time length during immersion at OCP, while Atapour et al. [90] compared i_{corr} of Ti6Al4V in deaerated 5% HCl (1.3 M) by using the Tafel extrapolation method on potentiodynamic polarisation curves.

The corrosion process in this study is complicated and not controlled by a single mechanism. As expected, active dissolution and possible passivation may co-exist since the applied potential is the primary passivation potential (-510 mV vs. SCE). In addition, the applied potential was not far from OCP (-670 mV vs. SCE), where cathodic reaction may also take place. Therefore, the current corrosion process of Ti6Al4V is different from the previously reported processes [53, 56, 90], which may lead to different activation energies.

4.5.3 Surface morphology of Ti6Al4V after potentiostatic test in 2M HCl

The current study demonstrated that the α phase of Ti6Al4V was preferentially attacked relative to the β phase in 2 M HCl at 37 °C after potentiostatic measurement at E_{pp} (-510 mV vs. SCE). This differs from Atapour's finding [105] that the β phase of Ti6Al4V-ELI (similar to Ti6Al4V but contains lower content of C, N, O and Fe) was preferentially attacked after exposure to 5 M HCl at 37 °C for 50 h. However, there is no over potential in their study. In addition, it has been reported that the preferential dissolution of α phase of Ti-15Mo (with α+β phases microstructure) was observed at potentials in the active region in 40% H_2SO_4 at 80 °C [177]. The α phase of Ti-15Mo-3Nb-3Al was also found to be preferentially attacked during anodic polarisation in 5 M HCl at 37 °C [175].

For Ti6Al4V used in this study, there is more Al and less V in α phase, while there is more V but less Al in β phase (Table 4-1 and Figure 4-2). Al is reported to have a detrimental influence on the passivity and corrosion resistance of α phase Ti in 5 M HCl [175], while dissolution of V coupled with conduction channels is also considered to be detrimental for the passive film in Hank's solution [178]. It is also suggested that both Al and V alloying component have bad effect on Ti passivity in 40% H_2SO_4 [177]. Considering the condition in this study, both active dissolution and possible passivation of Ti6Al4V would be expected. The detrimental effect of Al may dominate over other factors, resulting in preferential attack of α phase.

It is noted that there is also some Fe content (Table 4-1) in the β phase of Ti6Al4V in this study. Fe-containing β phase has been reported to possibly initiate hydride formation and proton reduction in acidic environment [5, 179]. It is likely that the cathodically active hydride sites on β phase co-exist with anodically active of α phase, which further result in preferential dissolution of α phase.

4.5.4 Effect of pH and LPS on Ti corrosion

It can be seen from Figure 4-9 that higher Ti release at pH 2 was observed compared with pH 4-7, consistent with previous work showing the observation of distinctly reduced Ti release at pH 4 and above [89, 93, 94]. However, the addition of LPS to the immersion solution significantly modified this pattern of Ti release, promoting corrosion at pH ≥4 but inhibiting it at pH 2, which has not been reported previously. It has been previously demonstrated that the solubility of Ti oxide surface layer is largely independent of acidity at pH ≥4 [89] and therefore the direct effect of LPS in lowering the solution pH is not considered to account for the increased Ti release at pH ≥4. Despite the differences in microstructure and composition

94

between the three grades of Ti studied, no differences in Ti release were observed in the immersion conditions used and, accordingly, only CP-Ti-G4 and the alloy Ti6Al4V were studied in electrochemical tests.

The increased solubility of the passive oxide film on Ti alloys in highly acidic conditions (pH 2) was confirmed by anodic polarisation and potentiostatic measurements on CP-Ti-G4 and Ti6Al4V samples. When physiological saline solution was maintained at pH 2, shifts towards higher anodic currents, higher cathodic currents and higher passive currents were all observed when compared with pH 4 (Figure 4-10, Figure 4-11 and Figure 4-12). Following addition of LPS to the pH 2 solution, the anodic, cathodic and passive currents were all decreased (Figure 4-10, Figure 4-11 and Figure 4-12). In contrast, addition of LPS to the pH 4 solution increased the anodic and cathodic currents when compared with an LPS-free environment (Figure 4-10 and Figure 4-11). There was no significant change for the passive current at pH 4 with and without the addition of LPS for both Ti6Al4V and CP-Ti-G4 (Figure 4-12).

It is generally established that organic molecules can affect the corrosion behaviour of metals mediated by adsorption onto the surfaces and/or chelation with the released dissolved ions [19, 20, 24, 25, 95, 96]. Studies on serum proteins interaction with Ti surfaces, using potential sweep techniques, have established that surface adsorption processes are potential dependent [95]. Further electrochemical tests have demonstrated that serum proteins such as albumin and fibrinogen can decrease the cathodic current, but also decrease or increase the anodic current [19, 20, 24]. These findings have been used to support a proposal that mechanistically, the protein has a covering and/or blocking effect [20].

LPS are large molecules that are found in part of the cell walls of Gram-negative bacteria and comprise a lipid covalently bonded to a polysaccharide. LPS has been shown to have a high

affinity for adsorption onto Ti surfaces [131], and in the current study it is likely that LPS will rapidly adsorb onto the surface of the Ti samples following immersion. The observed decrease in corrosion at pH 2 can be explained by the covering of potential reaction sites by the adsorbed molecules, which may further block ion release during the corrosion process. LPS has been shown to present different charges dependent on solution pH, and in the current study, adsorption may have been promoted most at pH 2 and least at neutral conditions [180]. Furthermore, chain mobility, aggregation and the structure of LPS have been shown to be influenced by the presence of metal cations and pH, and this may further act to modulate the anticipated surface adsorption and/or the covering of reaction sites [181]. However, this mechanism does not fully explain the promoted corrosion found in the presence of LPS at pH ≥ 4 for the long-term immersion tests. Although this has not been specifically demonstrated with Ti, LPS is considered to readily complex with metal cations at its polysaccharide component [182, 183]. It is possible that complexation of Ti ions on the surface of the passive film may enhance dissolution. However, this effect is smaller than the suppression of dissolution at pH 2. It should be noted that addition of LPS did not increase the passive current density at pH 4 (expected if the passive film undergoes significant dissolution) in the short-term potentiostatic tests. The decrease in cathodic reactivity on addition of LPS at pH 2 may again be associated with adsorption of LPS on Ti [131]. However, the small increase in cathodic reactivity on addition of LPS at pH 4 is more surprising. It is possible that complexation by LPS may lead to a thinner passive oxide film, allowing easier electron transfer for the cathodic reaction.

The environment of many Ti implants including dental implants and cranial anchorage devices may contain LPS due to the presence of Gram-negative bacteria in the surface biofilm. LPS has

been shown to have a strong affinity to Ti, and the current study demonstrates a significant increase in Ti corrosion at the mildly acidic and neutral pH levels which are commonly encountered in the peri-implant environment. However, the pH measured in sites of mechanically-assisted crevice corrosion (between modular components and in crevices) may be considerably lower approaching pH 2.5 [7]. Under these conditions, LPS may act to suppress dissolution of Ti.

4.6 Conclusions

The effect of pH and LPS on corrosion behaviour of Ti alloys was investigated using solution analysis, surface analysis and electrochemical tests, and it was determined whether LPS, an important mediator of peri-implant inflammation, promotes or inhibits corrosion of three grades of Ti. The effect of 2 M HCl was also studied by electrochemical tests.

1.   Corrosion of Ti6Al4V in 2 M HCl is temperature dependent and the steady state current density at -510 mV vs. SCE (the primary passivation potential at 37 °C) becomes higher with increasing temperature.

2.   The α phase of Ti6Al4V is preferentially dissolved relative to the β phase after potentiostatic measurement at primary passivation potential (E_{pp}) in 2 M HCl at 37 °C.

3.   LPS increases corrosion of CP-Ti-G4 and Ti6Al4V in physiological saline at pH 4-7, increasing the rate of both the anodic reaction and the cathodic reaction.

4.   LPS inhibits corrosion of CP-Ti-G4 and Ti6Al4V at pH 2 in physiological saline solution, decreasing both the anodic and cathodic reactions.

5   EFFECT OF H$_2$O$_2$ AND ALBUMIN ON TI CORROSION

5.1 Introduction

The aim of the work described in this chapter is to investigate the corrosion behaviour of three grades of Ti (CP-Ti-G2, CP-Ti-G4 and Ti6Al4V) in the presence of H$_2$O$_2$, which is an important inflammation product in the peri-implant environment. The corrosion behaviour of Ti6Al4V was also studied in the presence of albumin, which is an abundant protein found in blood and extracellular environments. The influence of the combination of H$_2$O$_2$ and albumin on corrosion of Ti6Al4V was also investigated. Solution analysis, surface analysis and electrochemical tests were used to investigate the corrosion of Ti.

5.2 Effect of H$_2$O$_2$ on Ti corrosion

5.2.1   Solution analysis

Figure 5-1 shows that the concentrations of Ti released from all three grades of Ti were increased in the presence of H$_2$O$_2$. Ti levels in the control (no Ti disc) solutions were negligible. The amount of Ti released from the three Ti grades increased with the concentration of H$_2$O$_2$ (Table 5-1 and Figure 5-1). The concentration of Ti released from Ti6Al4V was ten to hundred times higher than that from CP-Ti-G2 and CP-Ti-G4 for the same concentrations of H$_2$O$_2$, while there was no significant difference between the Ti released from CP-Ti-G2 and CP-Ti-G4 for all H$_2$O$_2$ concentrations.

Observation of the Ti samples following immersion identified yellow precipitates in the 10% H$_2$O$_2$ solutions after 4 weeks immersion for all three grades of Ti, probably due to detachment of the surface corrosion product (Ti-H$_2$O$_2$ complex [184]). Therefore, the released Ti

concentrations from three grades of Ti were not measured in 10% H_2O_2 to avoid an inaccuracy in reporting.
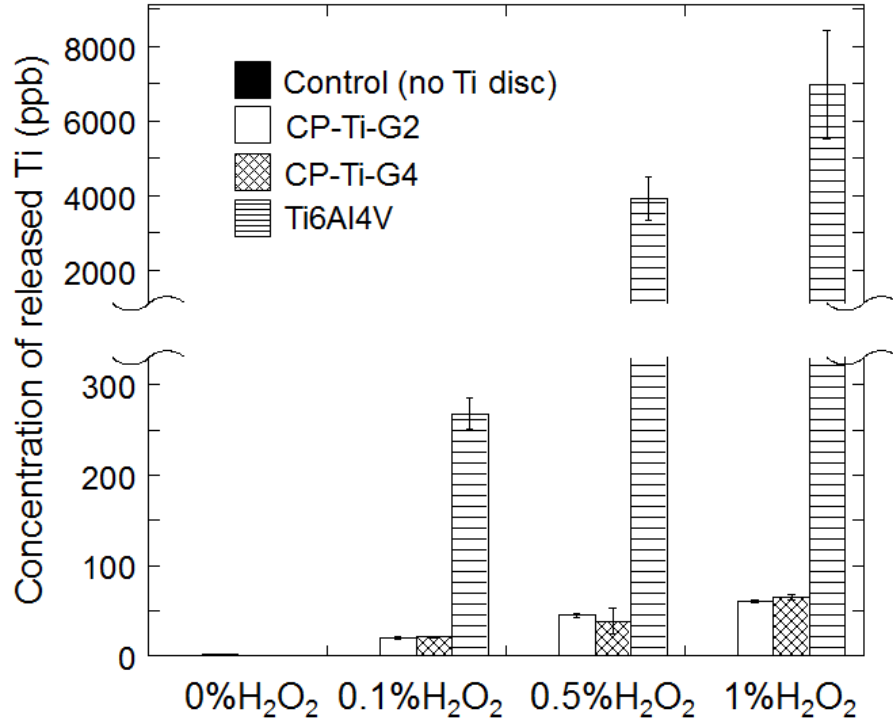
Figure 5-1 Mean concentrations (ppb) measured with ICP-MS of Ti released from mirror-polished CP-Ti-G2, CP-Ti-G4 and Ti6Al4V following immersion in physiological saline (0.15 M NaCl) with and without different levels of H_2O_2 for 4 weeks at 37 °C. Error bars refer to 1 standard deviation (n=3); control group: solutions without any Ti disc.

Table 5-1 Mean concentrations and standard deviations (ppb) measured with ICP-MS of elemental Ti released from mirror-polished CP-Ti-G2, CP-Ti-G4 and Ti6Al4V following immersion in physiological saline (0.15 M NaCl) with and without different levels of H_2O_2 for 4 weeks at 37 °C (n=3); control group: solutions without any Ti disc.

	Control group	CP-Ti-G2 group	CP-Ti-G4 group	Ti6Al4Vgroup
0% H_2O_2	<0.2	1.7±0.6	1±0.2	0.7±0.1
0.1% H_2O_2	<0.2	20±2	21±0.7	270±20
0.5% H_2O_2	0.4±0.2	45±2	40±10	3900±600
1% H_2O_2	0.2±0.1	60±1	65±3	7000±1000

Figure 5-2 and Table 5-2 show the concentrations of V and Al released from Ti6Al4V. It can be seen that the amount of released V and Al increased with increasing concentration of H_2O_2 demonstrating a similar pattern to the Ti released from Ti6Al4V. There appeared to be increased V release when compared with Al, especially following immersion in lower concentrations of H_2O_2.
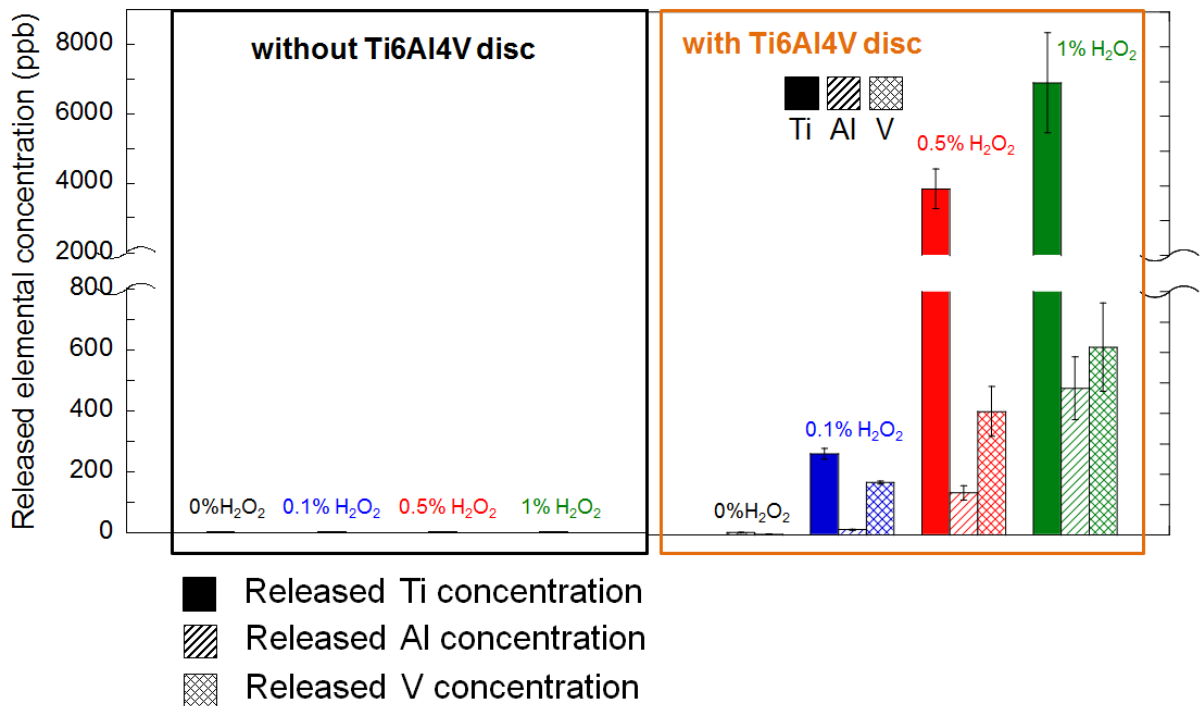
Figure 5-2 The mean concentrations (ppb) measured with ICP-MS of Ti, Al and V released from mirror-polished Ti6Al4V following immersion in physiological saline (0.15 M NaCl) with and without different levels of H_2O_2 for 4 weeks at 37 °C. Error bars refer to 1 standard deviation (n=3).

Table 5-2 The mean concentrations and standard deviations (ppb) measured with ICP-MS of Al and V released from mirror-polished Ti6Al4V following immersion in physiological saline (0.15 M NaCl) with and without different levels of H_2O_2 for 4 weeks at 37 °C (n=3); control group: solutions without any Ti disc.

	Control-Al	Ti6Al4V-Al	Control-V	Ti6Al4V-V
0% H_2O_2	1.4±0.2	7±1	<0.2	3±1
0.1% H_2O_2	1.3±0.01	17±2	0.3±0.01	173±5
0.5% H_2O_2	1.7±0.3	140±20	0.3±0.05	410±80
1% H_2O_2	1.6±0.2	500±100	0.3±0.04	600±100

5.2.2 Surface morphology

5.2.2.1 Characterisation after immersion tests

When Ti samples were immersed in physiological saline without H_2O_2 for 4 weeks, the original shiny polished appearance was unchanged, while discoloration of three grades of Ti was observed after immersion tests in H_2O_2-containing solutions (Figure 5-3).

Figure 5-3 Images of mirror-polished CP-Ti-G2, CP-Ti-G4 and Ti6Al4V following immersion in physiological saline with and without different levels of H_2O_2 for 4 weeks at 37 °C.

Figure 5-4 shows that the surface morphologies of the three grades of Ti did not demonstrate significant changes after immersion in physiological saline when compared with the original surfaces (Figure 4-1). CP-Ti-G2 showed no significant second phase particles (Figure 5-4a), whereas CP-Ti-G4 contained $TiFe_x$ intermetallic particles (Figure 5-4f). Ti6Al4V showed the characteristic α phase and β phase microstructure (Figure 5-4k).
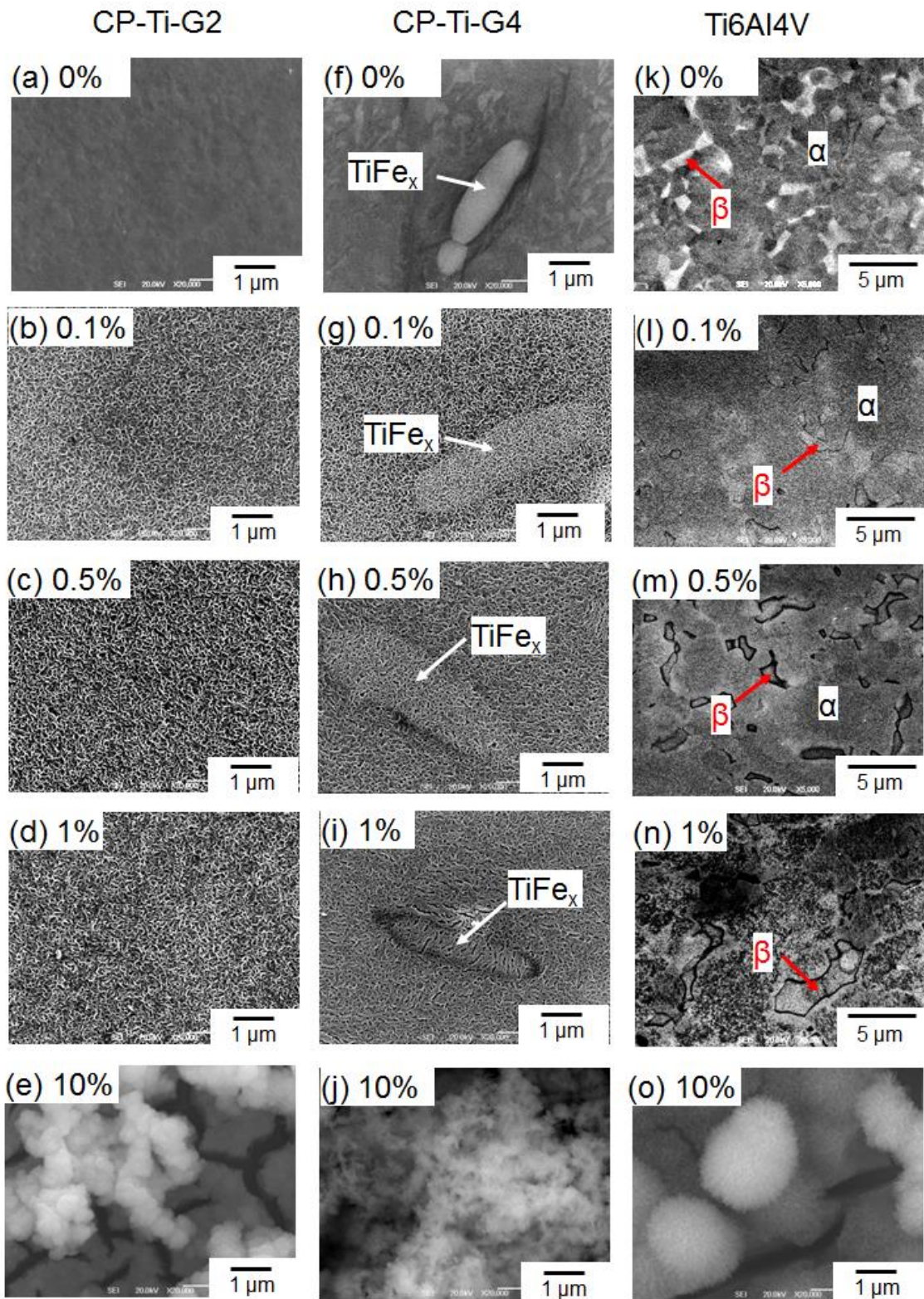
Figure 5-4 Surface morphologies of mirror-polished (a-e) CP-Ti-G2, (f-j) CP-Ti-G4 and (k-o) Ti6Al4V following immersion in physiological saline (0.15 M NaCl) with and without different levels of H_2O_2 for 4 weeks at 37 °C.

(a) 0% H$_2$O$_2$ (b) 0.1% H$_2$O$_2$

α   β   α   β

1 µm

(c) 0.5% H$_2$O$_2$ (d) 1% H$_2$O$_2$

β   α   β   α
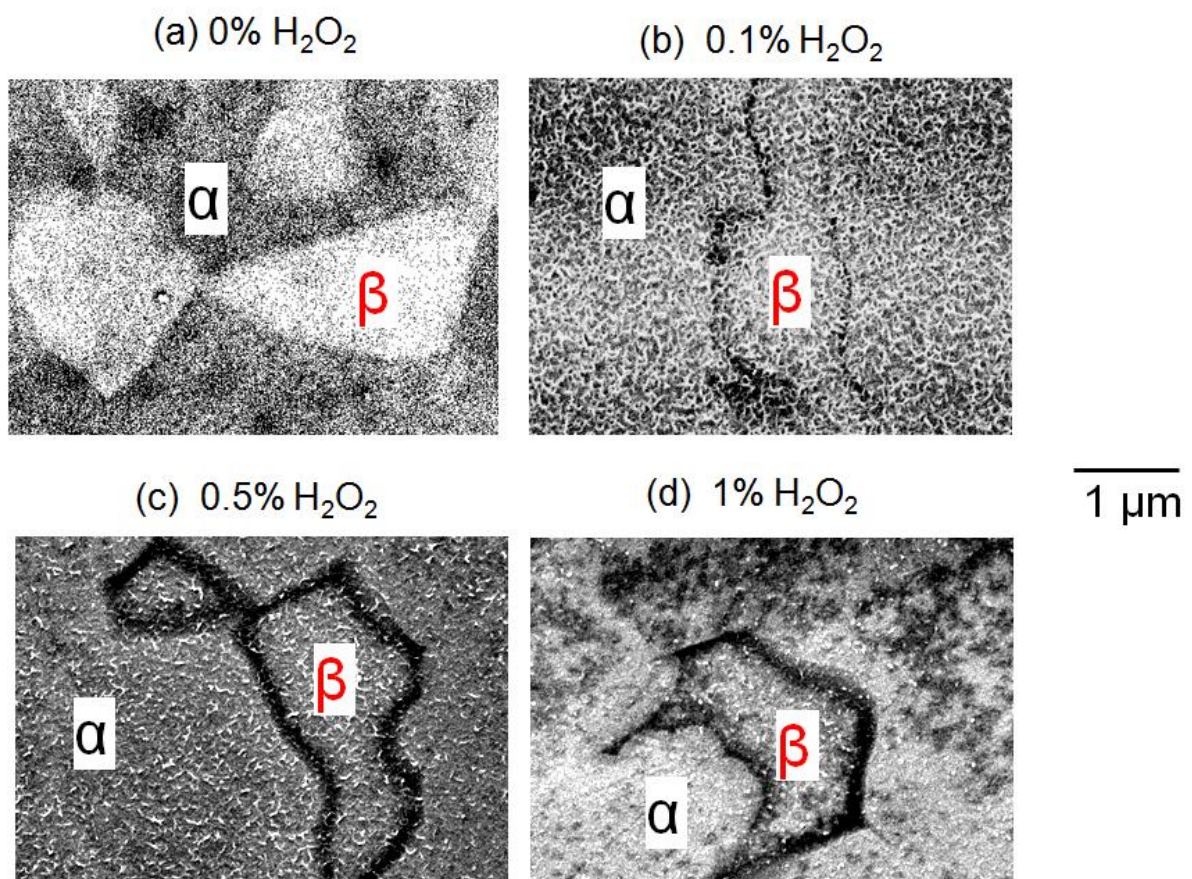
Figure 5-5 Surface morphologies of mirror-polished Ti6Al4V following immersion in physiological saline (0.15 M NaCl) with and without different levels of H$_2$O$_2$ for 4 weeks at 37 °C.

Clear changes in surface morphology were observed for the samples immersed in H$_2$O$_2$, as shown in Figure 5-4 and Figure 5-5. It can be seen that the corrosion products on the surfaces of CP-Ti-G2 and CP-Ti-G4 became much more porous following 4 weeks immersion in H$_2$O$_2$. Specifically the β phase of Ti6Al4V was preferentially attacked, accompanying the surface roughening in H$_2$O$_2$ solutions (Figure 5-5).

The most noticeable change in surface morphologies was observed following 4 weeks immersion in the highest concentration of H$_2$O$_2$ (10%), and differences between Ti grades were evident. Finer precipitates aggregated on the CP-Ti-G2 and CP-Ti-G4 surfaces whilst larger

precipitates formed on the Ti6Al4V surface. All samples immersed in H_2O_2-containing solutions showed the presence of oxygen based on EDX analysis (data not shown).

5.2.2.2 Characterisation after potentiostatic tests

Figure 5-6 compares the surface morphologies of mirror-polished Ti6Al4V before and after potentiostatic measurements in physiological saline with H_2O_2. It can be seen that Ti6Al4V showed a characteristic α/β two phase microstructure based on the BSE image and there was no variation surface topography based on the AFM mapping before the test. However, after the test, AFM mapping (Figure 5-6f) shows that β phase of Ti6Al4V was attacked more than α phase in the H_2O_2-containing solution.
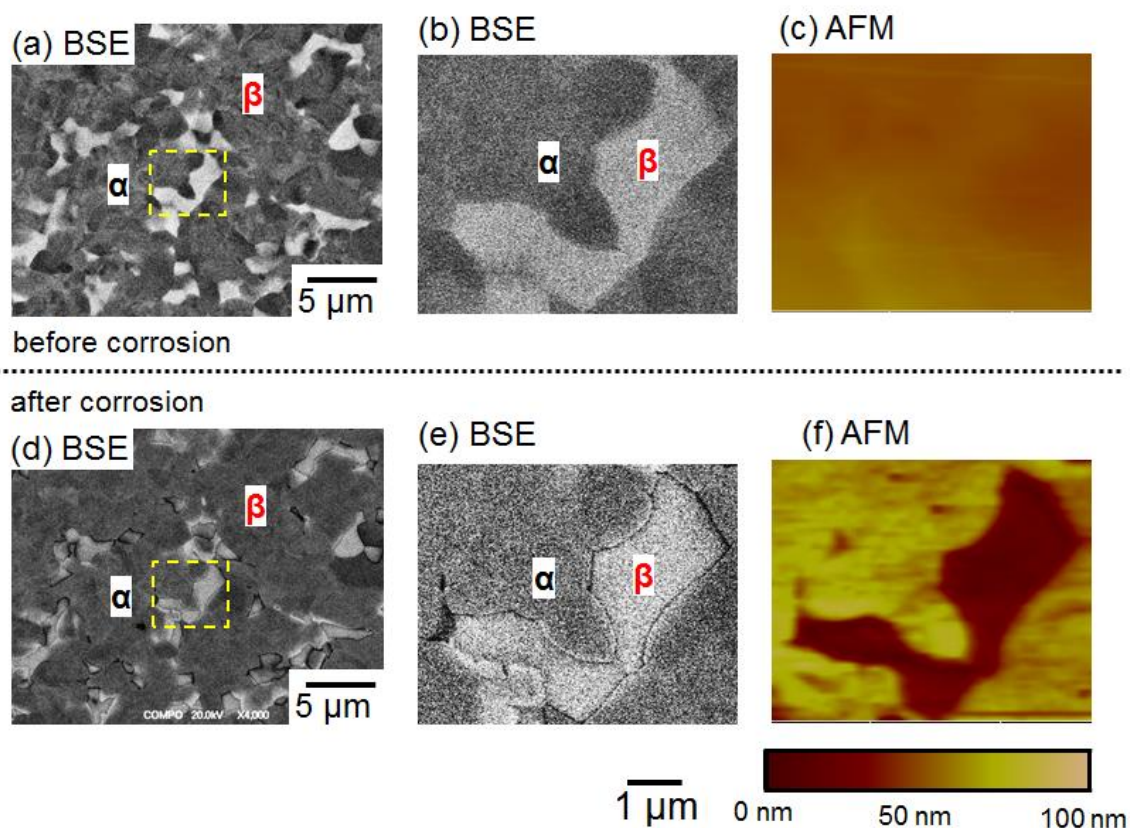
Figure 5-6 Surface morphology/topography of (a-c) before and (d-f) after potentiostatic measurement of mirror-polished Ti6Al4V in 10% H_2O_2-containing physiological saline (0.15 M NaCl) at 600 mV vs. SCE for 30 min at 37 °C. BSE: backscatter electron SEM image.

5.2.3 Electrochemical tests

5.2.3.1 OCP behaviour

Figure 5-7 shows the OCP as a function of time for CP-Ti-G4 (Figure 5-7a) and Ti6Al4V (Figure 5-7b). The OCP increased with time and the values were almost 300 mV higher in the presence of H_2O_2. The OCP of Ti6Al4V was close to that of CP-Ti-G4 for the same concentrations of H_2O_2.
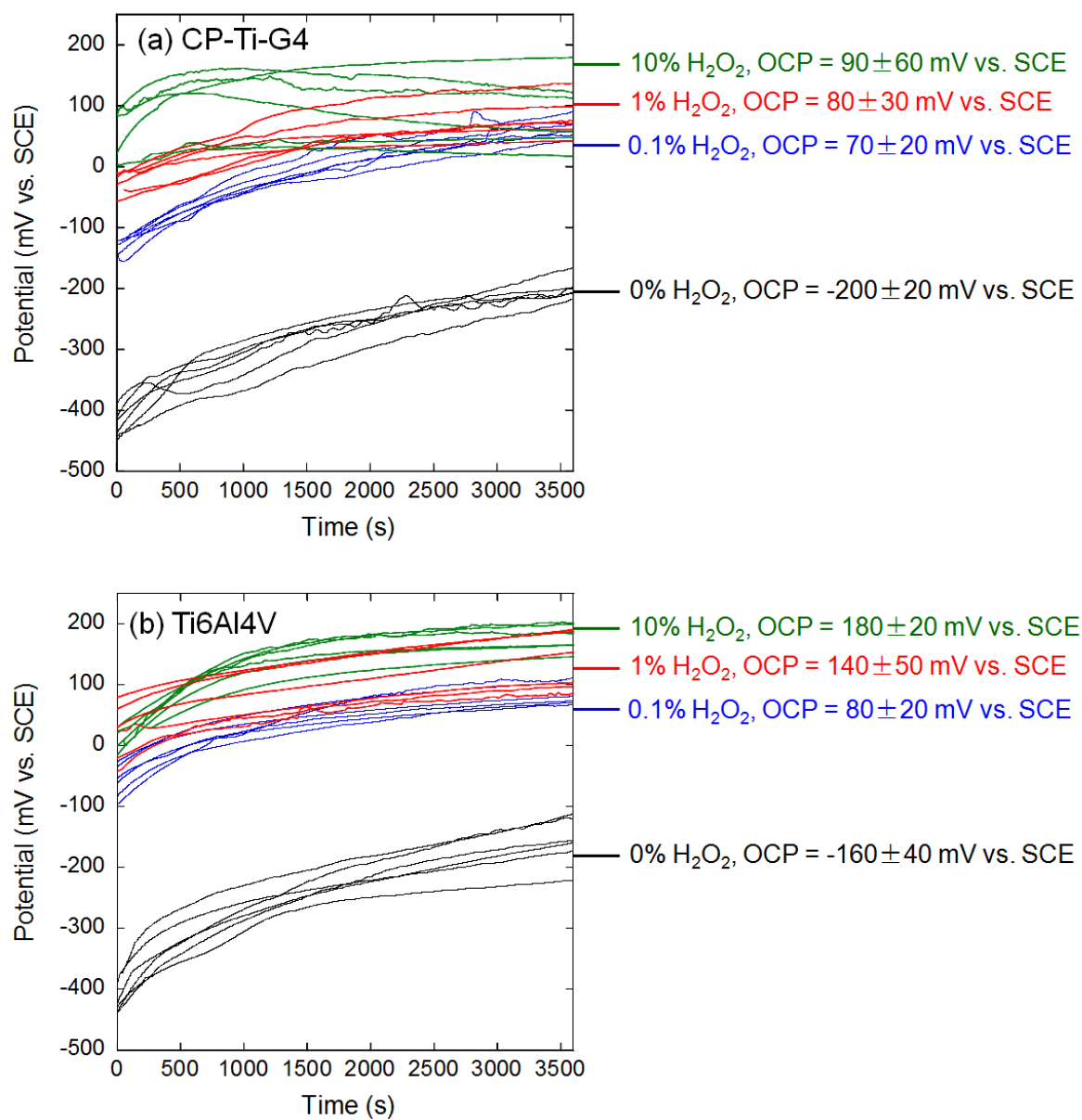
Figure 5-7 OCP as a function of time for mirror-polished (a) CP-Ti-G4 and (b) Ti6Al4V in physiological saline (0.15 M NaCl) with and without different levels of H_2O_2 at 37 °C. The average final OCP is shown.

5.2.3.2 Cathodic polarisation

Figure 5-8 shows cathodic polarisation curves for mirror-polished CP-Ti-G4 and Ti6Al4V measured in physiological saline with and without H_2O_2. A cathodic current plateau was observed for CP-Ti-G4 and Ti6Al4V under very negative potentials (less than -1 V vs. SCE) due to limited oxygen diffusion.

With the addition of H_2O_2, the cathodic current densities of both CP-Ti-G4 and Ti6Al4V were increased due to the reduction reaction of H_2O_2. It can also be seen that the cathodic current densities increased with increasing concentration of H_2O_2 and the cathodic current densities of CP-Ti-G4 and Ti6Al4V exhibited similar values at the same concentrations of H_2O_2. In addition, the value of OCP of Ti6Al4V and CP-Ti-G4 moved to more positive values in the presence of H_2O_2, which is consistent with OCP measurements in Figure 5-7.
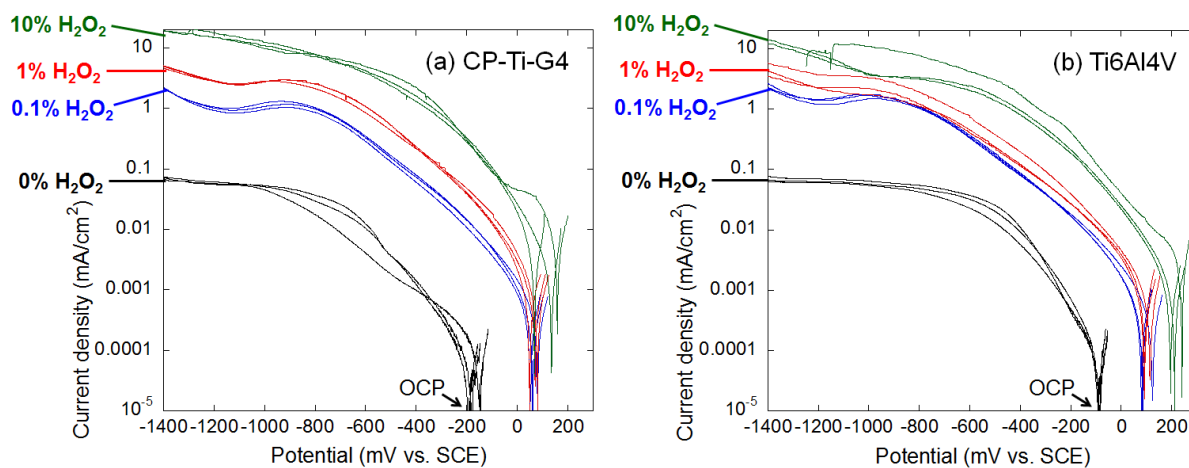
Figure 5-8 Cathodic polarisation curves of mirror-polished (a) CP-Ti-G4 and (b) Ti6Al4V in physiological saline (0.15 M NaCl) with and without different levels of H_2O_2 at 37 °C. The potential was swept in the negative direction from just 50 mV above OCP to -1400 mV vs. SCE at a rate of 1 mV/s.

5.2.3.3 Anodic polarisation

Figure 5-9 shows anodic polarisation curves for mirror-polished CP-Ti-G4 and Ti6Al4V. Both CP-Ti-G4 and Ti6Al4V showed passive behaviour in physiological saline and no significant change of anodic current density was observed up to a potential of 1200 mV vs. SCE.

In the presence of H_2O_2, the anodic current densities of CP-Ti-G4 and Ti6Al4V became higher compared with those measured in physiological saline without H_2O_2. The anodic current densities increased with increasing concentration of H_2O_2. In addition, Ti6Al4V showed higher anodic current densities than CP-Ti-G4 with exposure to the same concentrations of H_2O_2, consistent with Ti release shown in Figure 5-1. Furthermore the anodic current densities of CP-Ti-G4 and Ti6Al4V in the presence of H_2O_2 were slightly increased with increasing potential until an abrupt increase was observed at 600-800 mV vs. SCE, possibly due to oxygen evolution.
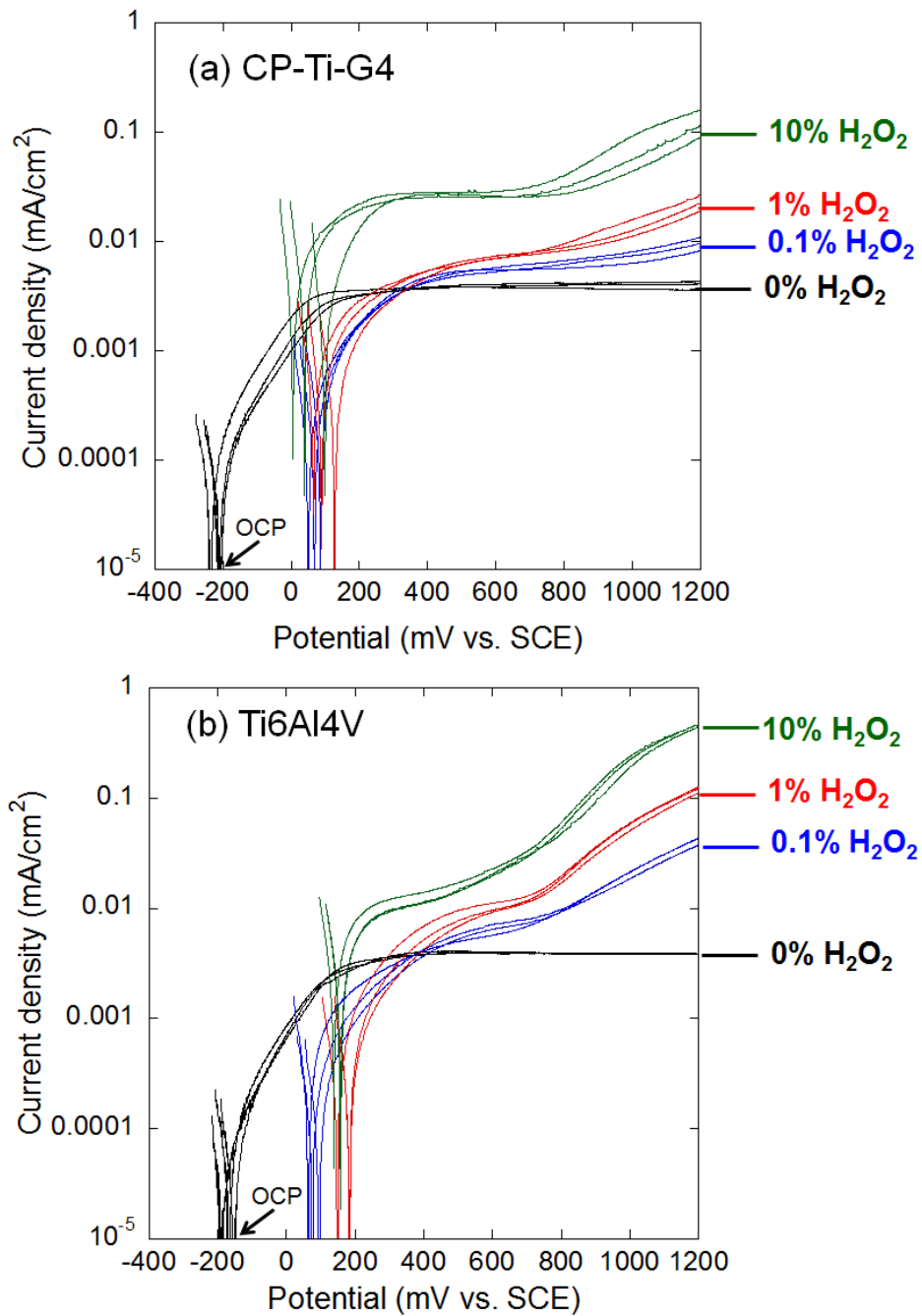
Figure 5-9 Anodic polarisation curves of mirror-polished (a) CP-Ti-G4 and (b) Ti6Al4V in physiological saline (0.15 M NaCl) with and without different levels of H_2O_2 at 37 °C. The potential was swept in the positive direction from just -50 mV below OCP to 1200 mV vs. SCE at a rate of 1 mV/s.

5.3 Effect of albumin on corrosion of Ti6Al4V

5.3.1 Electrochemical tests

5.3.1.1 OCP behaviour

Figure 5-10 shows the OCP as a function of time for mirror-polished Ti6Al4V. The OCP increased with time and was almost 300 mV lower in the presence of albumin. The OCP of Ti6Al4V did not show significant differences in solutions containing different levels of albumin.
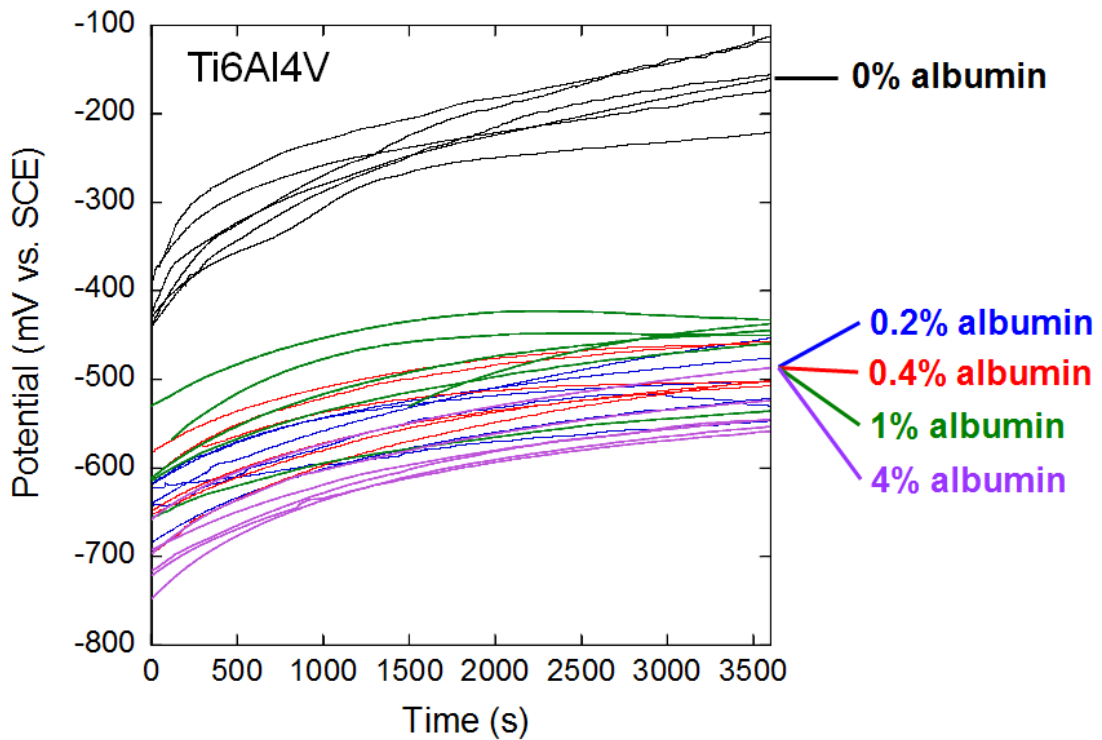
Figure 5-10 OCP as a function of time for mirror-polished Ti6Al4V in physiological saline (0.15 M NaCl) with and without different levels of albumin at 37 °C.

5.3.1.2 Anodic and cathodic polarisation

Figure 5-11 shows anodic and cathodic polarisation curves for mirror-polished Ti6Al4V. When compared with the cathodic reaction in physiological saline, albumin addition significantly inhibited the cathodic reaction. The decreased cathodic current densities did not show significant differences in the solutions containing different levels of albumin. In addition, OCP of Ti6Al4V moved to more negative values in the presence of albumin, which is consistent with OCP measurements in Figure 5-10.

The anodic current density was observed to be higher in the presence of albumin. This is possibly due to the suppressed cathodic reaction or an enhanced anodic reaction or a combination of both. A particularly sharp active peak was found in 4% albumin (Figure 5-11c).
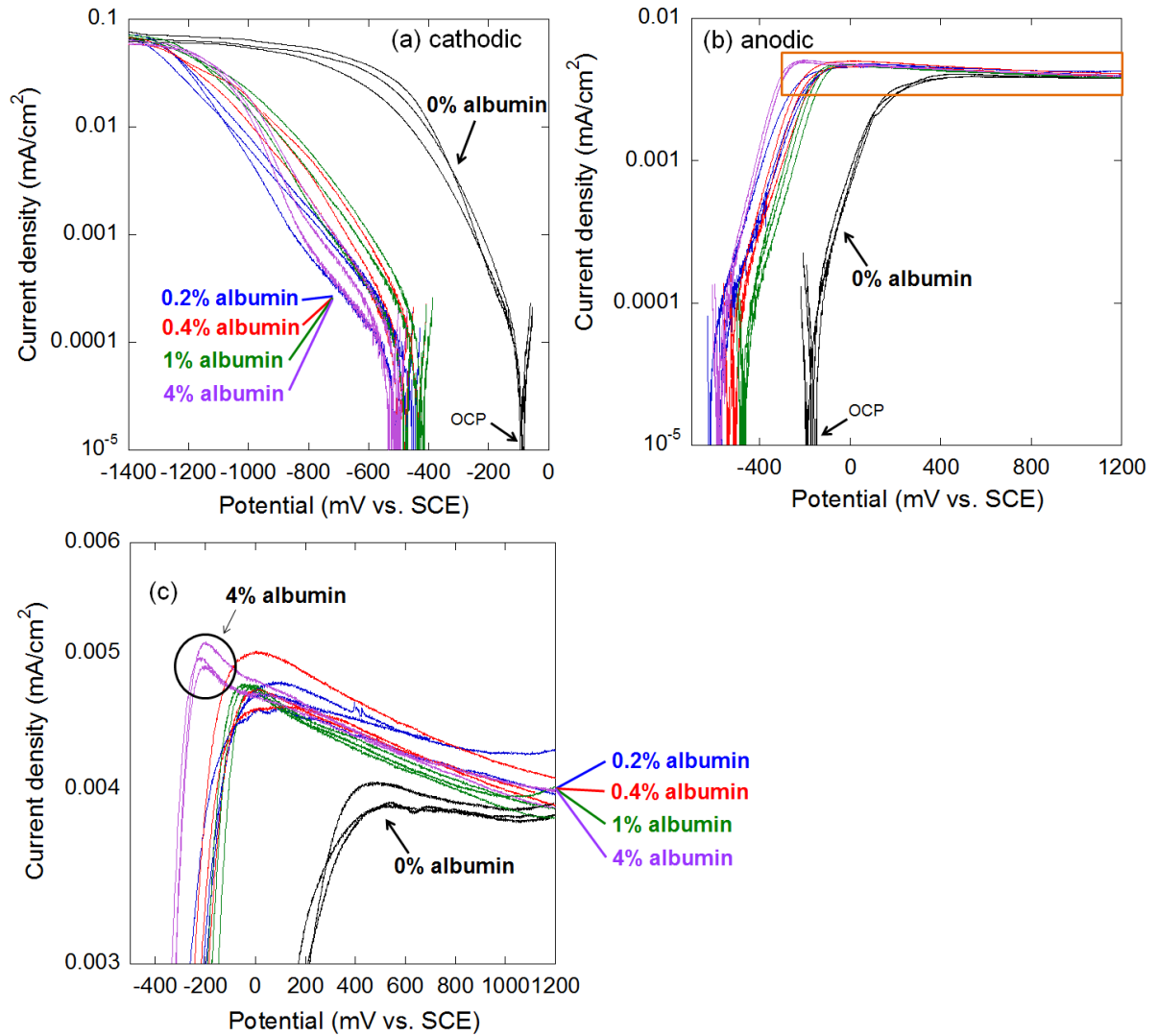
Figure 5-11 (a) cathodic and (b) anodic polarisation curves; (c) enlarged image of the region outlined in (b) of mirror-polished Ti6Al4V in physiological saline (0.15 M NaCl) in the presence and absence of different levels of albumin at 37 °C. For cathodic polarisation, the potential was swept in the negative direction from 50 mV above OCP to -1400 mV vs. SCE at a rate of 1 mV/s. For anodic polarisation, the potential was swept in the positive direction from -50 mV below OCP to 1200 mV vs. SCE at a rate of 1 mV/s.

5.4 Effect of the combination of H_2O_2 and albumin on corrosion of Ti6Al4V

5.4.1 Solution analysis

Figure 5-12 shows the concentrations of Ti, Al and V released from mirror-polished Ti6Al4V in the absence and presence of H_2O_2 and albumin. Ti, Al and V levels in the control (without a Ti6Al4V disc) solutions were negligible, except for the Al level in the albumin control sample (15 ± 10 ppb) (Table 5-3) and it is possible that this was due to one contaminated sample. There were three measurements and one sample showed high Al level (26 ppb, 8 ppb and 10 ppb).

A higher concentration of Ti measured in the immersion solution was observed from Ti6Al4V in the presence of H_2O_2 when compared with H_2O_2-free solution. Similar to the 4 week immersion tests in physiological saline with H_2O_2 (see Figure 5-2), the amount of released V was greater than Al.

In the presence of albumin, a small increase in the measured Ti concentration (65 ± 5 ppb) was observed when compared with the (albumin-free) physiological saline control. Immersion in mixed solutions of H_2O_2 and albumin resulted in a considerable increase in the release of Ti, Al and V, which increased with the increasing concentration of albumin in the mixed solutions. The concentration of Al measured in the mixed solutions was greater than that in the presence of H_2O_2 without albumin.

114

	without Ti6Al4V disc (control)			with Ti6Al4V disc						
albumin (%)	0	4	0	0	4	0	0.2	0.4	1	4
H₂O₂ (%)	0	0	0.1	0	0	0.1	0.1	0.1	0.1	0.1

Released Ti concentration
Released Al concentration
Released V concentration
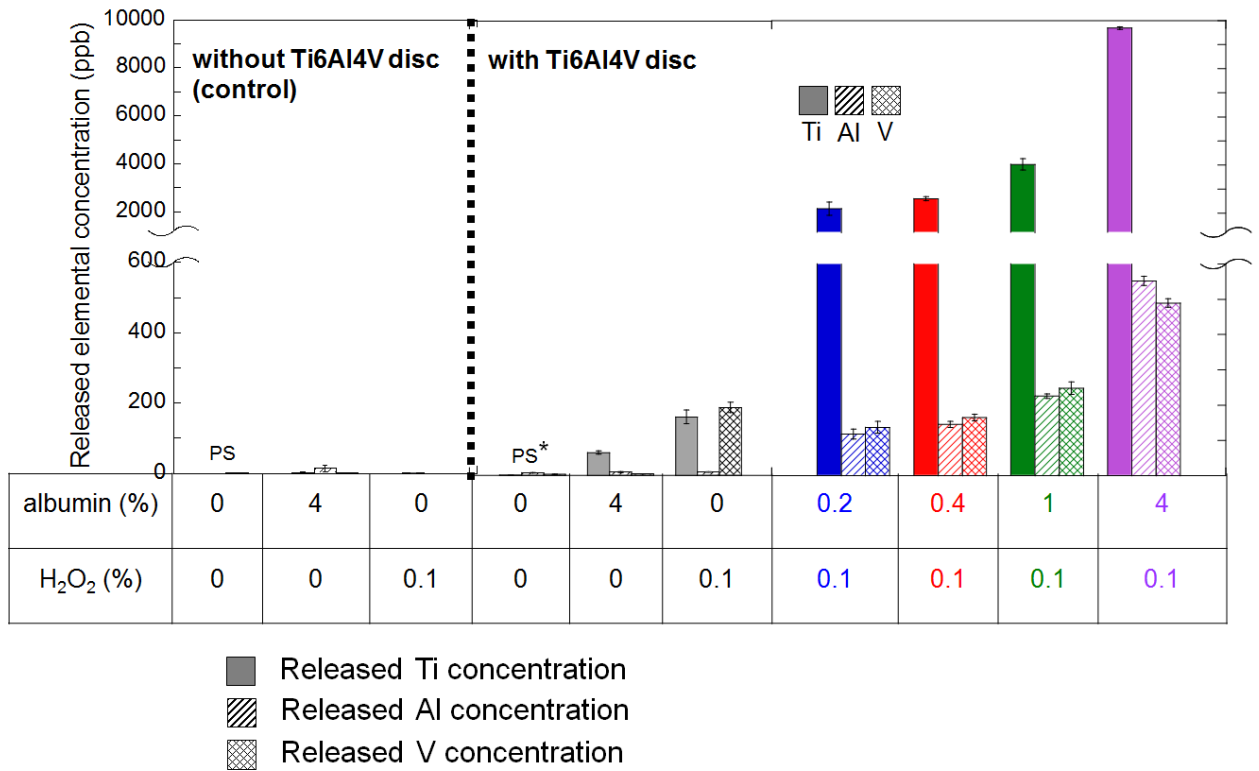
Figure 5-12 The mean concentrations and standard deviations (ppb) measured with ICP-MS of Ti, Al and V released from mirror-polished Ti6Al4V following immersion in physiological saline (PS, 0.15 M NaCl) with and without H_2O_2 and albumin for 2 weeks at 37 °C (n=3); the results indicated * were from 4 week immersion test.

Table 5-3 The mean concentrations and standard deviations (ppb) measured with ICP-MS of Ti, Al and V released from mirror-polished Ti6Al4V following immersion in physiological saline (PS, 0.15 M NaCl) with and without H_2O_2 and albumin for 2 weeks at 37 °C (n=3); the results indicated * were from 4 week immersion test.

	Ti	Al	V
PS without Ti6Al4V	<0.5	0.8±0.1	<0.2
4% albumin without Ti6Al4V	2±1	15±10	1.5±0.4
0.1% H_2O_2 without Ti6Al4V	<0.5	1.1±0.5	<0.2
PS + Ti6Al4V*	0.7±0.1	7±1	3±1
4% albumin + Ti6Al4V	65±5	10±1	4.3±0.5
0.1% H_2O_2 + Ti6Al4V	170±20	10±1	190±10
0.2% albumin + 0.1% H_2O_2 + Ti6Al4V	2200±300	120±10	140±20
0.4% albumin + 0.1% H_2O_2 + Ti6Al4V	2600±90	146±9	170±10
1% albumin + 0.1% H_2O_2 + Ti6Al4V	4000±200	226±6	250±20
4% albumin + 0.1% H_2O_2 + Ti6Al4V	9690±50	550±10	490±10

5.4.2 Surface morphology after immersion tests

Figure 5-13 shows that the corrosion products on the Ti6Al4V surface appeared porous in the presence of H_2O_2 based on the secondary electron image (SE), and the β phase appeared to be preferentially attacked based on the backscatter electron image (BSE), which was similar to the observation in the following 4 week immersion in H_2O_2 (Figure 5-5).

Figure 5-13 also shows that the surface of Ti6Al4V after immersion in albumin did not show a significant difference from the sample immersed in physiological saline alone. However, the surface of Ti6Al4V was relatively smooth and β phase was also preferentially attacked after immersion in the mixed solutions of H_2O_2 and albumin. In addition, the surface of Ti6Al4V was likely to show clearer attack features with an increasing albumin concentration in the mixed solutions (Figure 5-14).
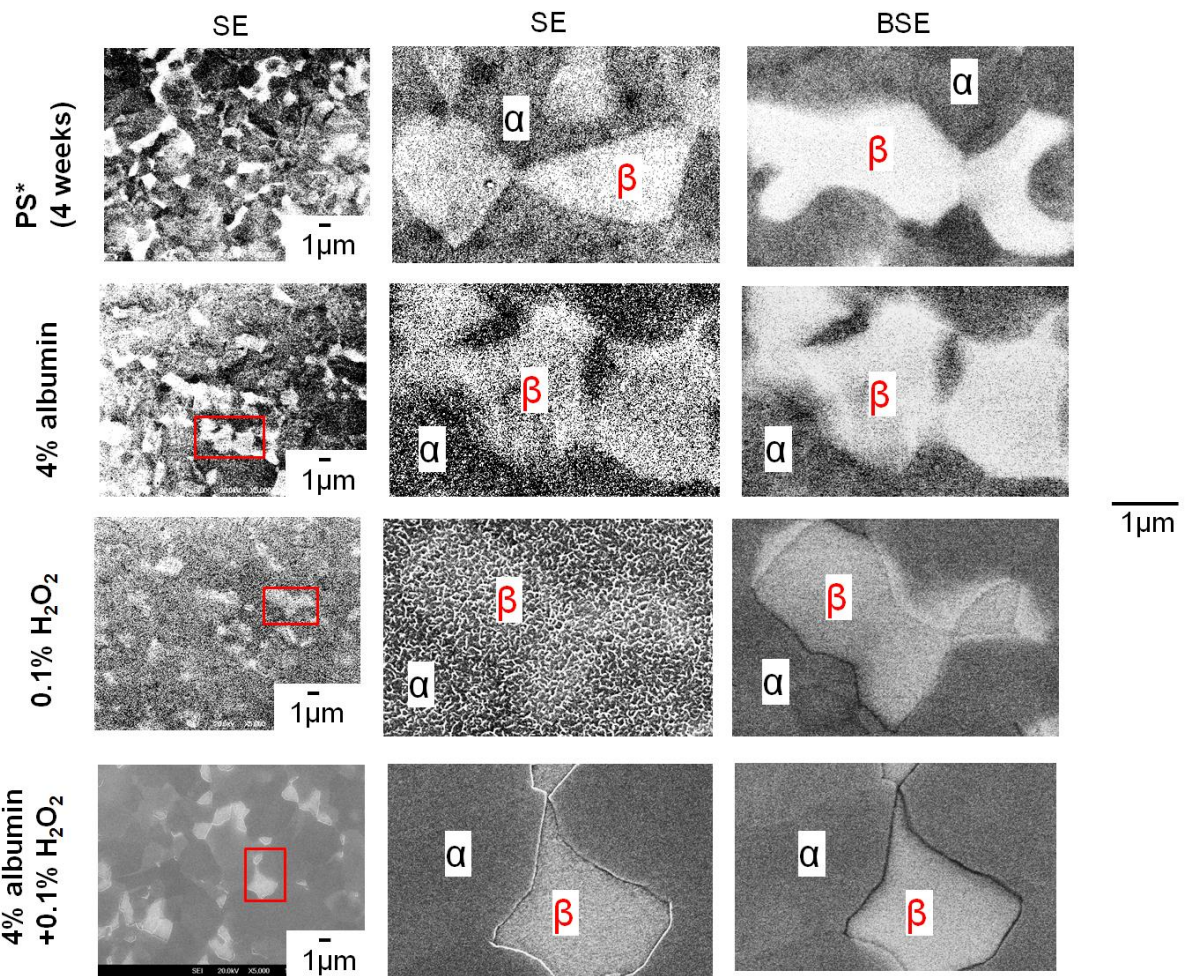
Figure 5-13 Surface morphology of mirror-polished Ti6Al4V following 2 week immersion in physiological saline (PS, 0.15 M NaCl) with or without H_2O_2 and/or albumin at 37 °C; the results indicated * were from 4 week immersion test. SE: secondary electron SEM image; BSE: backscatter electron SEM image.
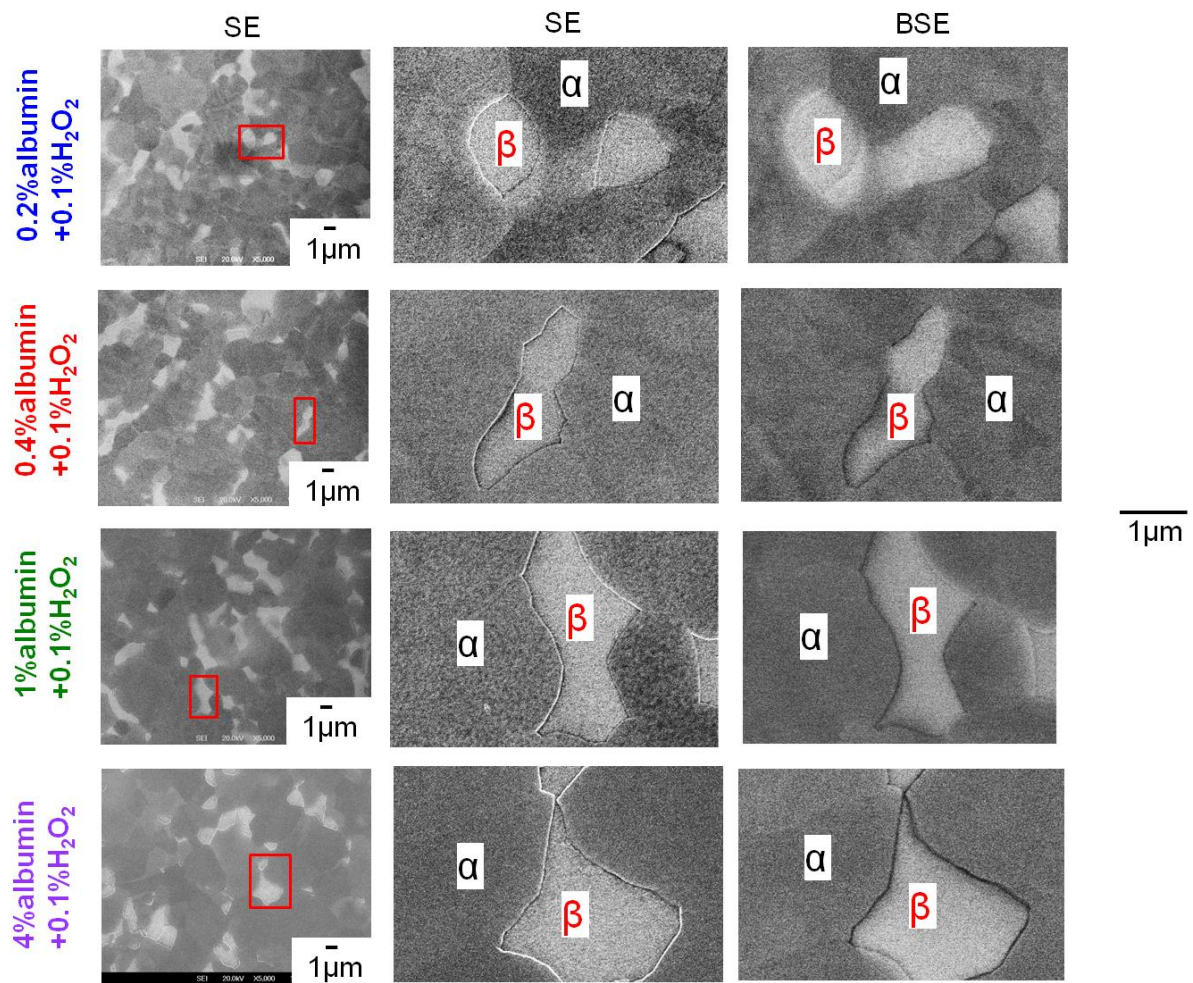
Figure 5-14 Surface morphology of mirror-polished Ti6Al4V following 2 week immersion in physiological saline (0.15 M NaCl) in the presence of H_2O_2 and different levels of albumin at 37 °C. SE: secondary electron SEM image; BSE: backscatter electron SEM image.

5.4.3 Electrochemical tests

5.4.3.1 OCP behaviour

Figure 5-15 shows the OCP as a function of time for mirror-polished Ti6Al4V in the absence and presence of H_2O_2 and albumin. The OCP was higher in the presence of H_2O_2 compared with (H_2O_2-free) physiological saline, which was decreased after the addition of albumin. The OCP was lower in the presence of albumin compared with (albumin-free) physiological saline, which was increased after the addition of H_2O_2. The OCP of Ti6Al4V in the presence of mixed solutions of H_2O_2 and albumin was close to that in physiological saline control. In addition, the OCP was not found to depend on the concentration of albumin in the mixed solutions.
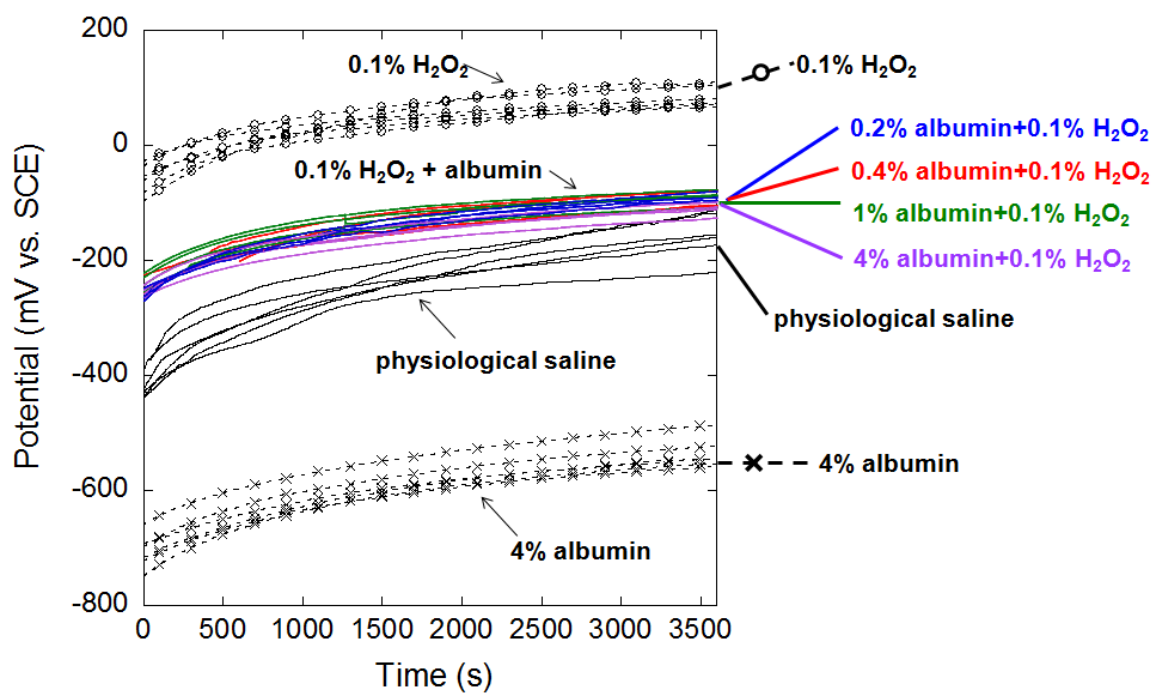

Figure 5-15 OCP as a function of time for mirror-polished Ti6Al4V in physiological saline (0.15 M NaCl) with and without H_2O_2 and different levels of albumin at 37 °C.

5.4.3.2 Anodic and cathodic polarisation

Figure 5-16 shows the anodic and cathodic polarisation curves for mirror-polished Ti6Al4V in the absence and presence of H_2O_2 and albumin. It can be seen that the addition of albumin decreased the cathodic current density in the presence of H_2O_2 alone, and the addition of H_2O_2 increased the cathodic current density in the presence of albumin alone.

For anodic polarisation curves (Figure 5-16b), Ti6Al4V exhibited higher anodic current densities in mixed solutions of H_2O_2 and albumin compared with physiological saline, and this appears to be mainly due to an enhanced anodic reaction. In addition, the anodic current densities of Ti6Al4V in mixed solutions were increased with an increasing concentration of albumin in the mixed solutions (Figure 5-16c), which is consistent with the metal release results (Figure 5-12). The anodic current density of Ti6Al4V showed an abrupt increase in the presence of mixed solutions at 600 ± 80 mV vs. SCE, which was similar to that observed in H_2O_2 (see Section 5.2.3.3) and is possibly due to oxygen evolution.
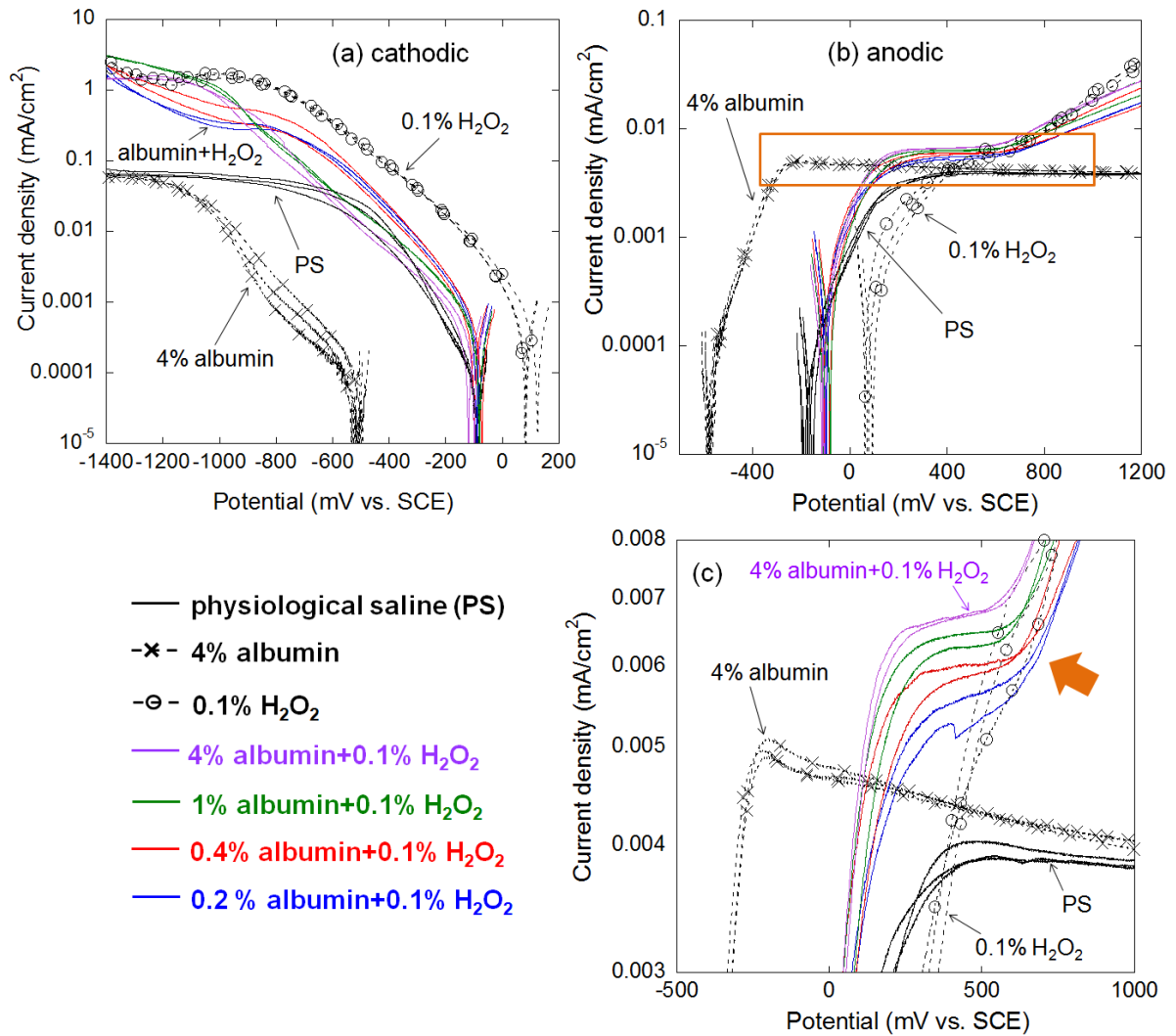
Figure 5-16 (a) cathodic and (b) anodic polarisation curves; (c) enlarged image of the region outlined in (b) of mirror-polished Ti6Al4V in physiological saline (PS, 0.15 M NaCl) with and without H_2O_2 and different levels of albumin at 37 °C. For cathodic polarisation, the potential was swept in the negative direction from 50 mV above OCP to -1400 mV vs. SCE at a rate of 1 mV/s. For anodic polarisation, the potential was swept in the positive direction from -50 mV below OCP to 1200 mV vs. SCE at a rate of 1 mV/s.

5.4.3.3 Potentiostatic measurements

Figure 5-17 shows potentiostatic measurements of mirror-polished Ti6Al4V in physiological saline with addition of albumin and/or H_2O_2 at different potentials. The solution was stirred at ~1000 s intervals to ensure complete mixing. H_2O_2 and/or albumin were added just prior to stirring for some of the measurements.

Figure 5-17a shows that the cathodic steady state current densities of Ti6Al4V at the cathodic potential were decreased following addition of albumin at the 1st ~1000 s interval, consistent with the cathodic polarisation results (Figure 5-11a). It can also be seen that the cathodic steady state current densities in the absence and presence of albumin were increased after addition of H_2O_2 at the 2nd ~1000 s interval, consistent with the cathodic polarisation results in Figure 5-16. In addition, the cathodic steady state current densities in H_2O_2-containing solution were decreased following addition of albumin at the 3rd ~1000 s interval, which is also consistent with the cathodic polarisation results (Figure 5-16).

Figure 5-17b and Figure 5-17c show that anodic steady state current densities of Ti6Al4V at both two anodic potentials decreased after addition of albumin at the 1st ~1000 s interval. It has also been shown that at the 2nd ~1000 s interval, the anodic steady state current densities in the absence and presence of albumin were increased after addition of H_2O_2. In addition, at the 3rd ~1000 s interval, the anodic steady state current densities in the presence of H_2O_2 were also decreased after addition of albumin.

122

1st ~1000s	100s stir	2nd ~1000s	100s stir	3rd ~1000s	100s stir	1000s
PS	+1% albumin		+0.1%H_2O_2			
PS			+0.1%H_2O_2		+1% albumin	
PS			+0.1%H_2O_2			
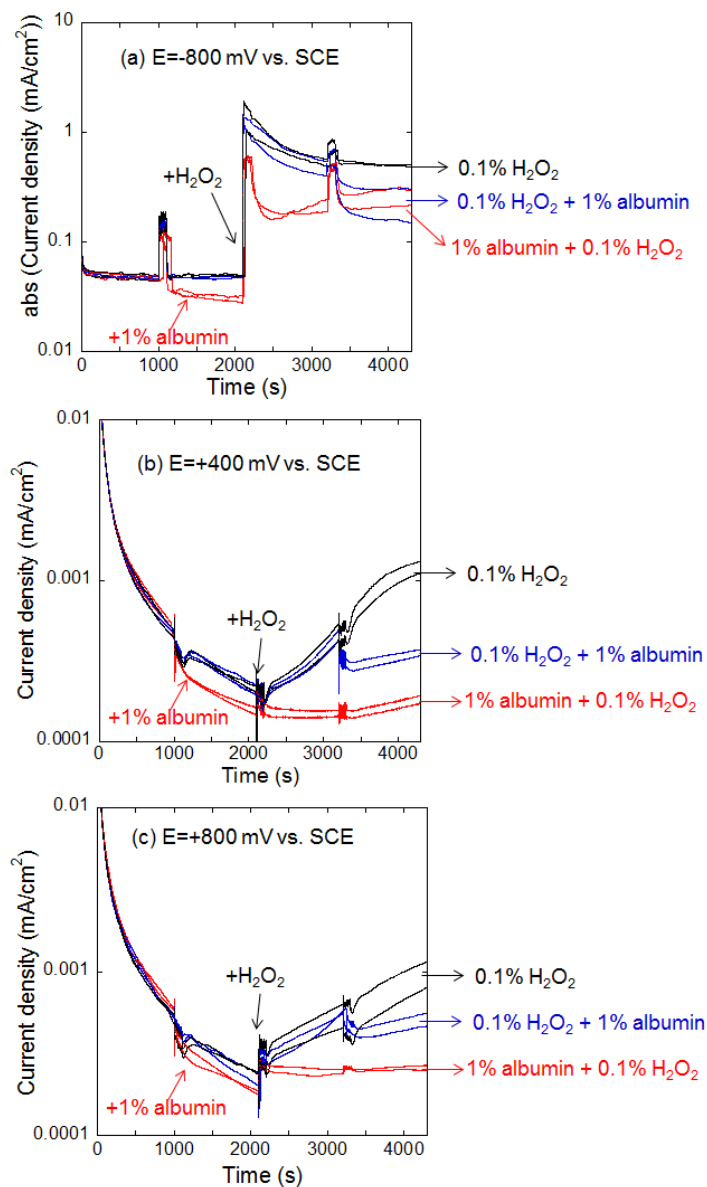
Figure 5-17 Potentiostatic measurements of mirror-polished Ti6Al4V at (a) -800 mV; (b) 400 mV and (c) 800 mV vs. SCE in physiological saline (PS, 0.15 M NaCl) with addition of H_2O_2 and/or albumin at 37°C. The solution was stirred for ~100 s at ~1000 s intervals to ensure complete mixing; for some experiments, a specific amount of H_2O_2 or albumin (in PS) was added at ~1000 s intervals immediately before stirring to give a final concentration of 0.1% or 1%.

5.4.4 Long-time (24 h) OCP behaviour

Figure 5-18 shows the OCP as a function of time for 24 h for mirror-polished Ti6Al4V in physiological saline with and without H_2O_2 and albumin. The solution was stirred at intervals to ensure complete mixing. H_2O_2 or albumin was added just prior to stirring at ~1 h or ~4 h for some of the measurements (see Figure 5-18).

At ~1 h following addition of H_2O_2, the OCP of Ti6Al4V shifted to a higher value when compared with the OCP in physiological saline alone. At ~4 h when albumin was added into the H_2O_2-containing solution, the OCP decreased and this was consistent with the 1 h OCP measurement (Figure 5-15).

At ~1 h following addition of albumin, the OCP of Ti6Al4V decreased when compared with the OCP measured in physiological saline alone. Subsequently at ~4 h when H_2O_2 was added into the albumin-containing solution, the OCP of Ti6Al4V increased, which again was consistent with the 1 h OCP measurement (Figure 5-15).

After 24 h exposure, Ti6Al4V exhibited the highest OCP value in H_2O_2 and the lowest in albumin whilst the OCP in mixed solutions was close to that in physiological saline, which also agreed with the previous observations (see Section 5.4.3.1).
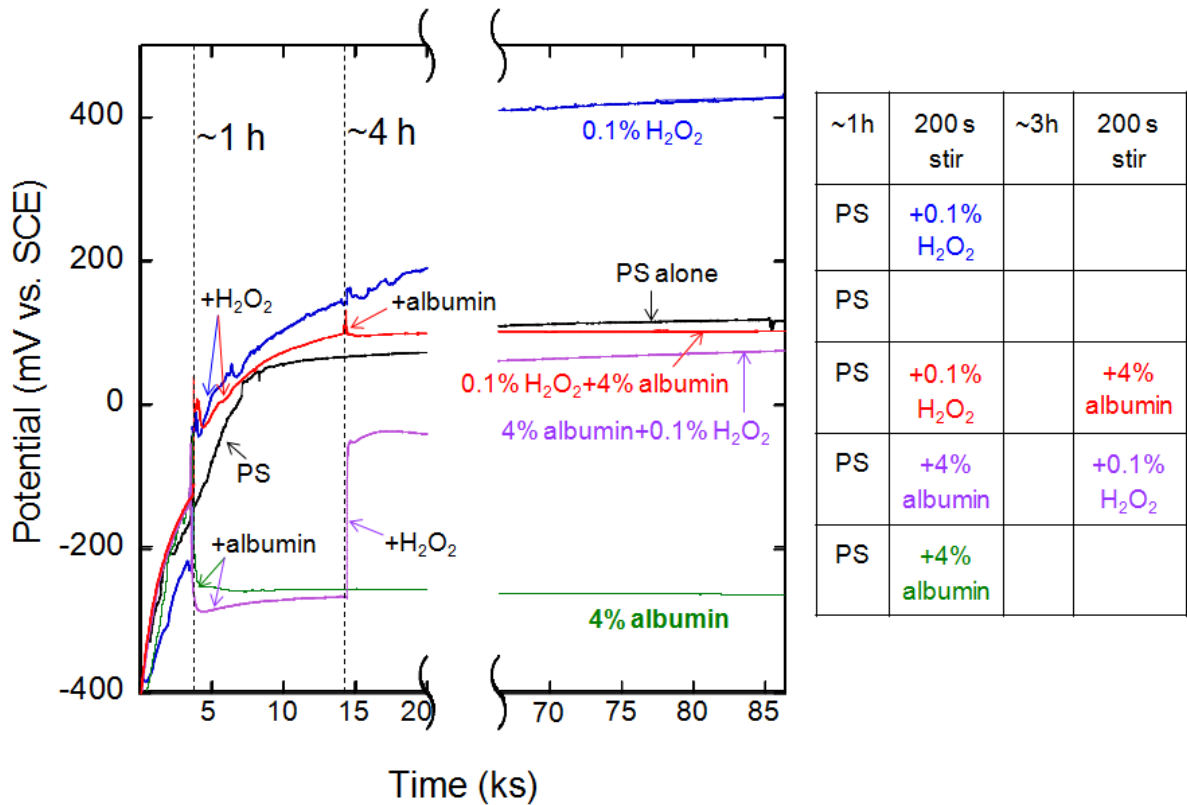
Figure 5-18 OCP as a function of time for 24 h for mirror-polished Ti6Al4V in physiological saline (PS, 0.15 M NaCl) with and without addition of H_2O_2 and/or albumin at 37 °C. The solution was stirred for ~200 s at ~1 h and ~4 h to ensure complete mixing; for some experiments, a specific amount of H_2O_2 or albumin (in PS) was added at ~1 h or ~4 h immediately before stirring to give a final concentration of 0.1% or 4%.

5.5 Discussion

5.5.1 Effect of H_2O_2 on Ti corrosion

5.5.1.1 Quantification of Ti release

Dissolution of Ti from the three grades of Ti (CP-Ti-G2, CP-Ti-G4 and Ti6Al4V) was observed

following addition of H_2O_2 (Figure 5-1), indicating decreased corrosion resistance. The finding

is consistent with other studies which have used electrochemical impedance spectroscopy (EIS)

to study the same or similar exposure conditions [17, 111, 112, 132, 185-188]. The Ti

concentrations quantified in the control solutions (no Ti discs) were negligible. It was observed that there was no significant difference on the concentration of Ti released from CP-Ti-G2 and CP-Ti-G4 in the presence of H_2O_2. Therefore, only CP-Ti-G4 and Ti6Al4V were conducted in the electrochemical tests.

5.5.1.2 Electrochemistry of Ti corrosion

It is well known that H_2O_2 is a strong oxidiser and has a high standard reduction potential ($E° = 1.54$ V vs. SCE) [57]. Since all experiments were carried out under naturally-aerated conditions, it is assumed that the cathodic reaction in physiological saline is oxygen reduction. Whilst in the presence of H_2O_2 the cathodic reaction is likely to be dominated by the reduction reaction of H_2O_2 (Equation 2-9), leading to a higher cathodic current density and also resulting in a more positive OCP according to the basis of the Evans diagram (mixed potential theory) [64].

It was observed that the anodic current densities were higher for CP-Ti-G4 and Ti6Al4V in the presence of H_2O_2 due to the complexation interaction between Ti and H_2O_2 [106, 108, 184, 189]. In addition, a higher anodic current density was observed for both CP-Ti-G4 and Ti6Al4V for a higher concentration of H_2O_2 and the magnitude of the increase was greater for Ti6Al4V than CP-Ti-G4, suggesting inferior corrosion resistance of Ti6Al4V, which was consistent with the Ti release results following immersion studies (Figure 5-1) and other studies [185, 187].

The anodic current density was slightly increased with increasing potential, and an abrupt increase was observed at 600-800 mV vs. SCE possibly due to O_2 evolution from H_2O_2 (Equation 2-10) or H_2O (Equation 5-1). Based on the E-pH (Pourbaix) diagram of H_2O/H_2O_2 system (Figure 2-15), oxidation reaction of H_2O_2 to form O_2 can happen thermodynamically at

a lower potential (0 mV vs. SCE) and O_2 evolution from H_2O is also thermodynamically possible at potential >580 mV vs. SCE in neutral solutions (Equation 5-1) [175]. However, O_2 evolution was not observed for CP-Ti-G4 and Ti6Al4V in physiological saline at the applied potentials, which could be attributed to the stable and/or insulating passive film on the surface [48, 175]. However, Fonseca and Barbosa [112] reported that the oxide film formed in the presence of H_2O_2 showed higher ionic conductivities, which may lead to occurrence of O_2 evolution reaction kinetically.

Equation 5-1 $O_2 + 4H^+ + 4e^- = 2H_2O$; E (V vs. SCE) = 0.99 - 0.059pH + 0.0015logp(O_2)

5.5.2 Effect of albumin on corrosion of Ti6Al4V

It can be seen from Figure 5-11 that the presence of albumin significantly inhibited the cathodic reaction of Ti6Al4V, resulting in lower OCP (Figure 5-10), which is consistent with other studies on Ti alloys [20, 122]. It has also been shown that the cathodic steady state current was decreased after addition of albumin (Figure 5-17). It has been established that albumin strongly adsorbs on the surfaces of metals including Ti by chemisorption through amino group or carboxylate group or through electrostatic interactions [19, 24, 190]. In the current study, it is possible that albumin rapidly adsorbs onto the surface of Ti6Al4V following immersion and covers the potential reaction sites or blocks the mass transportation for the cathodic reaction, which results in a decrease in cathodic current and cathodic steady state current.

In terms of anodic polarisation, higher anodic current densities were observed in the presence of albumin, possibly due to the suppressed cathodic reaction (stated above) or an enhanced anodic reaction or even a combination of both. It is reported that albumin can form a complex or chelate with the metal cations and promote anodic reaction (e.g. stainless steel [19]). A

127

similar chelation effect was also proposed on CP-Ti to explain the insignificantly changed corrosion resistance at open circuit since albumin decreased cathodic current [20]. However, in the current study, the anodic steady state current densities were decreased following addition of albumin (Figure 5-17), indicating that the anodic reaction was actually suppressed. Therefore, the higher anodic current density is more likely to be due to the suppressed cathodic reaction. It is possible that the cover/block effect by adsorption of albumin also inhibits the anodic reaction of Ti6Al4V, resulting in lower anodic steady state current. A decreased anodic current of CP-Ti in a high anodic region was also reported [20]. A lower passive current density of Ti6Al4V-ELI in the presence of albumin during anodic polarisation was claimed by Padilla and Bronson [25] using a rotating disc electrode, but there were no details about conducting the anodic polarisation experiment.

A particularly sharp active peak was found in the presence of 4% albumin (Figure 5-11), which has not been previously reported, possibly due to the different polarisation methods in previous studies [26, 28, 122]. In the current study, anodic and cathodic polarisation tests were conducted separately to reduce the effect of prior cathodic polarisation on anodic polarisation and vice versa, while the polarisation from very negative cathodic potential (e.g. -1 V vs Ag/AgCl [122]) to a very positive anodic potential (e.g. 1.5 V vs Ag/AgCl [122]) was used in previous studies [26, 28, 122]. The history of cathodic reaction may have an influence on anodic behaviour of Ti6Al4V during the polarisation tests. However, the "whole region" polarisation method (i.e., cathodic and anodic polarisations are carried out in one single potentiodynamic test) is widely used in most studies, and the reported stability of Ti6Al4V is mainly based on the change of anodic current, which may lead to inconsistent results in the literature [25, 28, 122].

In addition, a small increase in Ti release from Ti6Al4V was observed in the presence of albumin after the immersion test (Figure 5-12). However, the presence of albumin inhibited the cathodic and anodic reaction in physiological saline. Karimi and Alfantazi [26] reported that the anodic current density of Ti6Al4V decreased in PBS containing 0.2% and 0.4% albumin, indicating the increased stability of passive film, but Karimi and Alfantazi [27] also reported in a following study that more Ti release was found at the same conditions. However, there is no clear explanation for the contradictory results. They believed that the phosphates leaching from passive film on the Ti6Al4V surface increase Ti release rate in albumin solutions [27]. Similar contradictory results can be found in Padilla and Bronson's work [25] that the passive current density of Ti6Al4V-ELI decreased in the presence of albumin but corrosion resistance (from EIS) was also decreased at the same condition. In the current study, it is proposed that the lower OCP brought about by the suppressed cathodic reaction may drive the dissolution of Ti6Al4V into the active region, so the presence of albumin increased corrosion rate of Ti6Al4V at the open circuit.

5.5.3 Effect of the combination of albumin and H_2O_2 on corrosion of Ti6Al4V

It can be seen from Figure 5-16 and Figure 5-17 that the cathodic current density and cathodic steady state current density were lower in the presence of both H_2O_2 and albumin when compared with that in H_2O_2 alone, suggesting that the presence of albumin inhibited the cathodic reaction of Ti6Al4V in H_2O_2-containing solutions. Higher anodic current densities were observed in the presence of mixed solutions when compared with that in the presence of H_2O_2 alone (Figure 5-16), which is more likely due to the suppressed cathodic reaction. Potentiostatic studies showed that the anodic steady state current densities (Figure 5-17) in the

presence of H_2O_2 were decreased after addition of albumin, indicating that the presence of albumin suppressed anodic reaction of Ti6Al4V in H_2O_2-containing solutions.

It also can be seen from Figure 5-16 and Figure 5-17 that cathodic current density and cathodic steady state current density of Ti6Al4V were higher in the presence of both H_2O_2 and albumin when compared with that in albumin alone, suggesting that the presence of H_2O_2 promoted the cathodic reaction of Ti6Al4V in albumin-containing solutions. Potentiostatic studies showed that the anodic steady state current densities in the presence of albumin were increased after addition of H_2O_2 (Figure 5-17), indicating that the presence of H_2O_2 promoted anodic reaction in albumin-containing solutions. For anodic polarisation, an abrupt increase in anodic current was observed in the mixed solution around potential 600 ± 80 mV vs SCE, which is similar to the observation in H_2O_2, possibly due to O_2 evolution reaction (see Section 5.5.1.2).

Specifically, a considerably higher rate of metal release from Ti6Al4V was observed in the presence of mixed solutions than that in either albumin or H_2O_2 alone after the immersion test (Table 5-3 and Figure 5-12), which has not been reported previously. Although Padilla and Bronson [25] mentioned the possible effect of H_2O_2 and albumin because H_2O_2 was regarded as an intermediate species in oxygen reduction, there was no direct investigation about the synergistic effect of H_2O_2 and albumin on corrosion of Ti alloys. In the current study, it is proposed that the suppressed cathodic reaction by the addition of albumin taking the potential of Ti6Al4V into the active region and considerably promotes corrosion.

Figure 5-19 shows a diagram that provides a hypothesis to explain the combined effect of albumin and H_2O_2 in the current work.

Firstly, Ti6Al4V is passivated in physiological saline as shown in Figure 5-19 (point A), which is consistent with the negligible released Ti concentration (Figure 5-12) and the very low passive anodic current (Figure 5-16). Ti6Al4V also showed a stable OCP value after 24 h exposure in physiological saline (Figure 5-18).

Secondly, the presence of H_2O_2 promotes cathodic and anodic reaction in physiological saline, resulting in higher E_{corr} and higher i_{corr} (point B in Figure 5-19). It was observed from 24 h OCP measurements that OCP of Ti6Al4V was the highest in the presence of H_2O_2.

Thirdly, it has been observed that the presence of albumin inhibited cathodic reaction and anodic reaction of Ti6Al4V in physiological saline. The inhibited cathodic reaction induced by albumin results in a lower OCP, which may drive the dissolution of Ti6Al4V from the passive region (point A in Figure 5-19) to the active region (point C in Figure 5-19) and promote Ti6Al4V corrosion. E_{corr} is decreased, and it showed the lowest value in albumin after 24 h measurement (Figure 5-18), while i_{corr} is increased in albumin-containing solution (Figure 5-12).

It has also been shown that the presence of albumin inhibited cathodic reaction and anodic reaction of Ti6Al4V in H_2O_2-containing solutions. The inhibited cathodic reaction in the mixed solutions resulted in a lower OCP when compared with that in the presence of H_2O_2 alone, at which the anodic dissolution may lie in the active region (point D in Figure 5-19), resulting in considerable dissolution of Ti6Al4V in mixed solutions. It was also observed that the OCP of Ti6Al4V after 24 h exposure in mixed solutions was higher than that in albumin alone but lower than that in H_2O_2 alone (Figure 5-18). Also, the concentration of released V was similar in between the mixed solutions and H_2O_2 alone, but there were more released Al in the mixed solutions after immersion test (Figure 5-12), which may suggest that both α phase and β phase

dissolve in the active region, since higher Al levels are found in the α phase, whereas higher V levels are found in the β phase (Figure 4-2).
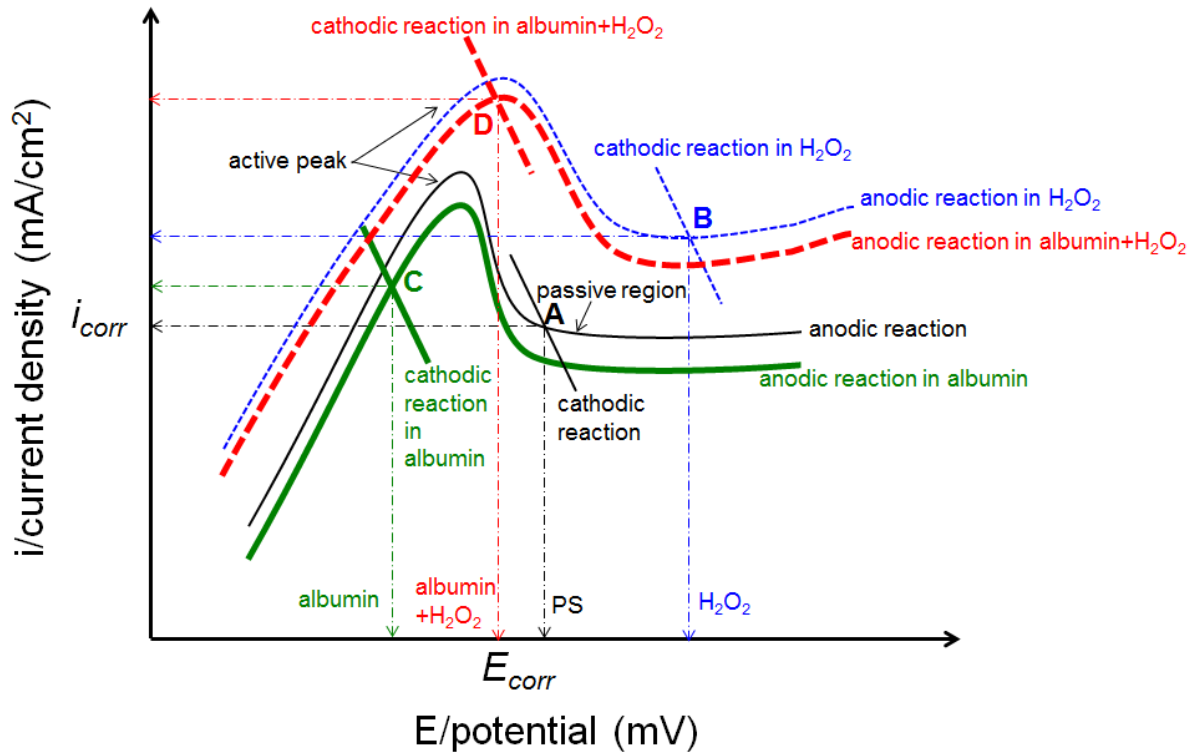
Figure 5-19 Schematic Evans diagram (mixed potential theory) to show the effect of H_2O_2, albumin and the combination of albumin and H_2O_2 on corrosion potential (E_{corr}) and corrosion current density (i_{corr}) of Ti6Al4V in physiological saline (PS).

5.5.4 Surface morphology

Both CP-Ti-G2 and CP-Ti-G4 showed similar porous corrosion product morphologies after 4 week immersion tests, which is correlated with previous work [17, 111, 112, 130, 132]. It is firstly proposed by Pan [17, 132] that the oxide films formed on Ti exposed to H_2O_2 containing PBS can be described by a two-layer model, which consisted of a thin inner compact layer and a porous outer layer. In addition, the discoloration of CP-Ti was consistent with other studies,

possibly due to the difference on the thickness of the corrosion products formed in the presence of H_2O_2 [17, 88, 191].

It was observed that the β phase of Ti6Al4V is preferentially attacked in the presence of H_2O_2 after potentiostatic tests (using SEM and AFM, see Figure 5-6), as well as after immersion tests (using SEM, see Figure 5-5). This is also consistent with the metal release measurement in this study, where V (predominately in the β phase) release was more than Al (predominately in the α phase) release (Figure 5-2). The preferential attack of β phase is also consistent with previous studies [113, 114]. In addition, the β phase attack with relatively smooth surface was observed in the mixed solutions of albumin and H_2O_2 (Figure 5-13 and Figure 5-14). Since it is speculated that the dissolution of Ti6Al4V at OCP is in the active region in the presence of mixed solution, the porous corrosion products formed in the presence of H_2O_2 might dissolve and the concentrations of released metal increase.

It may be worth mentioning that the preferential attack of β phase was recently reported in the retrieved hip implant parts [75], which might be explained by the observation in the current study in the presence of H_2O_2, since H_2O_2 is known as an important inflammatory product *in vivo*. It is likely that the presence of H_2O_2 is at play in the peri-implant environment. Crystal structures of α phase (hcp) and β phase (bcc) of Ti6Al4V are different, which may affect the oxide film forming on the surface [75]. In addition, there are more V and less Al contents in the β phase compared with the α phase, so more V-rich oxides may be present over β phase, which can destroy the passivity of titanium by providing conduction channels [178] and lead to the preferential corrosion.

5.6 Conclusions

The effect of H_2O_2 which is an important inflammation product found in the peri-implant environment was investigated on CP-Ti (CP-Ti-G2 and CP-Ti-G4) and Ti6Al4V using solution analysis, surface analysis and electrochemical tests. The influence of albumin, the principle protein component of blood and extracellular fluid, on the corrosion of Ti6Al4V was also evaluated. The effect of the co-existence of albumin and H_2O_2, which will be a better biological approximation of peri-implant environment under inflammatory conditions, was also characterised.

1. The presence of H_2O_2 promotes corrosion of CP-Ti-G2, CP-Ti-G4 and Ti6Al4V, and the amount of Ti release increases with an increasing concentration of H_2O_2 in physiological saline. Ti6Al4V shows the greatest Ti release amongst the three grades of Ti studied. The electrochemical measurements on CP-Ti-G4 and Ti6Al4V were consistent with the quantification of Ti release following immersion studies.

2. The presence of albumin strongly inhibits the cathodic reaction and slightly inhibits the anodic reaction of Ti6Al4V in physiological saline resulting in a lower OCP. During anodic polarisation, a particularly sharp active peak is observed following addition of albumin (4%) owing to suppression of the cathodic reaction. The presence of albumin causes a small increase in Ti release from Ti6Al4V in the long-term immersion tests, which is attributed to decreased OCP brought about by an inhibited cathodic reaction, leading to dissolution of Ti6Al4V in the active region.

3. The cathodic reaction rate is higher in the presence of H_2O_2, which is decreased after the addition of albumin. The suppression of the cathodic reaction results in a shift of OCP to a more active region for anodic dissolution and leads to a considerably higher rate of metal release in

immersion tests in the presence of both albumin and H_2O_2 when compared with that for either albumin or H_2O_2 alone.

4. In the presence of H_2O_2 the corrosion products of three grades of Ti become more porous and the β phase of Ti6Al4V is preferentially attacked. Preferential attack of β phase is also found in albumin and H_2O_2 mixed solutions.

6   CELLULAR EFFECTS ON TI CORROSION

6.1 Introduction

The aim of the work described in this chapter was to investigate the corrosion behaviour of Ti alloys in the presence of microbes that have been shown to colonise implant surfaces. The corrosion behaviour of Ti alloys was also studied in the presence of polymorphous nuclear leukocytes (neutrophils) which are abundant immune cells present in the peri-implant tissues. Corrosion in the presence of the oral microbe *Streptococcus sanguinis* (*S. sanguinis*), which is an early coloniser of dental implants, was studied on three grades of Ti (CP-Ti-G2, CP-Ti-G4 and Ti6Al4V) which possessed two types of surface finish (either mirror-polished or sandblasted-acid-etched (SLA) surfaces) that mimicked the surfaces of dental implants. The corrosion behaviours of CP-Ti and Ti6Al4V were investigated by culturing *S. sanguinis* on Ti surfaces in artificial saliva followed by measuring the concentration of released Ti and using SEM to characterise the surface morphology. The methods for culturing bacteria are described in Section 3.3. To study the influence of neutrophils on Ti corrosion, three grades of Ti with mirror-polished surfaces were immersed in Tris-buffer and cultured with neutrophils which were in an un-stimulated or stimulated (by exposure to opsonised *Staphylococcus aureus* (Ops *Sa*)) state. The concentration of the released Ti was measured using ICP-MS and the Ti surfaces imaged using SEM. The detailed procedures for isolating and culturing neutrophils on Ti alloys are described in Section 3.4.

6.2 Effect of *S. sanguinis* on Ti corrosion in artificial saliva

6.2.1 Surface morphologies of Ti samples

SEM imaging of the Ti samples prior to culturing with *S. sanguinis* demonstrated that the mirror-polished CP-Ti-G2 (G2P) surfaces did not appear to exhibit second phase particles, whereas the CP-Ti-G4 (higher Fe level) (G4P) surfaces contained $TiFe_x$ intermetallic particles, and Ti6Al4V (G5P) surfaces possessed the characteristic α/β two phase microstructure (Figure 6-1). When compared with mirror-polished samples, the SLA surfaces appeared as a fine network of peaks and depressions with an irregular spacing between peaks of 1-5 μm (Figure 6-1). The SLA surfaces generated on CP-Ti-G2 (G2S) and on CP-Ti-G4 (G4S) exhibited similar surfaces profiles whereas the SLA surfaces generated on Ti6Al4V (G5S) were more irregular with shallower wider depressions and flatter peaks.

After incubating *S. sanguinis* in artificial saliva for 3 days the bacteria were observed to adhere to both types of surfaces prepared on all three grades of Ti (Figure 6-2). For the mirror-polished surfaces, the density of adhered *S. sanguinis* was typically heterogeneous, however all samples imaged (n=3 per Ti grade) appeared to possess similar cell numbers. For the SLA surfaces, *S. sanguinis* appeared to adhere predominantly inside the surface depressions where they were potentially shielded from displacing shear forces (Figure 6-2d and Figure 6-2e).
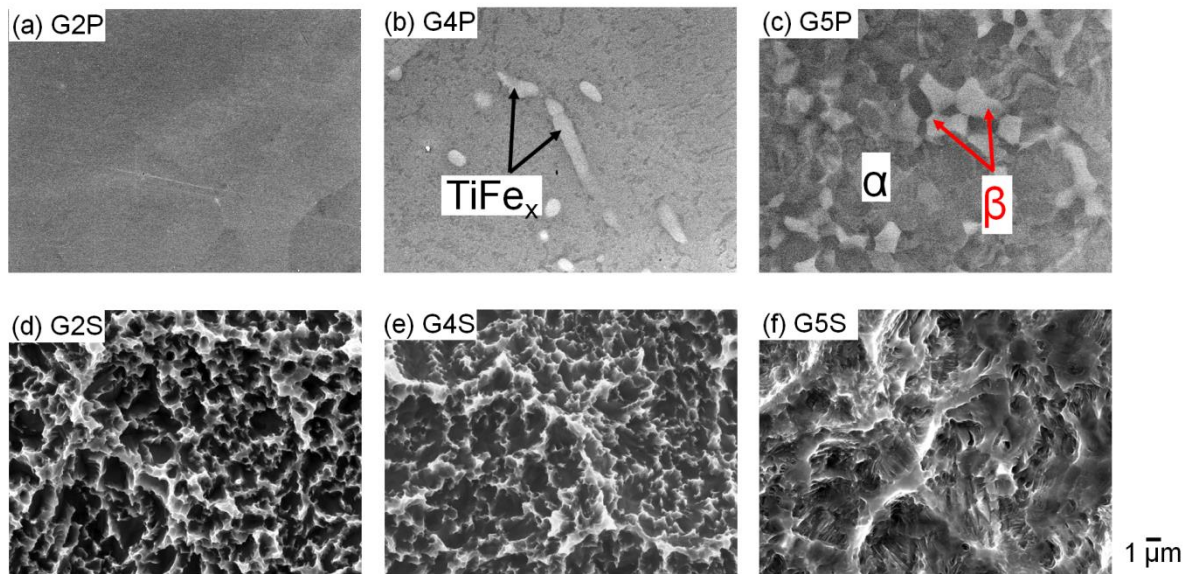
Figure 6-1 SEM images demonstrating the surface morphology of (a) mirror-polished CP-Ti-G2 (G2P); (b) mirror-polished CP-Ti-G4 (G4P); (c) mirror-polished Ti6Al4V (G5P); (d) CP-Ti-G2 with SLA treatment (G2S); (e) CP-Ti-G4 with SLA treatment (G4S); and (f) Ti6Al4V with SLA treatment (G5S).
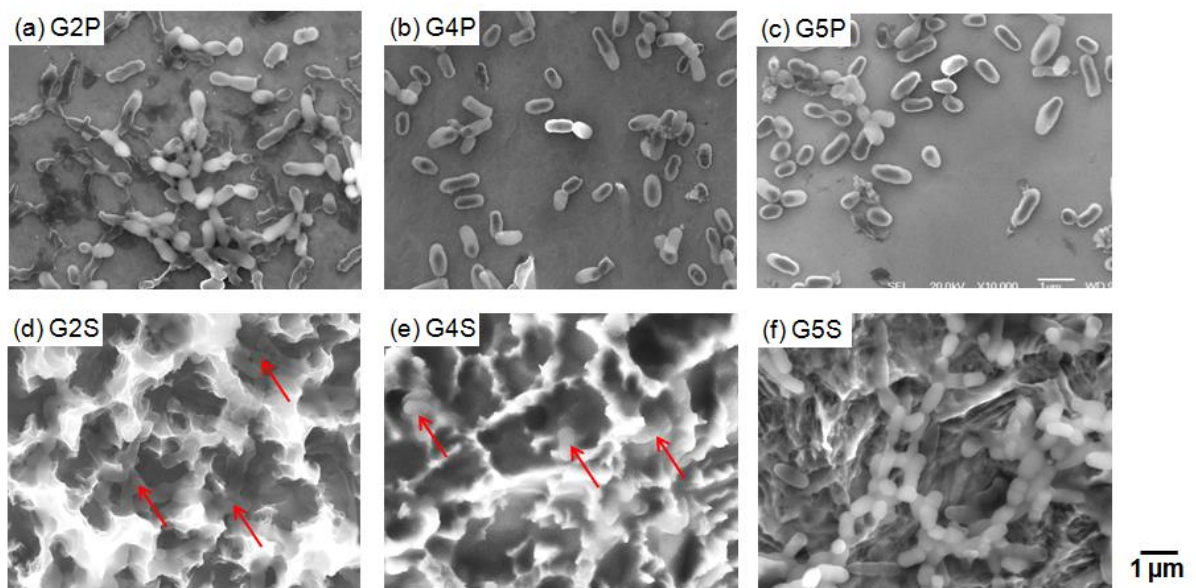
Figure 6-2 SEM images demonstrating the formation of a *S. sanguinis* biofilm on the surface of (a) mirror-polished CP-Ti-G2 (G2P); (b) mirror-polished CP-Ti-G4 (G4P); (c) mirror-polished Ti6Al4V (G5P); (d) CP-Ti-G2 with SLA treatment (G2S); (e) CP-Ti-G4 with SLA treatment (G4S); and (f) Ti6Al4V with SLA treatment (G5S) following 3 days culture in artificial saliva at 37 °C.

6.2.2 Quantification of Ti release in artificial saliva

The concentrations of Ti released when *S. sanguinis* was cultured on Ti samples in artificial saliva were measured using ICP-MS. The concentration of Ti in the artificial saliva culture medium (supernatant) and the Ti concentration in the bacteria themselves (bacterial pellet) were measured separately (Figure 6-3). Increased Ti concentrations were measured in the artificial saliva for the SLA surface finish samples when compared with mirror-polished samples following both the bacterial culture and the cell-free immersion. The Ti concentrations in the supernatants from *S. sanguinis* bacterial cultures were highest on day 3 when compared with subsequent measurements taken on day 12, day 21 and day 30 (Figure 6-4). The immersion medium was retrieved and replaced with fresh medium and new bacterial inoculum every 3 days as detailed in Section 3.3. In terms of the concentration of released Ti from the SLA samples, the highest concentration of Ti was associated with G2S, followed by G4S and G5S. The differences could be potentially related to the variability in the SLA surface modification for the three different Ti grades, leading to differences in the surface areas generated.

For all samples cultured with bacteria, the higher Ti concentrations were associated with measurements on the bacterial pellets when compared with the supernatant. The relatively high Ti concentration in the bacteria cultured with Ti compared with the control Ti-free bacteria culture demonstrates uptake of Ti into the cells. Again the SLA samples of the three grades of Ti showed increased Ti release when compared with the mirror-polished samples which is likely to be due to minor variation in the Ti surface area exposed to the culture medium and available for microbial colonisation.
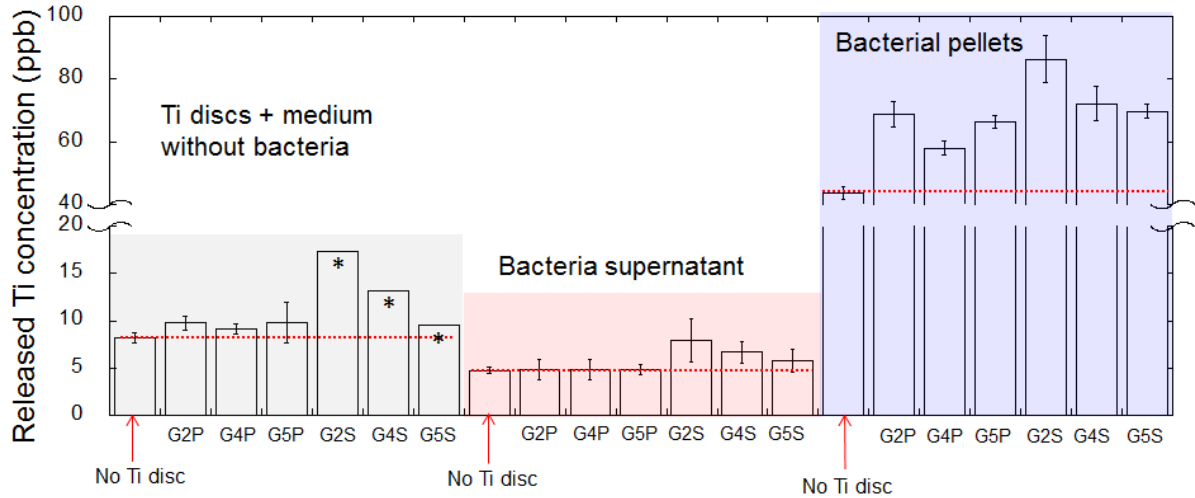
Figure 6-3 Plot of the concentration (ppb) of released Ti measured with ICP-MS from the Ti samples in the absence and presence of *S. sanguinis* after 3 days incubation in artificial saliva at 37 °C; n=3 for each condition with the exception of measurements indicated with *, for which n=1. Error bars refer to 1 standard deviation. G2P: mirror-polished CP-Ti-G2; G4P: mirror-polished CP-Ti-G4; G5P: mirror-polished Ti6Al4V; G2S: CP-Ti-G2 with SLA treatment; G4S: CP-Ti-G4 with SLA treatment; and G5S: Ti6Al4V with SLA treatment.

Table 6-1 Mean concentration and standard deviation (ppb) of released Ti measured with ICP-MS from the Ti samples in the absence and presence of *S. sanguinis* after 3 days incubation in artificial saliva at 37 °C; n=3 for each condition with the exception of measurements indicated with *, for which n=1. G2P: mirror-polished CP-Ti-G2; G4P: mirror-polished CP-Ti-G4; G5P: mirror-polished Ti6Al4V; G2S: CP-Ti-G2 with SLA treatment; G4S: CP-Ti-G4 with SLA treatment; and G5S: Ti6Al4V with SLA treatment.

	Control group without bacteria	Bacteria supernatant group	Bacterial pellet group
No Ti disc	8±0.5	5±0.4	44±2
G2P	10±0.7	5±1	69±4
G4P	9±0.6	5±1	58±2
G5P	10±2	5±0.5	66±2
G2S	17*	8±2	86±7
G4S	13*	7±1	72±5
G5S	10*	6±1	70±2
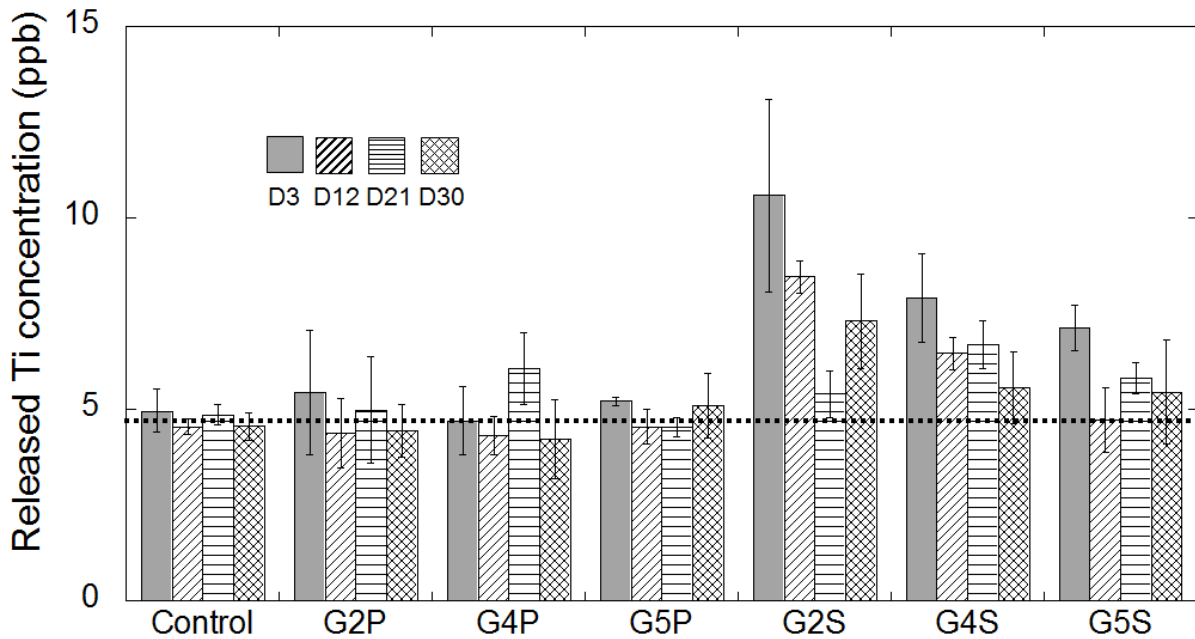
Figure 6-4 Mean concentration (ppb) of released Ti measured with ICP-MS from the Ti samples in bacteria supernatant at day 3 (D3), day 12 (D12), day 21 (D21) and day 30 (D30) during *S. sanguinis* culture in artificial saliva at 37 °C. Error bars refer to 1 standard deviation (n=3). Control: medium without any Ti disc. G2P: mirror-polished CP-Ti-G2; G4P: mirror-polished CP-Ti-G4; G5P: mirror-polished Ti6Al4V; G2S: CP-Ti-G2 with SLA treatment; G4S: CP-Ti-G4 with SLA treatment; and G5S: Ti6Al4V with SLA treatment.

6.3 Discussion - effect of *S. sanguinis* on Ti corrosion

S. sanguinis is a Gram-positive bacterium which is found in oral biofilms which can form on Ti dental implant surfaces [135]. The influence of *S. sanguinis* on Ti corrosion was investigated in this study by culturing the bacteria on prepared Ti surfaces. It was observed that an immature biofilm of *S. sanguinis* formed easily on the samples with either surface finish and on all three Ti grades (CP-Ti-G2, CP-Ti-G4 and Ti6Al4V) following 3 days of culture. It was observed that there was high Ti level in bacterial pellets when cultured in the absence of any Ti disc, which is likely due to the selective uptake of some components from artificial saliva culture-media, because some Ti level has been observed in artificial saliva medium alone. However, the Ti

concentrations in the bacteria cultured with Ti were all increased when compared with the control Ti-free bacteria culture. Ti released from all Ti samples was increased following culture with *S. sanguinis* when compared with the bacteria-free controls which indicates that the microbes promoted Ti corrosion.

These findings can be compared with other studies where decreased corrosion resistance of Ti has been reported following exposure of Ti surfaces to a number of different bacteria [29, 98, 141]. Investigators comparing the corrosion susceptibility of CP-Ti before and after bacteria incubation with *Streptococcus mutans* and *Actinomyces naeslundii* have reported that the bacteria cultured on Ti surfaces reduced the corrosion resistance [98, 141]. However, in two studies, the biofilm had been removed from Ti surface (e.g. by ultrasonically cleaning [98]) before electrochemical tests [98, 141]. In another case, a Ti sample covered with biofilm was used for electrochemical measurements whilst the test solution was different from the growth medium for biofilm formation [29]. The state of the interface between biofilm and Ti surface is likely to have changed and therefore interpretation of the data is complicated.

In addition, studies into the mechanical properties of Ti implants following exposure to *Lactobacillus salivarius* and/or *S. sanguinis* have shown an associated deterioration of mechanical properties [99]. It has also been reported that the surface roughness of Ti was increased after culture with *Streptococcus mitis* [93]. However, in none of these studies was an increase in Ti release demonstrated which is presumably due to the difficulty of making the measurements. There is considerable variability in bacterial growth *in vitro*, and the use of long incubation periods without media supplementation or exchange complicates accurate metal release measurements. In this study a short culture time (3 days) was repeated consecutively for 10 episodes, with fresh culture medium and bacterial inoculum on each occasion, allowing

greater standardisation of cell-numbers and cell viability for each sample throughout the study. The short culture time also limited the concentration of Ti within the culture medium.

It is established that metabolic products of *S. sanguinis* include acids [143], and when cultured in an aerobic environment millimolar levels of extracellular H_2O_2 are also produced [144, 145, 192]. Both acids and H_2O_2 may result in the degradation of Ti surfaces, and locally high concentrations of such metabolic products may develop in micro-environments between the bacterial cells and the Ti surface. Biofilms which were observed on the surfaces of the Ti samples are associated with more established micro-environments, which are less influenced by components from the culture medium. Therefore acid and H_2O_2 could both accumulate in the micro-environment under the adherent bacteria (Figure 6-5). The observation that similar Ti release was observed for all Ti grades suggests that the effect of acidity (no significant differences among the Ti grades in Chapter 4) is the more important contributor to the observed Ti release when compared with H_2O_2 (more Ti release from Ti6Al4V than CP-Ti following exposure to H_2O_2 in Chapter 5).
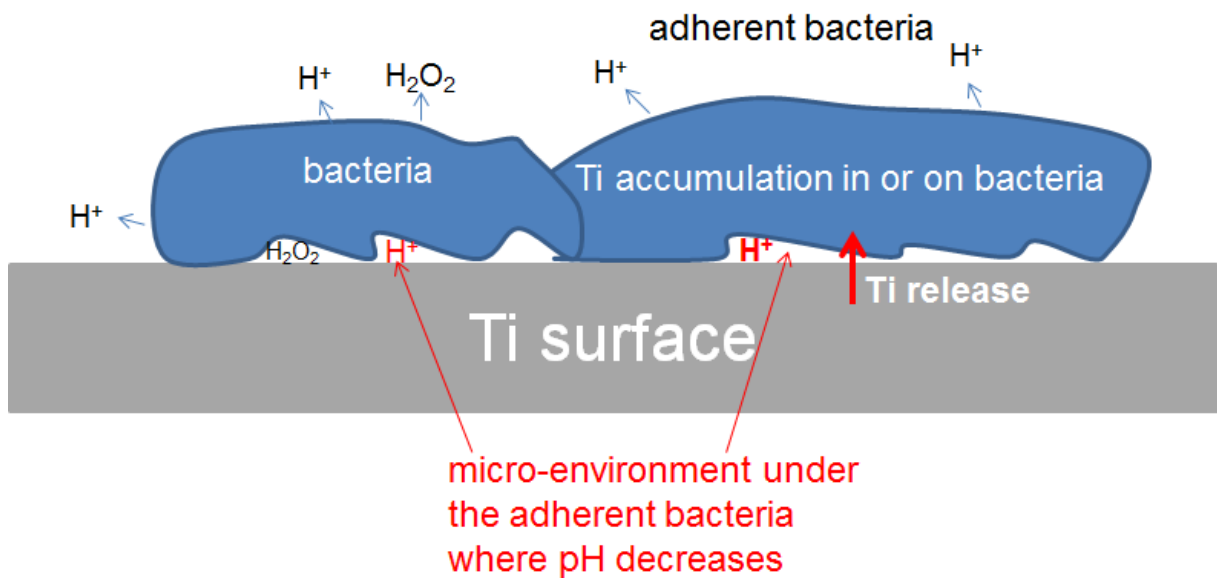
Figure 6-5 Schematic diagram demonstrating the possibility of the presence of micro/macro crevice or gap between bacteria aggregates and Ti surfaces; both acid (H^+) and H_2O_2 may accumulate in the micro-environment under the adherent *S. sanguinis*.

It was observed that the highest Ti release in the supernatants from *S. sanguinis* bacterial cultures was found on day 3 when compared with subsequent measurements on day 12, day 21 and day 30. This is likely to be due to a larger fresh surface area exposed to the culture medium and bacteria aggregates on day 3 when compared with the following culture time since the Ti samples were not changed during the whole immersion time.

It was also observed that there was greater Ti release from the SLA samples when compared with a mirror-polished surface finish (Figure 6-3). Although not quantified in this study, it is clear that the SLA samples which possessed a surface made up of a fine network of peaks and depressions (Figure 6-1) had a larger surface area exposed to the culture medium. In addition, more Ti was released from G2S, followed by G4S and then G5S. The hardness of Ti6Al4V is higher than CP-Ti-G4 and CP-Ti-G2 [2] and therefore differences in deformation would be expected to take place among the three Ti grades during the sandblasting process. Moreover,

S. sanguinis was observed to adhere predominantly in the depressions of the net-like structure of the SLA surface; however greater cell numbers were not determined (Figure 6-2d and Figure 6-2e). Significantly higher bacterial adhesion has been reported on roughened surfaces compared with that on the flat surfaces [137, 138]. Therefore more *S. sanguinis* cells were expected on the SLA surfaces when compared with mirror-polished surfaces in this study, which may increase the chance of developing micro-environments and result in more Ti release.

6.4 Effect of neutrophils on Ti corrosion

6.4.1 Surface morphology

Figure 6-6 shows SEM images of neutrophils in an un-stimulated or stimulated (by Ops *Sa*) state on mirror-polished Ti surfaces. It was observed that neutrophils interacted with the surfaces of all three Ti grades. In the absence and presence of microbial stimulation (Ops *Sa*), neutrophils were observed to be similarly activated exhibiting membrane protrusions, evidence of degranulation (visible "footprints" on the Ti surface which are attributed to deposits of lysosome granule contents or cell lysis) and neutrophil extracellular traps (NETs) on all Ti surfaces [16]. Figure 6-7 shows high magnification of "footprint" on Ti surface. It can be seen that there was not an "attack" on Ti surface, rather a release of intracellular contents which becomes adhered to the Ti surface.
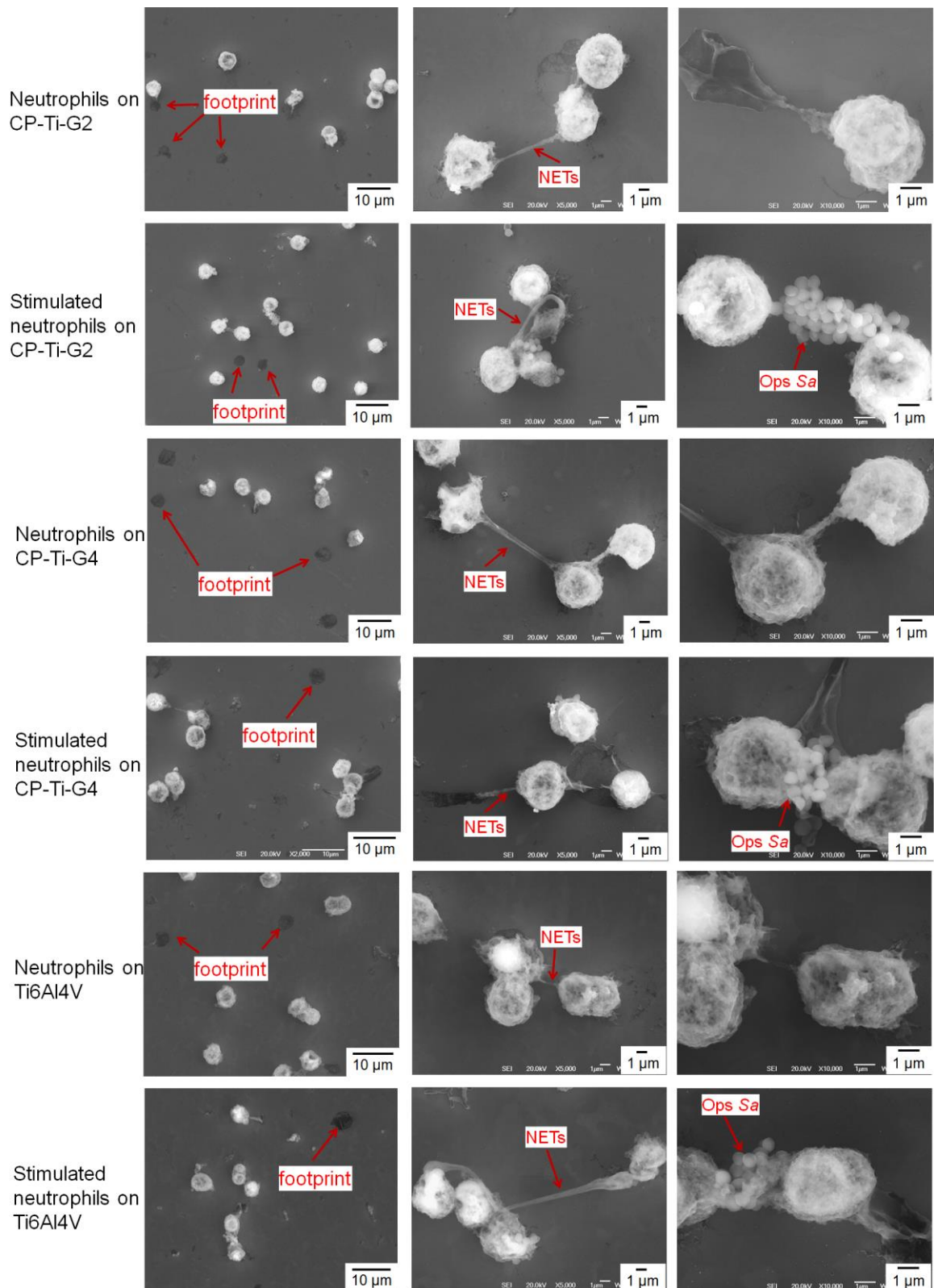
Figure 6-6 SEM images of un-stimulated neutrophils and neutrophils stimulated by Ops *Sa* on three grades of Ti surfaces after 8 h incubation in Tris-buffer at 37 °C. NETs: neutrophil extracellular traps.

146
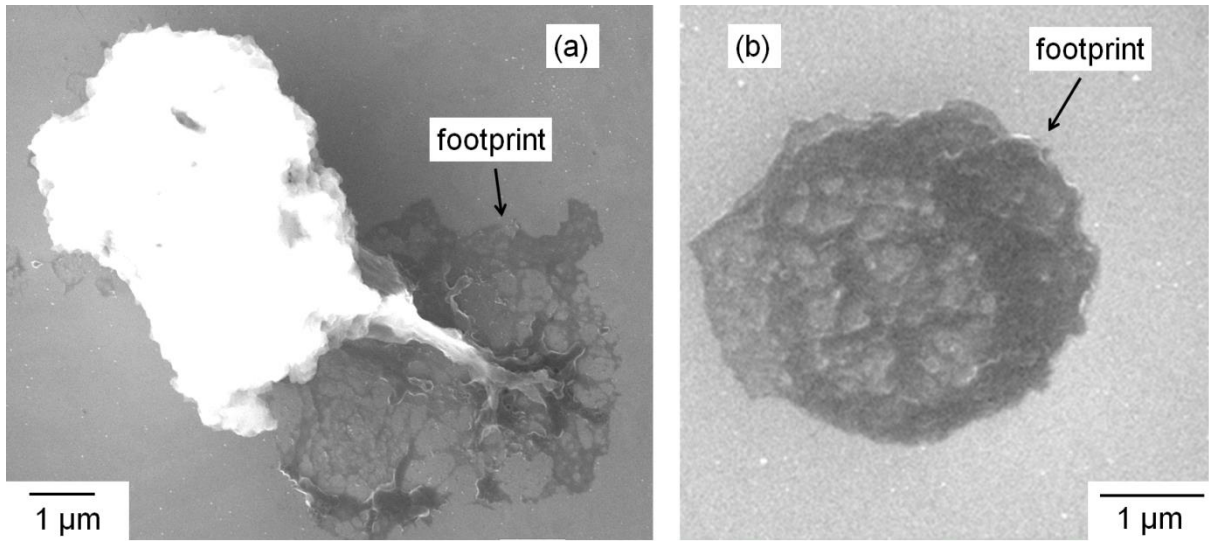
Figure 6-7 High magnification of "footprint" (due to degranulation or cell lysis) created by un-stimulated neutrophils on CP-Ti-G2 surface after 8 h incubation in Tris-buffer at 37 °C.

6.4.2 Quantification of Ti release

Figure 6-8 and Table 6-2 show the concentrations of Ti released from three grades of Ti in the absence and presence of neutrophils in an un-stimulated or stimulated state. It should be noted that the sample measured with ICP-MS for each test under each condition was created by pooling together 24 experimental repeat samples generated under the same conditions to achieve the required sample volume for the ICP-MS measurements. For each test, neutrophils were isolated from 4 or 5 individuals to obtain enough cells to be distributed among the 8 groups (n=24, per group). The detailed experimental procedures are described in Section 3.4.1. The concentrations of Ti released from CP-Ti-G2, CP-Ti-G4 and Ti6Al4V groups (control groups without neutrophils) were negligible (Figure 6-8 and Table 6-2).

Increased Ti release from the three grades of Ti was observed in the presence of neutrophils. A relatively higher Ti concentration was found in the control cell group (without Ti disc) in test 3

which may be possibly due to previous exposure of one or more of the individual cell donors to Ti. However, the increase in the amount of released Ti in test 3 remained larger when compared with the other two tests relative to the baseline concentration of Ti in the control sample. Natural variability in the concentration of Ti released between tests would be expected as there is considerable variability in the reactivity of neutrophils obtained from different donors. In addition, no significant difference was observed for the Ti release between the un-stimulated neutrophils and neutrophils stimulated with Ops *Sa*. Ti level was also observed in the control Ops *Sa* group, which could be due to low level exposure of the *Sa* culture to Ti or polyatomic interferences because of the complexity of the samples.
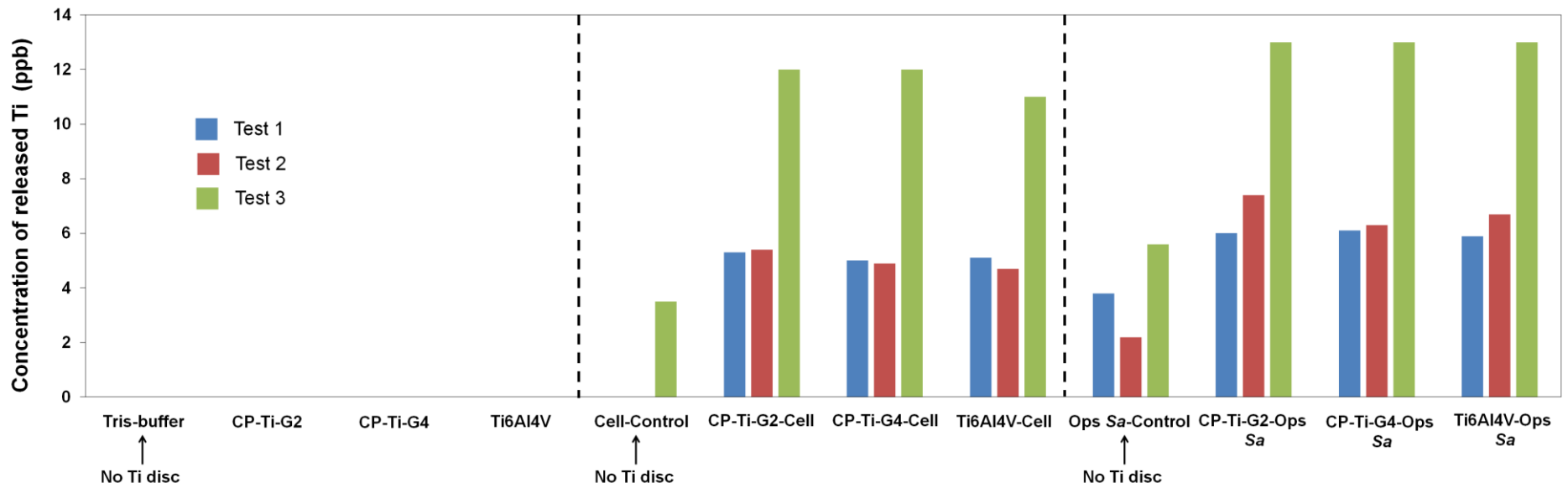
Figure 6-8 Concentration (ppb) of Ti released measured with ICP-MS from mirror-polished CP-Ti-G2, CP-Ti-G4, Ti6Al4V in the absence and presence of neutrophils in an un-stimulated or stimulated (by Ops *Sa*) state after 8 h incubation in Tris-buffer at 37 °C. Cell-Control: Tris-buffer+cell without any Ti disc. Ops *Sa*-Control: Tris-buffer+cell+Ops *Sa* without any Ti disc.

Table 6-2 The concentration (ppb) of Ti released measured with ICP-MS from mirror-polished CP-Ti-G2, CP-Ti-G4, Ti6Al4V in the absence and presence of neutrophils in an un-stimulated or stimulated (by Ops *Sa*) state after 8 h incubation in Tris-buffer at 37 °C. The detection limit is 1 ppb, the value less than 1 ppb is for information only. Cell-Control: Tris-buffer+cell without any Ti disc. Ops *Sa*-Control: Tris-buffer+cell+Ops *Sa* without any Ti disc.

Condition	Test 1	Test 2	Test 3
Tris-buffer	<0.2	<0.2	<0.2
CP-Ti-G2	0.3	0.4	0.5
CP-Ti-G4	0.2	0.3	0.5
Ti6Al4V	0.5	0.5	0.5
Cell-Control	0.4	0.4	3.5
CP-Ti-G2-Cell	5.3	5.4	12
CP-Ti-G4-Cell	5	4.9	12
Ti6Al4V-Cell	5.1	4.7	11
Ops *Sa* -Control	3.8	2.2	5.6
CP-Ti-G2-Ops *Sa*	6	7.4	13
CP-Ti-G4-Ops *Sa*	6.1	6.3	13
Ti6Al4V-Ops *Sa*	5.9	6.7	13

6.5 Discussion - effect of neutrophils on Ti corrosion

Neutrophils migrate in large numbers into the tissues surrounding implants as the body's first line of defence against infection or injury [152, 153]. The neutrophil has a number of killing mechanisms which include the release of antimicrobial proteins (degranulation) and the generation of reactive oxygen species (ROS) through a process termed "respiratory burst" due to its consumption of oxygen [154, 156, 193]. During "respiratory burst", ROS species are directly or indirectly produced, which include superoxide (O_2^-), hypochlorous acid (HOCl), H_2O_2 and chloramines (Figure 6-9) [16, 155, 156]. It is established that bacteria, Ti ions and Ti dioxide particles can stimulate ROS production from neutrophils which is then released into the

immediate extracellular environment [16, 157, 158]. In this study, evidence of activated neutrophils present on Ti surfaces included the "footprints" of degranulation and the formation of NETs even when no deliberate stimulation with Ops *Sa* was performed (Figure 6-6).
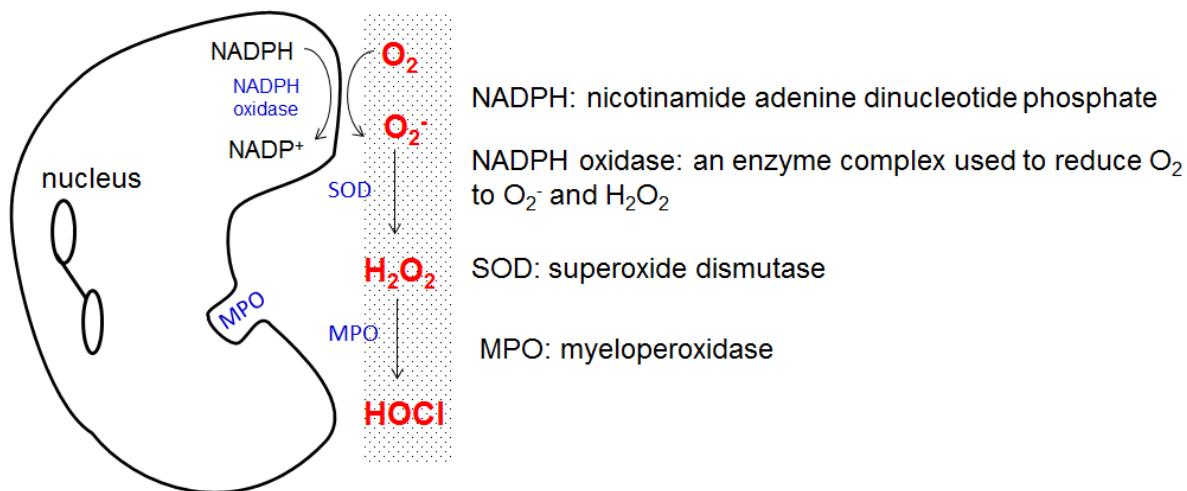
Figure 6-9 Schematic representation of ROS release from neutrophils [16, 194].

Figure 6-8 shows that the presence of neutrophils resulted in increased Ti release from all three grades of Ti. No significant effect of Ti grade on the magnitude of Ti release was observed. The level of Ti in the neutrophils can be estimated if it is assumed that the released Ti is concentrated within the neutrophils. The neutrophil is assumed to be a sphere with a diameter of 5 μm [152] and the concentration of neutrophils used was 2.5×10^6 cells/mL. Thus the volume of neutrophils in the solution is 1.6×10^{-4} mL per mL, so the Ti level in the cellular volume varies between 30 and 60 ppm in this study.

ROS release by macrophages has been previously demonstrated to lead to the release of Ti when cultured in the presence of a Ti surface [30], but has not been demonstrated in association with neutrophils. The observed effect of neutrophils is important as neutrophils are the most abundant immune cells in dental peri-implant sites and the findings confirm that ROS species

produced are capable of destabilising the passive film on Ti surfaces leading to Ti dissolution. Apart from H_2O_2 there is little literature regarding the interactions of ROS species with Ti. However although not been specifically demonstrated on Ti, HOCl and chloramines have been reported to induce copper or lead dissolution [195, 196]. Further systematic studies are required to understand the potential effects of other ROS on Ti to identify which, if any, is more important in inducing Ti dissolution.

Although increased ROS production has been observed in neutrophils in the presence of Ops *Sa* when compared with un-stimulated cells [16], this study demonstrated that the addition of Ops *Sa* did not lead to significantly greater Ti release (Figure 6-8). However, for the neutrophils not exposed to Ops *Sa*, there was also evidence of stimulation, and it is well accepted that neutrophils produce a resting level of extracellular ROS [16]. It is possible that the additional ROS produced by the neutrophils stimulated with Ops *Sa* interacts directly with these bacteria and is therefore consumed before it has a chance to encounter the Ti surface. As a result the actual exposures of ROS species to the Ti surface may have been similar although this was not demonstrated empirically.

Increased Ti release was observed in test 3 when compared with the other two tests (Figure 6-8). It is known that the neutrophils of different people behave differently as a function of a variety of factors including age [197]. Hence, in this study different peoples' neutrophils may have different activity and reactivity which is directly related to the magnitude and kinetics of ROS release. This will directly influence the ROS exposure to the Ti sample, and the consistent elevation of Ti concentration detected from all experimental groups in test 3 supports this assumption that the neutrophils isolated for this measurement were more reactive. Unfortunately, this individual variability is extremely difficult to predict and subsequently

control. The study is also complicated by the knowledge that Ti released as a consequence of corrosion can itself potentially stimulate further ROS release from neutrophils or prime neutrophils to produce more ROS [16]. Stimulation of ROS production from neutrophils has been demonstrated by metallic Ti particles and TiO_2 particles in various sizes or concentrations [152, 157, 158].

6.6 Conclusions

1. The effect of *S. sanguinis* on corrosion behaviour of three grades of Ti possessing two types of surface finish (mirror-polished and sandblasted-acid-etched (SLA)) was investigated using solution analysis and SEM. The presence of *S. sanguinis* leads to increased Ti release by promoting Ti corrosion, especially for the SLA samples.

2. Neutrophils, which are the predominant immune cells in the peri-implant environment, were incubated with Ti *in vitro* to investigate the influence on Ti degradation. The presence of neutrophils leads to more Ti release but this effect may vary between different individuals.

7 MECHANICALLY-ASSISTED CREVICE CORROSION OF TI

7.1 Introduction

The aim of the work described in this chapter is to design a novel mechanically-assisted crevice corrosion (MACC) apparatus to simulate the interface between an implant and bone/bone cement, or the taper interface of modular hip implant for *in vitro* investigation of MACC behaviour of Ti alloys. Firstly, the MACC device was tested on a Ti6Al4V/Ti6Al4V couple in physiological saline with pH indicator to investigate the chemistry of MACC. The surface morphologies of abrasion scars and abrasion debris were also characterised by SEM. Secondly, to understand the differences under the static and abrasion conditions, anodic and cathodic polarisation curves of the Ti6Al4V couple were analysed. The influence of the mechanical parameters including rotation speed and load in the abrasion status on MACC of Ti6Al4V was studied in physiological saline. In addition, the preliminary study was also conducted to explore the influence of albumin, LPS and H_2O_2 on MACC behaviour of Ti6Al4V using this apparatus. The average abrasion current and accumulated abrasion charge of the Ti6Al4V couple during abrasion process were compared in the absence and presence of albumin, LPS and H_2O_2.

7.2 Results

7.2.1 MACC apparatus with designed crevice geometry

Figure 7-1a shows that the OCP of the Ti6Al4V couple exhibited a gradually increasing trend when there was no motion between the two components (static condition) during 1 h immersion. After this, a potential of 10 mV vs. Ag/AgCl was applied and the current was monitored (Figure 7-1b, MACC test-1). The steady state current under the static condition (static current) was very small (<0.1 µA) before rotation. Immediately after rotation started, the current rapidly increased to ~6 µA (Figure 7-1c) due to the rupture/removal of passive film and exposure of the underlying bare metal to the solution. The abrasion current slightly increased during the 7 h abrasion process, possibly due to the development of a more aggressive environment in the crevice. When the rotation was stopped, the current immediately decreased (Figure 7-1d) because of repassivation of the metal.
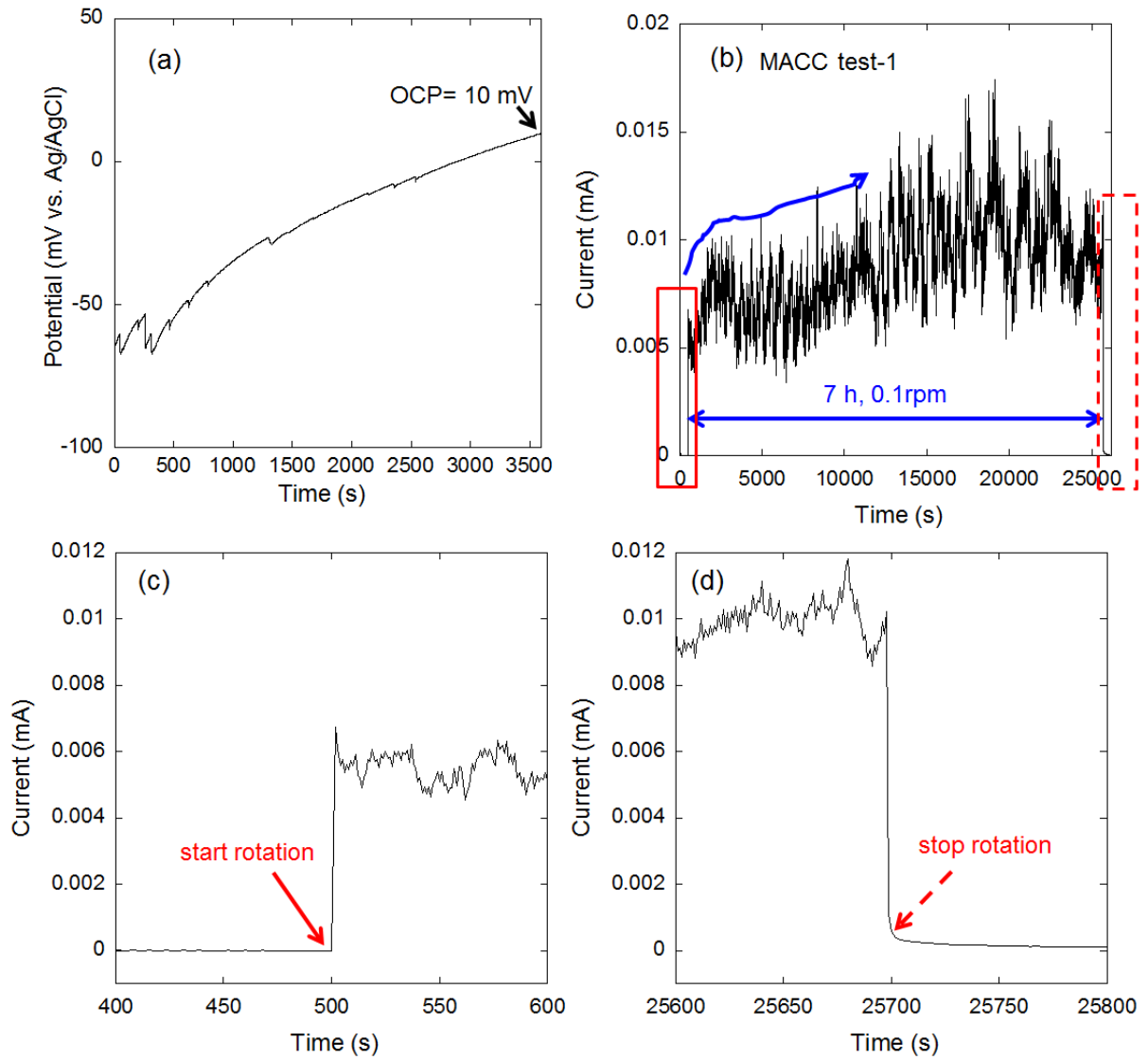
Figure 7-1 (a) OCP as a function of time for 1 h under static condition (no rotation); (b) current as a function of time at 10 mV vs. Ag/AgCl with rotation; (c) details of the start of rotation (solid red box in (b)); (d) end of rotation (dashed red region outlined in (b)) for a Ti6Al4V couple before, during and after rotation at 0.1 rpm under an applied load of 2400 g in physiological saline with pH indicator at room temperature (MACC test-1).

Figure 7-2 shows the pH change of the solution during MACC test-1. The acidic region (at the mouth of the Ti6Al4V couple) and alkaline region (near the Pt mesh) were clearly observed according to the colour change of the solution. In addition, after uncoupling the rotating and

156

stationary parts in the end of the test, the solution inside the cavity of the stationary part (crevice geometry) was also found to be highly acidic (corrected pH ~2).
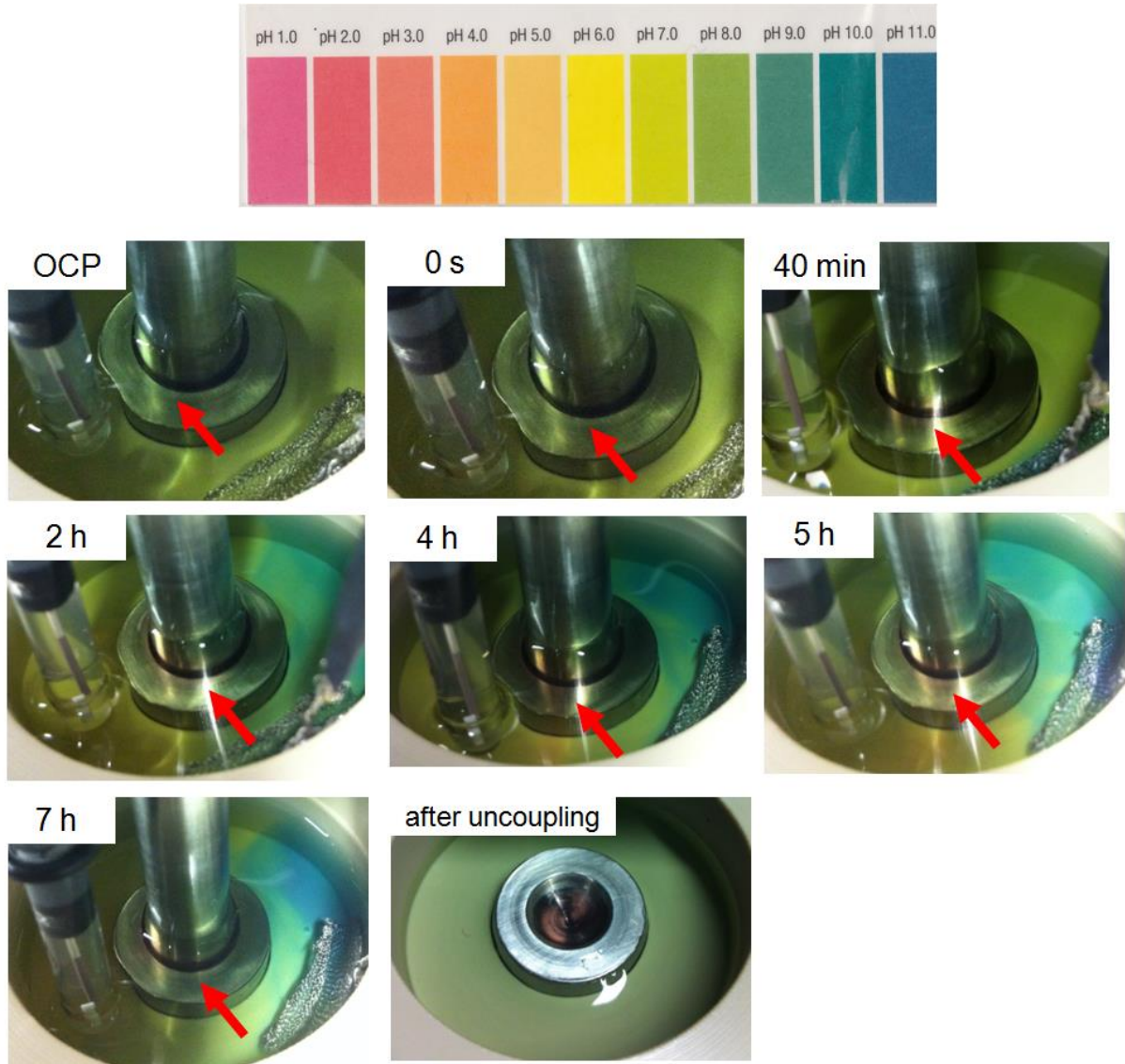
Figure 7-2 pH changes during static OCP measurement (no rotation), abrasion process (0-7 h rotation) and after uncoupling rotating and stationary parts in the end of MACC test-1 (described in Figure 7-1, applied potential: 10 mV vs. Ag/AgCl, load: 2400 g, rotation speed: 0.1 rpm) at room temperature; the outer diameter of the stationary part is 20 mm. The red arrow points towards the red-coloured acidic region at the crevice site.

Figure 7-3 shows the OCP as a function of time for the Ti6Al4V couple under static and abrasion conditions. It can be seen that after the rotation started the OCP rapidly decreased to ~-450 mV vs. Ag/AgCl due to the removal of passive film and exposed bare metal surface to the solution. The abrasion process lasted for 7 h. When the rotation was stopped the OCP rapidly increased because of repassivation of the metal. It also can be seen that the pH of the solution became a little alkaline after abrasion. The solution in the cavity of the stationary part was found to be highly acidic (corrected pH ~2) after uncoupling the rotating and stationary parts in the end of the OCP test (Figure 7-3).
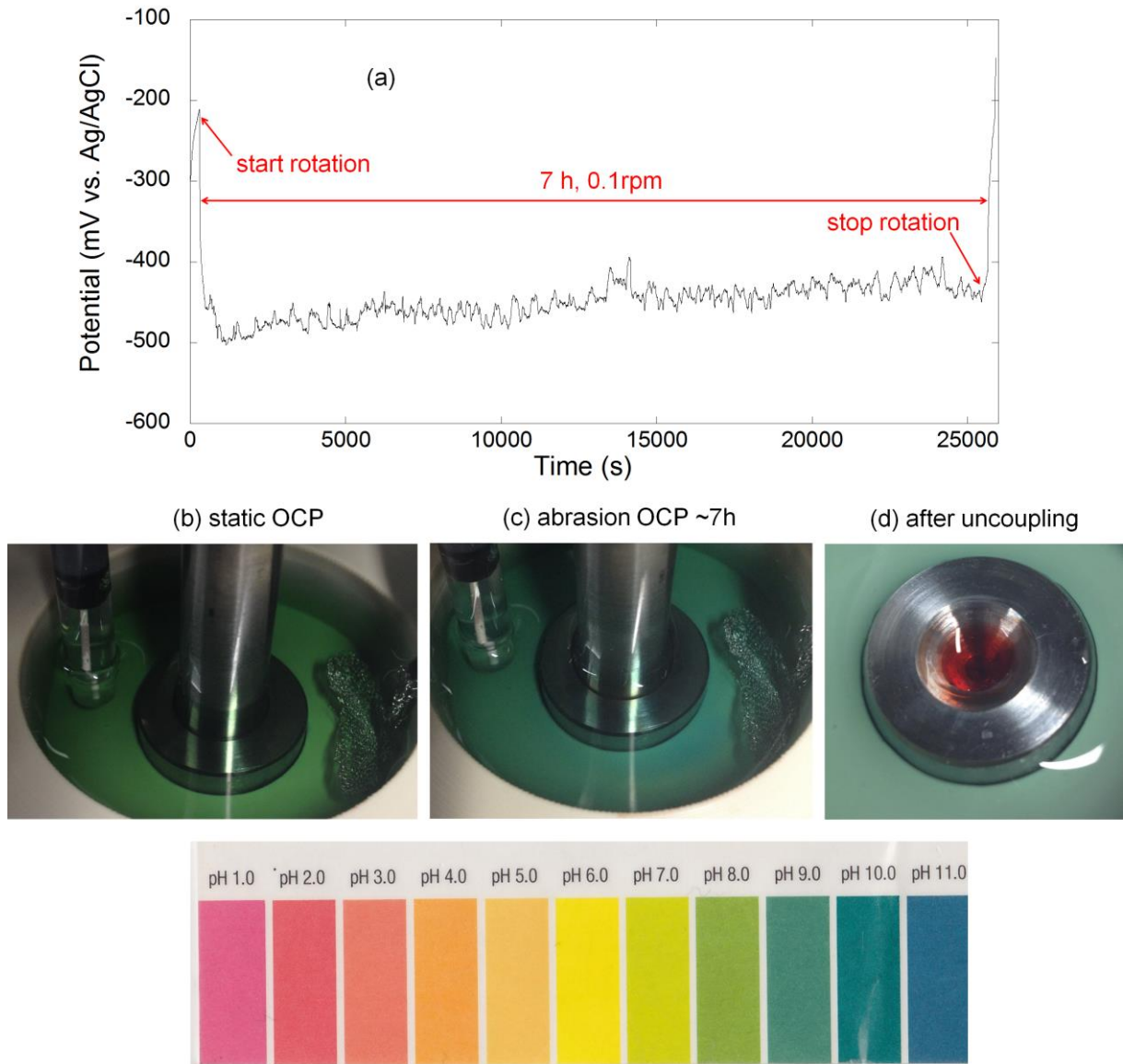
Figure 7-3 (a) OCP as a function of time for the Ti6Al4V couple and (b-d) pH change of physiological saline during static and abrasion (rotation 0.1 rpm) conditions under an applied load of 3200 g at room temperature; the outer diameter of the stationary part is 20 mm.

7.2.2 Surface morphology

Figure 7-4 shows the stationary part of the Ti6Al4V couple before and after MACC test-1. It can be seen that more abrasion scars appeared on the stationary part after the MACC test-1. Some abrasion scars can be seen before the test, because the Ti6Al4V couple had previously been used for preliminary experiments.

Figure 7-5 shows SEM images of the abrasion scars. Severe plastic deformation of the Ti6Al4V surface with detached particles with different sizes and shapes was observed over the abrasion area.
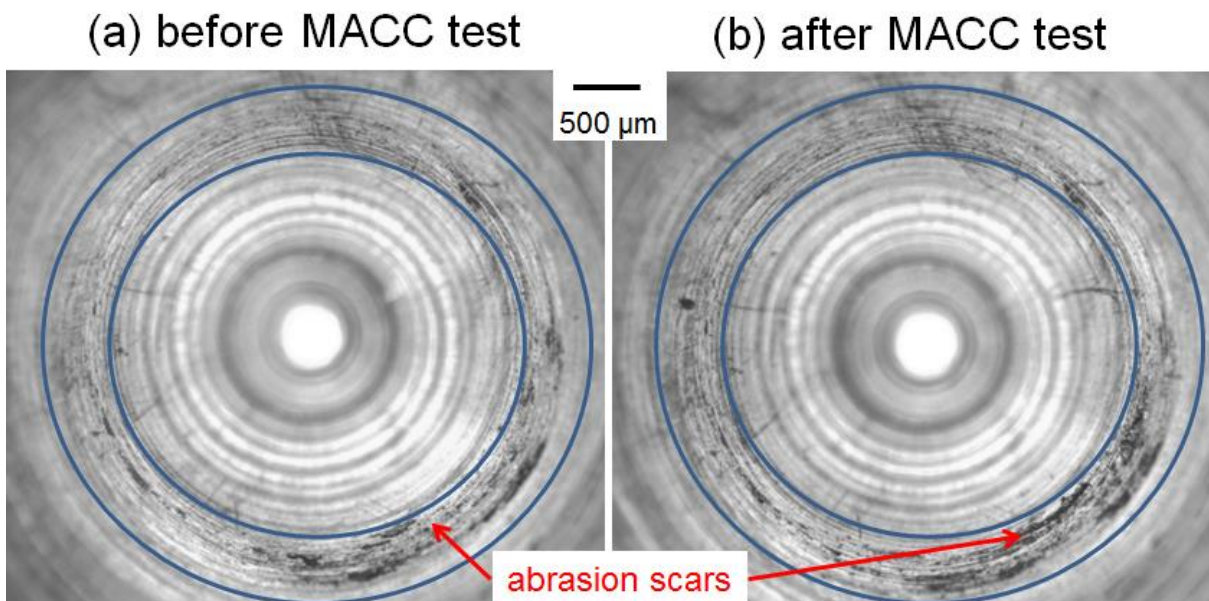
Figure 7-4 Optical images of the stationary part (a) before and (b) after MACC test-1 (described in Figure 7-1, applied potential: 10 mV vs. Ag/AgCl, load: 2400 g, rotation speed: 0.1 rpm) in physiological saline at room temperature.
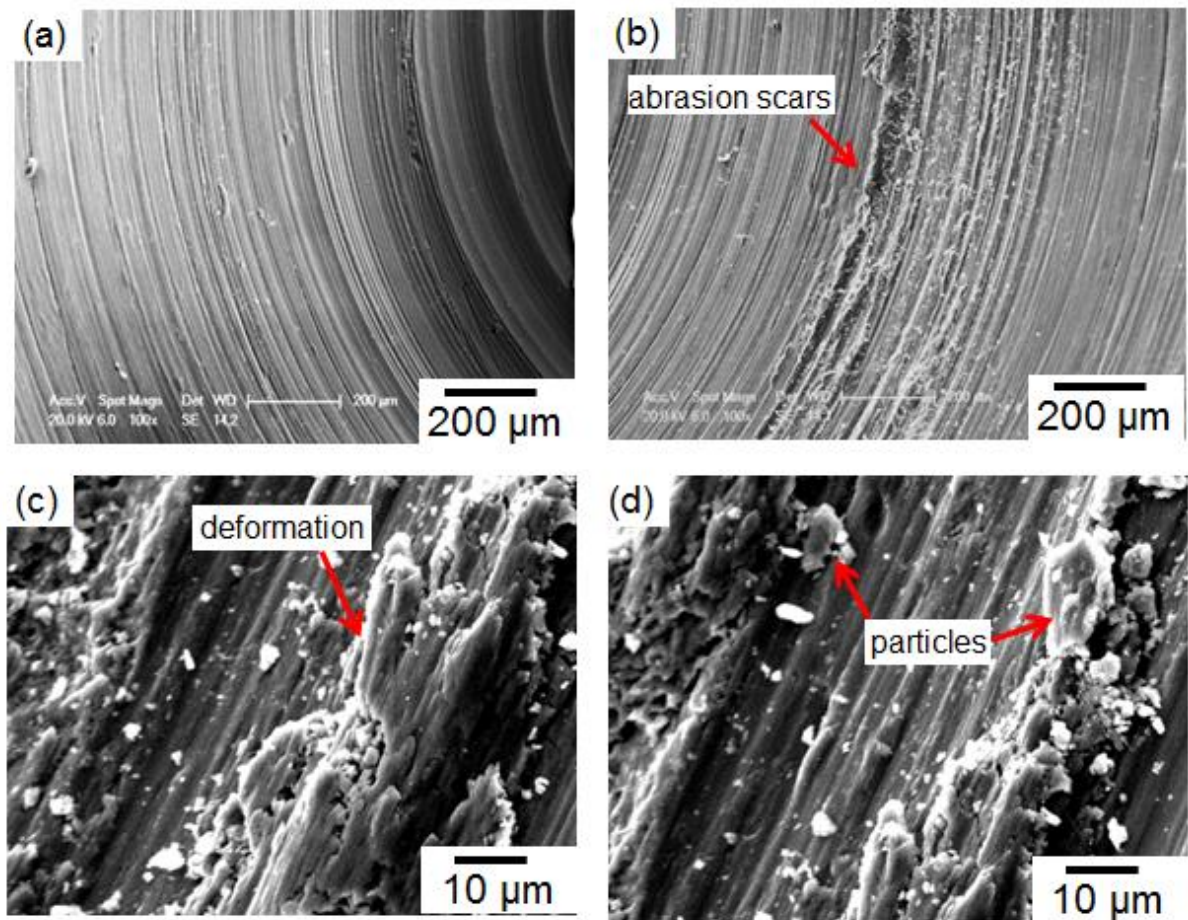
Figure 7-5 SEM images of (a) regions with few scars; (b-d) regions with clear abrasion scars on the stationary part after MACC-test 1 (described in Figure 7-1, applied potential: 10 mV vs. Ag/AgCl, load: 2400 g, rotation speed: 0.1 rpm) at room temperature.

To characterise the black debris collected from the cavity in the stationary part, another MACC test (MACC test-2) was conducted in physiological saline without pH indicator. Similar to MACC test-1, the OCP of the Ti6Al4V couple showed a gradually increasing trend under static conditions during 1 h immersion (data not shown). After this, a potential of 40 mV vs. Ag/AgCl (the final OCP) was applied and current was monitored (load: 3200 g, rotation speed: 0.1 rpm, abrasion time: 7 h, data not shown).

Figure 7-6 shows the morphology of the collected black debris after MACC test-2. The fragments were variously shaped with sizes from several to hundreds of micrometres, which are similar to the detached particles on the stationary part (Figure 7-5). The fragments were mainly Ti6Al4V metallic particles (EDX in Figure 7-6c).
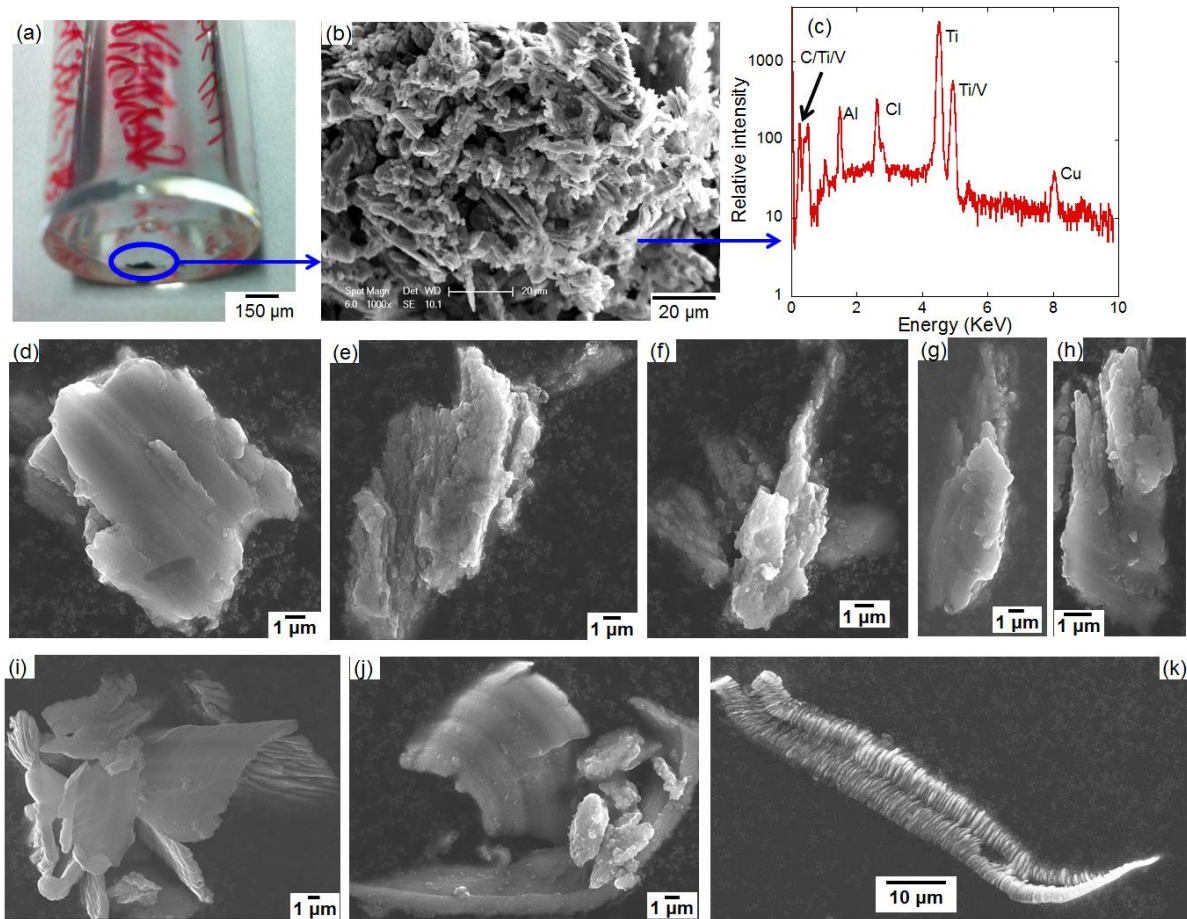
Figure 7-6 (a) A picture of the collected black debris; (b, d-k) SEM images and (c) EDX spectrum of abrasion black debris after MACC test-2 in physiological saline without pH indicator (applied potential: 40 mV vs. Ag/AgCl, load: 3200 g, rotation speed: 0.1 rpm) at room temperature.

7.2.3 Anodic and cathodic polarisation curves

Figure 7-7a shows the OCP as a function of time for the Ti6Al4V couple under the static and abrasion conditions before anodic and cathodic polarisation measurements. It can be seen that the Ti6Al4V couple exhibited a gradually increasing trend under static conditions (static OCP) while the OCP of the Ti6Al4V rapidly decreased at the start of rotation (abrasion OCP). The abrasion OCP was much more negative than the static OCP. Since the final static OCP of the Ti6Al4V couple were not exactly the same, a potential of 0 mV vs. Ag/AgCl was chosen for the potentiostatic measurements in the following sections.

Figure 7-7b shows the anodic and cathodic polarisation curves of the Ti6Al4V couple in physiological saline under static and abrasion conditions. The cathodic polarisation curves under the static and abrasion conditions were similar, while the anodic current under the abrasion condition became higher than the static condition, due to the increased anodic reaction of bare metal as a result of destruction of passive film during the abrasion process.
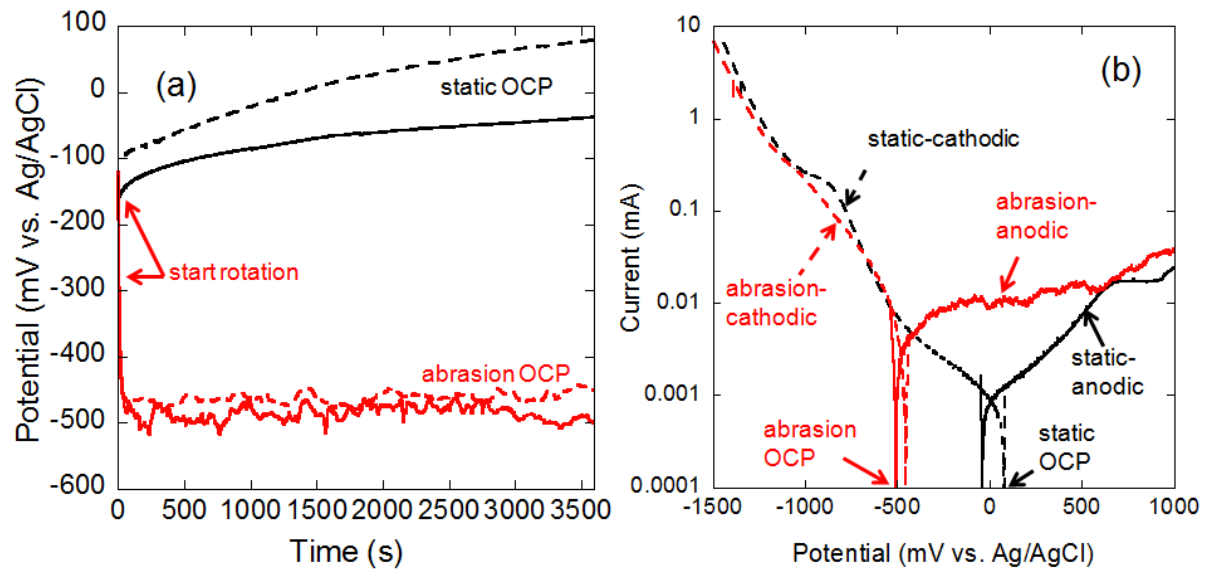
Figure 7-7 (a) OCP as a function of time; (b) anodic (solid line) and cathodic (dash line) polarisation curves of the Ti6Al4V couple in physiological saline during the static and abrasion (rotation at 0.1 rpm) processes under an applied load of 3200 g at room temperature. The anodic polarisation curves were measured by sweeping the potential from -50 mV below the OCP to 1000 mV vs. Ag/AgCl at a rate of 1 mV/s, and the cathodic polarisation curves were measured by sweeping the potential from 50 mV above the OCP to -1500 mV vs. Ag/AgCl at a rate of 1 mV/s.

7.2.4 Effect of rotation speed and load on abrasion OCP

Figure 7-8 shows the schematic diagram of the sequence of different rotation speeds applied to investigate its effect on abrasion OCP of the Ti6Al4V couple in physiological saline.
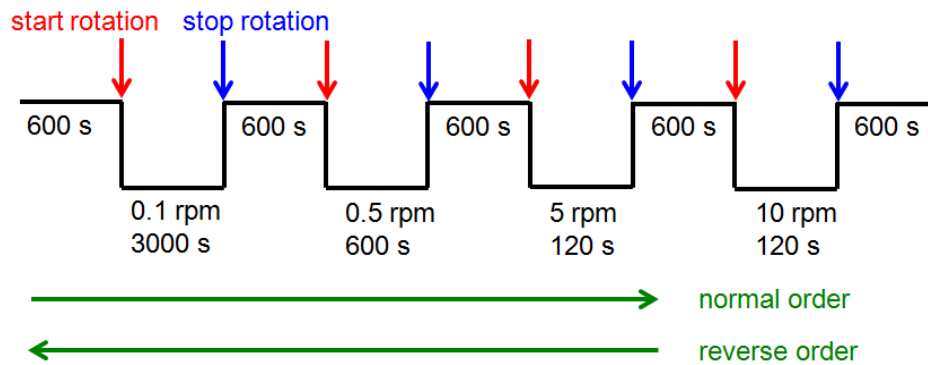
Figure 7-8 Schematic diagram of one sequence of rotation speeds used to study the effect of rotation speed on abrasion OCP, the reverse order was also used for comparison with the normal order.

Figure 7-9 shows the OCP change of the Ti6Al4V couple with different rotation speeds under different loads. When the applied load was 250 g, the abrasion OCP decreased with increasing rotation speed (Figure 7-9a). To confirm that the change in OCP was not a time-dependent change (a "history effect"), the OCP was also monitored as the rotation speed was progressively decreased. With a decrease in rotation speed, the abrasion OCP became less negative (shown in Figure 7-9b). The similar trend of abrasion OCP was also observed when a higher load of 3200 g was used (Figure 7-9c and Figure 7-9d).

Figure 7-10 shows that the abrasion OCP became more negative under a greater load than under a smaller load, possibly due to the increased contact area under a higher load.
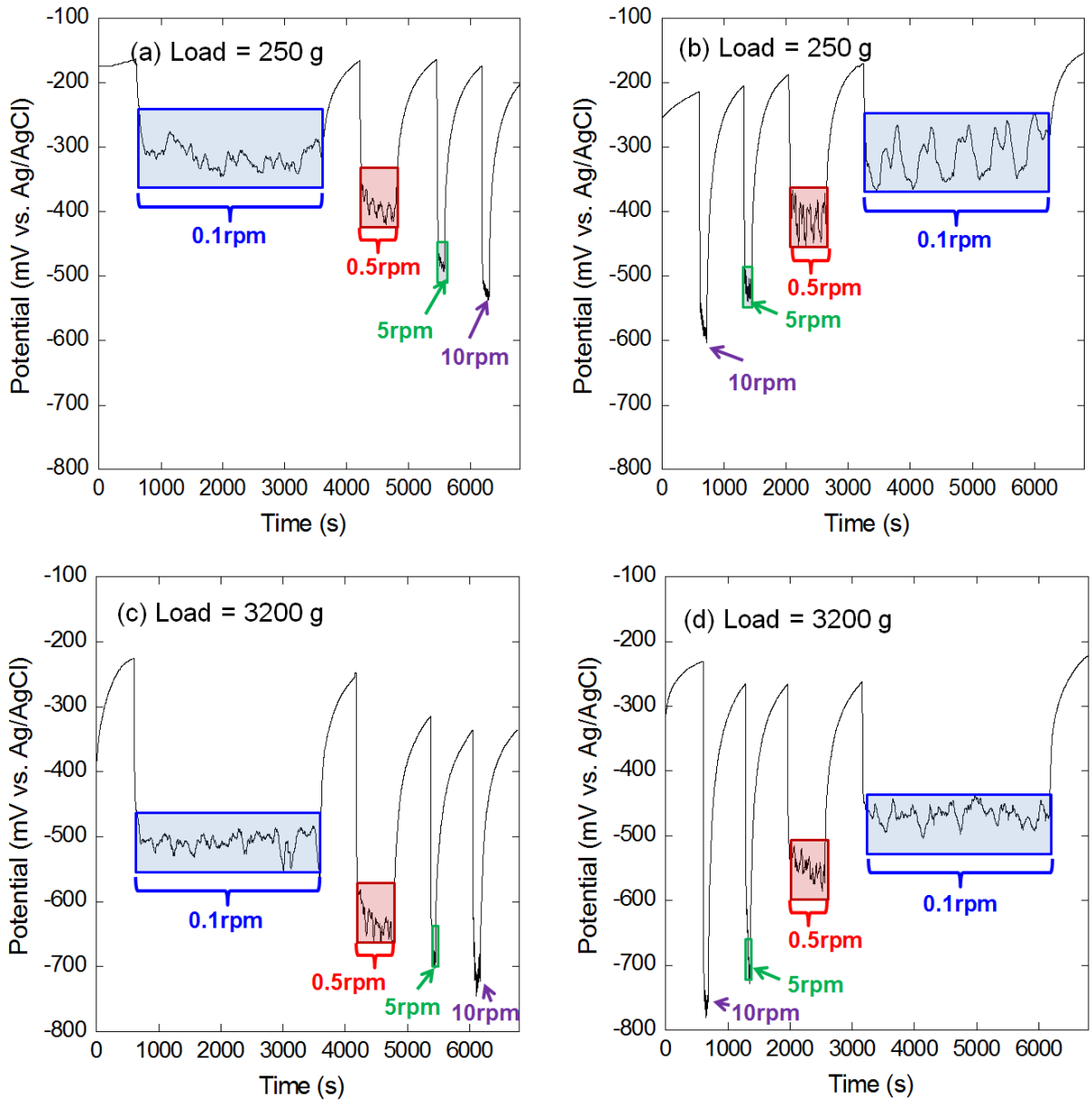
Figure 7-9 OCP of the Ti6Al4V couple in physiological saline before, during and after rotation at different speeds under applied loads (a-b) 250 g and (c-d) 3200 g at room temperature (the sequence of the used rotation speeds is shown in Figure 7-8).
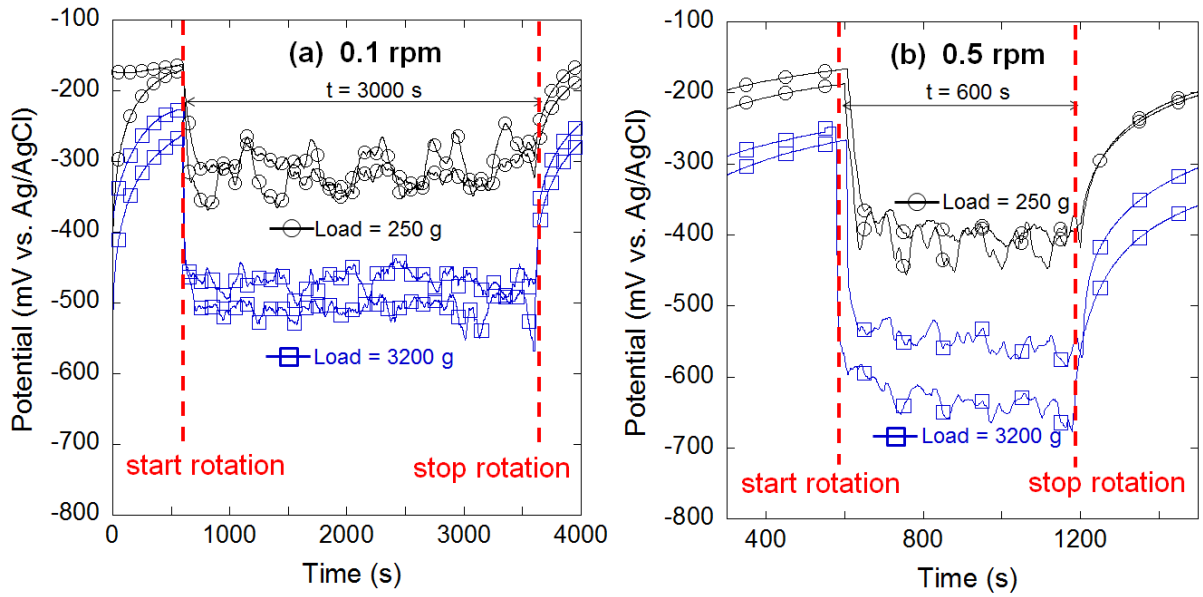
Figure 7-10 OCP comparison of the Ti6Al4V couple in physiological saline at (a) 0.1 rpm and (b) 0.5 rpm under different applied loads at room temperature.

7.2.5 Effect of rotation speed and load on abrasion current

Figure 7-11 shows the schematic diagram of the sequence of applied rotation speed to investigate its effect on abrasion current of the Ti6Al4V couple in physiological saline.
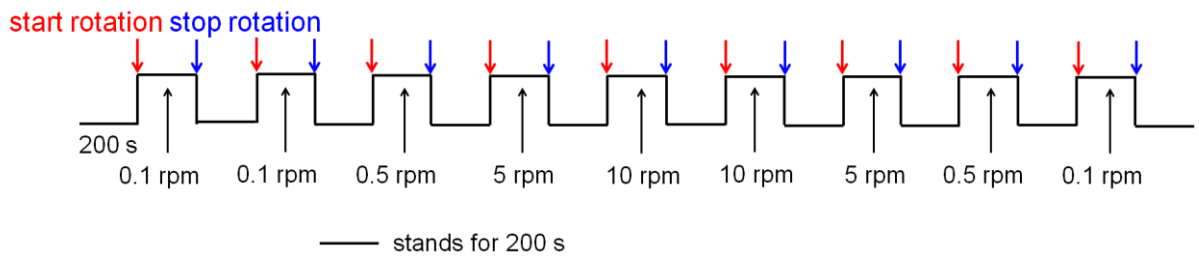
Figure 7-11 Schematic diagram of one sequence of applied rotation speed to study its effect on abrasion current.

Figure 7-12 shows the current as a function of time for the Ti6Al4V couple in physiological saline at a potential of 0 mV vs. Ag/AgCl with different rotation speeds and different loads. The abrasion current of the Ti6Al4V couple increased with increasing rotation speed for both applied loads.

In addition, Figure 7-13 shows that the abrasion current was much higher under a greater load than a smaller load at a same rotation speed, and also demonstrates that this behaviour is consistent over time since the traces shown for each rotation speed were carried out before and after measurements at higher rotation speeds (see Figure 7-12).
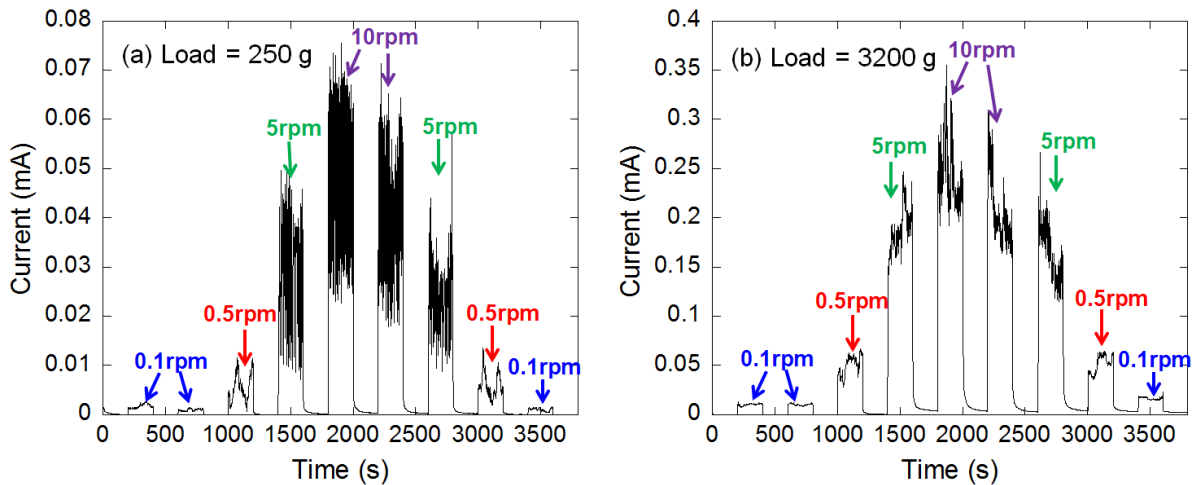
Figure 7-12 Current as a function of time for the Ti6Al4V couple in physiological saline at different rotation speeds under applied loads of (a) 250 g and (b) 3200 g at 0 mV vs. Ag/AgCl at room temperature.
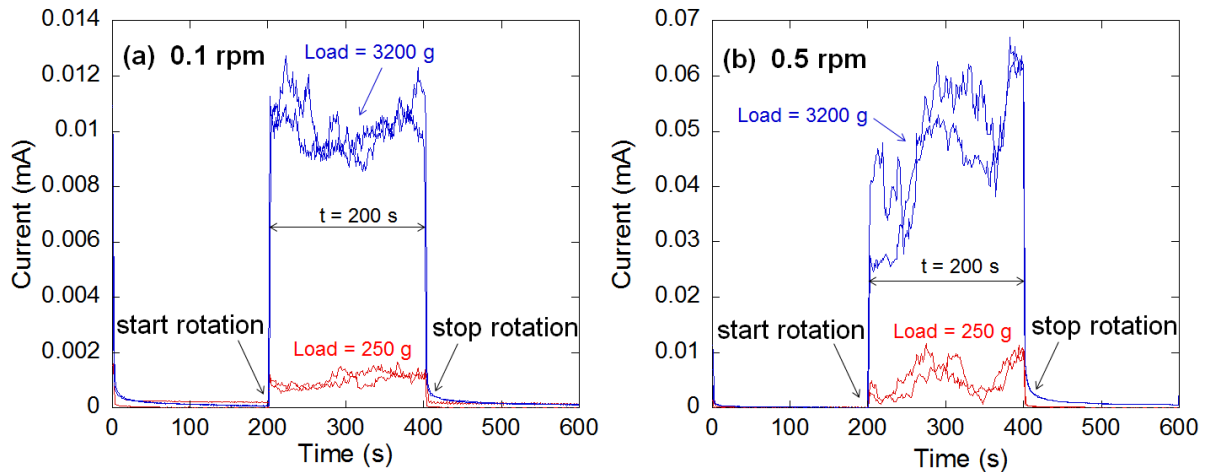
Figure 7-13 Abrasion current comparison of the Ti6Al4V couple in physiological saline at a rotation speed of (a) 0.1 rpm and (b) 0.5 rpm under different applied loads at 0 mV vs. Ag/AgCl at room temperature. The same data are shown as a function of time in Figure 7-12.

7.2.6 Effect of albumin, LPS and H_2O_2 on MACC of Ti6Al4V

7.2.6.1 Effect of time at OCP for the static couple on the subsequent abrasion current

Figure 7-14a shows the OCP as a function of different time for the static Ti6Al4V couple in physiological saline for four different tests. The values of the static OCP varied amongst the different tests (Table 7-1), possibly due to different levels of damage to the passive films on the two surfaces during assembly. Figure 7-14b shows the subsequent abrasion currents as a function of time, which show that the value of static OCP and the time at OCP before the abrasion test did not have a significant effect on the average abrasion current. Figure 7-14c and Figure 7-14d show the average values of the abrasion current in the four tests and the corrected pH of the solution in the cavity at the bottom of stationary part after the tests as a function of the final OCP prior to the test and the time length at OCP prior to the test, respectively. It is clear that neither the final OCP nor the length of time at OCP had an effect on the subsequent

169

abrasion currents or corrected pH, so the subsequent experiments were all carried out with 10 minutes of static OCP measurements prior to abrasion tests.
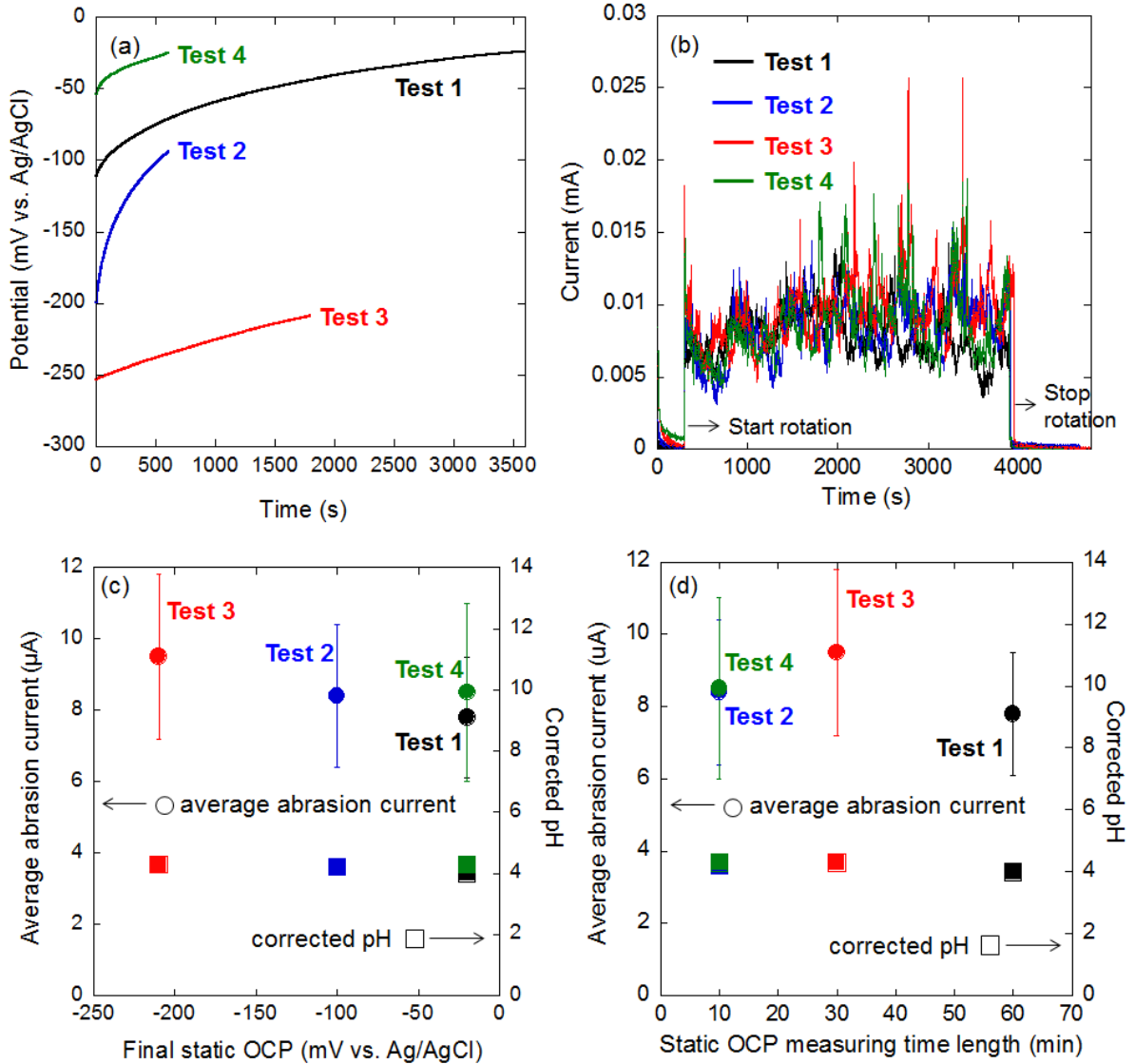
Figure 7-14 (a) Static OCP as a function of time prior to MACC (abrasion at 0.1 rpm) tests; (b) current as a function of time at a potential of 0 mV vs. Ag/AgCl following OCP measurements; (c) average abrasion current and corrected pH vs. final static OCP and (d) average abrasion current and corrected pH vs. static OCP measuring time length of the Ti6Al4V couple in physiological saline under an applied load of 3200 g at room temperature. Error bars refer to 1 standard deviation. The corrected pH refers to the pH of the solution in the cavity in the stationary part of the couple.

Table 7-1 Experimental parameters during static OCP measurements and subsequent MACC (abrasion at 0.1 rpm) tests of the Ti6Al4V couple at 0 mV vs. Ag/AgCl under applied load of 3200 g in physiological saline at room temperature. The corrected pH refers to the pH of the solution in the cavity in the stationary part of the couple.

	Final static OCP (mV vs. Ag/AgCl)	Static OCP measuring time length (min)	Average abrasion current (μA)	Corrected pH
Test 1	-20	60	8±2	3.9
Test 2	-100	10	8±2	4.1
Test 3	-210	30	10±2	4.2
Test 4	-20	10	9±3	4.2

7.2.6.2 Typical MACC Experiment

For each experiment, a sequence of 12 tests was carried out to examine the effect of a species (albumin, LPS or H_2O_2) on MACC behaviour of the Ti6Al4V couple. In between each test, the solution was removed; the Ti6Al4V couple, MACC cell and electrodes were all cleaned with deionised water. Afterwards, the cell was reassembled and a fresh solution was added. In each experiment, the sequence of the solution used in individual tests was ABBA or BAAB (A: physiological saline, B: physiological saline with addition of albumin, LPS or H_2O_2) to reduce the "history" effect (time-dependence).

Figure 7-15 shows one typical MACC test of the Ti6Al4V couple in physiological saline at 0.1 rpm (i.e. 600 s per cycle) under a load of 3200 g at room temperature. The abrasion process lasted for 3600 s (6 cycles). The average abrasion current and total accumulated abrasion charge during the whole abrasion process (3600 s) was calculated and compared for a series of MACC tests in the following sections. Moreover, the accumulated abrasion charge in each cycle of the abrasion process was also calculated and compared separately.

It should be noted that a potential of 0 mV vs. Ag/AgCl was applied to investigate the effect of albumin and LPS on MACC of Ti6Al4V in physiological saline. For the effect of H_2O_2, a potential of 300 mV vs. Ag/AgCl was applied due to a more positive OCP value of the Ti6Al4V couple in physiological saline with addition of H_2O_2.
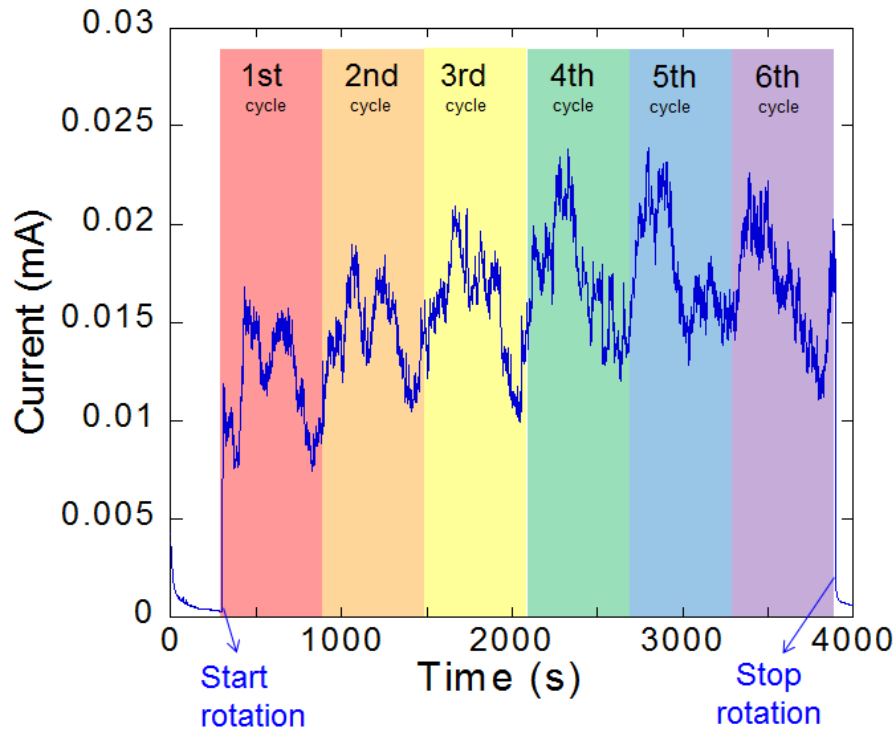
Figure 7-15 A typical MACC test of the Ti6Al4V couple in physiological saline at 0 mV vs. Ag/AgCl at 0.1 rpm (i.e. 600 s per cycle) under an applied load of 3200 g at room temperature. The abrasion process lasted for 3600 s (6 cycles).

7.2.6.3 Effect of albumin on MACC of Ti6Al4V

Table 7-2 lists the experimental parameters from a series of MACC tests of Ti6Al4V in physiological saline in the absence and presence of albumin. It can be seen that the static OCP in each test was negative to 0 mV vs. Ag/AgCl and the static current was very small ($<0.3 \mu A$) before rotation (Table 7-2). After each test, the cavity in the stationary part of the couple was

acidic, but the corrected pH did not show any significant change between the solutions with and

without albumin.

Table 7-2 Experimental parameters from a series of MACC tests of the Ti6Al4V couple at 0.1 rpm under an applied load of 3200 g in physiological saline (PS) with and without 1% albumin (A*) at 0 mV vs. Ag/AgCl at room temperature. Total accumulated abrasion charge refers to the values during the whole abrasion process (3600 s). The corrected pH refers to the pH of the solution in the cavity in the stationary part of the couple.

No.		Final static OCP (mV vs. Ag/AgCl)	Average abrasion current (μA)	Corrected pH	Static current before rotation (μA)	Total accumulated abrasion charge (Q/mC)
1	PS	-220	10±3	3.9	<0.3	36
2	PS+A*	-260	7±2	3.6	<0.3	27
3	PS+A*	-260	9±1	3.5	<0.2	31
4	PS	-230	11± 2	3.9	<0.2	39
5	PS	-110	16±4	3.9	<0.1	59
6	PS+A*	-170	10±2	4	<0.2	36
7	PS+A*	-130	8±2	4.1	<0.2	27
8	PS	-130	9± 2	4	<0.1	32
9	PS+A*	-50	9±3	4.1	<0.1	31
10	PS	-90	12±4	3.9	<0.1	43
11	PS	-90	14±4	3.9	<0.1	50
12	PS+A*	-120	9±2	4	<0.2	32

Figure 7-16 shows the average abrasion current and total accumulated abrasion charge during

each test. They follow the same trend since both are calculated by using all the data points of

currents in each test. There is significant variation from test to test, which may be a result of

differences in the way in which the cell was reassembled between every test. However, the

average abrasion current and total accumulated abrasion charge tend to be smaller in the presence of albumin.
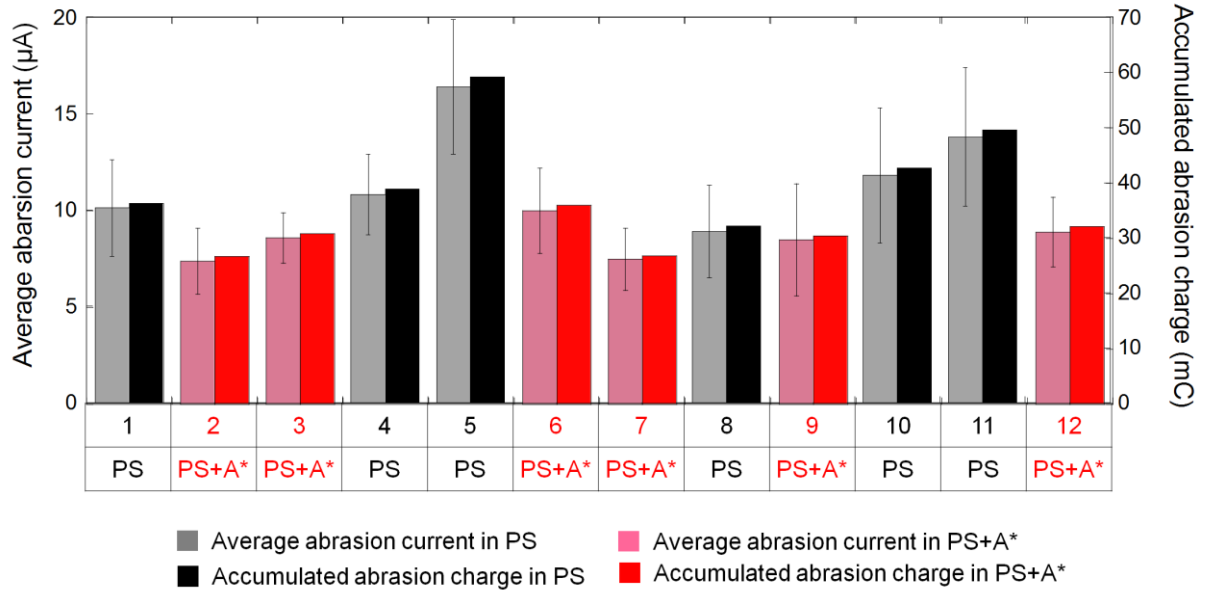
Figure 7-16 Average abrasion current and total accumulated abrasion charge during the whole abrasion process (3600 s) from a series of MACC tests of the Ti6Al4V couple at 0.1 rpm under an applied load of 3200 g in physiological saline (PS) with and without 1% albumin (A*) at 0 mV vs. Ag/AgCl at room temperature.

Figure 7-17a shows the accumulated abrasion charge for each cycle of the abrasion process from a series of MACC tests. It can be seen that the 1st cycle of the abrasion process has a similar charge in physiological saline with and without albumin. The accumulated abrasion charge tends to become higher in subsequent cycles in physiological saline without albumin, possibly due to the formation of a more aggressive solution in the crevice. In contrast, the accumulated abrasion charge tends to become lower for subsequent cycles in albumin-containing solutions. Figure 7-17b also shows the presence of albumin decreased the total accumulated abrasion charge of the Ti6Al4V couple over all the tests.
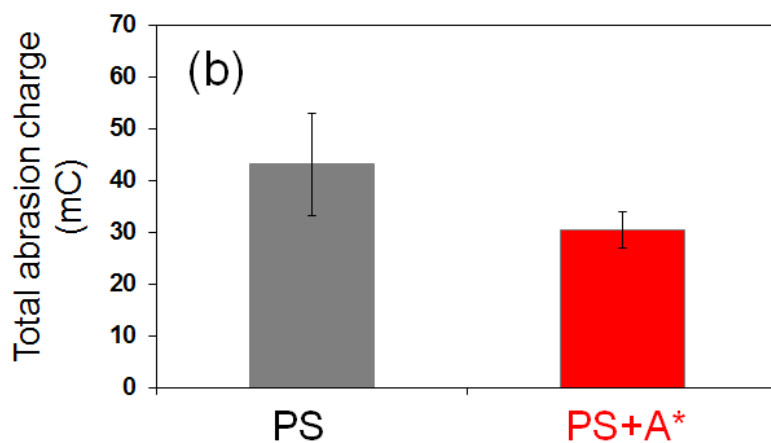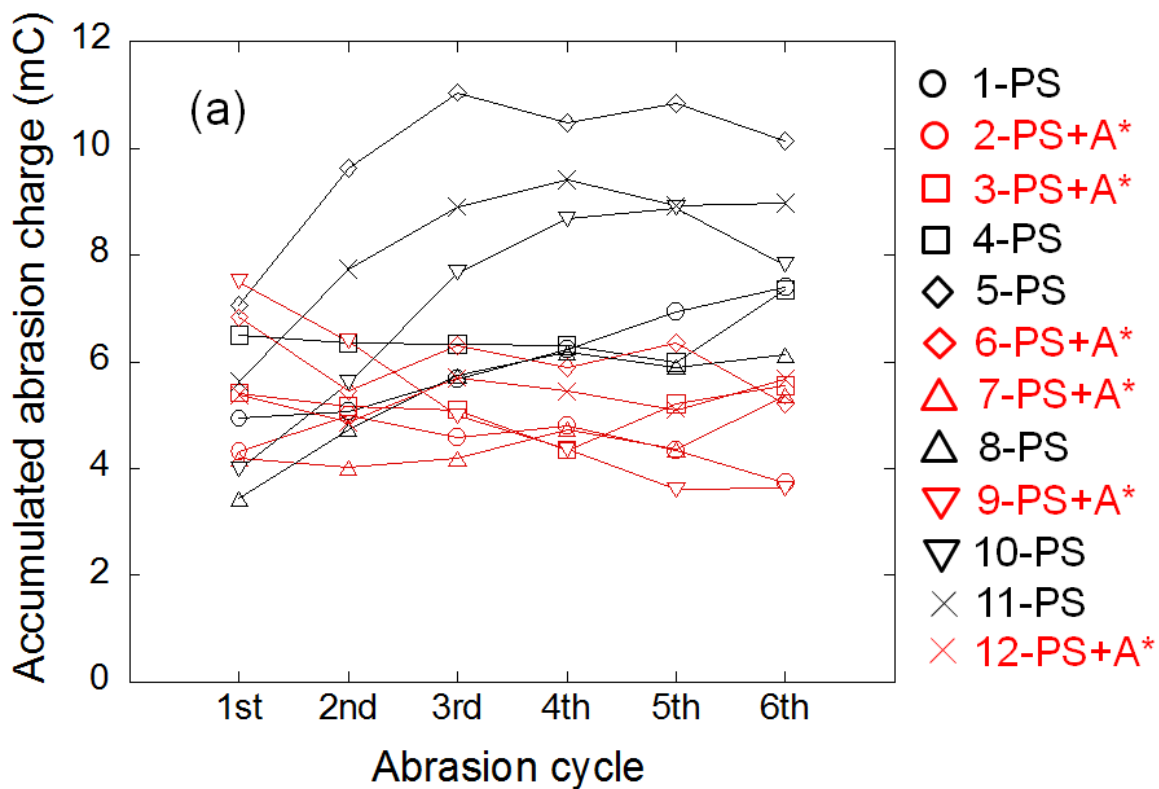
Figure 7-17 (a) Accumulated abrasion charge for each cycle of the abrasion process from a series of MACC tests; (b) total accumulated abrasion charge over all tests of the Ti6Al4V couple at 0.1 rpm under an applied load of 3200 g in physiological saline (PS, black) with or without 1% albumin (A*, red) at 0 mV vs. Ag/AgCl at room temperature.

7.2.6.4 Effect of LPS on MACC of Ti6Al4V

Table 7-3 lists the experimental parameters from a series of MACC tests of the Ti6Al4V couple in the absence and presence of LPS. The final static OCP in each test was less than 0 mV vs. Ag/AgCl and the static current was also very small (<0.2 µA) before rotation (Table 7-3). The solution in the cavity of the stationary part was also acidic but there was no significant difference in corrected pH between the solutions with and without addition of LPS.

Table 7-3 Experimental parameters from a series of MACC tests of the Ti6Al4V couple at 0.1 rpm under an applied load of 3200 g in physiological saline (PS) with and without 150 µg/mL LPS at 0 mV vs. Ag/AgCl at room temperature. Total accumulated abrasion charge refers to the values during the whole abrasion process (3600 s). The corrected pH refers to the pH of the solution in the cavity in the stationary part of the couple.

No.		Final static OCP (mV vs. Ag/AgCl)	Average abrasion current (µA)	Corrected pH	Static current before rotation (µA)	Total accumulated abrasion charge (Q/mC)
1	PS	-30	11±3	4	<0.1	40
2	LPS	-150	15±4	3.8	<0.2	52
3	LPS	-130	9±2	4.2	<0.1	32
4	PS	-120	12±2	3.8	<0.1	42
5	PS	-50	14±2	4	<0.1	49
6	LPS	-130	15±4	3.8	<0.1	52
7	LPS	-110	9±2	4	<0.1	31
8	PS	-180	11±3	4.1	<0.2	41
9	LPS	-120	10±2	3.9	<0.1	35
10	PS	-170	9±2	4.2	<0.2	33
11	PS	-150	11±2	3.9	<0.2	39
12	LPS	-140	12±3	3.8	<0.2	41

Figure 7-18 shows that the average abrasion current and total accumulated abrasion charge during each test. They follow the same trend and there is no significant difference of either abrasion current or abrasion charge between the LPS-containing and LPS-free solutions. However, the variation of abrasion current and abrasion charge for each test at the same conditions was also very big.
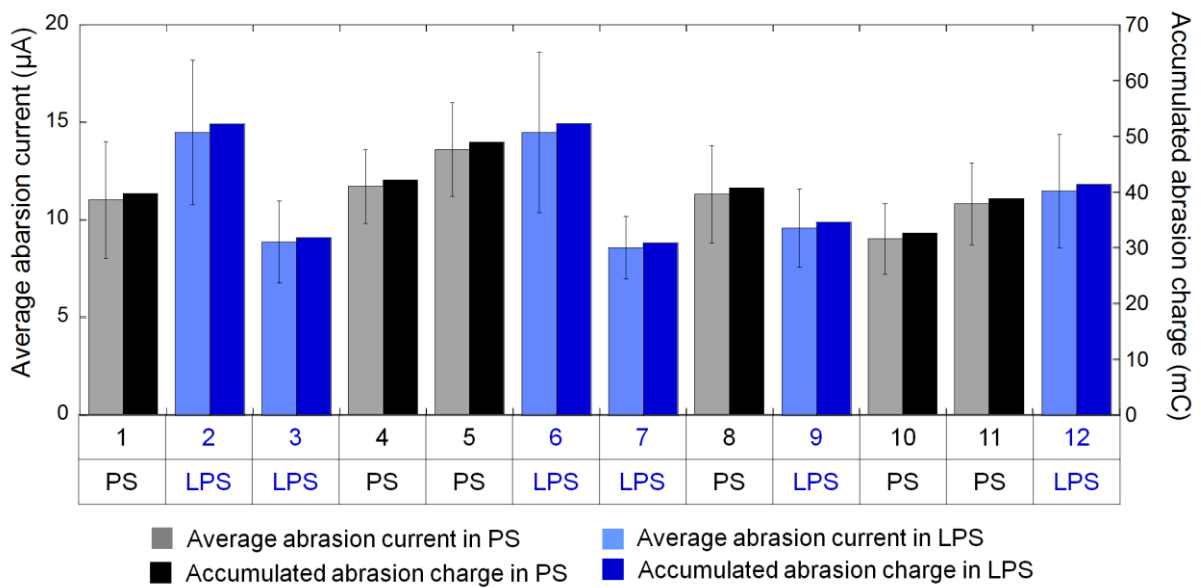
Figure 7-18 Average abrasion current and total accumulated abrasion charge during the whole abrasion process (3600 s) from a series of MACC tests of the Ti6Al4V couple at 0.1 rpm under an applied load of 3200 g in physiological saline (PS) with and without 150 μg/mL LPS at 0 mV vs. Ag/AgCl at room temperature.

Figure 7-19a shows the accumulated abrasion charge for each cycle of the abrasion process. It can be seen that the accumulated abrasion charge has a similar trend in physiological saline with and without LPS. The abrasion charge appears to be higher following abrasion cycles in both types of solutions, possibly due to the formation of a more aggressive crevice environment. However, the variation of the abrasion charge for each test at the same conditions was also very

177

big. The presence of LPS did not show measurable effect on the abrasion charge. Figure 7-19b also shows no measurable differences between the solutions with and without LPS in the total abrasion charge over all the tests.
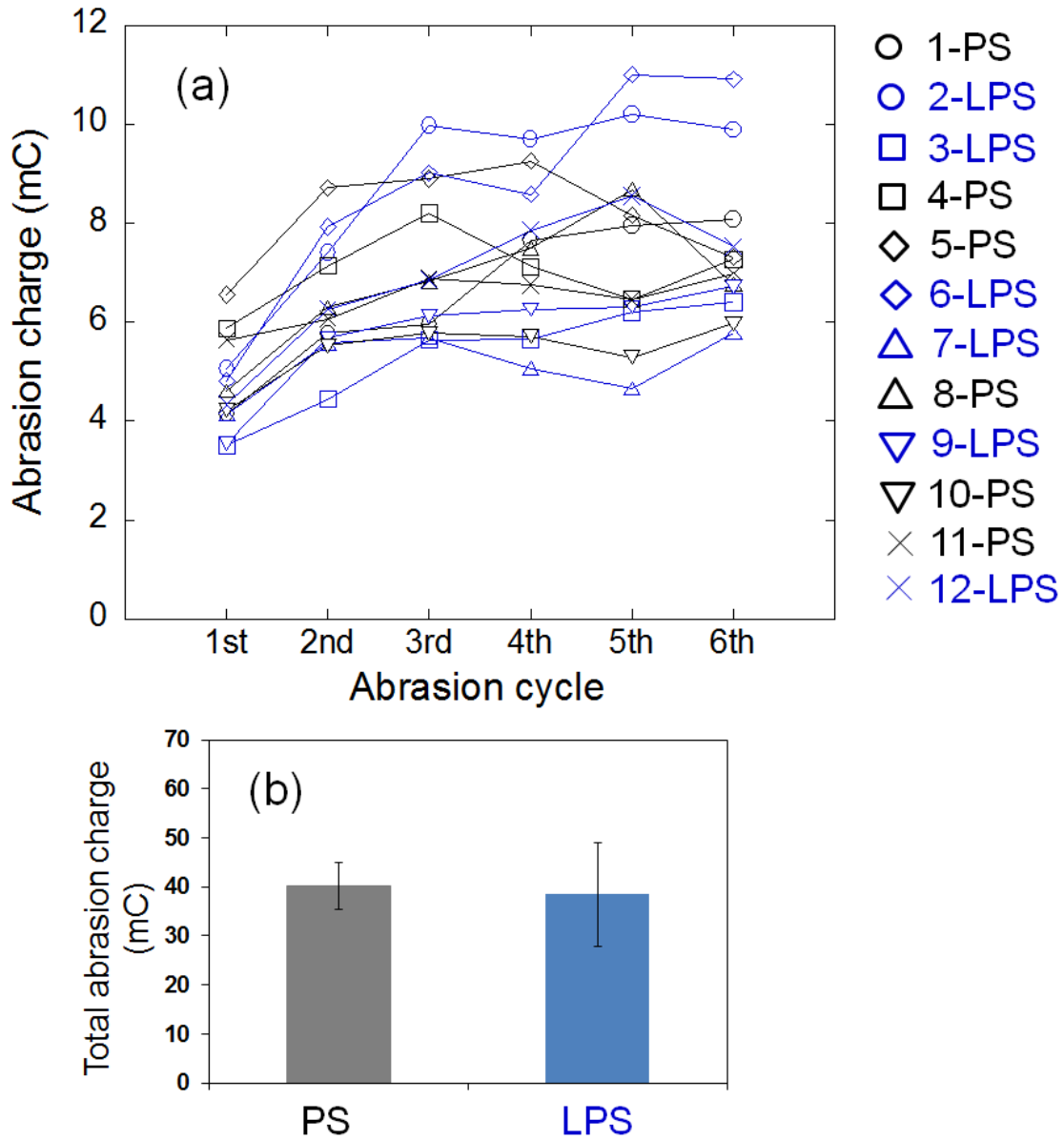
Figure 7-19 (a) Accumulated abrasion charge for each cycle of the abrasion process from a series of MACC tests; (b) total abrasion charge over all tests of the Ti6Al4V couple at 0.1 rpm under an applied load of 3200 g in physiological saline (PS) with and without 150 μg/mL LPS at 0 mV vs. Ag/AgCl at room temperature.

7.2.6.5 Effect of H_2O_2 on MACC of Ti6Al4V

Figure 7-20 shows polarisation curves for the Ti6Al4V couple in physiological saline with and without H_2O_2 in the presence and absence of rotation (abrasion at 0.1 rpm) following 10 min OCP measurements. It can be seen that the static OCP, cathodic current and anodic current of the Ti6Al4V couple under static conditions were all increased in the presence of H_2O_2, which is consistent with the previous observations noted in Chapter 5. The abrasion OCP and cathodic current under abrasion conditions were also increased after the addition of H_2O_2. However, the anodic current did not show a significant change between the static condition and abrasion condition. Due to the increased static OCP in the presence of H_2O_2, a potential of 300 mV vs. Ag/AgCl was applied for the following tests.
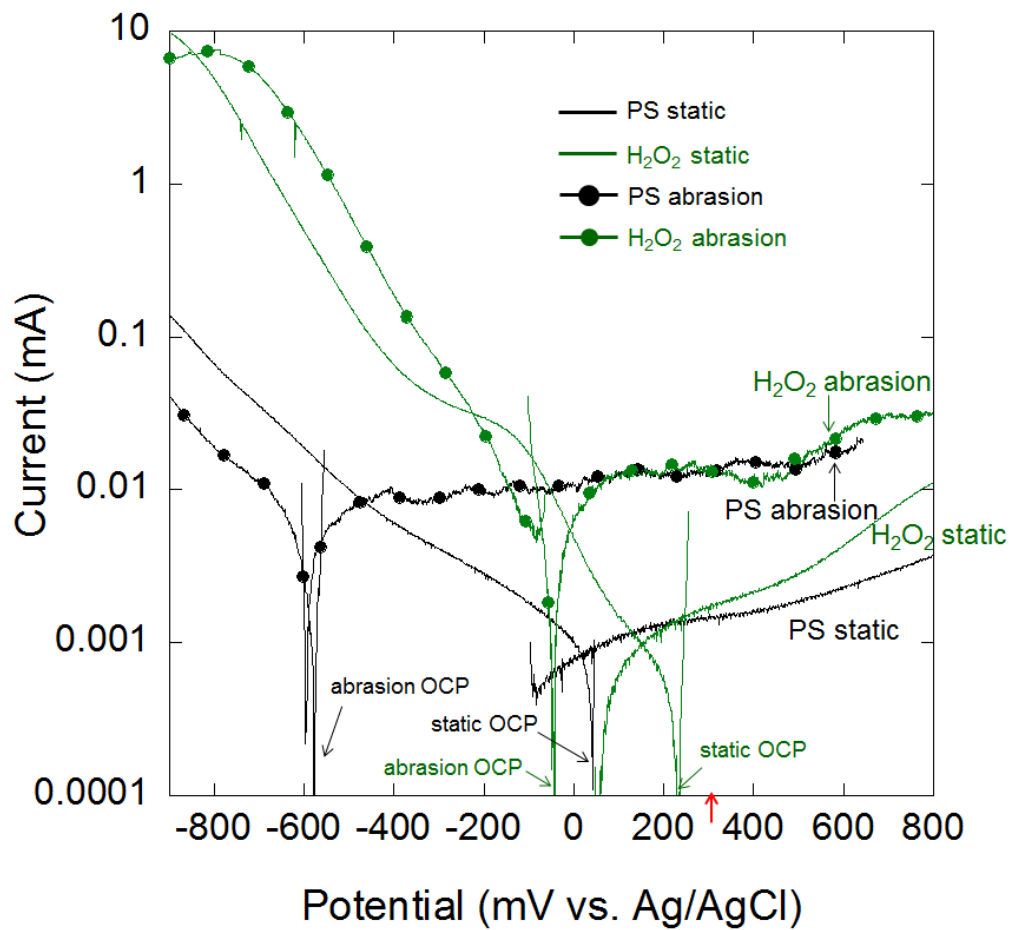
Figure 7-20 Anodic and cathodic polarisation curves of the Ti6Al4V couple in physiological saline (PS) with and without 0.1% H_2O_2 under static and abrasion (0.1 rpm) conditions with an applied load of 3200 g at room temperature. A potential of 300 mV vs. Ag/AgCl (shown as a red arrow in the figure) was chosen for the subsequent experiments. The anodic polarisation curves were measured by sweeping the potential from -50 mV below the OCP to 800 mV vs. Ag/AgCl at a rate of 1 mV/s, and the cathodic polarisation curves were measured by sweeping the potential from 50 mV above the OCP to -900 mV vs. Ag/AgCl at a rate of 1 mV/s.

Table 7-4 lists the experimental parameters from a series of MACC tests of Ti6Al4V in physiological saline in the absence and presence of H_2O_2. The final static OCP in each test was less than 300 mV vs. Ag/AgCl and the static current was small (<1 μA) before rotation (Table 7-4). The solution in the cavity in the stationary part of the Ti6Al4V couple after each

test was acidic, but the corrected pH did not show a significant difference between in the

presence and absence of H_2O_2.

Table 7-4 Experimental parameters from a series of MACC tests of the Ti6Al4V couple at 0.1 rpm under an applied load of 3200 g in physiological saline (PS) with and without 0.1% H_2O_2 at 300 mV vs. Ag/AgCl at room temperature. Total accumulated abrasion charge refers to the values during the whole abrasion process (3600 s). The corrected pH refers to the pH of the solution in the cavity in the stationary part of the couple.

No.		Final static OCP (mV vs. Ag/AgCl)	Average abrasion current (µA)	Corrected pH	Static current beforerotation (µA)	Total accumulated abrasion charge (Q/mC)
1	H_2O_2	170	15±2	3.8	<1	53
2	PS	90	13±2	4	<0.8	47
3	PS	140	14±4	4	<0.3	50
4	H_2O_2	240	13±2	3.8	<0.2	47
5	PS	120	10±2	4	<0.2	37
6	H_2O_2	250	11±2	3.8	<0.2	39
7	H_2O_2	280	9±2	3.8	<0.2	34
8	PS	140	10±2	4	<0.3	35
9	H_2O_2	270	12±3	3.6	<0.1	44
10	PS	120	11±2	3.6	<0.3	39
11	PS	100	11±2	3.6	<0.3	39
12	H_2O_2	250	12±2	3.6	<0.1	43

Figure 7-21 shows the average abrasion current and total accumulated abrasion charge during

each test. They have the same trend in each test and there is no noticeable change in H_2O_2-

containing and H_2O_2-free solutions.
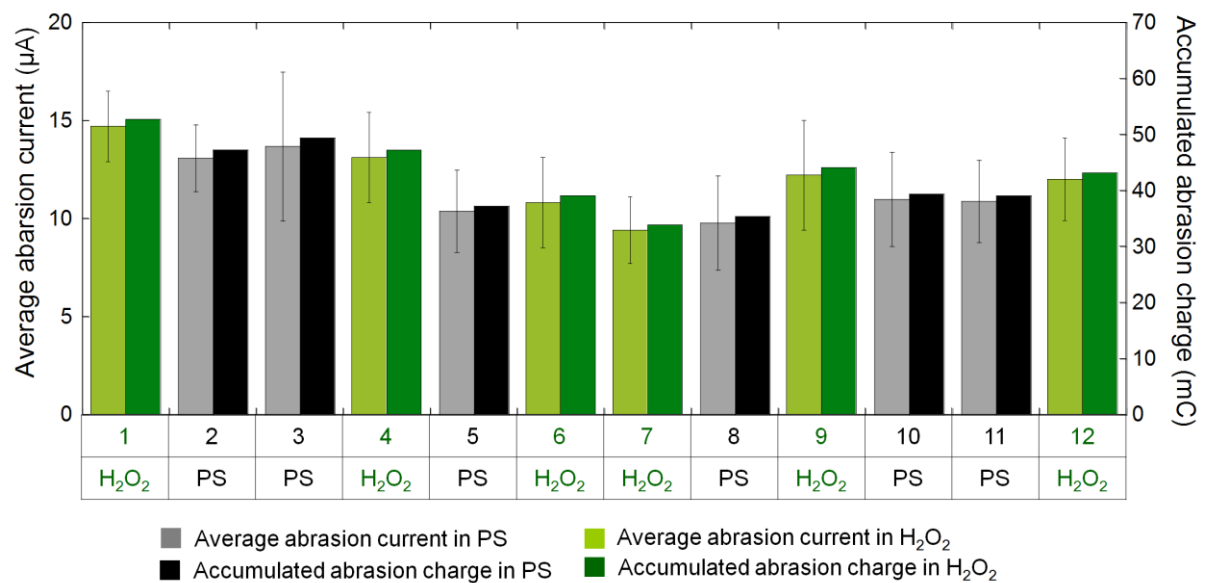
Figure 7-21 Average abrasion current and accumulated abrasion charge during the whole abrasion process (3600 s) from a series of MACC tests of the Ti6Al4V couple at 0.1 rpm under an applied load of 3200 g in physiological saline (PS) with and without 0.1% H_2O_2 at 300 mV vs. Ag/AgCl at room temperature.

Figure 7-22a shows the accumulated abrasion charge for each cycle of the abrasion process. It can be seen that the abrasion process has a similar charge in the absence and presence of H_2O_2. There is relatively small increase in the accumulated abrasion charge following abrasion cycles in both types of solutions. The addition of H_2O_2 did not show measurable effect on the abrasion charge. The variation of the accumulated abrasion charge for each test at the same condition was also very big. Figure 7-22b shows no measurable differences between the solutions with and without H_2O_2 in total abrasion charge over all the tests.
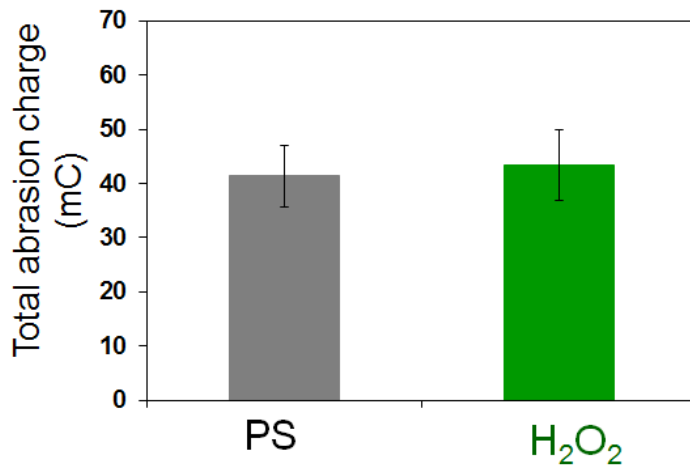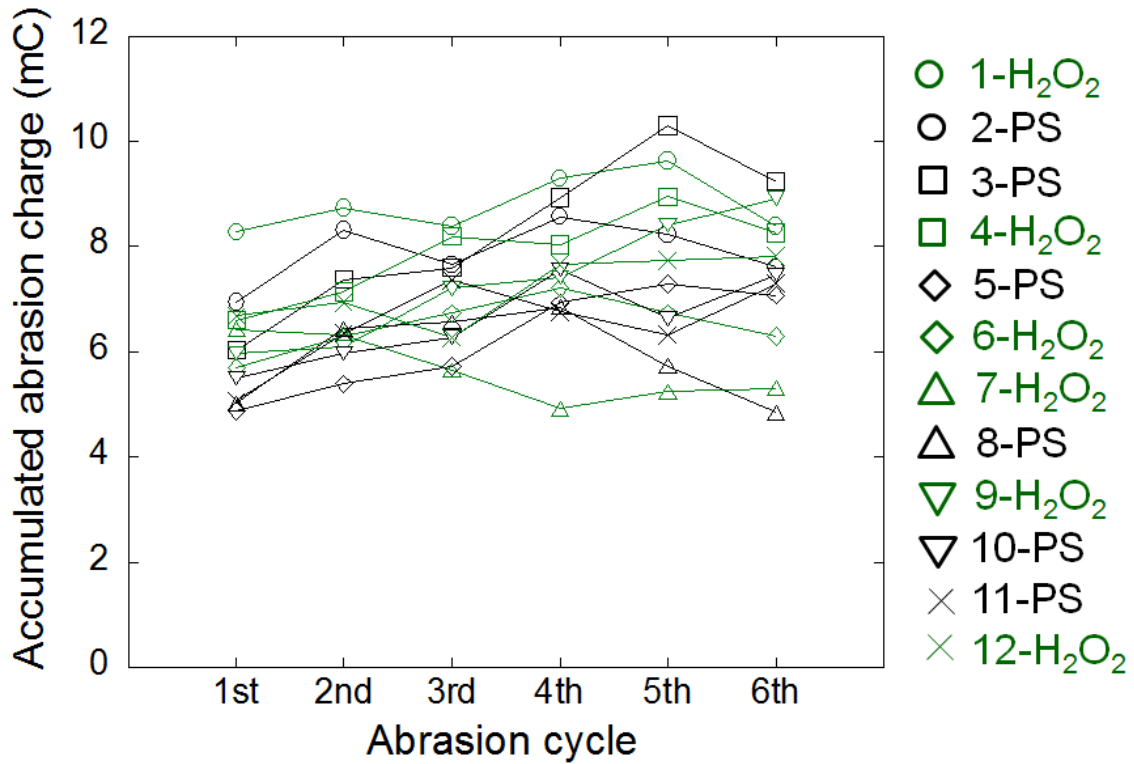
Figure 7-22 (a) Accumulated abrasion charge for each cycle of the abrasion process from a series of MACC tests; (b) total abrasion charge over all tests of the Ti6Al4V couple at 0.1 rpm under an applied load of 3200 g in physiological saline (PS) with and without 0.1% H_2O_2 at 300 mV vs. Ag/AgCl at room temperature.

7.3 Discussion

7.3.1 MACC apparatus

Mechanically-assisted crevice corrosion (MACC) plays a decisive role in implant degradation. MACC may take place in any Ti biomedical implants in human body where two metal components are in contact or where a metal component is in contact with another surface such as bone or cement. It can take place at dental implants [15, 16], bone-anchored hearing aids (BAHA) [14], hip stem [7, 8] and the modular implant interfaces [33, 74, 77], leading to Ti release and degradation/failure of the implants. Severe degradation of contacting surfaces has been widely observed in modular hip prostheses e.g. at the neck-stem interface [33, 75, 76]. For example, severe corrosion was observed for hip implants at the junction between CoCrMo heads and Ti6Al4V necks after only 2.5 months of implantation [33]. In addition, it has been demonstrated that cemented Ti stems are also susceptible to MACC and the pH of body fluid around corroded cemented Ti stems can reach a value as low as 2.5 [7]. The presence of an occluded crevice between modular taper interfaces and stem and cement interfaces can induce a significant change in the solution chemistry [7, 8, 33].

For modular tapers, there is little exchange between the solution in the crevice and the exterior solution due to the small scale of movement (<250 µm [78, 83]) compared with the large contact area (up to 600 mm^2 [76]) of modular implants, which results in formation of a more aggressive environment inside the crevice and active corrosion of the metal implant.

In the current study, the pH change of the solution was clearly observed during the abrasion process of the Ti6Al4V couple in the MACC apparatus (Figure 7-2). The acidic region was clearly observed near the Ti6Al4V couple and an alkaline region was located near the Pt mesh.

In addition, after the abrasion process, the pH of solution in the cavity in the stationary part (crevice geometry) was acidic (pH ~2-4 depending on the time length of abrasion). It has also been shown that the solution in the cavity in the stationary part became highly acidic after abrasion under freely corroding conditions (Figure 7-3), which agrees with the MACC study that used manufactured implants [37]. They found the pH between the modular taper junctions was decreased by 0-3 units after long-time cyclic loading tests.

During MACC tests, the mechanical process induces rupture of the passive oxide film on the surface of the Ti6Al4V couple, leading to a burst of Ti dissolution and freshly-exposed bare metal surface [33]. The anodic reaction is promoted under abrasion conditions compared with the static conditions. Increased anodic reaction takes place when there are more Ti ions in the crevice. Hydrolysis of the accumulated Ti ions can produce more H^+ ions; Cl^- ions are also drawn into the crevice to maintain the charge balance, which results in forming a strong HCl solution with a very low pH in the crevice. Therefore an acidic region is observed around the Ti6Al4V couple. Outside the couple, the bulk solution is neutral and O_2-rich. O_2 reduction reaction is expected to take place on the Pt mesh, producing OH^- ions and leading to an alkaline region.

Most research in this area has involved "fretting corrosion" apparatus with relatively small contact areas (Table 2-2, e.g. 0.1-0.5 mm^2 on pin-on-disc geometry in Swaminathan and Gilbert's study [34]) to investigate fretting behaviour of metal implants [34, 35, 82]. During these "fretting corrosion" movements with the small scale amplitudes (Table 2-2, <200 μm), part or majority of the abrasion areas can be exposed and may be readily flushed by bulk solution and further repassivated. Meanwhile, the dissolved metal ions can also escape easily and aggressive crevice chemistry cannot be developed. Although Swaminathan and Gilbert [34]

reported the possibility of the presence of crevice corrosion in their "fretting corrosion" device, there was no direct evidence apart from a slight increase in recovery time of metal couples after long-time fretting under high loads.

The MACC device used in this work has an occluded crevice with a large contact area (110 mm^2, Figure 3-5). During the abrasion process, there was almost no abrasion area exposed to the bulk solution and it was also difficult for the metal ions to escape, which facilitated the development of the type of aggressive crevice chemistry that modular tapers may experience *in vivo*.

Although most "fretting corrosion" devices have small amplitudes (<200 μm [34, 35, 82]) that are much closer to the movement of modular implants (<250 μm [78, 83]), they may not be able to develop crevice chemistry that modular implants experience *in vivo*. 1 Hz (i.e. the average frequency of human walking) is normally used in these "fretting corrosion" studies [34, 82, 168]. However, it is very difficult to control the precise reciprocating micro-movement for the MACC apparatus in the current work. Therefore, a continuous rotational motion with a very small rotation rate (<100 μm/s at 0.1 rpm) was applied in this MACC apparatus. The mechanical process during rotation results in continuous removal of passive film and exposure of bare metal surface, which further increases the amount of metal ions and results in forming an aggressive environment. Therefore, the MACC test in the current work is an accelerated experiment.

7.3.2 Abrasion scars and debris

Many *in vivo* studies have shown the existence of Ti particles/debris of different sizes in peri-implant tissues around dental implants [15, 16, 71], BAHA [14], and modular tapers [77, 198]. For example, Ti particles in a range of 0.01 to 200 μm were found in the tissue around modular

interfaces [77]. In the current study, it has been shown that both surface deformation and large and fine abrasion particles were present over the abrasion area (Figure 7-5), as well as the black debris with various shapes and sizes collected in the cavity at the bottom of the stationary part (Figure 7-6).

During the abrasion process, contacting asperities are expected to experience severe plastic deformation and bare Ti6Al4V metal surface can be exposed to the solution for oxidation. Repeated deformation results in more oxidation of the metal surface [163]. The mechanical force can lead to mixture of the bare metal and oxide and the formation of an initial deformed layer on the surface. Depending on the extent of deformation and oxidation, some abrasion regions might be entirely oxidised [34], leading to a deformed layer that can become brittle and prone to form detached particles [169]. In the presence of mechanical force, the detached metallic particles and oxides smear into the deformed layer (a third body), which contributes to increased degradation [160, 170]. Some large detached particles may be crushed into fine particles over the abrasion area. In addition, surface oxide may reduce the adhesive strength between detached particles and the metal surface, facilitating their ejection from the abrasion area into the surrounding environment [169]. Therefore both large flakes and fine debris were observed in the crevice geometry of the stationary part.

The abrasion debris was easily collected from the cavity in the stationary part of the MACC couple. The Ti particles/debris released into the human body which has been reported to induce adverse cellular reactions e.g. pain, peri-inflammation even failure of the implants [7, 14, 71, 85]. Therefore, the collected abrasion debris after MACC tests in this study may be used to investigate the potential effect on responses/functions of human cells through *in vitro* and/or *in vivo* tests.

7.3.3 Effect of rotation speed and load on MACC of Ti6Al4V

As expected, the OCP of the Ti6Al4V couple rapidly decreased upon the onset of rotation. With an increase in the rotation speed and load, the abrasion OCP became more negative (Figure 7-9 and Figure 7-10). The current of the Ti6Al4V couple rapidly increased at the beginning of abrasion and the abrasion current increased with increasing rotation speed and load (Figure 7-12 and Figure 7-13). The mechanical process removed the surface oxide film and the bare surface was exposed to the solution for oxidation, which resulted in decreased OCP and increased current.

With an increase in the rotation speed, i.e. increasing rotation frequency, more bare metal surfaces per unit time were exposed to the corrosion environment, which resulted in higher abrasion current and lower abrasion OCP [165, 169, 171]. With an increase in the load, the pressure between the contact surfaces was increased resulting in more effective exposure of the fresh bare metal surface to abrasion and yielding the observed increase in abrasion current and decrease in OCP [96, 122].

7.3.4 Effect of albumin, LPS and H_2O_2 on abrasion charge

7.3.4.1 Effect of albumin on abrasion charge

It has been observed that the presence of albumin decreased the accumulated abrasion charge of the Ti6Al4V couple in physiological saline (Figure 7-17). A similar inhibition effect of albumin on average abrasion current or abrasion charge has been reported for Ti6Al4V-ELI during an intermittent tribocorrosion test [166] and 316 stainless steel during "fretting corrosion" test [81].

However, in other tribocorrosion experiments on Ti6Al4V, albumin has been found to increase average abrasion current at a high potential but decrease abrasion current at a low potential [36]. Whilst in "fretting corrosion" experiment on Ti6Al4V, the presence of albumin has been reported to cause no change to the average abrasion current [122]. In both tribocorrosion and "fretting corrosion" studies, a small contact area with an Al_2O_3 sphere (10 mm in diameter) on Ti6Al4V disc was used (Table 2-2), where an effective crevice chemistry cannot be developed, which is different from the current MACC study.

Protein is thought to affect abrasion current by acting as lubricant or by interfering with the oxidation [166]. It is well established that albumin can strongly adsorb on Ti surfaces [24]. It was found that the addition of albumin inhibited the anodic reaction under static conditions (in Chapter 5). It is likely that the presence of albumin may also block the reaction sites on the surface under abrasion conditions, decreasing abrasion current and the according accumulated abrasion charge.

It has been reported that the presence of serum (containing albumin as the main protein) can have an effective lubricating function during tribological tests on CoCrMo alloy [124, 199]. This lubricant layer may modify the mechanical stress, probably decreasing effective abrasion area, resulting in decreased abrasion current [124, 199]. In the current study, the accumulated abrasion charge of the Ti6Al4V couple was observed to be similar at the 1st cycle of the abrasion process in physiological saline in the absence and presence of albumin. From the 2nd cycle the accumulated abrasion charge tended to become noticeably lower in the albumin-containing solutions (Figure 7-17). This suggests that the development of the protective effect of albumin is not immediate, which may provide evidence for the gradual formation of a protein-rich lubricating layer on the surface.

7.3.4.2 Effect of LPS and H_2O_2 on abrasion charge

Average abrasion current and accumulated abrasion charge of the Ti6Al4V couple did not change significantly after addition of LPS or H_2O_2. There is little previous work on the effect of LPS or H_2O_2 on tribocorrosion or "fretting corrosion" of metallic implants [121, 172]. One paper stated that the presence of LPS increased wear-corrosion weight loss and reduced the corrosion resistance of CP-Ti and Ti6Al4V by comparing impedance before and after tribocorrosion tests [121]. The presence of H_2O_2 was found to increase the weight loss and Ti release from Ti6Al4V plates and screws [172]. However, none of these studies compared the abrasion current or abrasion charge during abrasion process.

LPS was found to promote Ti dissolution at pH 4-7 after immersion test, possibly due to the potential complex effect through its polysaccharide component [182, 183] (see Chapter 4). The presence of H_2O_2 was also observed to promote Ti corrosion due to the Ti-H_2O_2 complex reactions [184] (see Chapter 5). Therefore, the presence of LPS or H_2O_2 is expected to increase abrasion current and accumulated abrasion charge. However, no measurable change on abrasion charge was observed in the presence of LPS or H_2O_2, possibly suggesting that the complexation effect is insignificant compared with the MACC process. In addition, the variations of the abrasion current were very large, which may also result in the unmeasurable change in the presence and absence of LPS or H_2O_2.

7.4 Conclusions

A new experimental device with a large contact-area crevice and a low frequency of movement has been developed for the investigation of MACC of metallic implants. An experimental study focused on MACC of the Ti6Al4V couple in physiological saline confirmed the evolution of

chemistry and the presence of abrasion debris in the occluded crevice at a low rotation speed by means of potentiostatic techniques. It also confirmed the importance of controlling mechanical variables such as applied load and rotation speed as well as the presence of albumin, LPS and H_2O_2 for the study of MACC behaviour.

1.   This is the first time that a MACC apparatus has been specifically designed with a crevice geometry with a large contact area and a continuous rotational motion with a very small rotation rate (<100 μm/s at 0.1 rpm). Crevice corrosion with a clearly observed acidic environment was found on a Ti6Al4V couple.

2.   Both fine and large abrasion debris were observed on the Ti6Al4V couple surface and the solutions in the crevice, which can be easily collected and may be used for *in vitro* and/or *in vivo* toxicity tests.

3.   With an increase in the rotation speed and load, abrasion OCP of the Ti6Al4V couple was decreased while abrasion current at a potential of 0 mV vs. Ag/AgCl was increased.

4.   The presence of albumin decreased the accumulated abrasion charge of the Ti6Al4V couple while LPS did not show measurable change under a potential of 0 mV vs. Ag/AgCl in this MACC apparatus. In addition, the presence of H_2O_2 did not induce measurable change on the abrasion charge of the Ti6Al4V couple at 300 mV vs. Ag/AgCl.

8   GENERAL DISCUSSION AND FUTURE WORK

8.1 General discussion

8.1.1   Introduction

The work presented in this thesis has focused on the role of important chemical species found in the peri-implant environment (albumin, LPS and H_2O_2) and their effect on MACC, which is an important mechanism of failure of Ti implants in the body. The presence of LPS in the peri-implant environment is likely to be a result of bacterial colonisation, since LPS is a component of Gram-negative bacterial cell walls and surface biofilms are found in many types of biomedical implanted devices [133]. The effect of viable bacteria on Ti release (using *S. sanguinis* as a model system) has also been studied. The presence of H_2O_2 is often a consequence of inflammatory reactions caused by immune cells such as neutrophils. Thus Ti release in the presence of neutrophils has also been investigated.

8.1.2   Effect of bacteria and bacterial products on Ti corrosion

The presence of bacteria is observed in many peri-implant environments [133, 134] and associated peri-implant infection can ultimately lead to failure of Ti implants at early or late stages following implantation [136]. An significant bacterial product LPS, which is an important mediator of peri-implant inflammation, has also been demonstrated to be present on Ti implant surfaces [131]. However, the effect of bacteria and bacterial products on Ti corrosion has not been investigated extensively.

Ti dental implants are modular systems with the components that are integrated into the jaw bones connecting to several other components that penetrate the oral mucosa to emerge into

mouth and restore the form and functionality of a missing tooth. The parts of dental implants that emerge from the gingiva (gum) are exposed to the oral environment and soft tissues which form a pocket around them. The pocket which forms between the soft tissues of the gum and the implant is of particular interest as there is a low flow of saliva, the composition is close to tissue fluid and a bacterial biofilm is always present on adjacent Ti implant surface.

In this study it has been found that the presence of bacteria *S. sanguinis*, an early coloniser of Ti surfaces in the oral cavity, increased Ti release. Furthermore, the presence of LPS which is detected on Ti dental implant surfaces was found to promote Ti dissolution under slightly acidic and neutral conditions (pH 4-7), which are the common environmental conditions in peri-implant sites. These findings suggest that the presence of bacteria or bacterial products can accelerate corrosion of Ti implants.

In addition, it was observed during MACC simulation that highly acidic conditions could be generated (corrected pH ~2-4 depending on the abrasion time). Although bacterial viability in such aggressive environments is itself unlikely, bacterial products such as LPS might be present and diffuse into the crevice environment. LPS was however observed to decrease Ti release in highly acidic environment (pH 2) during immersion tests and the significance is that under such conditions LPS may actually protect Ti implants from very severe corrosion. However, there was no measureable change in abrasion charge/abrasion current in the absence and presence of LPS during MACC experiment, indicating that no inhibition effect of LPS was detectable. It should, however, be noted that for the MACC tests the abrasion time was only 1 h (after which the actual pH may not be as low as 2) whilst the immersion test lasted for 4 weeks (pH 2).

8.1.3   Effect on inflammation cells and chemical species on Ti corrosion

When there is bacterial infection around the biomedical implants, an inflammatory response occurs, involving activation of the innate and adaptive immune systems. In acute inflammation innate immune cells, which include neutrophils and macrophages, are the first to migrate into the infected or damage tissue. In inflammation associated with dental implants, neutrophils are the most abundant immune cells found in the inflammatory lesions [71] and these cells have the capacity to initiate a number of microbial killing mechanisms including the release of chemical species [152, 153, 200], which may conceivably promote Ti corrosion. Despite a good understanding of the potential corrosion-promoting chemical species that the host cells produce, it is surprising that little attention has been paid on the role of neutrophils in Ti corrosion.

H_2O_2 has been regarded as an important inflammation product in the peri-implant environment and is generated extracellular alongside species such as superoxide (O_2^-) and hypochlorous acid (HOCl) during neutrophil oxidative burst [194]. The ICP-MS results following culturing of neutrophils with the three grades of Ti suggest that neutrophils produce species that promote Ti corrosion. Furthermore, there was little difference between the three grades of Ti studied. There were, however, considerable differences between tests using neutrophils isolated from different individuals and we know that such cells display variation which affects their physiology which could explain the findings.

In this study, the presence of H_2O_2 when investigated in isolation has been observed to significantly accelerate corrosion of Ti6Al4V when compared with CP-Ti. The observed lack of difference between the three grades of Ti in the presence of neutrophils suggests the mechanisms underpinning neutrophil-assisted Ti corrosion may be different from those

194

mediated by H_2O_2, or may be due to the fact that the corrosion process was at very early stages when induced in culture with the cells. It is important to note that whilst H_2O_2 is one of the key species generated extracellularlly by neutrophils other ROS species could also be affecting Ti corrosion. However the key alternative ROS species generated include O_2^- which has an extremely short half-life extracellularly and $HOCl$ which is a weak acid. Future studies should include investigations to identify their respective effects on Ti corrosion.

Interestingly, it has been found that β phase of Ti6Al4V was preferentially attacked in the presence of H_2O_2, which agrees with a recent report about preferential attack of β phase of a retrieved modular taper [75]. This may suggest that corrosion of Ti in the presence of H_2O_2 *in vivo* is significant.

8.1.4   Effect of presence of albumin and H_2O_2 on Ti corrosion

The effect of albumin on the corrosion of biomedical implant alloys has been the subject of considerable attention because albumin is the most abundant protein in the blood and in the extracellular environment [23]. The effect of albumin on the corrosion rate of Ti and other biomedical alloys is disputed within the literature [19, 20, 25, 122]. In the current study, the addition of albumin has been found to significantly inhibit the cathodic reaction and also slightly inhibit the anodic reaction in physiological saline while a small increase of Ti release was observed in the presence of albumin at open circuit. It is proposed that the presence of albumin decreases the cathodic reaction, which may drive dissolution of Ti6Al4V into the active region, therefore promoting corrosion of Ti6Al4V.

A better approximation of the peri-implant environment under inflammatory conditions has also been simulated by considering the effects of combinations of biomolecules on Ti corrosion.

It has been found that there was a considerably higher rate of metal release from Ti6Al4V in mixed solutions of albumin and H_2O_2 compared with albumin alone or H_2O_2 alone. Again it is proposed that the presence of albumin decreases the cathodic reaction, taking the potential of Ti6Al4V into the active region, where the higher rate of anodic dissolution in H_2O_2 leads to significantly enhanced corrosion of Ti6Al4V.

8.1.5 MACC

MACC is now considered to be a particularly important corrosion mechanism for Ti implants in human body. The MACC mechanism of biomedical Ti was firstly proposed by Gilbert et al. [33] in 1993 to explain severe corrosion observed on modular Ti tapers. Increasingly, investigators have reported the presence of significant quantities of corrosion products in the tissues and fluids adjacent to implants that have been associated with no obvious tribological processes, e.g. cemented Ti stems [7, 8], bone-anchored hearing aid (BAHA) [14] and dental implants [15, 16] and these findings further support the presence of MACC of Ti implants in the body.

However, the majority of *in vitro* research has focused on the tribocorrosion effects [36, 121]. Some investigators have studied "fretting corrosion" with small scale vibrational motion, but such studies have employed a relatively small contact area [34, 35, 82]. However, none of them has paid attention to the development of the effective crevice chemistry, which is the main feature of MACC, with the exception of some work conducted on manufactured modular tapers using real orthopaedic components [37, 38].

To obtain a better insight into MACC, a novel MACC apparatus has been designed and tested on a Ti6Al4V couple in the current study. The chemistry of MACC was explored with the

observation of pH change of the solutions. It has shown that highly acidic environment can be formed in the crevice of a Ti6Al4V couple. In addition, it has been reported clinically that patients implanted with cemented hip stems experienced severe pain although the stems were well-fixed and without evidence of infection [7, 8, 79]. The pH of the retrieved stems was found to be highly acidic, causing pain [7, 79]. The presence of peri-implant inflammation may provide an explanation for the acidic peri-implant environment [8]. In addition, the current study also clearly demonstrates the occurrence of low pH during MACC, which may be another important explanation for the clinical observation.

Inconsistent and incomplete results have been reported about the effect of albumin [36, 122], LPS [121] and H_2O_2 [172] on tribocorrosion or "fretting corrosion" of Ti alloys. More importantly, none of their experimental setups contained effective crevice geometry or could develop effective crevice chemistry. In this study, the effect of albumin, LPS and H_2O_2 have been preliminarily studied in the MACC apparatus. It has been found that the presence of albumin decreased the abrasion charge of the Ti6Al4V couple while there is no measurable influence in the presence of both LPS and H_2O_2.

8.2 Future work

8.2.1 Effect of combination of albumin and H_2O_2 on Ti corrosion

A new hypothesis has been proposed to explain the considerably higher Ti release in the mixed solution of albumin and H_2O_2 compared with albumin or H_2O_2 alone. To test this hypothesis, more investigations are needed, e.g. further electrochemical tests including electrochemical impedance spectroscopy (EIS) and potentiostatic measurements.

8.2.2 Effect of cells on Ti corrosion

It has been found that the presence of neutrophils leads to increased Ti release, which is detrimental for Ti biomedical implants and should draw people's attention. Except for investigation on the effect of H_2O_2 on Ti corrosion, other key alternative ROS species e.g. O_2^- and HOCl on Ti corrosion have not been identified. Further work is needed.

8.2.3 Further studies on MACC

The new MACC apparatus has been designed and established in the current study. However, it is essential to develop an updated apparatus in which the rotation motion can be reciprocating with an amplitude of ~100 μm or less (i.e. controlling the frequency between clockwise and anti-clockwise movements since the rotation rate is <100 μm/s at 0.1 rpm), which is more close to the micro-movement of implants *in vivo*.

It has been observed that the variation of abrasion current was relatively large. This is not surprising because the surface finish of the Ti6Al4V couple was limited to machining tolerances during device manufacture which was not at a precision level. In addition, the Ti6Al4V couple was re-used without surface treatment except for cleaning with deionised water. For the future work, grinding or polishing procedures will be needed to obtain a controllable surface finish and an even micro-gap between two components. It should however be noted that the machining accuracy of biomedical components is also limited with micro-gaps between modular components extensively reported in the literature [201].

It has been shown that the corrosion of Ti6Al4V in 2 M HCl was temperature dependent and higher current was observed at higher temperature. It has also been observed that the crevice chemistry of the Ti6Al4V couple became highly acidic and may be more aggressive during

MACC. However, all MACC tests were conducted at room temperature in this study. More severe MACC would be expected at body temperature (37 °C). Therefore, the effect of temperature should be considered for the future experiment and the whole MACC apparatus may be placed in a chamber, where temperature can be controlled.

A preliminary study on the effect of chemical species (albumin, LPS and H_2O_2) on MACC compared the abrasion current and abrasion charge in the current study. However, this is not sufficient. More detailed investigations will be needed, including analysis of the crevice solution and characterisation of the abrasion debris. In terms of the analysis of crevice solution, a corrected pH value was given in the current study due to the small volume of the solution in the cavity in the stationary part of the couple. For future experiments, a pH electrode with a micron-scale diameter can be helpful to obtain more accurate and reliable results. In addition, to investigate the effect of abrasion debris on human cells will also contribute to the understanding of the role of Ti corrosion products *in vivo*.

The MACC apparatus with the Ti6Al4V couple in the current study can easily be extended to investigation on MACC of the Ti/cement couple and galvanic couple by making new couples of other materials.

8.2.4 Summary: the need for improved simulation of the peri-implant environment for future corrosion tests

Although the effects of H_2O_2, albumin and LPS have been studied in the literature, a better approximation of the peri-implant environment should be simulated *in vitro* for the future experiment to investigate the corrosion of Ti by combining the effects of such species.

The current experimental condition of involving the use of both albumin and H_2O_2 is a good case for the better approximation of peri-implant environment. No same or similar study has been conducted previously. This can be extended to investigate corrosion of other Ti alloys and other metallic implant materials, and this will also help explore different corrosion mechanisms of biomedical implants.

Other combination effects of the three species should be considered for future experiment, e.g. the combination of H_2O_2 and LPS and the combination of albumin, H_2O_2 and LPS, which are better approximations of co-existence of peri-implant infection and inflammation.

In addition, MACC of Ti implants may also take place concurrently with biologically-mediated effects. In the current work, the effect of albumin, LPS or H_2O_2 was investigated separately without combination of any. Further MACC investigations in the presence of combination of a series of factors (albumin and H_2O_2, LPS and H_2O_2 and all three species) will provide greater insight into *in vivo* corrosion of Ti implants.

9 CONCLUSIONS

The corrosion of three grades of Ti (CP-Ti-G2, CP-Ti-G4 and Ti6Al4V) has been investigated under better simulated conditions of peri-implant environment.

1.   The presence of *S. sanguinis* an early coloniser of Ti surfaces in the oral environment has been found to promote Ti release from three grades of Ti. More corrosion was observed for sandblasted-acid-etched surface than mirror-polished surface of three grades of Ti.

2.   The presence of LPS, a component of Gram-negative bacterial cell walls, increases Ti dissolution in slightly acidic and neutral conditions (pH 4-7) that are commonly encountered in the peri-implant environment. Whilst LPS protects Ti from severe corrosion in a highly acidic conditions (pH 2).

3.   The presence of neutrophils, the most abundant acute immune cells in the peri-implant environment, has been observed to enhance the corrosion of three grades of Ti. This effect is likely to be varied with different individuals. In addition, corrosion of CP-Ti and Ti6Al4V did not show significant difference in the presence of neutrophils.

4.   The presence of H_2O_2, an important inflammation product in the peri-implant environment, has been characterised on corrosion of Ti. The corrosion resistance of CP-Ti was found to be higher than Ti6Al4V. Specifically, the β phase of Ti6Al4V was observed to be preferentially attacked relative to the α phase.

5.   The presence of albumin, an abundant protein in the blood and the extracellular environment has been found to inhibit the cathodic and anodic reaction of Ti6Al4V in physiological saline but promote corrosion of Ti6Al4V at open circuit.

6. The presence of both albumin and H_2O_2, which is a better approximation of peri-implant environment, has been identified to considerably promote corrosion of Ti6Al4V. A new hypothesis has been proposed to interpret the significantly more corrosion of Ti6Al4V in the combination of albumin and H_2O_2 compared with albumin or H_2O_2 alone.

7. A novel MACC apparatus has been designed and tested on a Ti6Al4V couple, which further support and help better understand the mechanism of MACC of biomedical implants.

8. The presence of albumin, LPS and H_2O_2 on MACC of Ti6Al4V has been preliminarily studied. The addition of albumin was found to decrease the abrasion charge at a potential of 0 V vs. Ag/AgCl during MACC. However, no measurable change was observed in the presence of LPS at a potential of 0 V vs. Ag/AgCl or in the presence of H_2O_2 at a potential of 300 mV vs. Ag/AgCl.

10 REFERENCES

1. Liu, X.Y., P.K. Chu, and C.X. Ding, Surface modification of titanium, titanium alloys, and related materials for biomedical applications. Materials Science and Engineering, R: Reports, 2004. 47(3-4): p. 49-121.

2. Long, M. and H.J. Rack, Titanium alloys in total joint replacement - a materials science perspective. Biomaterials, 1998. 19(18): p. 1621-1639.

3. Brunette, M.D., P. Tengvall, M. Textor, and P. Thomsen, Titanium in medicine: material science, surface science, engineering, biological reponses, and medical applications. 2001, New York: Springer-Verlag Berlin Heidelberg.

4. He, X.H., J.J. Noel, and D.W. Shoesmith, Temperature dependence of crevice corrosion initiation on titanium grade-2. Journal of the Electrochemical Society, 2002. 149(9): p. B440-B449.

5. Yan, L., J.J. Noel, and D.W. Shoesmith, Hydrogen absorption into Grade-2 titanium during crevice corrosion. Electrochimica Acta, 2011. 56(4): p. 1810-1822.

6. Virtanen, S. and C. Curty, Metastable and stable pitting corrosion of titanium in halide solutions. Corrosion, 2004. 60(7): p. 643-649.

7. Hallam, P., F. Haddad, and J. Cobb, Pain in the well-fixed, aseptic titanium hip replacement - The role of corrosion. Journal of Bone and Joint Surgery-British Volume, 2004. 86B(1): p. 27-30.

8. Thomas, S.R., D. Shukla, and P.D. Latham, Corrosion of cemented titanium femoral stems. Journal of Bone and Joint Surgery-British Volume, 2004. 86B(7): p. 974-978.

9. Cadosch, D., E. Chan, O.P. Gautschi, and L. Filgueira, Metal is not inert: Role of metal ions released by biocorrosion in aseptic loosening-Current concepts. Journal of Biomedical Materials Research Part A, 2009. 91A(4): p. 1252-1262.

10. Sarmiento-Gonzalez, A., J.M. Marchante-Gayon, J.M. Tejerina-Lobo, J. Paz-Jimenez, and A. Sanz-Medel, High-resolution ICP-MS determination of Ti, V, Cr, Co, Ni, and Mo in human blood and urine of patients implanted with a hip or knee prosthesis. Analytical and Bioanalytical Chemistry, 2008. 391(7): p. 2583-2589.

11. Sarmiento-Gonzalez, A., J.R. Encinar, J.M. Marchante-Gayon, and A. Sanz-Medel, Titanium levels in the organs and blood of rats with a titanium implant, in the absence of wear, as determined by double-focusing ICP-MS. Analytical and Bioanalytical Chemistry, 2009. 393(1): p. 335-343.

12.   Rubio, J.C., M.C. Garcia-Alonso, C. Alonso, M.A. Alobera, C. Clemente, L. Munuera, and M.L. Escudero, Determination of metallic traces in kidneys, livers, lungs and spleens of rats with metallic implants after a long implantation time. Journal of Materials Science. Materials in Medicine, 2008. 19(1): p. 369-75.

13.   Nuevo-Ordonez, Y., M. Montes-Bayon, E. Blanco-Gonzalez, J. Paz-Aparicio, J. Dianez Raimundez, J.M. Tejerina, M.A. Pena, and A. Sanz-Medel, Titanium release in serum of patients with different bone fixation implants and its interaction with serum biomolecules at physiological levels. Analytical and Bioanalytical Chemistry, 2011. 401(9): p. 2747-2754.

14.   Addison, O., A.J. Davenport, R.J. Newport, S. Kalra, M. Monir, J.F.W. Mosselmans, D. Proops, and R.A. Martin, Do 'passive' medical titanium surfaces deteriorate in service in the absence of wear? Journal of the Royal Society Interface, 2012. 9(76): p. 3161-3164.

15.   Uo, M., K. Asakura, A. Yokoyama, M. Ishikawa, K. Tamura, Y. Totsuka, T. Akasaka, and F. Watari, X-ray absorption fine structure (XAFS) analysis of titanium-implanted soft tissue. Dental Materials Journal, 2007. 26(2): p. 268-273.

16.   Kalra, S., PhD thesis: The distribution and pro-inflammatory impact of titanium debris accumulation in the peri-implant environment. 2013, University of Birmingham. Available from: http://etheses.bham.ac.uk/4759/5/Kalra14PhD.pdf. [Accessed 20 March 2015].

17.   Pan, J., D. Thierry, and C. Leygraf, Hydrogen peroxide toward enhanced oxide growth on titanium in PBS solution: Blue coloration and clinical relevance. Journal of Biomedical Materials Research, 1996. 30(3): p. 393-402.

18.   Barao, V.A., M.T. Mathew, W.G. Assuncao, J.C. Yuan, M.A. Wimmer, and C. Sukotjo, The role of lipopolysaccharide on the electrochemical behavior of titanium. Journal of Dental Research, 2011. 90(5): p. 613-618.

19.   Omanovic, S. and S.G. Roscoe, Electrochemical studies of the adsorption behavior of bovine serum albumin on stainless steel. Langmuir, 1999. 15(23): p. 8315-8321.

20.   Cheng, X.L. and S.G. Roscoe, Corrosion behavior of titanium in the presence of calcium phosphate and serum proteins. Biomaterials, 2005. 26(35): p. 7350-7356.

21.   Wang, L.N., X.Q. Huang, A. Shinbine, and J.L. Luo, Influence of albumin on the electrochemical behaviour of Zr in phosphate buffered saline solutions. Journal of Materials Science-Materials in Medicine, 2013. 24(2): p. 295-305.

22.   Wang, W., F. Mohammadi, and A. Alfantazi, Corrosion behaviour of niobium in phosphate buffered saline solutions with different concentrations of bovine serum albumin. Corrosion Science, 2012. 57: p. 11-21.

23. Francis, G.L., Albumin and mammalian cell culture: implications for biotechnology applications. Cytotechnology, 2010. 62(1): p. 1-16.

24. Jackson, D.R., S. Omanovic, and S.G. Roscoe, Electrochemical studies of the adsorption behavior of serum proteins on titanium. Langmuir, 2000. 16(12): p. 5449-5457.

25. Padilla, N. and A. Bronson, Electrochemical characterization of albumin protein on Ti-6Al-4V alloy immersed in a simulated plasma solution. Journal of Biomedical Materials Research Part A, 2007. 81A(3): p. 531-543.

26. Karimi, S. and A.M. Alfantazi, Electrochemical corrosion behavior of orthopedic biomaterials in presence of human serum albumin. Journal of the Electrochemical Society, 2013. 160(6): p. C206-C214.

27. Karimi, S. and A.M. Alfantazi, Ion release and surface oxide composition of AISI 316L, Co-28Cr-6Mo, and Ti-6Al-4V alloys immersed in human serum albumin solutions. Materials Science & Engineering C-Materials for Biological Applications, 2014. 40: p. 435-444.

28. Karimi, S., T. Nickchi, and A. Alfantazi, Effects of bovine serum albumin on the corrosion behaviour of AISI 316L, Co-28Cr-6Mo, and Ti-6Al-4V alloys in phosphate buffered saline solutions. Corrosion Science, 2011. 53(10): p. 3262-3272.

29. Souza, J.C.M., P. Ponthiaux, M. Henriques, R. Oliveira, W. Teughels, J.P. Celis, and L.A. Rocha, Corrosion behaviour of titanium in the presence of Streptococcus mutans. Journal of Dentistry, 2013. 41(6): p. 528-34.

30. Mu, Y., T. Kobayashi, M. Sumita, A. Yamamoto, and T. Hanawa, Metal ion release from titanium with active oxygen species generated by rat macrophages in vitro. Journal of Biomedical Materials Research, 2000. 49(2): p. 238-243.

31. Hiromoto, S., Corrosion of metallic biomaterials in cell culture environments. The Electrochemical Society Interface, 2008: p. 41-44.

32. Hiromoto, S. and T. Hanawa, Corrosion of implant metals in the presence of cells. Corrosion Reviews, 2006. 24(5-6): p. 323-351.

33. Gilbert, J.L., C.A. Buckley, and J.J. Jacobs, In vivo corrosion of modular hip-prosthesis components in mixed and similar metal combinations - the effect of crevice, stress, motion and alloy coupling. Journal of Biomedical Materials Research, 1993. 27(12): p. 1533-1544.

34. Swaminathan, V. and J.L. Gilbert, Fretting corrosion of CoCrMo and Ti6Al4V interfaces. Biomaterials, 2012. 33(22): p. 5487-5503.

35. Barril, S., N. Debaud, S. Mischler, and D. Landolt, A tribo-electrochemical apparatus for in vitro investigation of fretting-corrosion of metallic implant materials. Wear, 2002. 252(9-10): p. 744-754.

36. Runa, M.J., M.T. Mathew, and L.A. Rocha, Tribocorrosion response of the Ti6Al4V alloys commonly used in femoral stems. Tribology International, 2013. 68: p. 85-93.

37. Goldberg, J.R., C.A. Buckley, J.J. Jacobs, and J.L. Gilbert, Corrosion testing of modular hip implants, in Modularity of Orthopedic Implants, D.E. Marlowe, J.E. Parr, and M.B. Mayor, Editors., American Society for Testing and Materials Special Technical Publication. STP 1301, Philadelphia, PA. March 1997. p. 157-176.

38. Goldberg, J.R. and J.L. Gilbert, In vitro corrosion testing of modular hip tapers. Journal of Biomedical Materials Research Part B-Applied Biomaterials, 2003. 64B(2): p. 78-93.

39. Albrektsson, T., P.I. Branemark, H.A. Hansson, and J. Lindstrom, Osseointegrated titanium implants - requirements for ensuring a long-lasting, direct bone-to-implant anchorage in man. Acta Orthopaedica Scandinavica, 1981. 52(2): p. 155-170.

40. Elias, C.N., J.H.C. Lima, R. Valiev, and M.A. Meyers, Biomedical applications of titanium and its alloys. Journal of the Minerals Metals and Materials Society, 2008. 60(3): p. 46-49.

41. Lutjering, G. and J.C. Williams, Titanium (2nd edition). 2007, New York: Springer-Verlag Berlin Heidelberg.

42. He, X., J.J. Noel, and D.W. Shoesmith, Effects of iron content on microstructure and crevice corrosion of Grade-2 titanium. Corrosion, 2004. 60(4): p. 378-386.

43. Atapour, M., A. Pilchak, G.S. Frankel, J.C. Williams, M.H. Fathi, and M. Shamanian, Corrosion behavior of Ti6Al4V with different thermomechanical treatments and microstructures. Corrosion, 2010. 66(6).

44. Hanawa, T., Metal ion release from metal implants. Materials Science and Engineering: C, 2004. 24(6-8): p. 745-752.

45. Tun, Z., J.J. Noel, and D.W. Shoesmith, Electrochemical modification of the passive oxide layer on a Ti film observed by in situ neutron reflectometry. Journal of the Electrochemical Society, 1999. 146(3): p. 988-994.

46. Shibata, T. and Y.C. Zhu, Effect of film formation conditions on the structure and composition of anodic oxide films on titanium. Corrosion Science, 1995. 37(2): p. 253-270.

47. Zhu, R., C. Nowierski, Z. Ding, J.J. Noel, and D.W. Shoesmith, Insights into grain structures and their reactivity on grade-2 Ti alloy surfaces by scanning electrochemical microscopy. Chemistry of Materials, 2007. 19(10): p. 2533-2543.

48.   Kelly, R.G., J.R. Scully, D.W. Shoesmith, and R.G. Buchheit, Electrochemical techniques in corrosion science and engineering. 2003, New York: Marcel Dekker Inc.

49.   Revie, R.W., Uhlig's Corrosion Handbook (3rd Editon). 2011, New Jersey: John Wiley & Sons Ltd.

50.   Marcus, P. and J. Oudar, Corrosion mechanisms in theory and practice. 1995, New York: Marcel Dekker, Inc.

51.   Tomashov, N.D., R.M. Altovsky, and G.P. Chernova, Passivity and corrosion resistance of titanium and its alloys. Journal of the Electrochemical Society, 1961. 108(2): p. 113-119.

52.   Stern, M. and H. Wissenberg, The influence of noble metal alloy additions on the electrochemical and corrosion behavior of titanium. Journal of the Electrochemical Society, 1959. 106(9): p. 759-764.

53.   Yu, S.Y., C.W. Brodrick, M.P. Ryan, and J.R. Scully, Effects of Nb and Zr alloying additions on the activation behavior of Ti in hydrochloric acid. Journal of the Electrochemical Society, 1999. 146(12): p. 4429-4438.

54.   Yu, S.Y., J.R. Scully, and C.M. Vitus, Influence of niobium and zirconium alloying additions on the anodic dissolution behavior of activated titanium in HCl solutions. Journal of the Electrochemical Society, 2001. 148(2): p. B68-B78.

55.   Dyer, C.K. and J.S.L. Leach, Reversible reactions within anodic oxide films on titanium electrodes. Electrochimica Acta, 1978. 23(12): p. 1387-1394.

56.   Blackwood, D.J., L.M. Peter, and D.E. Williams, Stability and open circuit breakdown of the passive oxide film on titanium. Electrochimica Acta, 1988. 33(8): p. 1143-1149.

57.   Pourbaix, M., Atlas of electrochemical equilibria in aqueous solutions. 1974, Houston: TX. NACE.

58.   Casillas, N., S. Charlebois, W.H. Smyrl, and H.S. White, Pitting corrosion of titanium. Journal of the Electrochemical Society, 1994. 141(3): p. 636-642.

59.   Basame, S.B. and H.S. White, Pitting corrosion of titanium - the relationship between fitting potential and competitive anion adsorption at the oxide film/electrolyte interface. Journal of the Electrochemical Society, 2000. 147(4): p. 1376-1381.

60.   Shoesmith, D.W., Assessing the corrosion performance of high-level nuclear waste containers. Corrosion, 2006. 62(8): p. 703-722.

61.   Virtanen, S., I. Milosev, E. Gomez-Barrena, R. Trebse, J. Salo, and Y.T. Konttinen, Special modes of corrosion under physiological and simulated physiological conditions. Acta Biomaterialia, 2008. 4(3): p. 468-476.

62.   Burstein, G.T., C. Liu, and R.M. Souto, The effect of temperature on the nucleation of corrosion pits on titanium in Ringer's physiological solution. Biomaterials, 2005. 26(3): p. 245-256.

63.   Burstein, G.T. and C. Liu, Depassivation current transients measured between identical twin microelectrodes in open circuit. Corrosion Science, 2008. 50(1): p. 2-7.

64.   Davenport, A.J., Second Year Corrosion Lecture Notes. 2013, University of Birmingham.

65.   Cheng, F.T., K.H. Lo, and H.C. Man, An electrochemical study of the crevice corrosion resistance of NiTi in Hanks' solution. Journal of Alloys and Compounds, 2007. 437(1-2): p. 322-328.

66.   Yaya, K., Y. Khelfaoui, B. Malki, and M. Kerkar, Numerical simulations study of the localized corrosion resistance of AISI 316L stainless steel and pure titanium in a simulated body fluid environment. Corrosion Science, 2011. 53(10): p. 3309-3314.

67.   Jacobs, J.J., A.K. Skipor, L.M. Patteson, N.J. Hallab, W.G. Paprosky, J. Black, and J.O. Galante, Metal release in patients who have has a primary total hip arthroplasty - A prospective, controlled, longitudinal study. Journal of Bone and Joint Surgery-American Volume, 1998. 80A(10): p. 1447-1458.

68.   Kasai, Y., R. Iida, and A. Uchida, Metal concentrations in the serum and hair of patients with titanium alloy spinal implants. Spine, 2003. 28(12): p. 1320-1326.

69.   Boyer, P., J.-Y. Lazennec, J. Poupon, M.-A. Rousseau, P. Ravaud, and Y. Catonne, Clinical and biological assessment of cemented titanium femoral stems: an 11-year experience. International Orthopaedics, 2009. 33(5): p. 1209-1215.

70.   Jacobs, J.J., J.L. Gilbert, and R.M. Urban, Current concepts review - corrosion of metal orthopaedic implants. The journal of bone and joint surgery, 1998. 80(2): p. 268-282.

71.   Olmedo, D.G., G. Nalli, S. Verdu, M.L. Paparella, and R.L. Cabrini, Exfoliative cytology and titanium dental implants: a pilot study. Journal of Periodontology, 2013. 84(1): p. 78-83.

72.   Olmedo, D.G., M.L. Paparella, D. Brandizzi, and R.L. Cabrini, Reactive lesions of peri-implant mucosa associated with titanium dental implants: a report of 2 cases. International Journal of Oral and Maxillofacial Surgery, 2010. 39(5): p. 503-507.

73.   Olmedo, D.G., M.L. Paparella, M. Spielberg, D. Brandizzi, M.B. Guglielmotti, and R.L. Cabrini, Oral mucosa tissue response to titanium cover screws. Journal of Periodontology, 2012. 83(8): p. 973-980.

74. Rodrigues, D.C., R.M. Urban, J.J. Jacobs, and J.L. Gilbert, In vivo severe corrosion and hydrogen embrittlement of retrieved modular body titanium alloy hip implants. Journal of Biomedical Materials Research Part B-Applied Biomaterials, 2009. 88B(1): p. 206-219.

75. Gilbert, J.L., S. Mali, R.M. Urban, C.D. Silverton, and J.J. Jacobs, In vivo oxide-induced stress corrosion cracking of Ti-6Al-4V in a neck-stem modular taper: Emergent behavior in a new mechanism of in vivo corrosion. Journal of Biomedical Materials Research Part B-Applied Biomaterials, 2012. 100B(2): p. 584-594.

76. Witt, F., B.H. Bosker, N.E. Bishop, H.B. Ettema, C.C.P.M. Verheyen, and M.M. Morlock, The relation between titanium taper corrosion and cobalt-chromium bearing wear in large-head metal-on-metal total hip prostheses: a retrieval study. The Journal of bone and joint surgery. American volume, 2014. 96(18): p. e157-e157.

77. Urban, R.M., J.L. Gilbert, and J.J. Jacobs, Corrosion of modular titanium alloy stems in cementless hip replacement, in Titanium, niobium, zirconium, and tantalum for medical and surgical applications, L.D. Zardiackas, M.J. Kraay, and H.L. Freese., Editors., American Society for Testing and Materials International, STP 1471, Ann Arbor, MI, Dec 2005. p. 215-224.

78. Grupp, T.M., T. Weik, W. Bloemer, and H.-P. Knaebel, Modular titanium alloy neck adapter failures in hip replacement - failure mode analysis and influence of implant material. BMC Musculoskeletal Disorders, 2010. 11:3.

79. Willert, H.G., L.G. Broback, G.H. Buchhorn, P.H. Jensen, G. Koster, I. Lang, P. Ochsner, and R. Schenk, Crevice corrosion of cemented titanium alloy stems in total hip replacements. Clinical Orthopaedics and Related Research, 1996(333): p. 51-75.

80. Jasty, M., W.J. Maloney, C.R. Bragdon, D.O. Oconnor, T. Haire, and W.H. Harris, The initiation of failure in cemented femoral components of hip arthroplasties. Journal of Bone and Joint Surgery-British Volume, 1991. 73(4): p. 551-558.

81. Geringer, J., J. Pellier, M.L. Taylor, and D.D. Macdonald, Electrochemical Impedance Spectroscopy: Insights for fretting corrosion experiments. Tribology International, 2013. 68: p. 67-76.

82. Baxmann, M., S.Y. Jauch, C. Schilling, W. Bloemer, T.M. Grupp, and M.M. Morlock, The influence of contact conditions and micromotions on the fretting behavior of modular titanium alloy taper connections. Medical Engineering & Physics, 2013. 35(5): p. 676-683.

83. Jauch, S.Y., G. Huber, K. Sellenschloh, H. Haschke, M. Baxmann, T.M. Grupp, and M.M. Morlock, Micromotions at the taper interface between stem and neck adapter of a bimodular hip prosthesis during activities of daily living. Journal of Orthopaedic Research, 2013. 31(8): p. 1165-1171.

84.   COM/06/S1. 2006 Biological effects of metal wear debris generated from hip implants: genotoxicity. Medicines and Healthcare products Regulatory Agency: London, UK. Available from: http://cot.food.gov.uk/sites/default/files/cot/comsection06.pdf. [Assessed 27 March 2015].

85.   Katou, F., N. Andoh, K. Motegi, and H. Nagura, Immuno-inflammatory responses in the tissue adjacent to titanium miniplates used in the treatment of mandibular fractures. Journal of Cranio-Maxillofacial Surgery, 1996. 24(3): p. 155-162.

86.   Flatebo, R.S., A.C. Johannessen, A.G. Gronningsaeter, O.E. Boe, N.R. Gjerdet, B. Grung, and K.N. Leknes, Host response to titanium dental implant placement evaluated in a human oral model. Journal of Periodontology, 2006. 77(7): p. 1201-1210.

87.   Olmedo, D., M.M. Fernandez, M.B. Guglielmotti, and R.L. Cabrini, Macrophages related to dental implant failure. Implant Dentistry, 2003. 12(1): p. 75-80.

88.   Noguchi, T., S. Takemoto, M. Hattori, M. Yoshinari, E. Kawada, and Y. Oda, Discoloration and dissolution of titanium and titanium alloys with immersion in peroxide- or fluoride-containing solutions. Dental Materials Journal, 2008. 27(1): p. 117-123.

89.   Okazaki, Y. and E. Gotoh, Comparison of metal release from various metallic biomaterials in vitro. Biomaterials, 2005. 26(1): p. 11-21.

90.   Atapour, M., M.H. Fathi, and M. Shamanian, Corrosion behavior of Ti6Al4V alloy weldment in hydrochloric acid. Materials and Corrosion-Werkstoffe Und Korrosion, 2012. 63(2): p. 134-139.

91.   Koike, M. and H. Fujii, The corrosion resistance of pure titanium in organic acids. Biomaterials, 2001. 22(21): p. 2931-2936.

92.   Koike, M. and H. Fujii, In vitro assessment of corrosive properties of titanium as a biomaterial. Journal of Oral Rehabilitation, 2001. 28(6): p. 540-548.

93.   Mabilleau, G., S. Bourdon, M.L. Joly-Guillou, R. Filmon, M.F. Basle, and D. Chappard, Influence of fluoride, hydrogen peroxide and lactic acid on the corrosion resistance of commercially pure titanium. Acta Biomaterialia, 2006. 2(1): p. 121-129.

94.   Strietzel, R., A. Hosch, H. Kalbfleisch, and D. Buch, In vitro corrosion of titanium. Biomaterials, 1998. 19(16): p. 1495-1499.

95.   Contu, F., The cathodic behavior of titanium: Serum effect. J Biomed Mater Res Part B, 2012. 100B(2): p. 544-552.

96.   Contu, F., B. Elsener, and H. Bohni, Serum effect on the electrochemical behaviour of titanium, Ti6A14V and Ti6Al7Nb alloys in sulphuric acid and sodium hydroxide. Corrosion Science, 2004. 46(9): p. 2241-2254.

97.   Williams, R.L., S.A. Brown, and K. Merritt, Electrochemical studies on the influence of proteins on the corrosion of implant alloys. Biomaterials, 1988. 9(2): p. 181-186.

98.   Zhang, S.M., J. Qiu, F. Tian, X.K. Guo, F.Q. Zhang, and Q.F. Huang, Corrosion behavior of pure titanium in the presence of Actinomyces naeslundii. Journal of Materials Science-Materials in Medicine, 2013. 24(5): p. 1229-1237.

99.   Javier Gil, F., A. Rodriguez, E. Espinar, J. Maria Llamas, E. Padulles, and A. Juarez, Effect of oral bacteria on the mechanical behavior of titanium dental implants. International Journal of Oral and Maxillofacial Implants, 2012. 27(1): p. 64-68.

100.   Lin, H.Y. and J.D. Bumgardner, In vitro biocorrosion of Ti-6Al-4V implant alloy by a mouse macrophage cell line. Journal of Biomedical Materials Research Part A, 2004. 68A(4): p. 717-724.

101.   Rodrigues, D.C., P. Valderrama, T.G. Wilson, Jr., K. Palmer, A. Thomas, S. Sridhar, A. Adapalli, M. Burbano, and C. Wadhwani, Titanium corrosion mechanisms in the oral environment: a retrieval study. Materials, 2013. 6(11): p. 5258-5274.

102.   Barao, V.A.R., M.T. Mathew, W.G. Assuncao, J.C.-C. Yuan, M.A. Wimmer, and C. Sukotjo, Stability of cp-Ti and Ti-6Al-4V alloy for dental implants as a function of saliva pH - an electrochemical study. Clinical Oral Implants Research, 2012. 23(9): p. 1055-1062.

103.   Souza, M.E.P., L. Lima, C.R.P. Lima, C.A.C. Zavaglia, and C.M.A. Freire, Effects of pH on the electrochemical behaviour of titanium alloys for implant applications. Journal of Materials Science-Materials in Medicine, 2009. 20(2): p. 549-552.

104.   Kelly, E.J., Anodic dissolution and passivation of titanium in acidic media. 3. chloride solutions. Journal of the Electrochemical Society, 1979. 126(12): p. 2064-2075.

105.   Atapour, M., A.L. Pilchak, G.S. Frankel, and J.C. Williams, Corrosion behavior of beta titanium alloys for biomedical applications. Materials Science & Engineering C, 2011. 31(5): p. 885-891.

106.   Tengvall, P., I. Lundstrom, L. Sjoqvist, H. Elwing, and L.M. Bjursten, Titanium-hydrogen peroxide interaction - model studies of the influence of the inflammatory response on titanium implants. Biomaterials, 1989. 10(3): p. 166-175.

107.   Hattori, M. and Y. Oda, EQCM analysis of titanium corrosion in peroxide- or fluoride-containing solutions. The Bulletin of Tokyo Dental College, 2013. 54(3): p. 135-40.

108.   Tengvall, P., L. Bertilsson, B. Liedberg, H. Elwing, and I. Lundstrom, Degradation of dried ti-peroxy gels made from metallic titanium and hydrogen-peroxide. Journal of Colloid and Interface Science, 1990. 139(2): p. 575-580.

109. Mohanchandra, K.P., Y. Chun, S.V. Prikhodko, and G.P. Carman, TEM characterization of super-hydrophilic Ni-Ti thin film. Materials Letters, 2011. 65(8): p. 1184-1187.

110. Assis, S.L.d. and I. Costa, The effect of hydrogen peroxide on the electrochemical behaviour of Ti-13Nb-13Zr alloy in Hanks' solution. Materials Research, 2006. 9(4).

111. Fadl-Allah, S.A., R.M. El-Sherief, and W.A. Badawy, Electrochemical formation and characterization of porous titania TiO_2 films on Ti. Journal of Applied Electrochemistry, 2008. 38(10): p. 1459-1466.

112. Fonseca, C. and M.A. Barbosa, Corrosion behaviour of titanium in biofluids containing H_2O_2 studied by electrochemical impedance spectroscopy. Corrosion Science, 2001. 43(3): p. 547-559.

113. Gilbert, J.L., Method of preparing biomedical surface. Patent #8,012,338, September 6, 2011.

114. Chandrasekaran, N., Z. Bai, and J.L. Gilbert, Titanium electrochemistry in the presence of the inflammatory species H_2O_2. Translation society for biomaterials annual meeting, 2006.

115. Hedberg, Y. and I.O. Wallinder, Metal release and speciation of released chromium from a biomedical CoCrMo alloy into simulated physiologically relevant solutions. Journal of Biomedical Materials Research Part B-Applied Biomaterials, 2014. 102(4): p. 693-699.

116. Mareci, D., R. Chelariu, D.-M. Gordin, G. Ungureanu, and T. Gloriant, Comparative corrosion study of Ti-Ta alloys for dental applications. Acta Biomaterialia, 2009. 5(9): p. 3625-3639.

117. Khan, M.A., R.L. Williams, and D.F. Williams, The corrosion behaviour of Ti-6Al-4V, Ti-6Al-7Nb and Ti-13Nb-13Zr in protein solutions. Biomaterials, 1999. 20(7): p. 631-637.

118. Huang, H.H., Effect of fluoride and albumin concentration on the corrosion behavior of Ti-6Al-4V alloy. Biomaterials, 2003. 24(2): p. 275-282.

119. Contu, F., B. Elsener, and H. Bohni, Characterization of implant materials in fetal bovine serum and sodium sulfate by electrochemical impedance spectroscopy. I. Mechanically polished samples. Journal of Biomedical Materials Research, 2002. 62(3): p. 412-421.

120. Faverani, L.P., W.G. Assuncao, P.S.P. de Carvalho, J.C.-C. Yuan, C. Sukotjo, M.T. Mathew, and V.A. Barao, Effects of dextrose and lipopolysaccharide on the corrosion behavior of a Ti6Al4V alloy with a smooth surface or treated with double-acid-etching. PLoS One, 2014. 9(3).

121. Mathew, M.T., V.A. Barao, J.C.-C. Yuan, W.G. Assuncao, C. Sukotjo, and M.A. Wimmer, What is the role of lipopolysaccharide on the tribocorrosive behavior of titanium? Journal of the Mechanical Behavior of Biomedical Materials, 2012. 8: p. 71-85.

122. Hiromoto, S. and S. Mischler, The influence of proteins on the fretting-corrosion behaviour of a Ti6Al4V alloy. Wear, 2006. 261(9): p. 1002-1011.

123. Huang, H.H. and T.H. Lee, Electrochemical impedance spectroscopy study of Ti-6Al-4V alloy in artificial saliva with fluoride and/or bovine albumin. Dental Materials, 2005. 21(8): p. 749-755.

124. Yan, Y., A. Neville, D. Dowson, and S. Williams, Tribocorrosion in implants - assessing high carbon and low carbon Co-Cr-Mo alloys by in situ electrochemical measurements. Tribology International, 2006. 39(12): p. 1509-1517.

125. Valero Vidal, C., A. Olmo Juan, and A. Lgual Munoz, Adsorption of bovine serum albumin on CoCrMo surface: Effect of temperature and protein concentration. Colloids and Surfaces B-Biointerfaces, 2010. 80(1): p. 1-11.

126. Ban, S., J. Hasegawa, and S. Maruno, Electrochemical corrosion behavior of hydroxyapatite glass titanium composite. Biomaterials, 1991. 12(2): p. 205-209.

127. Munoz, A.I. and S. Mischler, Interactive effects of albumin and phosphate ions on the corrosion of CoCrMo implant alloy. Journal of the Electrochemical Society, 2007. 154(10): p. C562-C570.

128. Mareci, D., G. Bolat, R. Chelariu, D. Sutiman, and C. Munteanu, The estimation of corrosion behaviour of ZrTi binary alloys for dental applications using electrochemical techniques. Materials Chemistry and Physics, 2013. 141(1): p. 362-369.

129. Walivaara, B., I. Lundstrom, and P. Tengvall, An in vitro study of hydrogen peroxide-treated titanium surfaces in contact with blood plasma and a simulated body fluid. Clinical Materials, 1993. 12(3): p. 141-148.

130. Nagassa, M.E., A.E. Daw, W.G. Rowe, A. Carley, D.W. Thomas, and R. Moseley, Optimisation of the hydrogen peroxide pre-treatment of titanium: surface characterisation and protein adsorption. Clinical Oral Implants Research, 2008. 19(12): p. 1317-1326.

131. Ragab, A.A., R. Van de Motter, S.A. Lavish, V.M. Goldberg, J.T. Ninomiya, C.R. Carlin, and E.M. Greenfield, Measurement and removal of adherent endotoxin from titanium particles and implant surfaces. Journal of Orthopaedic Research, 1999. 17(6): p. 803-809.

132. Pan, J., D. Thierry, and C. Leygraf, Electrochemical impedance spectroscopy study of the passive oxide film on titanium for implant application. Electrochimica Acta, 1996. 41(7-8): p. 1143-1153.

133. The marshall protocol knowledge base: biofilm bacteria. Autoimmunity Research Foundation 2014. [Online]. [Accessed 27 March 2015]. Available from: http://mpkb.org/home/pathogenesis/microbiota/biofilm.

134. Monksfield, P., I.L.C. Chapple, J.B. Matthews, M.M. Grant, O. Addison, A.P. Reid, D.W. Proops, and R.L. Sammons, Biofilm formation on bone-anchored hearing aids. Journal of Laryngology and Otology, 2011. 125(11): p. 1125-1130.

135. Hauser-Gerspach, I., E.M. Kulik, R. Weiger, E.-M. Decker, C. Von Ohle, and J. Meyer, Adhesion of Streptococcus sanguinis to dental implant and restorative materials in vitro. Dental Materials Journal, 2007. 26(3): p. 361-366.

136. Paquette, D.W., N. Brodala, and R.C. Williams, Risk factors for endosseous dental implant failure. Dental Clinics of North America, 2006. 50(3): p. 361-vi.

137. Rodriguez-Hernandez, A.G., A. Juarez, E. Engel, and F.J. Gil, Streptococcus sanguinis adhesion on titanium rough surfaces: effect of shot-blasting particles. Journal of Materials Science-Materials in Medicine, 2011. 22(8): p. 1913-1922.

138. Rodriguez-Hernandez, A.G., J.A. Munoz-Tabares, M. Godoy-Gallardo, A. Juarez, and F.-J. Gil, S. sanguinis adhesion on rough titanium surfaces: effect of culture media. Materials Science & Engineering C-Materials for Biological Applications, 2013. 33(2): p. 714-720.

139. Le Guehennec, L., A. Soueidan, P. Layrolle, and Y. Amouriq, Surface treatments of titanium dental implants for rapid osseointegration. Dental Materials, 2007. 23(7): p. 844-854.

140. da Rocha, S.S., A.C. Abreu Bernardi, A.C. Pizzolitto, G.L. Adabo, and E.L. Pizzolitto, Streptococcus mutans attachment on a cast titanium surface. Materials Research-Ibero-American Journal of Materials, 2009. 12(1): p. 41-44.

141. Fukushima, A., G. Mayanagi, K. Nakajo, K. Sasaki, and N. Takahashi, Microbiologically induced corrosive properties of the titanium surface. Journal of Dental Research, 2014. 93(5): p. 525-529.

142. Nobbs, A.H., R.J. Lamont, and H.F. Jenkinson, Streptococcus adherence and colonization. Microbiology and Molecular Biology Reviews, 2009. 73(3): p. 407-450.

143. Desoet, J.J., F.A. Toors, and J. Degraaff, Acidogenesis by oral streptococci at different pH values. Caries Research, 1989. 23(1): p. 14-17.

144. Zheng, L., Z. Chen, A. Itzek, M. Ashby, and J. Kreth, Catabolite control protein a controls hydrogen peroxide production and cell death in Streptococcus sanguinis. Journal of Bacteriology, 2011. 193(2): p. 516-526.

145. Ryan, C.S. and I. Kleinberg, Bacteria in human mouths involved in the production and utilization of hydrogen-peroxide. Archives of Oral Biology, 1995. 40(8): p. 753-763.

146. Hiromoto, S., K. Noda, and T. Hanawa, Electrochemical properties of an interface between titanium and fibroblasts L929. Electrochimica Acta, 2002. 48(4): p. 387-396.

147. Hiromoto, S. and T. Hanawa, pH near cells on stainless steel and titanium. Electrochemical and Solid State Letters, 2004. 7(3): p. B9-B11.

148. Cadosch, D., M.S. Al-Mushaiqri, O.P. Gautschi, J. Meagher, H.-P. Simmen, and L. Filgueira, Biocorrosion and uptake of titanium by human osteoclasts. J Biomed Mater Res Part A, 2010. 95A(4): p. 1004-1010.

149. Lin, H.Y. and J.D. Bumgardner, Changes in surface composition of the Ti-6Al-4V implant alloy by cultured macrophage cells. Applied Surface Science, 2004. 225(1-4): p. 21-28.

150. Hiromoto, S. and T. Hanawa, Electrochemical properties of 316L stainless steel with culturing L929 fibroblasts. Journal of the Royal Society Interface, 2006. 3(9): p. 495-505.

151. Lin, H.Y. and J.D. Bumgardner, Changes in the surface oxide composition of Co-Cr-Mo implant alloy by macrophage cells and their released reactive chemical species. Biomaterials, 2004. 25(7-8): p. 1233-1238.

152. Kumazawa, R., F. Watari, N. Takashi, Y. Tanimura, M. Uo, and Y. Totsuka, Effects of Ti ions and particles on neutrophil function and morphology. Biomaterials, 2002. 23(17): p. 3757-3764.

153. Brinkmann, V., U. Reichard, C. Goosmann, B. Fauler, Y. Uhlemann, D.S. Weiss, Y. Weinrauch, and A. Zychlinsky, Neutrophil extracellular traps kill bacteria. Science, 2004. 303(5663): p. 1532-1535.

154. Wright, H.L., R.J. Moots, R.C. Bucknall, and S.W. Edwards, Neutrophil function in inflammation and inflammatory diseases. Rheumatology, 2010. 49(9): p. 1618-1631.

155. Test, S.T. and S.J. Weiss, Quantitative and temporal characterization of the extracellular H_2O_2 pool generated by human neutrophils. Journal of Biological Chemistry, 1984. 259(1): p. 399-405.

156. Battino, M., P. Bullon, M. Wilson, and H. Newman, Oxidative injury and inflammatory periodontal diseases: the challenge of antioxidants to free radicals and reactive oxygen species. Critical Reviews in Oral Biology & Medicine, 1999. 10(4): p. 458-476.

157.   Goncalves, D.M., S. Chiasson, and D. Girard, Activation of human neutrophils by titanium dioxide (TiO$_2$) nanoparticles. Toxicology In Vitro, 2010. 24(3): p. 1002-1008.

158.   Goncalves, D.M. and D. Girard, Titanium dioxide (TiO$_2$) nanoparticles induce neutrophil influx and local production of several pro-inflammatory mediators in vivo. International Immunopharmacology, 2011. 11(8): p. 1109-1115.

159.   Mattei, L., F. Di Puccio, B. Piccigallo, and E. Ciulli, Lubrication and wear modelling of artificial hip joints: A review. Tribology International, 2011. 44(5): p. 532-549.

160.   Lomholt, T.C., K. Pantleon, and M.A.J. Somers, In-vivo degradation mechanism of Ti-6Al-4V hip joints. Materials Science & Engineering C-Materials for Biological Applications, 2011. 31(2): p. 120-127.

161.   Mathew, M.T., S. Abbey, N.J. Hallab, D.J. Hall, C. Sukotjo, and M.A. Wimmer, Influence of pH on the tribocorrosion behavior of CpTi in the oral environment: synergistic interactions of wear and corrosion. Journal of Biomedical Materials Research Part B-Applied Biomaterials, 2012. 100B(6): p. 1662-1671.

162.   Licausi, M.P., A. Igual Munoz, and V. Amigo Borras, Tribocorrosion mechanisms of Ti6Al4V biomedical alloys in artificial saliva with different pHs. Journal of Physics D-Applied Physics, 2013. 46(40).

163.   Cvijovic-Alagic, I., Z. Cvijovic, S. Mitrovic, V. Panic, and M. Rakin, Wear and corrosion behaviour of Ti-13Nb-13Zr and Ti-6Al-4V alloys in simulated physiological solution. Corrosion Science, 2011. 53(2): p. 796-808.

164.   Advanced mechanical engineering solutions: hertzian contact stress calculator. [Online]. Available from: http://www.amesweb.info/HertzianContact/HertzianContact.aspx. [Accessed 27 March 2015].

165.   Komotori, J., N. Hisamori, and Y. Ohmori, The corrosion/wear mechanisms of Ti-6Al-4V alloy for different scratching rates. Wear, 2007. 263: p. 412-418.

166.   Dimah, M.K., F. Devesa Albeza, V. Amigo Borras, and A. Igual Munoz, Study of the biotribocorrosion behaviour of titanium biomedical alloys in simulated body fluids by electrochemical techniques. Wear, 2012. 294: p. 409-418.

167.   Contu, F., B. Elsener, and H. Bohni, A study of the potentials achieved during mechanical abrasion and the repassivation rate of titanium and Ti6Al4V in inorganic buffer solutions and bovine serum. Electrochimica Acta, 2004. 50(1): p. 33-41.

168.   Barril, S., S. Mischler, and D. Landolt, Influence of fretting regimes on the tribocorrosion behaviour of Ti6Al4V in 0.9wt.% sodium chloride solution. Wear, 2004. 256(9-10): p. 963-972.

169. Barril, S., S. Mischler, and D. Landolt, Electrochemical effects on the fretting corrosion behaviour of Ti6Al4V in 0.9% sodium chloride solution. Wear, 2005. 259(1-6): p. 282-291.

170. Vieira, A.C., A.R. Ribeiro, L.A. Rocha, and J.P. Celis, Influence of pH and corrosion inhibitors on the tribocorrosion of titanium in artificial saliva. Wear, 2006. 261(9): p. 994-1001.

171. Swaminathan, V. and J.L. Gilbert, Potential and frequency effects on fretting corrosion of Ti6Al4V and CoCrMo surfaces. Journal of Biomedical Materials Research Part A, 2013. 101(9): p. 2602-2612.

172. Montague, A., K. Merritt, S. Brown, and J. Payer, Effects of Ca and H_2O_2 added to RPMI on the fretting corrosion of Ti6Al4V. Journal of Biomedical Materials Research, 1996. 32(4): p. 519-526.

173. May, T.W. and R.H. Wiedmeyer, A table of polyatomic interferences in ICP-MS. Atomic Spectroscopy, 1998. 19(5): p. 150-155.

174. Pratten, J., A.W. Smith, and M. Wilson, Response of single species biofilms and microcosm dental plaques to pulsing with chlorhexidine. Journal of Antimicrobial Chemotherapy, 1998. 42(4): p. 453-459.

175. Yu, S.Y. and J.R. Scully, Corrosion and passivity of Ti-13% Nb-13% Zr in comparison to other biomedical implant alloys. Corrosion, 1997. 53(12): p. 965-976.

176. Atapour, M., A.L. Pilchak, M. Shamanian, and M.H. Fathi, Corrosion behavior of Ti8Al1Mo1V alloy compared to Ti6A14V. Materials and Design, 2011. 32(3): p. 1692-1696.

177. Tomashov, N.D., G.P. Chernova, Y.S. Ruscol, and G.A. Ayuyan, Passivation of alloys on titanium bases. Electrochimica Acta, 1974. 19(4): p. 159-172.

178. Metikos-Hukovic, M., A. Kwokal, and J. Piljac, The influence of niobium and vanadium on passivity of titanium-based implants in physiological solution. Biomaterials, 2003. 24(21): p. 3765-3775.

179. Yan, L., S. Ramamurthy, J.J. Noel, and D.W. Shoesmith, Hydrogen absorption into alpha titanium in acidic solutions. Electrochimica Acta, 2006. 52(3): p. 1169-1181.

180. Schromm, A.B., K. Brandenburg, H. Loppnow, U. Zahringer, E.T. Rietschel, S.F. Carroll, M.H.J. Koch, S. Kusumoto, and U. Seydel, The charge of endotoxin molecules influences their conformation and IL-6-inducing capacity. Journal of Immunology, 1998. 161(10): p. 5464-5471.

181. Garidel, P., M. Rappolt, A.B. Schromm, J. Howe, K. Lohner, J. Andra, M.H.J. Koch, and K. Brandenburg, Divalent cations affect chain mobility and aggregate structure of lipopolysaccharide from Salmonella minnesota reflected in a decrease of its biological activity. Biochimica et Biophysica Acta: Protein Structure and Molecular Enzymology, 2005. 1715(2): p. 122-131.

182. Sourek, J., M. Tichy, and J. Levin, Effect of certain cations (Fe, Zn, Mg and Ca) on bacterial endotoxins. Infection and Immunity, 1978. 21(2): p. 648-654.

183. Coughlin, R.T., S. Tonsager, and E.J. McGroarty, Quantitation of metal-cations bound to membranes and extracted lipopolysaccharide of Escherichia-coli. Biochemistry, 1983. 22(8): p. 2002-2007.

184. Tengvall, P., H. Elwing, L. Sjoqvist, I. Lundstrom, and L.M. Bjursten, Interaction between hydrogen-peroxide and titanium - a possible role in the biocompatibility of titanium. Biomaterials, 1989. 10(2): p. 118-120.

185. Al-Mobarak, N.A., A.M. Al-Mayouf, and A.A. Al-Swayih, The effect of hydrogen peroxide on the electrochemical behavior of Ti and some of its alloys for dental applications. Materials Chemistry and Physics, 2006. 99(2-3): p. 333-340.

186. Zhang, B.B., B.L. Wang, Y.B. Wang, L. Li, Y.F. Zheng, and Y. Liu, Development of Ti-Ag-Fe ternary titanium alloy for dental application. Journal of Biomedical Materials Research Part B-Applied Biomaterials, 2012. 100B(1): p. 185-196.

187. Al-Mobarak, N.A., A.A. Al-Swayih, and F.A. Al-Rashoud, Corrosion Behavior of Ti-6Al-7Nb Alloy in Biological Solution for Dentistry Applications. International Journal of Electrochemical Science, 2011. 6(6): p. 2031-2042.

188. Pan, J., D. Thierry, and C. Leygraf, Electrochemical and xps studies of titanium for biomaterial applications with respect to the effect of hydrogen-peroxide. Journal of Biomedical Materials Research, 1994. 28(1): p. 113-122.

189. Tengvall, P., H. Elwing, and I. Lundstrom, Titanium gel made from metallic titanium and hydrogen-peroxide. Journal of Colloid and Interface Science, 1989. 130(2): p. 405-413.

190. Burgos-Asperilla, L., M.C. Garcia-Alonso, M.L. Escudero, and C. Alonso, Study of the interaction of inorganic and organic compounds of cell culture medium with a Ti surface. Acta Biomaterialia, 2010. 6(2): p. 652-661.

191. Takemoto, S., M. Hattori, M. Yoshinari, E. Kawada, and Y. Oda, Discoloration of titanium alloy in acidic saline solutions with peroxide. Dental Materials Journal, 2013. 32(1): p. 19-24.

192. Zheng, L.Y., A. Itzek, Z.Y. Chen, and J. Kreth, Oxygen dependent pyruvate oxidase expression and production in Streptococcus sanguinis. International Journal of Oral Science, 2011. 3(2): p. 82-89.

193. Babin, K., F. Antoine, D.M. Goncalves, and D. Girard, TiO_2, CeO_2 and ZnO nanoparticles and modulation of the degranulation process in human neutrophils. Toxicology Letters, 2013. 221(1): p. 57-63.

194. Robinson, J.M., Reactive oxygen species in phagocytic leukocytes. Histochemistry and Cell Biology, 2008. 130(2): p. 281-297.

195. Hong, P.K.A. and Y.Y. MacAuley, Corrosion and leaching of copper tubing exposed to chlorinated drinking water. Water Air and Soil Pollution, 1998. 108(3-4): p. 457-471.

196. Woszczynski, M., J. Bergese, and G.A. Gagnon, Comparison of Chlorine and Chloramines on Lead Release from Copper Pipe Rigs. Journal of Environmental Engineering, 2013. 139(8): p. 1099-1107.

197. Gautam, N., S.P. Chakraborty, P.K. Kundu, and S. Roy, Age associated changes in antioxidant and antioxidative enzymes in human neutrophil of different aged people. Asian Pacific Journal of Tropical Biomedicine, 2012: p. S423-S428.

198. Molloy, D.O., S. Munir, C.M. Jack, M.B. Cross, W.L. Walter, and W.K. Walter, Sr., Fretting and Corrosion in Modular-Neck Total Hip Arthroplasty Femoral Stems. Journal of Bone and Joint Surgery-American Volume, 2014. 96A(6): p. 488-493.

199. Yan, Y., A. Neville, and D. Blowson, Biotribocorrosion of CoCrMo orthopaedic implant materials - Assessing the formation and effectof the biofilm. Tribology International, 2007. 40(10-12): p. 1492-1499.

200. Zhou, J., Y.-T. Tsai, H. Weng, E.N. Tang, A. Nair, D.P. Dave, and L. Tang, Real-time detection of implant-associated neutrophil responses using a formyl peptide receptor-targeting NIR nanoprobe. International Journal of Nanomedicine, 2012. 7: p. 2057-68.

201. Kop, A.M., C. Keogh, and E. Swarts, Proximal component modularity in THA-at what cost? An implant retrieval study. Clinical Orthopaedics and Related Research, 2012. 470(7): p. 1885-1894.